ANL-78-76

DR-760

ANL-78-76

DO NOT MICROFILM
COVER

330
2/28/80

MASTER

CHEMICAL ENGINEERING DIVISION

FUEL CYCLE PROGRAMS PROGRESS REPORT

April—June 1978

by

M. J. Steindler, Milton Ader, R. E. Barletta, J. K. Bates, C. H. Bean, G. J. Bernstein, R. A. Couture, K. F. Flynn, T. J. Gerding, L. J. Jardine, D. K. Kroeck, Michael Krumpelt, B. J. Kullen, R. A. Leonard, W. J. Mecham, J. H. Meisenhelder, K. M. Myles, R. H. Pelto, B. B. Saunders, W. B. Seefeldt, M. G. Seitz, A. A. Siczek, L. E. Trevorrow, Seymour Vogler, A. A. Ziegler, D. S. Webster, and Leslie Burris

ARGONNE NATIONAL LABORATORY, ARGONNE, ILLINOIS

Prepared for the U. S. DEPARTMENT OF ENERGY
under Contract W-31-109-Eng-38

DISCLAIMER

The facilities of Argonne National Laboratory are owned by the United States Government. Under the terms of a contract (W-31-109-Eng-38) among the U. S. Department of Energy, Argonne Universities Association and The University of Chicago, the University employs the staff and operates the Laboratory in accordance with policies and programs formulated, approved and reviewed by the Association.

MEMBERS OF ARGONNE UNIVERSITIES ASSOCIATION

The University of Arizona
Carnegie-Mellon University
Case Western Reserve University
The University of Chicago
University of Cincinnati
Illinois Institute of Technology
University of Illinois
Indiana University
The University of Iowa
Iowa State University
The University of Kansas
Kansas State University
Loyola University of Chicago
Marquette University
The University of Michigan
Michigan State University
University of Minnesota
University of Missouri
Northwestern University
University of Notre Dame
The Ohio State University
Ohio University
The Pennsylvania State University
Purdue University
Saint Louis University
Southern Illinois University
The University of Texas at Austin
Washington University
Wayne State University
The University of Wisconsin-Madison

Printed in the United States of America
Available from
National Technical Information Service
U. S. Department of Commerce
5285 Port Royal Road
Springfield, VA 22161

NTIS price codes
Printed copy: A14
Microfiche copy: A01

Distribution Categories:
Nuclear Waste Management (UC-70)
Chemical Separations Processes
for Plutonium and Uranium (UC-10)

ANL-78-76

ANL-78-76

ARGONNE NATIONAL LABORATORY
9700 South Cass Avenue
Argonne, Illinois 60439

CHEMICAL ENGINEERING DIVISION

FUEL CYCLE PROGRAMS QUARTERLY PROGRESS REPORT

April—June 1978

by

M. J. Steindler, Milton Ader, R. E. Barletta, J. K. Bates, C. H. Bean, G. J. Bernstein, R. A. Couture, K. F. Flynn, T. J. Gerding, L. J. Jardine, D. K. Kroeck, Michael Krumpelt, B. J. Kullen, R. A. Leonard, W. J. Mecham, J. H. Meisenhelder, K. M. Myles, R. H. Pelto, B. B. Saunders, W. B. Seefeldt, M. G. Seitz, A. A. Siczek, L. E. Trevorrow, Seymour Vogler, A. A. Ziegler, D. S. Webster, and Leslie Burris

December 1979

Previous reports in this series

ANL-77-36	October-December 1976
ANL-78-11	January-September 1977
ANL-78-37	October-December 1977
ANL-78-68	January-March 1978

THIS PAGE

WAS INTENTIONALLY

LEFT BLANK

TABLE OF CONTENTS

TABLE OF CONTENTS (contd)

TABLE OF CONTENTS (contd)

LIST OF FIGURES

LIST OF FIGURES (contd)

LIST OF FIGURES (contd)

LIST OF FIGURES (contd)

LIST OF FIGURES (contd)

LIST OF FIGURES (contd)

LIST OF TABLES

LIST OF TABLES (contd)

LIST OF TABLES (contd)

CHEMICAL ENGINEERING DIVISION

FUEL CYCLE PROGRAMS QUARTERLY PROGRESS REPORT

April-June 1978

by

M. J. Steindler, Milton Ader, R. E. Barletta, J. K. Bates, C. H. Bean, G. J. Bernstein, R. A. Couture, K. F. Flynn, T. J. Gerding, L. J. Jardine, D. K. Kroeck, Michael Krumpelt, B. J. Kullen, R. A. Leonard, W. J. Mecham, J. H. Meisenhelder, K. M. Myles, R. H. Pelto, B. B. Saunders, W. B. Seefeldt, M. G. Seitz, A. A. Siczek, L. E. Trevorrow, Seymour Vogler, A. A. Ziegler, D. S. Webster, and Leslie Burris

ABSTRACT

Fuel cycle studies reported for this period include studies of advanced solvent extraction techniques focussed on the development of centrifugal contactors for use in Purex processes. Miniature eight-stage centrifugal contactors are being employed in studies of phase separation, residence times, holdup volumes, and extraction efficiencies. The extraction kinetics of ruthenium and zirconium in the presence of uranium are being studied. Modifications of the 9-cm-ID centrifugal contactor resulted in increased separating capacity and rapid recovery from flow upsets. In other work, tricaprylmethyl-ammonium nitrate and di-n-amyl-n-amylphosphonate are being evaluated as extractants in the Thorex process. In another investigation, literature on the dispersion of uranium and plutonium by fires is being reviewed to develop a systematic and coherent body of knowledge as a basis for realistic source terms for accidents in fuel reprocessing plants. Mechanisms for subdividing and dispersing liquids and solids were reviewed.

In the program on pyrochemical and dry processing of nuclear fuel, a facility for testing materials for containment vessels is under construction; a preliminary conceptual flowsheet for carbide fuel processing has been designed, and equipment for studying carbide reactions in bismuth is under construction; salt transport processes are being studied; the literature on fabrication of process-size refractory metal vessels is being reviewed and the spinning of 13-cm-ID tungsten crucibles atttempted; fuel cycles were examined to establish the feasibility of AIROX reprocessing; the behavior (especially the solubility) of (1) uranium dioxide, (2) uranium dioxide containing simulated fission products, and (3) plutonium dioxide in molten alkali metal nitrates has been investigated; work was continued on the development of a flowsheet for reprocessing actinide oxides in molten salts; the preparation

of thorium-uranium carbide from the oxide is being studied and a preliminary flowsheet prepared; new flowsheets (based on the Dow Aluminum Pyrometallurgical process) for reprocessing of spent uranium metal fuel have been prepared; the chloride volitility processing of thorium-based fuels is being studied; the reprocessing of $(Th,U)O_2$ solid solution in a KCl-LiCl salt containing $ThCl_4$ and thorium chips continues to be studied; and a preliminary process flow sheet for the processing of spent nuclear fuel in molten tin has been constructed.

Work on the encapsulation of solidified radioactive waste in a metal matrix included study of the leach rates of simulated encapsulated waste forms.

Nine criteria for the handling of waste cladding hulls have been established. In other work, the transport properties of nuclear waste in geologic media are being studied. Strontium and tin migration in glauconite columns, relative to flowing water, was measured. In other column infiltration experiments, radioactive strontium in a stream of water moved through oolitic limestone as rapidly as the water did, but in a stream of water that had been equilibrated with the limestone strontium moved through the limestone one-tenth as fast. The migration of trace quantities of cesium and iodine through kaolinite columns was studied at various temperatures and solution compositions.

SUMMARY

Development of Advanced Solvent Extraction Techniques

As part of the program to develop advanced solvent extraction processes for Purex reprocessing of LWR fuel, mechanical and hydraulic testing of the first and second eight-stage 2-cm-ID centrifugal contactors has been completed. Tested were phase separation under flow conditions, residence time in the annular mixing zone, and total unit holdup volumes. Extraction efficiency tests are continuing. Results to date indicate that extraction efficiencies for uranium are in the 85 to 94% range.

Fabrication of the large (25-cm-ID rotor) annular centrifugal contactor is proceeding on schedule. This unit will be tested as part of the program to develop a contactor sized to process LWR fuel at a rate of 10 Mg/day.

The study of extraction kinetics of ruthenium and zirconium has been extended to multistage extraction/scrubbing runs in the presence of uranium. The objective is to determine whether or not a significant improvement can be achieved in decontamination of uranium and plutonium from ruthenium and zirconium by taking advantage of the lower extraction rates of these fission products. The initial extraction/scrub test showed that the decontamination factors for ruthenium and zirconium were about 250. These values are considered to be good when there are only four extraction and four scrub stages. The results for tests made at longer residence times are not yet available.

Tests to measure the kinetics of thorium extraction were made initially in a single-stage unit in the presence of uranium and also with no uranium present. Additional tests were done in an eight-stage bank of centrifugal contactors. The analytical results are pending.

Two extractants, 0.73F tricapyrlmethylammonium nitrate in "Aromatic-100" (TCMA-AR100) and 2.0F di-n-amyl-n-amylphosphonate in n-dodecane (DA[AP]-nDD) are being investigated for the recovery of uranium, thorium, and plutonium from irradiated thorium-uranium oxide fuels. The TCMA-AR100 extracts uranium and thorium up to the limits set by stoichiometry (TCMA:Th = 2:1, TCMA:U = 1:1), without a second organic phase forming. The concentration-dependent distribution of uranium into TCMA-AR100 from 2M HNO_3 is given.

The DA[AP]-nDD distribution coefficients are shown for various concentrations of HCOOH, HNO_3, uranium, and thorium, and for tracer Pu(IV). A scrubbing experiment traces the transfer of uranium, thorium, NO_3^-, and total acid through successive equilibrations with a formic acid-nitric acid solution.

A new method for titrating acids in samples containing uranium and thorium is presented.

Changes to the 9-cm-ID annular centrifugal contactor housing and rotor resulted in increased separating capacity of 25 to 40% over a range of organic-to-aqueous (O/A) flow ratios of 0.1 to 10. Flow upset tests made over this range showed the unit recovered quickly from even the most severe upsets. Operating regions for organic-continuous and aqueous-continuous emulsions in the annular mixing zone have been established. When the O/A ratio is near 0.5, either phase may be continuous, depending upon startup conditions and recovery from any flow upsets.

A set of tests was run in a single-stage miniature contactor to determine the effectiveness of various scrub solutions in removing zirconium from solutions of di-n-butyl-phosphoric acid (HDBP) in 30% tri-n-butyl phosphate (TBP)/nDD. Uncertainties in sample analyses permit only qualitative evaluations: scrubbing with 0.01M HNO_3 or water does not remove zirconium-di-n-butyl-phosphate (DBP) complexes from the organic phase; and (2) scrubbing with 2.5% Na_2CO_3 or 1M citric acid is effective.

Environmental Effects (Accident Analysis Methodology for Fuel Reprocessing Plants)

The purpose of this program is to develop the scientific and technical basis for predicting and evaluating the effects of accidents in fuel reprocessing plants. The scope includes the qualitative and quantitative characterization of material airborne in postulated accidents and the modifications of this airborne material during in-plant transport and during penetration of the confinement and air-cleaning system. Accident categories include explosions, fires, and criticality events.

Analysis of tests of the explosive dispersion of liquids (reported previously) was reviewed for application to realistic plant conditions. An alternative particle-size distribution function, the semilog function, was proposed and evaluated as an alternative to the particle-size distribution lognormal function; the semilog function may have more appropriate mathematical properties for the required correlation of physical conditions--in particular, the correlation of the explosion energy, the mass of material at risk, and the fraction of that material dispersed as an aerosol of respirable size (<10μm).

A review and analysis was made of previous estimates of accident effects in fabrication plants, including empirical tests of airborne uranium and plutonium under conditions representative of plant fires.

Reviews were also made of basic mechanisms for subdividing liquids and solid bodies and for dispersing such particles in air to form a transportable aerosol. Minimum energy requirements per gram of particles were calculated as functions of particle size for comparison with data obtained from experimental tests. Basic mechanisms for air entrainment were similarly used to calculate the ratio of entrainment to settling (as a function of particle size) for consistency with entrainment data and for implications as to expected behavior under various plant conditions, including fires.

Pyrochemical and Dry Processing Methods

A Pyrochemical and Dry Processing Methods (PDPM) Program was established at the beginning of FY 1978 in the Fuel Cycle Section of Chemical Engineering Division at Argonne National Laboratory (ANL). This program is an expansion of the National Fuel Cycle Program for reprocessing fuel by processes that will reduce the risk of proliferation of nuclear weapons. Argonne has been designated by the U.S. Department of Energy (DOE) as the lead laboratory for PDPM, with various reprocessing developments being performed at other DOE laboratories and by industrial contractors.

A PDPM Program Review was held at DOE Germantown on May 5, 1978. Presentations were made describing the PDPM Program management and technical program plan. Comments and recommendations were made by DOE staff from the Office of Fuel Cycle R&D and the Technology Branch. No significant redirection of program effort was indicated.

A technical information exchange meeting was held at ANL on May 16 and 17, 1978. Representatives of eight contractors responsible for nine separate work packages, along with individuals responsible for three work packages at ANL, reported on the status of engineering analysis, separations processes, and materials development in support of the PDPM Program.

Planned procurement, program schedules, program requirements, and management controls for FY 1979 were reviewed with ANL budget, accounting, procurement, administrative, and quality assurance personnel. The authority and responsibility of individuals representing each of the above was identified. Schedules were set for completing the procurement actions needed to effect the transition to FY 1979 subcontracted effort without delay.

Materials Development. The PDPM Environmental Testing facility (PETF) for screening candidate ceramic and metallic materials in simulated PDPM process environments is under construction.

Samples of Mo-30 wt % W and W-25 wt % Re are being prepared for corrosion testing. A list of other possible process containment materials has been prepared, and samples will be obtained.

Tungsten coatings have been achieved on small crucibles fabricated of alumina (with 3% yttria) and are being tested for integrity under thermal cycling conditions.

Carbide Fuel Processing. A preliminary conceptual flowsheet has been designed. The separation of the fission products from the actinides is achieved upon the reaction or dissolution of certain of the carbides in molten bismuth to form bismuthides. The unreacted fission product carbides and bismthides are lighter than bismuth and are expected to float on the surface. Uranium carbide dissociates to a very limited extent, and the $PuBi_2$ and $ThBi_2$ are denser than bismuth, are of limited solubility in bismuth, and are expected to settle in bismuth along with unreacted UC.

Work has continued on the design, construction, and purchase of equipment in which carbide reactions in bismuth will be studied. These experiments are to be performed in an inert-atmosphere (argon) glove box.

A conceptual pyrochemical processing scheme employing partitions between immiscible molten cadmium and molten chloride salts has been devised for spent monocarbide fuels. Separations of actinides from fission products are achieved by volatilization of fission products, solubility differences in alloy phases, and differences in metal/salt distributions following oxidation-reduction reactions with $CdCl_2$, $MgCl_2$, or magnesium. Essentially similar processes are proposed for Pu-^{238}U, Pu-^{232}Th, and ^{233}U-^{238}U-^{232}Th fuels.

Thorium-Uranium Salt Transport Processing. A flowsheet for thorium-uranium salt transport reprocessing is presented. The major areas include decladding, reduction, uranium/plutonium separation, and plutonium/thorium recovery. Several metals or alloys have been considered, but initial experiments will focus on the cadmium-magnesium alloy. The recovery of plutonium/thorium/FP-3, FP-4* by a hydriding step is also being considered.

In the reduction step of the salt transport process, CaO is one product. Periodically, when the cover salt becomes saturated with CaO, it must either be purified of CaO or discarded as a waste. One method for achieving recycling is based on the fused salt ($CaCl_2$) electrolysis of CaO. The cathode reaction regenerates calcium metal for recycle to the reduction vessel. A small laboratory-scale cell is being designed and an inert atmosphere glove box is being readied for verifying the feasibility of this concept.

---

*FP-3 consists of the trivalent rare earths and yttrium; FP-4 consists of Zr, Nb, Mo, Tc, Ru, Rh, Pd, Ag, Cd, In, Sn, and Sb.

Uranium-Plutonium Salt Transport Processing. During the third quarter of FY 1978, three pyrochemical processes were selected for processing of LWR and FBR fuels, namely, (a) coprocessing of uranium and plutonium by the salt transport process, (b) coprocessing of uranium and plutonium by Pyroredox, and (c) making a uranium separation from plutonium by the salt transport process.

Reference LWR and FBR fuel assemblies were selected, and the ORIGEN code (provided by Oak Ridge National Laboratory) was obtained to provide fission product data which could be used in material balance calculations around the selected pyrochemical process options. Three material balances have been completed, and six more are left to do. The material balances will be used in evaluation studies which will (a) provide a basis for the selection of a reference flowsheet and (b) identify key problems which challenge the feasibility of the process.

The literature search is near completion, with abstracts complete on decladding, oxide-reduction, and fuel refabrication. Tables have been compiled on the free energies of formation of oxides, chlorides, and fluorides and the vapor pressures of the elements between 800 K and 1400 K.

Descriptive flow sheets, material balances and cost estimates for conceptual facilities for pyrochemical processing of uranium-plutonium core, uranium blanket, and thorium blanket spent reactor fuel by salt transport were completed for the INFCE study.

Almost all equipment has been selected and ordered for the salt purification laboratory. The facility should be operational during the fourth quarter of FY 1978.

Fabrication of Process-Size Refractory Metal Vessels. A survey of tungsten suppliers and fabricators was conducted during the Third Quarter of FY 1978. Commercial capabilities in sheet fabrication, sintering, roll forming and riveting, and coating were examined.

Scheduled completion of the literature search is set for the first week of July 1978.

Problems were encountered in attempting to spin a 13-cm (5-in.)-ID tungsten crucible. a consultant has been hired to assist in future spinning.

Techniques currently being examined for the production of full-scale 283.1-L (10 ft^3) crucibles include (1) fabrication of a tungsten liner using joining techniques by brazing and/or riveting; (2) chemical vapor deposition for coating tungsten, molybdenum, and graphite; (3) plasma spray and (4) sintering.

Various brazes have been used to join tungsten coupons and are currently being tested for corrosion resistance.

Aluminum Alloy Processing of Thorium-and Uranium-Based Fuels. The literature review is well under way, and a first draft of a topical report based on the review is in preparation. Several new alternative flowsheets have been formulated that reflect both the contributions of data obtained in an ongoing literature survey and concepts that seem worth investigating with respect to project goals.

Experimental work has begun, directed towards gathering the essential data not in the literature.

Chloride-Volatility Processing of Thorium-Based Fuels. From the literature review, prior work has been evaluated to obtain data and information about the current technology. This data and information has been organized to provide a block diagram (not included) of the chloride volatility process. Some problems associated with hydrogen chloride decladding have been identified.

Corrosion tests are to be carried out in an available experimental system, accepting the risk of attack on the reactor wall. The design of experiments continued and is about 75% complete. Three preliminary experiments were carried out to evaluate the oxidation of uranium tetrachloride.

AIROX,* CARBOX and RAHYD Processing Systems. Fuel cycles were examined to establish the feasibility of AIROX reprocessing. These analyses indicated that fission product recyle is feasible--for both the LWR and the FBR.

The decay heat and radiation levels for fuel burnups greater than 33,000 MW/MT (i.e., after AIROX reprocessing) have been successfully calculated with the ORIGEN Code. The isotope removal fractions and uranium enrichment requirements have been calculated by the AIMFIRE and HAMMER Codes.

Experiments were carried out with UO_2 pellets to evaluate the comminution of the oxide during oxidation and reduction steps. When the series of experiments is completed, one should be able to determine if an optimum oxidation temperature exists. Kinetic information for the AIROX process is being obtained. As the temperature is increased from 400 to 480°C, the oxidation rate increases and the induction time period decreases. Verification tests with cold UO_2-PuO_2 are planned to investigate the oxidation-inhibiting effect of PuO_2 in the fuel and to determine if oxidation-reduction cycling will enhance the oxidation of UO_2 to U_3O_8.

Preparations are being made for an AIROX process demonstration to show that the developed process is applicable to spent fuels.

---

*The AIROX process consists of multiple oxidation-reduction cycles of oxide fuels.

Molten Nitrate Salt Oxidation-Processes. The behavior of uranium dioxide containing simulated fission products, and plutonium dioxide in molten alkali metal nitrates has been investigated. Uranium dioxide reacts with the molten alkali metal nitrates to form a uranate species. Plutonium dioxide does not react with alkali metal nitrates in the temperature range studied ($\leq$525°C).

Addition of nitric acid vapor to a nitrate melt containing the uranate species produces a soluble uranium species that may be thermally decomposed. Upon the addition of nitric acid to the nitrate melt a portion of the plutonium dioxide dissolved, but definitive statements must await analytical results.

Quantitative analyses of molten-phase samples and solids produced in these experiments are currently in progress. The results of these analyses will allow (1) better definition of actinide and fission product behavior in molten alkali metal nitrates and (2) determination of possible process steps.

Molten Salt Processes Applied to Ceramic Fuels. A proliferation-resistant method of reprocessing spent nuclear reactor fuels consists of first converting fuel oxide to chlorides, dissolving the chlorides in LiCl, extracting fissile and fertile material into bismuth, transferring the fissile and fertile materials into NH_4AlCl_4, and finally volatilizing the NH_4AlCl_4, leaving behind the fissile and fertile chlorides. Modifications to the reprocessing flow sheet involving bismuth, lithium and lithium chloride were examined. If fluoride should be substituted for chlorides, the separation factors of fissile material from fission products would be smaller.

Ammonium chloroaluminate was prepared by reacting ammonium chloride with aluminum chloride and zone refining the reaction product.

Reprocessing of Thoria-Urania Fuel. During the preparation of thorium-uranium carbide from the mixed oxide, barium and strontium are removed almost completely, but the rare earth elements, cerium, lanthanum, neodymium, promethium, and yttrium are only partially removed. Ruthenium, molybdenum, and zirconium showed little if any change in concentration from those of the initial charge.

The reaction of ThC_2 with $ZnCl_2$ to yield $ThCl_4$, zinc, and carbon was demonstrated; the kinetics are not highly sensitive to the particle size of the carbide, but appear to be sensitive to the temperature of preparation of the carbide.

Recent experiments on the reaction of UO_2 in a $(Th,U)O_2$ solid solution with thorium metal chips in a KCl-LiCl-$ThCl_4$ salt to produce UCl_3 and uranium metal have shown that glovebox oxygen levels of 10-100 ppm can have a significant effect on the reactions carried out in open containers. A different glove box has been put in operation to improve the reaction atmosphere.

A preliminary flowsheet has been prepared for thoria-urania fuels. The flowsheet gives the material requirements for a 10-kg fuel charge which initially contained 9.3% uranium and has been irradiated to an exposure of 94,271 MWd/MT at a power of 65 MW and a flux of 8×10^{13} neutrons/cm^2-s.

Molten Process for Reactor Fuel. A new effort is directed to the processing of spent nuclear fuel elements by the precipitation of thorium nitride, and plutonium nitride from a molten tin solvent. A preliminary process flowsheet has been constructed for this system and once revised.

Encapsulation of Radioactive Wastes in Metal

Leach rate studies (based on neutron activation analytical techniques) of compounds representative of those formed in the reaction zone between simulated high-level calcine waste pellets and molten lead have been completed. The results establish that these compounds are relatively insoluble in water (i.e., their leach rates are lower than those for typical glasses) and hence are not detrimental to the overall leaching characteristics of the lead-encapsulated waste.

The leach rates for aluminum-12% silicon alloy in 25°C and 100°C distilled water, as well as those for Zircaloy in 25°C distilled water and 110°C saturated sodium chloride solution, have also been determined using neutron activation analytical techniques. The leach rates for both were low.

Studies of the leaching characteristics in water of metal-encapsulated composites consisting of simulated high-level waste forms dispersed in a metal matrix are continuing. Leach rates as a function of time and ingot size for specific isotopes, using a sintered waste form, have been completed. These tests are continuing, using a variety of waste forms, matrix metals, leachants, and leaching conditions.

Some initial leaching measurements have been made using water and a simulated high level waste glass containing uranium (which had been prepared by Battelle Pacific Northwest Laboratories as part of their waste-glass program). Preliminary results indicate that approximately ten elements are leached relatively uniformly. Studies are continuing, using more severe leaching conditions.

Establishment of Tentative Criteria for Hull Treatment

In recent work on this project, the criteria for handling hulls have been conceived as the elements of a matrix of interactions between a set of safety policies and a set of operational factors that are basic to the handling of hulls. This concept has been recognized as similar to a method used in the expression of criteria for engineering concepts in general--i.e., that a criterion is a primary variable of an engineering concept that is viewed as a linear function of other secondary variables and parameters.

Nine criteria have been defined, and current work is concerned with defining the parameters and the four classes of secondary variables that they depend on. This revised format will be incorporated into the document on hulls criteria that is soon to be reviewed by members of several organizations and agencies.

Transport Properties of Nuclear Waste in Geologic Media

In this report, the influence of water flow-rate on the migration of strontium in a column of 40 to 70-mesh glauconite* is described. Strontium is retarded in glauconite relative to flowing water, and its concentration in the eluate from the glauconite column has a peak shape that broadens with increased flow rate. Therefore, the condition of "local equilibrium" may not be met for strontium in glauconite, even at the lowest flow rate of 1.2 km/y. This indicates that a description of nuclide migration needs to consider the kinetics of reactions, even for the simple and well-behaved system of strontium in glauconite. A criterion is proposed for determining when "local equilibrium" may be used to model migration without a loss of accuracy.

In an infiltration experiment, in which solution was forced through a column of rock material, it was observed that tin precipitated from solution or that it otherwise reacted irreversibly in the presence of glauconite to form a relatively immobile phase. Subsequent migration of tin occurred in the column--possibly as a result of the movement of colloids of tin or of particles having adsorbed tin.

In other column infiltration experiments, radioactive strontium in a stream containing 0.01M calcium was found to move through oolitic limestone as rapidly as the fluid stream did, but in a stream of water equilibrated with the limestone (REW), strontium moved through the oolitic limestone ten times slower that did the water. Results with the REW solution and with a solution that simulated groundwater in limestone ("recipe" solution) were similar. The REW solution and the recipe solution were both dilute but differed greatly in their content of major and minor elements and suspended particulate matter. That these two solutions produced the same migration behavior for strontium suggests that the differences are not important. This result, if valid in general, would considerably simplify the modeling and prediction of nuclide migration.

The delay of strontium migration in oolitic limestone using the REW solution and the recipe solution indicates a small exchange capacity of 7×10^{-5} meq strontium per gram limestone but nevertheless a capacity which is significant in the migration of trace quantities of strontium. The migration of strontium in oolitic limestone is ten times faster than is predicted by the results of earlier batch experiments. This discrepancy may be due to differences in the strontium absorption characteristics of crushed and massive limestone.

---

*A hydrous alumino-silicate mica, nominally (K, Na) (Al, Fe^{3+}, Fe^{2+}, Mg)$_2$ (Al,Si)$_4O_{10}(OH)_2$.

Solutions used to elute strontium in both glauconite and limestone were analyzed (1) for major and trace concentrations of cations by spectrochemical means and (2) for bicarbonate and calcium concentrations by titration. Comparing the analysis of REW that had been equilibrated with limestone with analysis of the recipe solution, we see that the REW solution is more complex than the receipe solution; six elements were present at detectable levels that were not explicitly added to the recipe solution.

Trace-Element Transport in Lithic Material by Fluid Flow at High Temperatures

Column infiltration experiments were performed to study the migration of cesium and iodine in kaolinite by fluid flow. Kaolinite is a nonexpanding common clay of low exchange capacity, and cesium and iodine isotopes are important in nuclear waste disposal. The temperature and the composition of aqueous solutions were varied in the experiments.

At room temperature, kaolinite retards the motion of cesium ion relative to that of a flowing aqueous solution of low ionic strength (0.001M $NaHCO_3$). Under these conditions, cesium moves about 0.0003 times as fast as the water stream. However, kaolinite loses some of this retention capability in solutions of higher ionic strength (0.5M Na) or at elevated temperature. At 118°C, cesium moves 0.03 times as fast, and at 224°C about 0.5 times as fast as the aqueous stream. These results demonstrate the great sensitivity of trace-element migration to solution composition and temperature.

At ambient temperature, iodine moved through columns of kaolinite in as many as three peaks but the results were time-dependent, with one peak prominent in one experiment and absent in another experiment. Paper chromatographic techniques were used to characterize the iodine solutions, and the complex results from the column infiltration indicate the coexistence of at least three chemically distinct species of iodine in the solutions.

In experiments at ambient temperature with some solutions, the iodine was strongly bound to the kaolinite. In experiments at 130°C, in contrast, the kaolinite completely lost its capacity to bind iodine and the iodine moved through the column at the same rate as the fluid stream.

Few experiments have been performed to study ion exchange on minerals above 100°C. The infiltration experiments reported here are the first to measure trace-element migration by fluid flow at temperatures above 100°C.

I. DEVELOPMENT OF ADVANCED SOLVENT EXTRACTION TECHNIQUES

(G. J. Bernstein, R. A. Leonard, R. H. Pelto, B. B. Saunders, A. A. Siczek, J. H. Meisenhelder, A. A. Ziegler, J. L. Murdock,* and J. L. Stassin†)

A. Developments for the Reprocessing of Light Water Reactor (LWR) Fuel

1. Introduction

Continuing progress is being made in the program to develop advanced solvent extraction techniques for Purex reprocessing of LWR fuel. The program is being carried out in cooperation with the Savannah River Laboratory (SRL). Specific parts of the Argonne National Laboratory (ANL) program are: (1) design, construction, and testing of single-stage and multistage miniature annular centrifugal contactors; (2) design, construction, and testing of a large annular centrifugal contactor with a reprocessing capacity of 10 Mg/day of LWR fuel; (3) study of the chemistry and kinetics of the solvent extraction of ruthenium and zirconium for the purpose of achieving enhanced decontamination of uranium and plutonium based upon differences in extraction rates in short-residence contactors; (4) investigation of uranium-plutonium partition in short-residence or other types of contactors; and (5) investigation of alternative aqueous thorium processing systems, including the causes and effects of solvent damage.

2. Development of a 10 Mg/day Centrifugal Contactor

(G. Bernstein and R. Leonard)

Fabrication of the large annular centrifugal contactor designed to process 10 Mg/day of LWR fuel began during this period and is proceeding on schedule. This unit has a rotor of 25-cm-ID and a 42-cm length. The phases are mixed in the annular space between the rotor and a stationary housing and are fed into an orifice in the bottom of the hollow rotor. The mixed organic and aqueous phases are separated under centrifugal force at about 1750 rpm.

A requisition has been placed for purchase of a large-capacity solution pumping and metering system. This will be used if the existing system in the contactor test unit should prove inadequate for testing of the contactor at its maximum capacity.

3. Development of Mini-Contactors

(R. Leonard, R. Pelto, A. Ziegler, J. L. Murdock,* J. L. Stassin,† and G. Bernstein)

Work continues on the development and testing of single-stage and multistage miniature (2-cm-ID) centrifugal contactors. They are being used to develop flowsheets for nuclear fuel reprocessing and solvent cleanup. Flow performance tests on the first two eight-stage units (contactors I and

---

*Student aide.

†Undergraduate research participant.

II) have been completed. Tests to measure and improve extraction efficiency are being completed. A modified rotor has been built and is ready for testing in a single-stage unit.

a. Contactor Flow Performance

Mechanical and hydraulic testing of the second eight-stage miniature contactor (disk base) was completed during this quarter. The variation in hydraulic performance between individual stages (shown in Table 1) is less than that for the first eight-stage contactor (vane base) reported earlier [STEINDLER-1978B]. The effect of organic-to-aqueous flow ratio and rotor speed on the throughput of a single stage of Contactor II (disk base) is shown in Fig. 1. As with Contactor I (vane base), increasing the rotor speed improves throughput up to about 6000 rpm. Single-stage throughputs for the two units are compared in Fig. 2. Contactor I has more variability, but both units have essentially the same maximum throughput. In this same figure, the single-stage and eight-stage results for Contactor II are compared. The lower throughput with eight-stage operation than with single-stage operation is similar to that found for Contactor I [STEINDLER-1978B].

Table 1. Hydraulic Performance of Individual Stages in Eight-Stage Contactor

Equipment:	Eight-Stage, 2-cm-ID Centrifugal Contactor II
Aqueous Phase:	3.0M HNO_3
Organic Phase:	30 vol % TBP in nDD
Rotor Speed:	6000 rpm

Stage No.	A in O Contamination, %			
	Total Flow of 120 mL/min		Total Flow of 160 mL/min	
1	2.2[a]	0.3[b]	10.9[b]	0.7[c]
2	7.0[a]	0.3[b]	1.9[b]	0.6[c]
3	3.8[a]	0.3[b]	0.7[b]	0.4[c]
4	6.2[a]	0.1[b]	2.1[b]	0.7[c]
5	5.8[a]	0.2[b]	18.3[b]	0.4[c]
			0.6[d]	
6	3.1[a]	0.3[b]	2.4[b]	0.6[c]
7	3.4[a]	0.3[b]	0.5[b]	0.5[c]
8	2.7[a]	0.3[b]	12.4[b]	0.4[c]

[a] At O/A ratio of 0.5.

[b] At O/A ratio of 1.0.

[c] At O/A ratio of 2.0.

[d] O in A contamination. This is the only O in A contamination in greater than a trace amount.

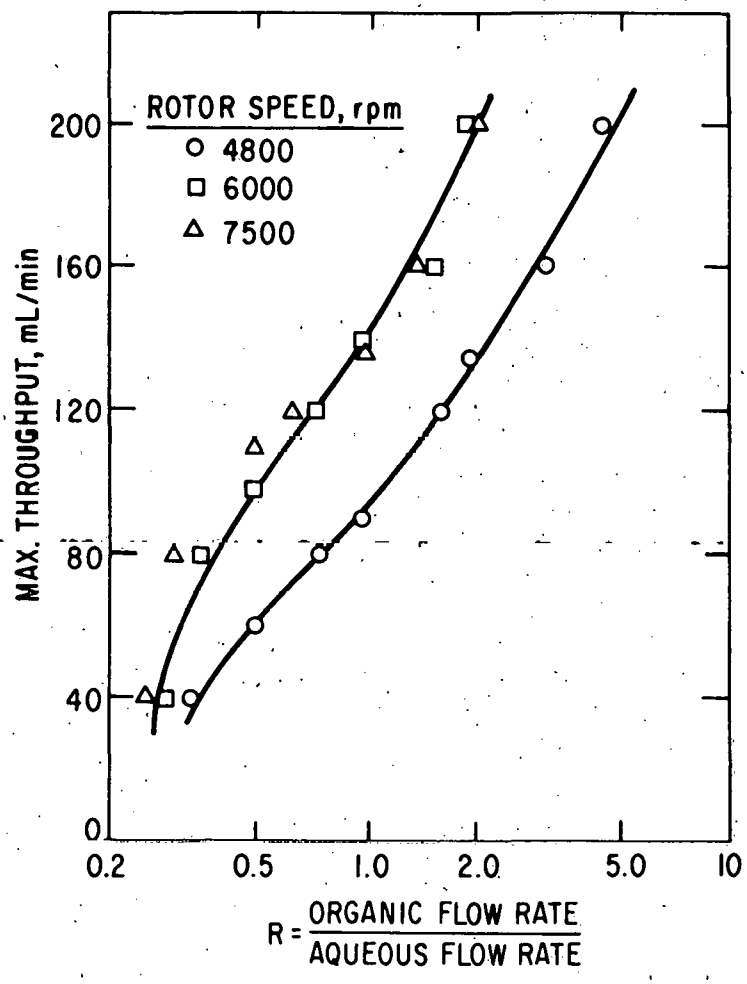

Fig. 1. Effect of O/A Ratio and Rotor Speed on Maximum Throughput of a Single Stage. Unit: Eight-stage 2-cm-ID Centrifugal Contactor. Stage No: 4 Aqueous Feed: 3.0M HNO_3. Organic Feed: 30 vol % TBP in nDD. Acceptable Performance: >99% phase separation in both effluent streams

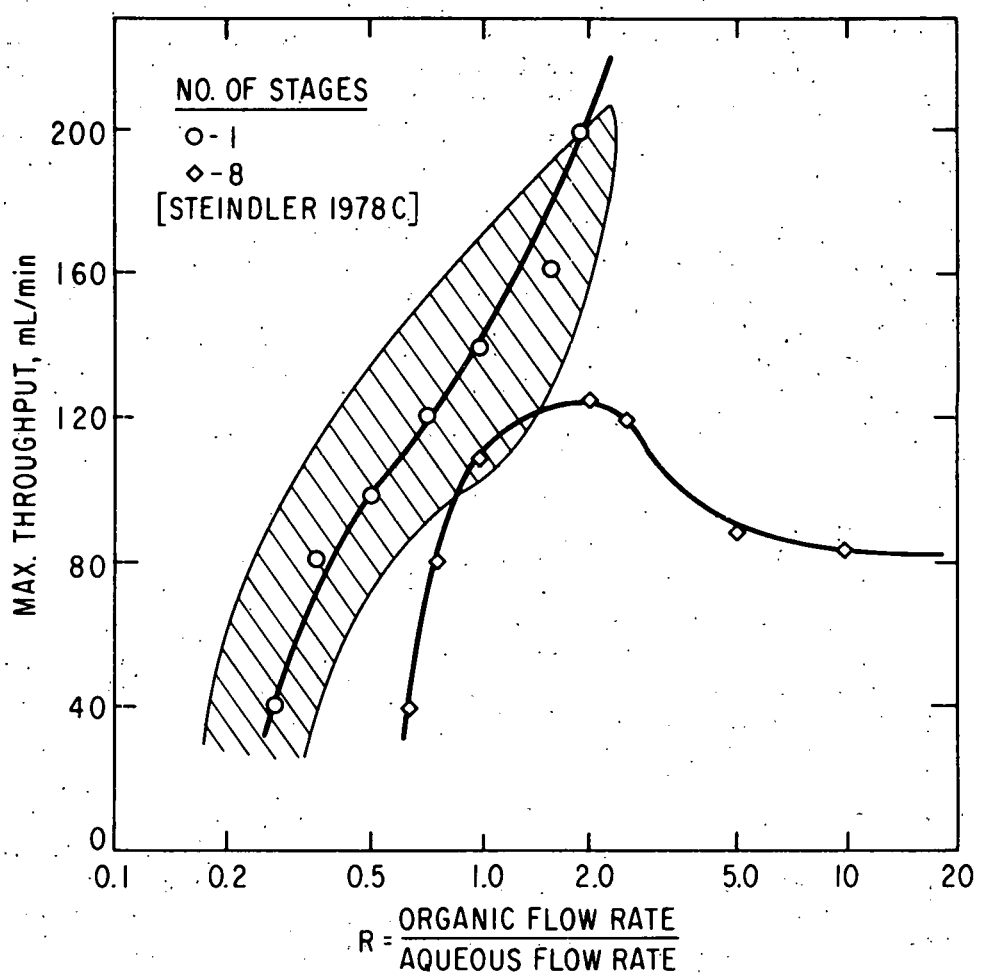

Fig. 2. Effect of O/A Ratio and Number of Stages on Maximum Throughput. Unit: Eight-stage 2-cm Centrifugal Contactor II (disk base). Rotor Speed: 6000 rpm. Aqueous Phase: 3.0M HNO_3. Organic Phase: 30 vol % TBP in nDD. Acceptable Performance: >99% phase separation in both exiting streams

NOTE: Shaded area indicates the range of single-stage results on the eight-stage 2-cm-ID Centrifugal Contactor I [STEINDLER-1977, -1978B].

From these tests, it is concluded that there is little difference in the flow performance of the two eight-stage contactors. The disk base unit will operate at slightly lower O/A ratios; it has its maximum capacity at a slightly higher O/A ratio, and it seems to be slightly more stable in operation. Also, as will be seen below, it has less liquid holdup in the annular mixing zone.

A modified single-stage rotor was built and is ready for testing. It has a diverter baffle in the lower region of the rotor that earlier rotors did not have. It also has a slightly larger aqueous weir ID intended to provide a more nearly equal holdup of aqueous and organic phases within the rotor. Our experience with the 9-cm-ID centrifugal contactor (see "Development of a 0.5 Mg/d Centrifugal Contactor" elsewhere in this report) suggests that this change should give us some increase in maximum throughput.

b. Measurement of Annular Volume

The annular volume is the space between the rotor and the housing that is filled by liquid. It is of special importance because the two phases are mixed and interphase diffusion occurs in this volume. Based upon the annular volume and the throughput, the residence time in this mixing zone can be calculated.

Single-stage tests in the eight-stage contactors were made to measure the annular volume. In such a test, the stage is isolated and fed through capillary tubes to avoid drainage of feed solutions into the stage when the inlet metering pumps are shut off. At the time the inlet pumps are shut off, the rotor motor is shut off and brought to a quick stop with a brake. The total liquid volume is drained from the stage, and the volume of each phase is measured. From this, the amounts calculated to be in the rotor and the drain line are subtracted. The residual volume is the effective volume of the annular mixing zone.

Results of these annular volume measurements are shown in Figs. 3, 4, and 5 as a function of the organic-to-aqueous phase ratio, total throughput, rotor speed, and base type. The annular volume increases as the O/A ratio decreases with both base types. When the annular space is filled with liquid (12.1 mL up to the emulsion breaker ring just below the organic collector ring), some of the mixture overflows into the organic collector ring and contaminates the organic phase effluent stream beyond the maximum allowable 1% aqueous phase in the organic phase. As total throughput increases, the level of the mixture in the annulus rises to provide the added head needed to pump the mixture through the rotor. At a given throughput, as the rotor speed increases, the pumping capacity of the rotor increases, and the additional head required from the liquid in the annulus decreases. However, Contactor I requires a higher annular liquid level than does Contactor II. This may be due to the fact that the vanes allow the development of some centrifugal force in the liquid below the Contactor I rotor, which inhibits flow through the rotor inlet orifice. In Contactor II, the liquid entering the rotor flows beneath the disk and is thereby shielded from the bottom of the spinning rotor.

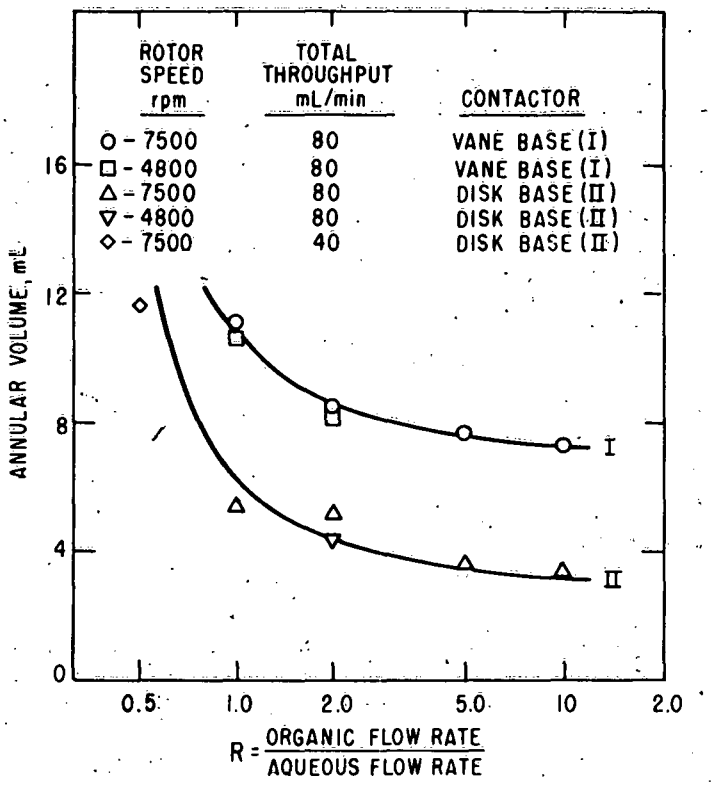

Fig. 3. Effect of O/A Ratio on Annular Volume in the Two Eight-Stage 2-cm-ID Centrifugal Contactors. Aqueous Phase: 3.0M HNO_3. Organic Phase: 30 vol % TBP in nDD. Single-Stage Tests

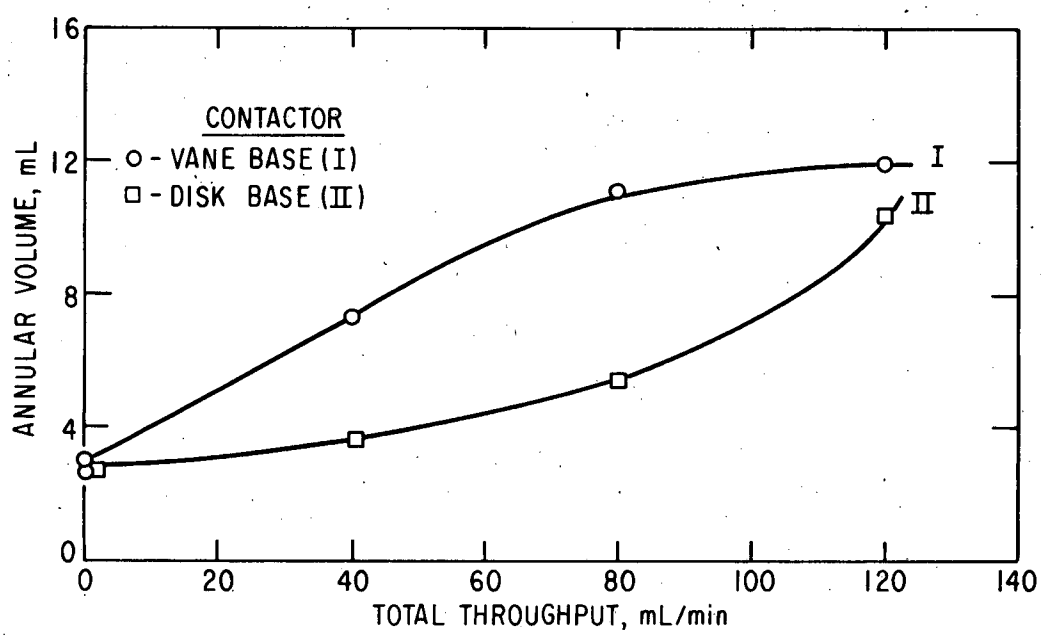

Fig. 4. Effect of Total Throughput on the Annular Volume in Eight-Stage 2-cm-ID Centrifugal Contactors. Aqueous Phase: 3.0M HNO_3. Organic Phase: 30 vol % TBP in nDD. Single-Stage Tests. Rotor Speed: 7500 rpm. Overall O/A Ratio: 1.0

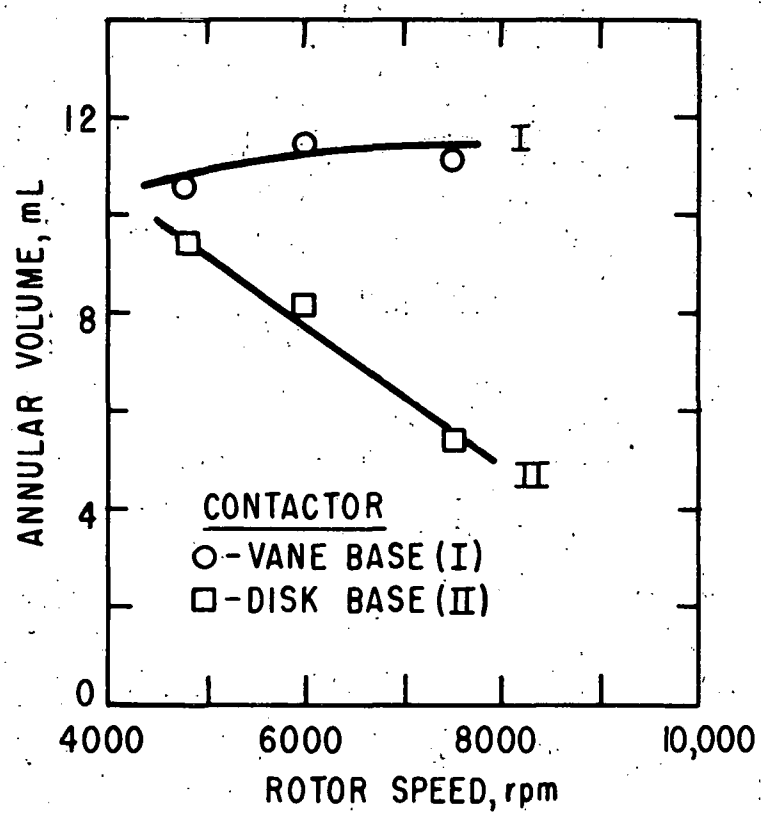

Fig. 5. Effect of Rotor Speed on the Annular Volume in the Eight-Stage 2-cm-ID Centrifugal Contactors. Aqueous Phase: 3.0M HNO_3. Organic Phase: 30 vol % TBP in nDD. Single-Stage Tests. Total Throughput: 80 mL/min. Overall O/A Ratio: 1.0

Measurements of the O/A ratio in the annular volume show it to be significantly lower than the overall O/A ratio as determined by the input flow rates. The effect is more pronounced with the vane base (Contactor I) than with the disk base (Contactor II). This apparent accumulation of aqueous phase in the annular mixing zone suggests that the aqueous phase is being held up below the rotor.

For purposes of estimating the rate of approach to steady state in Contactor II, the total volume of liquid was measured in each stage, including that in the rotor, the annulus, the collecting rings, and the interstage lines. This amounted to about 8 mL of organic phase per stage over a wide range of conditions: 40 to 120 mL/min, 4800 to 7500 rpm, and 1.0 to 10 O/A ratio. Over this same range of operating conditions, the aqueous phase holdup was 8 mL/stage at high O/A ratio or low rotor speed, and holdup increased to 14 mL/stage as O/A ratio decreased and rotor speed increased.

c. Extraction Efficiency Tests

Based on earlier single-stage [STEINDLER-1978B] and multistage [STEINDLER-1978C] extraction efficiency tests, a new set of single-stage uranium extraction efficiency tests were conducted. When analyses of samples from these tests are completed, they should contribute to improved understanding of factors contributing to extraction efficiency in miniature contactors in single-stage and multistage arrays.

Several factors that might affect extraction efficiency were tested. These included variation in annular gap within a single-stage contactor. In addition, individual stages of an eight-stage contactor were tested over a range of total solution throughputs, O/A flow ratios, and rotor speeds. Stripping efficiency tests were made under organic continuous and quasicontinuous aqueous conditions. Finally, to evaluate the relative performance of the vane base and the disk base, all single-stage tests made on the eight-stage unit (Contactor I) were repeated on Contactor II. Stage efficiency calculations will be made when results of stage sample analyses are available.

4. Extraction of Ruthenium and Zirconium in Centrifugal Contactors in the Purex Process
(A. Siczek and J. Meisenhelder)

The study of extraction kinetics of ruthenium and zirconium has been extended to multistage extraction scrubbing runs in the presence of uranium. The objective is to determine whether or not a significant improvement can be achieved in decontamination of uranium and plutonium from ruthenium and zirconium by taking advantage of the lower extraction rates of these fission products. In a short-residence-time contactor, such as a centrifugal contactor, mixing zone residence times of 2 to 4 s per stage can be achieved, as compared with several minutes per stage in pulse columns or mixer-settlers. Previous work with a single-stage annular centrifugal contactor showed that the extraction rates of uranium and of ruthenium and zirconium differed little at residence times of 2 to 7 s and that improvement in decontamination would

be modest. Multistage tests were made to determine whether this modest kinetic effect would be multiplied in a multistage operation and lead to improved decontamination.

a. Extraction/Scrub Tests

Multistage extraction/scrubbing tests were designed to measure the effect of multistage short-residence-time extraction upon the effectiveness of separating uranium from ruthenium and zirconium. They were carried out in an eight-stage miniature centrifugal contactor, with four stages serving as extraction stages and four as scrub stages. The experimental procedure was described in [STEINDLER-1978C]. Flow rates and approximate contact times in the mixing zone are given in Table 2. The analytical results are available only for Test No. 1 and presented in Table 3 as concentrations of uranium, ruthenium, and zirconium in the stage samples. As can be seen here, ruthenium and zirconium behavior was comparable. Extraction into the organic phase was highest in the stages where uranium concentration was lowest. As the uranium concentration in the solvent increased (to about 75% of saturation), the ruthenium and zirconium were largely displaced.

Table 2. Extraction/Scrub Tests in Multistage Centrifugal Contactor. Rotor Speed ∿6800 rpm

Test No.	Flow Rate mL/min			Contact Time, s	
	AF	AS	AX	Extraction	Scrub
1	20	12	56	∿2.0	∿2.5
2	7.5	3.7	20	∿3.5	∿4.0
3	2.9	1.6	7.3	∿11.5	∿9.0

Because ruthenium and zirconium concentrations in the solvent entering the scrub section were low (about 5 µg/mL), it is difficult to evaluate the effectiveness of scrubbing. As shown in Table 3, there was an apparent reduction in ruthenium and zirconium concentrations in the solvent as it moved through the scrub section, but analytical precision at these low concentrations may be inadequate to reveal the precise scrubbing performance. The increase in ruthenium and zirconium concentrations in the aqueous phase as it moved through the scrub section supports the idea that some scrubbing was taking place.

Table 3. Extraction/Scrub Tests of Uranium, Ruthenium, and Zirconium in an Eight-Stage Miniature Contactor

Extraction Section: Stages 1-4
Scrub Section: Stages 5-8
Rotor Speed: ~7000 rpm
The feed stream entered Stage 4, the AX stream entered Stage 1, and the AS stream entered Stage 8

Stream	Flow Rate, mL/min
AF - 1.2M U, 2M HNO_3; 0.02M Ru; 0.02M Zr	20
AX - 30% TBP/nDD	56
AS - 3M HNO_3	12

Stream Leaving Stage	Uranium mg/mL		Ruthenium µg/mL		Zirconium µg/mL		H^+, M
	aqueous	organic	aqueous	organic	aqueous	organic	aqueous
1	1.1	37.4	1334	249[a]	790	23	2.1
2	28.4	88.2	1645	69	813	26	2.8
3	129.6	112.9	1318	5	748	4	2.4
4	157.0	116.1	1245	5	738	5	2.3
5	72.9	112.3	12	5	11	4	2.6
6	51.8	107.3	4	5	7	5	2.7
7	39.0	103.6	<1	5	4	4	2.8
8	23.7	97.6	<1	3	2	2	2.8
Initial (AF)	283.0		2117		1342		2.0

[a]This is an unexpectedly high value which cannot be explained.

The overall distribution coefficients, $D_M = \frac{[M]_{AP}}{[M]_{AW}}$, for both ruthenium and zirconium were about 0.04, and the decontamination factors were as follows:

$$DF_{Ru} = \frac{2.12/283}{3 \times 10^{-3}/97.8} = 244$$

$$DF_{Zr} = \frac{1.34/283}{2 \times 10^{-3}/97.8} = 232$$

These are reasonably good values for the number of stages available.

The uranium loss in the AW stream (1.1 mg U/mL) was approximately equal to the loss calculated from the SEPHIS code using three extraction and three scrub stages. This result indicates that stage efficiency during the test was about 80%.

b. Spiking Test

An extraction/scrub test was made under conditions in which a low-acid feed stream (0.5M HNO_3) was spiked with concentrated nitric acid (8M) just before introduction into the contactor in proportions to give the same composition of AF stream as was used in tests 1, 2, and 3 (shown in Table 3). Spiking had been found to be very beneficial in reducing the extraction of ruthenium species in a test made in a single-stage contactor [STEINDLER-1978C]. The analytical results of this multistage test are pending.

c. Additional Zirconium and Ruthenium Extraction Studies

The effect of the purity of 30% TBP/nDD on zirconium or ruthenium extraction was checked in an experiment in which zirconium (0.01M) solution was mixed vigorously for 5 min with:

(1) organic solvent preequilibrated with HNO_3
(2) organic solvent previously washed with 2.5% Na_2CO_3
(3) untreated organic solvent

The results are given in Table 4. They show that washing TBP/nDD with sodium carbonate did not change the D_{Zr} value , indicating that no di- or monobutyl phosphate was present in the solvents in tests (1) and (2). The value of D_{zr} in test (3) reproduces the values found in earlier runs [STEINDLER-1978C].

Table 4. Effect of TBP/nDD Purity[a] on Zirconium Distribution Coefficients.
Initial Aqueous Solution:
[Zr] = 1.01 g/L;
[Ru] = 1.08 g/L;
[H+] = 2.98M

	Zirconium Concentration, mg/mL		
Test	Organic	Aqueous	D_{Zr}
1	0.093[b]	0.930	0.100
2	0.087	0.916	0.095
3	0.062	0.962	0.064

[a] See the text for identification of solvent condition in each test.

[b] Organic solvent in test 1 contained 0.54M H^+.

Tests were made on zirconium aging in the organic phase and its effect on back extraction, but analytical results are not yet available. Also, infrared studies of zirconium complexes/solvates in the tri-n-butyl phosphate/nDD phase have been started.

Tests have been made of the dependence of ruthenium extraction on nitric acid concentrations in the range 0.1 to 1.0M. Analytical results are not yet available.

5. Processing of Thorium Fuels in a Centrifugal Contactor Using Thorex Processes
(A. Siczek and J. Meisenhelder)

A literature review was conducted to gain familiarity with the various solvent extraction processes that have been identified as "Thorex" processes. On the basis of this review, a general type of Thorex process has been chosen to permit studies of extraction kinetics in single-stage and multistage centrifugal contactors.

Tests to measure the kinetics of thorium extraction with no uranium present and in the presence of uranium were made initially in a single-stage unit. They were followed by Thorex process runs carried out in an eight-stage bank of centrifugal contactors utilizing two different residence times. Partition of uranium and thorium was also tested. The detailed description of the experimental work will be given when analytical results become available.

6. Acknowledgment

The chemical analyses for the Purex and Thorex runs are being made by F. Williams, I. Fox, M. Bouchard, and R. Telford under the direction of K. Jensen of the Analytical Chemistry Group.

B. Aqueous Reprocessing Alternatives to the Thorex Process

(H. Diamond,* C. Sabau,* E. P. Horwitz,* G. Vandegrift,* and G. Mason*

1. Introduction

This program investigates aqueous reprocessing alternatives to the Thorex process. The objectives of the process are to recover the thorium, uranium, and plutonium that will result from the irradiation of mixed thorium-uranium oxide fuel. Uranium-238 is present in the mixed fuel in order to "denature" the ^{233}U. Protactinium will decay 1000-fold during cooling and will not be an important source of ^{233}U. The plutonium, which is produced from the ^{238}U in the fuel, must be recovered along with sufficient contamination so that a heavily shielded facility would be required for processing.

Irradiation of mixed oxides of ^{232}Th, ^{235}U and ^{238}U in a light water reactor and subsequent dissolution will provide a prototype dissolver solution containing 1.5M Th, 0.5M uranium, a small amount of plutonium, 0.5M aluminum, 0.01M zirconium, 0.0005M mercury, 0.05M fluoride (complexed), and 2M HNO_3. A process for thorium, uranium, and plutonium recovery should produce a thorium fraction, a uranium or uranium-plutonium fraction, a secure (i.e., fission product-contaminated and/or diluted) plutonium fraction, and waste streams that are depleted in the heavy elements and are subject to calcining and disposal.

Two extractants are under active consideration: tricaprylmethylamonium nitrate (TCMA) in "Aromatic 100" (AR100) and di-n-amyl-n-amylphosphonate (DA[AP]) in n-dodecane (nDD). Further, bis(2,6-dimethyl-4-heptyl) phosphoric acid, now being studied for other purposes, could lead to an alternative to the Thorex process, but is not considered here.

The previous quarterly report [STEINDLER-1978C] showed that concentrated solutions of TCMA in AR100 can extract large amounts of uranium and thorium without forming a second organic phase. This removes a principal difficulty in the exploitation of TCMA for process chemistry. In the current quarter, the extraction of uranium and uranium-thorium mixtures into TCMA-AR100 at 50°C continues to be studied; the concentration of heavy elements in the organic phase approaches, but does not exceed stoichiometric limits (TCMA:U = 1:1, TCMA:Th = 2:1).

---

*Chemistry Division

We have shown earlier [STEINDLER-1978C] that 2F DA[AP]-nDD extracts thorium and uranium from 2M HNO_3 and that thorium be selectively re-extracted into formic-nitric acid solutions. In this report, individual distributions of HNO_3, HCOOH, uranium, and thorium into 2F DA[AP]-nDD are given for various concentrations, and results of tracer studies of uranium, thorium, and Pu(IV) are reported. Thorium and uranium were extracted into 2F DA[AP]n-DD, and the organic phase was scrubbed with five successive portions of 1M HCOOH, 0.1M HNO_3; the behavior of uranium, thorium, HNO_3, and total acid was traced. A new method of titrating acid in the presence of uranium and thorium is reported.

2. Tricaprylmethylammonium Nitrate (TCMA)

An earlier survey has suggested that uranium and thorium could be extracted by TCMA-AR100 to a greater extent than would be expected from stoichiometric considerations. This has been re-investigated with careful attention to analytical problems. The investigation showed that the amount of heavy elements approaches but does not exceed stoichiometric ratios. The very large concentrations of uranium (0.7M and thorium (0.34M) in the organic phase occur without second organic phase formation, and this mode of extraction remains attractive for decontamination and separations.

a. Experimental--TCMA

The purification of TCMA from "Aliquat-336" was described earlier [STEINDLER 1978C]. The chloride form, TCMA-Cl, is titrated with standard $AgNO_3$, using Ag:AgCl and calomel electrodes to determine the endpoint. The TCMA-Cl is made 0.73M in AR100 (formerly called "Solvesso-100") and is scrubbed with 2M HNO_3 until all of the Cl^- has been removed. Portions of this solvent are equilibrated at 50°C with 2M HNO_3 containing uranium or uranium-thorium mixtures whose concentrations had been determined by titration.

Assays of the separate phases obtained after equilibration were made by gamma-ray counting: ^{235}U has a 185.7-keV gamma ray and ^{230}Th has a 67.8-keV peak. There are some minor problems associated with the gamma counting of ^{235}U and ^{230}Th. The nuclide ^{226}Ra, which can be found in some ^{230}Th tracer, has a 186-keV peak, and Bi K-X rays (of the progeny of ^{228}Th) have a tail that interferes with the 67.8-keV ^{230}Th peak. Standardization of the assay and counting procedures eliminates any important self-absorption error.

The uranium extraction distribution coefficient could also be measured by alpha scintillation counting. There is interference from the beta and gamma activity of ^{234}Th and ^{234}Pa found in equilibrium with ^{238}U, but these can be overwhelmed with sufficient ^{233}U tracer. Alpha-counting allows the easy accumulation of sufficient data to avoid any important statistical errors.

b. Results and Discussion--TCMA

Table 5 and Fig. 6 show the results of both alpha and gamma-counting measurements of the distribution of uranium between 2M HNO_3 and 2F TCMA-AR100 at 50°C. The gamma-counting results are more reliable at higher concentrations of uranium; the alpha-counting results are more precise at lower concentrations.

Table 5. Distribution of Uranium between 2M HNO_3 and 0.73F TCMA-AR100 at 50°C

By Alpha-Counting			By Gamma-Counting			
K_d	U_{org}, mol/L	U_{aq}, mol/L	K_d	U_{org}, mol/L	U_{aq}, mol/L	Disengagement Time,[a] s
2.29	0.707	0.308	2.12	0.692	0.326	129
2.83	0.681	0.241	2.90	0.685	0.236	116
3.52	0.578	0.164	3.67	0.583	0.159	85
4.57	0.293	0.0641	4.84	0.296	0.0611	118
5.44	0.0784	0.0144	4.97	0.0773	0.0155	111
6.17	0.0199	0.00323	7.05	0.0203	0.00287	87
6.41	0.00609	0.00095	6.20	0.00606	0.00098	74

[a]Time between cessation of agitation and appearance of a bubble-free interface upon standing at 50°C.

The limits of extraction by 0.73F TCMA-AR100 were also examined for mixtures of thorium and uranium in 2M HNO_3. Gamma analyses were used to show both the uranium and the thorium peaks simultaneously; the results are reported in Table 6. The right-hand column in Table 6 shows the sum of the uranium concentration plus two times the thorium concentration, corresponding to the extracted species given in the literature: $[R_3(CH_3)N][UO_2(NO_3)_3]$ [KOCH, 1965A], and $[R_3(CH_3)N]_2[Th(NO_3)_6]$ [KOCH-1965B]. The 0.73M limit set by the TCMA concentration is not significantly exceeded by this sum.

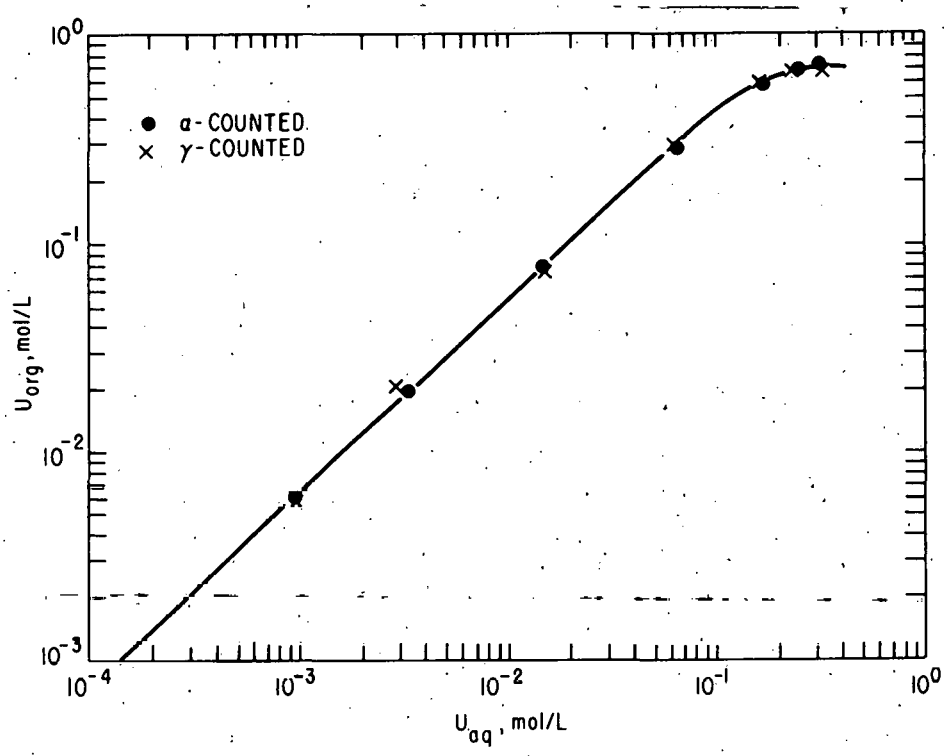

Fig. 6. Equilibrium Distribution of Uranium between 2.0M HNO_3 and 0.73F TCMA-AR100 at 50°C

Table 6. Distribution of Mixtures of Uranium and Thorium between 2.0M HNO_3 and 0.73F TCMA-AR100 at 50°C.

Total mmol Used[a]								
Th	U	K_d(U)	U_{org}, mol/L	U_{aq}, mol/L	K_d(Th)	Th_{org}, mol/L	Th_{aq}, mol/L	TCMA[b] Used, mol/L
0.923	0.299	0.29	0.0288	0.101	3.45	0.343	0.099	0.714
0.831	0.299	0.33	0.0320	0.098	6.94	0.354	0.0510	0.740
0.738	0.391	0.30	0.0387	0.0131	8.78	0.325	0.0370	0.688
0.738	0.207	0.36	0.0241	0.0661	14.1	0.340	0.0242	0.705

[a] 2.4 mL of aqueous were equilibrated with 2.0 mL organic in each case.

[b] Calculated from 2 x $[Th]_{org}$ + $[U]_{org}$ (see text).

3. Di-n-amyl-n-amylphosphonate (DA[AP])

Four types of measurements were made to help design a flow sheet for the extraction of uranium, thorium, and plutonium with DA[AP] from a dissolver solution and subsequent separation of the heavy elements. The distribution of uranium and thorium between 2M HNO_3 and 2F DA[AP]-nDD was measured for various metal concentrations. The distribution coefficients (K_ds) for tracer-level uranium, thorium, and Pu-IV were measured; some of the problems associated with these measurements are discussed. The distribution of uranium, thorium, NO_3^-, and total acid was traced in a scrubbing experiment in which a DA[AP] phase was scrubbed by five successive portions of HCOOH-HNO_3. A new method for determining total acid in the presence of uranium and thorium was developed in this work. The distributions of various concentrations of HCOOH and HNO_3 into 2F DA[AP]-nDD were also measured.

a. Experimental - DA[AP]

(1) Titration of Acids

The distribution of HNO_3 and HCOOH between aqueous solutions and 2F DA[AP]-nDD was measured at room temperature by titrating each phase with NaOH to a phenolphthalein end point.

The titration of acids in the presence of the polyvalent metal ions, uranium and thorium, is more difficult. This is especially true when weak acids are present. One can absorb the uranium and thorium onto a cation column and correct for the two- or fourfold H^+ ion thereby added to the eluate, but this requires highly accurate uranium and thorium assays. Another procedure [BOOMAN] uses $C_2O_4^{2-}$ complexing and a set of bias curves for titrating to an explicit pH, but this method does not work when uranium and thorium are present together, or for weak acids.

One can titrate the acid in the eluate from an anion exchange column that is operated in the presence of alkali metal oxalate and formate. Such a column will remove uranium and thorium and convert stronger acids to equivalent amounts of formic and oxalic acids. A recent paper (QURESHI) has shown that sodium formate solution holds uranium (but not thorium) onto an anion exchange resin and that potassium oxalate solution holds thorium (but uranium much less effectively). The distribution coefficients are not sensitive to the concentrations of the solutions.

In the new procedure, the unknown sample is mixed with an eluant solution of 0.25M $K_2C_2O_4$ and 0.5M NaCOOH. This is passed through a small anion column that has been conditioned with the eluant. The eluant and wash is titrated to a phenolphthalein end-point; further column elution into the colored solution assures that H^+ has been completely removed from the column. Preliminary tests of this method of titration led to agreement with a known sample within the expected 2-3%. More precise confirmations are planned.

Measurement of the total acid content of some (aqueous scrub) solutions was supplemented by measuring the NO_3^- content. Telford* measured this by the Kjeldahl and a colorimetric procedure: all nitrogen was ascribed to nitrate ion.

(2) Loading Uranium and Thorium into DA[AP]-nDD

The distribution of uranium and (separately) thorium between 2M HNO_3 and 2F DA[AP]-nDD was measured for different heavy metal ion concentrations. The DA[AP]-nDD solution was scrubbed with 2M HNO_3 to minimize the effect of HNO_3 extraction on the distribution coefficients. The 2M HNO_3 aqueous phases were prepared from titrated uranium, thorium and HNO_3 solutions; additional ^{230}Th (67.8-keV γ) or ^{235}U (186-keV γ) were added as tracers, and the distribution ratios were measured by the γ-ray procedures described in section B.2.a. above.

(3) Distribution Coefficient Measurements of U(VI), Th(IV), and Pu(IV) Tracers

Tracer solutions of ^{233}U, ^{230}Th and ^{239}Pu were used to assess the K_ds between 2M HNO_3 and 2F DA[AP]-nDD at 50°C; in the case of plutonium in 2M HNO_3, 0.1M $NaNO_2$ was used to preserve the Pu-IV state. Alpha-scintillation counting was used for ^{233}U and ^{239}Pu and γ-counting for ^{230}Th. The aqueous phase first equilibrated with ^{233}U was discarded to remove the small amount of ^{232}U progeny present in that tracer.

Unsuspected plutonium polymer or a small amount of disproportionation of Pu-IV can lead to erroneous K_d results. For confidence that neither of these effects interfered with measurements, a criterion was selected of three successive equilibrations of plutonium-spiked 2F DA[AP]nDD with 2M HNO_3 and 0.1M $NaNO_2$, each yielding a similar K_d. Earlier work (not reported) failed to meet the criterion when 2M HNO_3 but no NO_2^- was used; it is probable that disproportionation of Pu-IV to Pu-III and Pu-VI caused the failure.

Neutral phosphonate esters such as DA[AP] are subject to acid-catalyzed hydrolysis; the phosphonic acid hydrolytic products can then distort K_d measurements. The DA[AP] would be expected to have a very low K_d for Pu-IV in 0.1M HCl. In sharp distinction, the expected hydrolytic product, n-amyl-amylphosphonic acid, would have a very high K_d(Pu-IV) from 0.1M HCl. The plutonium remaining in an organic phase after extensive scrubbing with 0.1M HCl could then be reasonably ascribed to complexing by a hydrolytic product (two organic molecules per plutonium atom).

*Member of Chemical Engineering Division

Portions of the final plutonium-rich organic phases from three separate experiments (duration about four hours each, more than one hour at 50°C) were each scrubbed three times with ten times as much 0.098M HCl. The remaining plutonium concentrations were 1.5×10^{-3}M, 3.9×10^{-4}M, and 1.8×10^{-5}M. Such determination cannot quantify the amyl-amylphosphonic acid concentration, but they indicate its presence, and the order of magnitude concentration of heavy elements necessary to overwhelm any effect of the presence of this hydrolytic product. The uranium and thorium K_d determinations both used such high concentrations (and were completed so rapidly) that little error would be expected. The plutonium result is subject to the qualification that 13% of the plutonium remained in the organic phase following the 0.098M HCl scrubs.

(4) Successive Scrubbing Experiment

An aqueous solution of 2M HNO_3 containing titrated amounts of thorium, uranium, and ^{230}Th and ^{235}U tracers was equilibrated at 50°C with 2F DA[AP]-nDD. This was scrubbed at 50°C with five fresh portions of 1.00M HCOOH, 0.100M HNO_3; the volume of each scrub was equal to that of the organic phase. Aliquots from each phase were withdrawn for γ-ray analyses at each scrub, and the five residual aqueous phases were measured for total acid and for NO_3^-. At no time was there a phase inversion: the aqueous phase was always heavier than the organic phase.

b. Results and Discussion--DA[AP]

(1) Distribution of Acids

Figure 7 shows the concentration of acid in 2F DA[AP]-nDD (ordinate) in equilibrium with an aqueous phase whose concentration is shown on the abscissa. Clearly, the HCOOH is held more strongly by the organic phase than is HNO_3.

Free DA[AP], $(DA[AP]_f)$, is defined as the difference between the total organic phase DA[AP] concentration (2.0M) and the concentration of extracted formic acid. A plot of K_d(HCOOH) vs. $DA[AP]_f$ in Fig. 8 exhibits a reasonably straight line whose slope $\frac{\partial k_d}{\partial (DA[AP]_f)} = 0.91$ can be compared with a slope of about 0.62 obtained by Arsene and Germaine [ARSENE] for the extraction of formic acid into 30% TBP-nDD. Formic acid is extracted by DA[AP] more strongly than by TBP. No simple relationship between $DA[AP]_f$ and K_d was found for HNO_3.

The HNO_3 results in Fig. 7 are similar to but not identical with the results of Siddall [SIDDALL-1959A] for DA[AP] and for other neutral phosphonates. Siddall has also shown a very small temperature dependency for the extraction of HNO_3 into DA[AP] [SIDDALL-1959B].

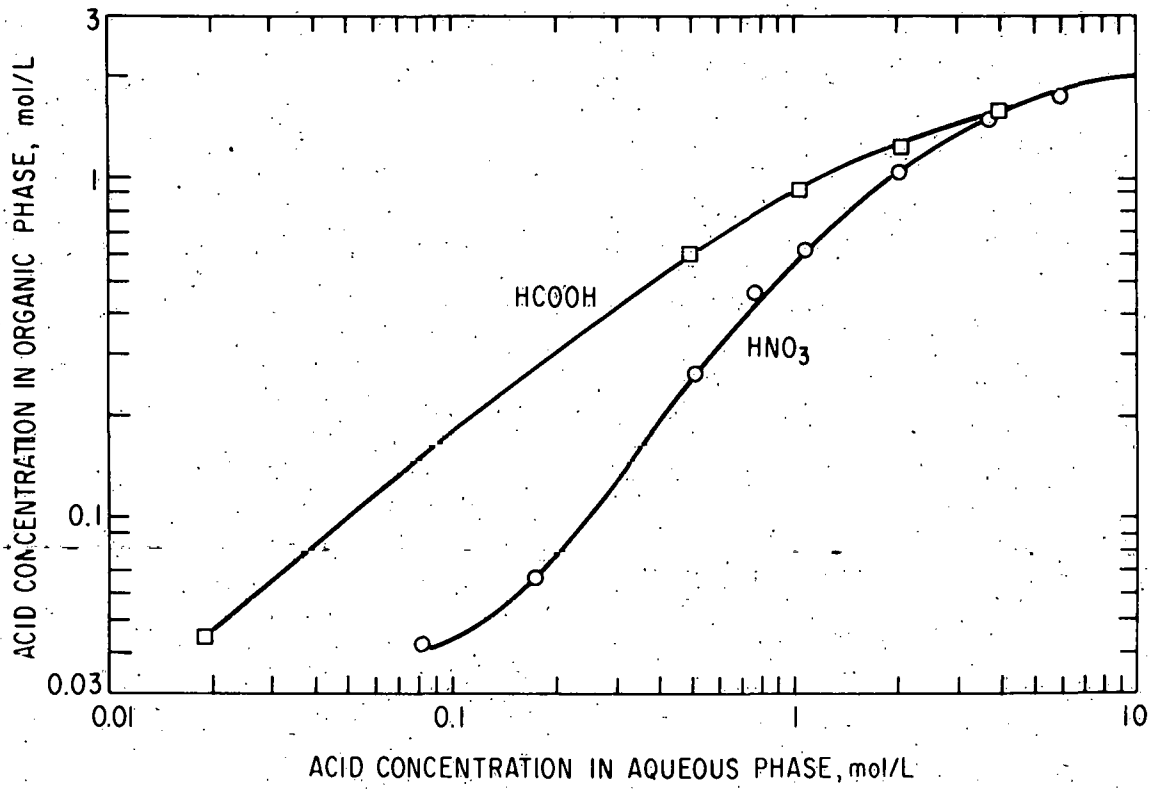

Fig. 7. Distribution of HNO_3 and HCOOH between Water and 2.0F DA[AP] at 23°C

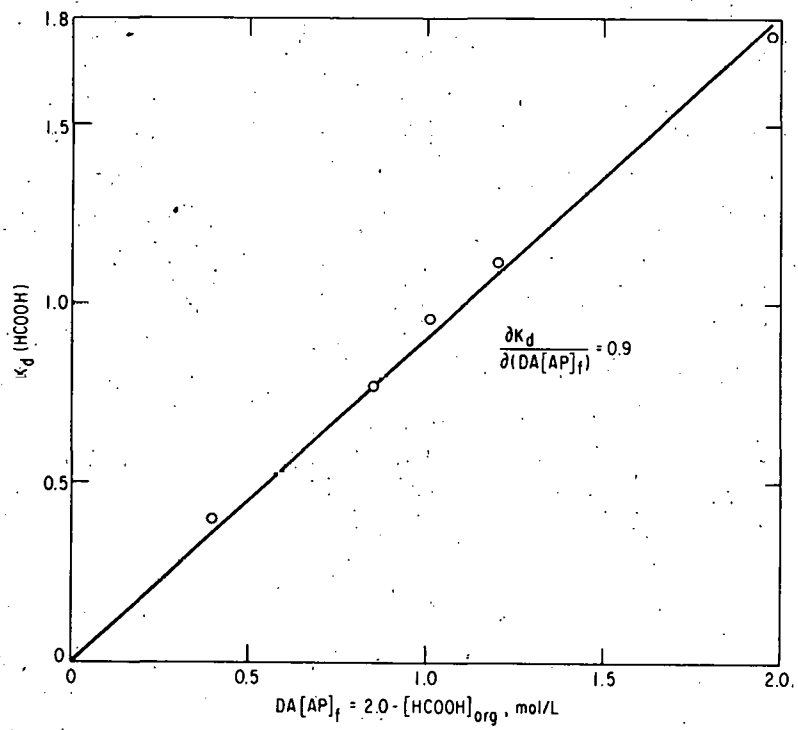

Fig. 8.

Effect of Free DA[AP] Concentration upon Distribution Coefficient of Formic Acid

The individual HNO_3 and HCOOH distribution measurements reported here are not directly applicable to a countercurrent system because of the effect of heavy metals and other acids upon the K_d. Such effects have been studied for TBP systems: Arsene and Germain [ARSENE] found that the K_d(HCOOH) declined only as the HNO_3 concentration reached 1M; McKay et al. [MCKAY] found that the presence of uranium depresses HCOOH extraction.

(2) Loading Curves for Uranium and Thorium in DA[AP]-nDD

The distribution of uranium and (separately) thorium between 2M HNO_3 and 2F DA[AP]-nDD at 50°C was measured for different heavy-metal ion concentrations. These simple systems allow the effect of concentration upon the distribution coefficients to be estimated and thus aid estimation of the extraction of uranium and thorium (and plutonium) from the more complex dissolver solutions. The results are shown in Fig. 9. Thorium saturates 2F DA[AP]-nDD at 0.48M; uranium saturates the organic phase at 0.86M. These values are higher than is attainable with TBP. There is no simple integral number of DA[AP] molecules tied up by each atom of extracted uranium or thorium.

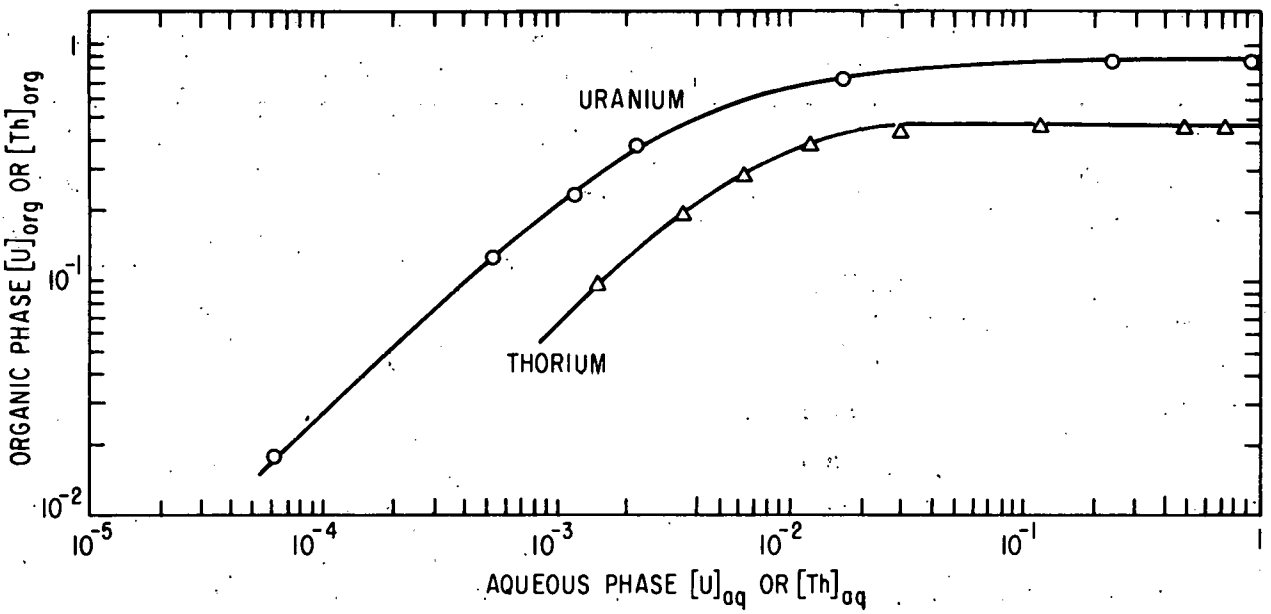

Fig. 9. Distribution of Uranium and Thorium Between 2M HNO_3 and 2F DA[AP]-nDD that had been Equilibrated with 2M HNO_3. Concentrations are in mol/L; all equilibrations were made at 50°C

(3) Distribution Coefficients for Tracer ^{233}U, ^{230}Th, and Pu-IV

Measurement of tracer K_ds for small amounts of ^{233}U, ^{230}Th, and Pu-IV between 2M HNO_3 and 2F DA[AP]-nDD at 50°C required avoidance of the potential errors caused by: disproportionation of Pu-IV, possible existence of Pu-IV polymer, the reduction of available organic DA[AP] concentration because of the extraction of significant amounts of heavy elements, and the formation of n-amyl amylphosphonic acid by the acid-catalyzed hydrolysis of DA[AP]. These problems are addressed in section B.3.a. above.

The results of the measurements are shown in Table 7. The right-hand column in Table 7 presents evaluated K_ds, corrected for the reduction of the concentration of available DA[AP] by the uranium and thorium. The data represented in Fig. 9 were used for this correction. The high K_ds reported here are an attractive feature of DA[AP] extraction.

Table 7. Distribution Coefficients for Small Amounts of Th, U, and Pu-IV between 2M HNO_3 and 2F DA[AP]-nDD at 50°C

Isotopes	Concentration in Organic Phase, mol/L	Forward or Reverse[a]	Counting Method	Measured K_d	Adopted K_d
^{230}Th, ^{232}Th	0.099	F	γ	66 ± 7	72 ± 8
^{233}U, ^{238}U	0.018	F	γ	283 ± 7	285 ± 15
^{233}U, ^{238}U	0.126	F	γ	244 ± 11	
^{233}U	0.006	R	α	252 ± 26	
^{239}Pu[c]	0.0005	F	α	333[b]	
^{239}Pu[c]	0.0005	R_1	α	343[b]	335b
^{239}Pu[c]	0.0005	R_2	α	334[b]	
^{239}Pu[c]	0.0005	R_3	α	333[b]	

[a]Forward direction is defined as the tracer moving from aqueous to the organic phase. Multiple success reverse strikes are labled R_1, R_2, R_3.

[b]No allowance is made for the 13% of the activity remaining in the organic phase upon scrubbing with HCl.

[c]The aqueous phase was 2M HNO_3, 0.1M $NaNO_2$.

(4) Successive Scrubbing Experiment

An organic phase, rich in uranium and thorium, was scrubbed five times with a formic-nitric acid mixture. The course of uranium, thorium, NO_3^-, and total acid was followed. The results give some insight into the competition of the various species for extraction sites in the organic phase.

A solution (1.64 mL) of 2.95M HNO_3, 0.913M Th and 0.32M U was equilibrated with 3 mL 2F DA[AP]-nDD at 50°C. The results are listed (scrub No. 0) in Table 8 along with those of five equal-volume 1.00M HCOOH, 0.100M HNO_3 scrubs.

Table 8. Concentrations of Uranium, Thorium, and Acid in Organic and Acidic Phases after Scrubbing[a]

	Scrub No.					
	0	1	2	3	4	5
$[U]_{org}$	0.148	0.1415	0.134	0.127	0.116	0.1019
$[U]_{aq}$	0.0497	0.0065	0.0073	0.0073	0.0113	0.0137
$K_d(U)$	2.98	21.9	18.4	17.3	10.3	7.45
$[Th]_{org}$	0.410	0.265	0.148	0.0646	0.0232	0.0052
$[Th]_{aq}$	0.164	0.145	0.117	0.0839	0.0413	0.0180
$K_d(Th)$	2.51	1.83	1.27	0.769	0.563	0.29
$\alpha = K_d(U)/K_d(Th)$	1.19	12.0	14.5	22.5	18.2	25.5
$[Total\ acid]_{aq}$		1.15	1.04	1.00	1.02	--
$[NO_3^-]_{aq}$	3.52	0.90	0.58	0.41	0.31	0.22

[a] An organic phase was formed (Scrub No. 0) by extracting into 2.0F DA[AP]-nDD from an aqueous phase containing titrated amounts of HNO_3, thorium, and uranium. Each n-numbered scrub was obtained by equilibrating the (n - 1)th organic phase with an equal volume of fresh 1.00M HCOOH, 0.100M HNO_3 at 50°C. Concentrations are in mol/L.

Very little acid was transferred to the scrubs by the organic phase; initially, the extraction sites were occupied by uranium and thorium, and as these elements passed into the aqueous phase, acid molecules went into the organic phase. There appears to be extensive transfer of NO_3^- to the aqueous phase. This must occur from the transfer of salts [$Th(NO_3)_4$, $UO_2(NO_3)_2$] and from the displacement of HNO_3 in the organic phase by HCOOH.

Although the total acid concentration and the α [$=K_d(U)/K_d(Th)$] approach steady values, the distribution coefficients for uranium and thorium are higher than expected and were still declining at Scrub No. 5. Study of pure formic acid systems is indicated.

C. Developments for Reprocessing of Fast Breeder Reactor Fuel

1. Introduction

Work is continuing in the program to develop improved solvent extraction techniques for Purex reprocessing of fast breeder reactor (FBR) fuels. This program is being carried out in cooperation with Oak Ridge National Laboratory (ORNL). The main objectives of the ANL program are: (1) design, construction, and testing of an annular centrifugal contactor to reprocess FBR fuel at a rate of 0.5 Mg/day in a unit that is critically safe for high plutonium concentrations; (2) adaptation of a Purex flow sheet for use in short-residence-time centrifugal contactors; and (3) a study of solvent cleanup techniques which may involve the use of short-residence-time contactors aimed at improving the cleanup process and reducing the impact of solvent cleanup upon waste handling.

2. Development of an 0.5 Mg/d Centrifugal Contactor

(R. A. Leonard, R. H. Pelto, A. A. Ziegler, J. L. Murdock,* J. L. Stassin,† and G. J. Bernstein)

Hydraulic testing of the 9-cm-ID (0.5 Mg/d) annular centrifugal contactor described in the previous quarterly report [STEINDLER-1978C] is continuing. Changes have been made to the rotor and the housing to improve flow performance. Initial continuous-phase measurements have been made.

a. Capacity Testing

A horizontal disk was installed in the rotor just above the inlet orifice. Such a disk was used in earlier designs but had been eliminated in the design of the present unit in order to simplify construction. Results of hydraulic testing of the contactor indicated that a diverter disk would be useful in causing the organic phase to be subjected to higher centrifugal force and would thereby improve phase separation. Tests were made to measure separating capacity over a range of O/A flow ratios. The results (Fig. 10) are compared with data obtained before the disk was installed. For O/A ratios greater than 0.2, a 30 to 40% increase in the maximum throughput was measured. At lower O/A ratios, the increase in maximum throughput was

---

*Student Aide.

†Undergraduate Research Participant.

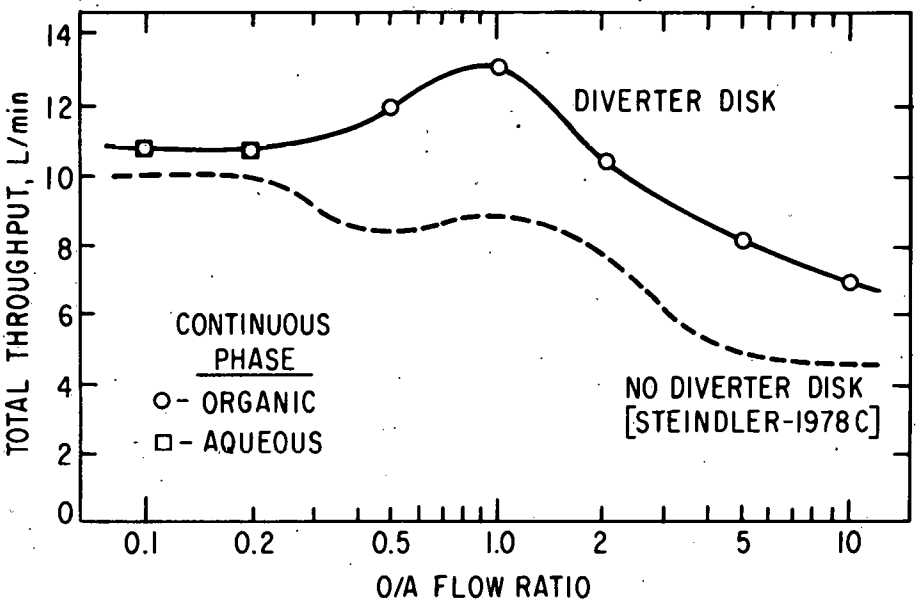

Fig. 10. Effect of Rotor Diverter Disk on 9-cm-ID Centrifugal Contactor Performance. Aqueous Phase: 0.5M HNO_3. Organic Phase: 30 vol % TBP in nDD. Rotor Speed: 1765 rpm. Acceptance Criteria: <1% entrainment and inlet head below the organic exit port

10% or less. At O/A ratios above 0.2, total acceptable capacity is based upon the capability of the rotor to separate the mixed phases. As anticipated, the diverter disk improves the contactor capacity. At O/A ratios of 0.2 and lower, the capacity would not be limited by phase separation but by a rise of liquid in the organic phase inlet line to the point where it would be above the level of the organic phase exit port in an adjacent contactor. It is assumed that in an array of contactors, such a rise would cause backup of organic phase in the collecting ring of the adjacent contactor, possibly leading to flooding. Accordingly, this criterion is used to determine maximum acceptable hydraulic capacity.

It is assumed that the rise of organic phase in its inlet line when the O/A was 0.2 or lower was due to the emulsion in the annular mixing zone then being aqueous continuous and due to greater organic phase inlet pressure being required to force the stream into the emulsion.* To reduce this problem, new inlet lines were installed in the contactor housing

*The same phenomenon applies at high O/A ratios when the mixture is organic continuous. There is some rise in the level of aqueous phase in its inlet line; however, the greater density of the aqueous phase and the higher elevation of the aqueous exit port prevent backup to the level of the port.

at an elevation that would put them above the normal operating level of emulsion in the annulus. In order to simplify fabrication, these lines were connected perpendicular to the housing rather than tangentially (as were the original lines).

Tests of separating capacity with the new inlet lines showed a 25% increase when the O/A ratio was 0.2 or less. At higher O/A ratios, separating capacity was unchanged (see Fig. 11).

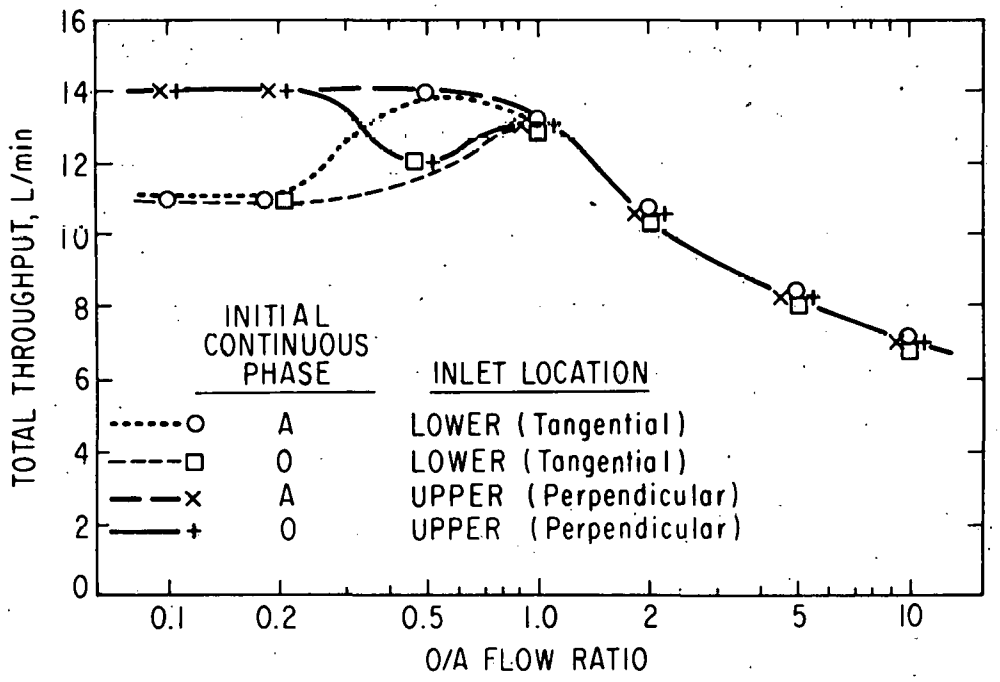

Fig. 11. Effect of Inlet Location and Initial Continuous Phase on 9-cm-ID Contactor Throughput. Rotor with diverter disk. Aqueous Phase: 0.5M HNO_3. Organic Phase: 30 vol % TBP in nDD. Rotor Speed: 1765 rpm. Acceptance Criteria: <1% Entrainment and inlet head below the organic exit port

b. Flow Upsets

A set of tests was performed to evaluate the capability of the contactor to re-establish stable hydraulic performance following a deliberate upset in flow conditions. As an extreme upset in flow conditions, the flow of one phase to the contactor was cut off entirely until the other phase became the continuous phase in the annular region, after which normal flows were restored. This was done for each test condition presented in Fig. 11. For O/A ratios of 1.0 or higher and 0.2 or lower, performance returned to the previous steady state condition regardless of which phase was made continuous by the flow upset. At an O/A ratio of 0.5, separation capacities measured

from initially aqueous-continuous conditions were significantly higher than those measured from initially organic-continuous conditions. Inasmuch as high O/A ratios favor organic-continuous emulsions and low O/A ratios favor aqueous-continuous emulsions, this suggests that the mixture is organic-continuous at an O/A ratio of 1.0 or above and is aqueous-continuous at an O/A ratio of 0.2 or below. Around an O/A ratio of 0.5, the emulsion in the mixing zone is metastable and can be either organic-continuous or aqueous-continuous, depending upon the startup or flow upset conditions. In all cases, the contactor recovered quickly from flow upsets.

c. Annular Region Conditions

Two annular probe ports have been added to the bottom of the contactor housing. These ports permit capillary tubes to be inserted into the annular mixing zone. These tubes can be used to verify which phase is the continuous phase during the flow upset tests. In addition, it was established that the O/A ratio in the annulus was 1 when the input flow O/A ratio was 1.

3. Solvent Cleanup
(B. B. Saunders and J. H. Meisenhelder)

A major product of solvent damage due to both hydrolysis and radiolysis of the solvent [30% tri-n-butyl phosphate (TBP) and 70% n-dodecane (nDD)] used in the Purex and Thorex processes is di-n-butyl phosphoric acid (HDBP). This acid forms strong complexes with zirconium, thorium, plutonium, and uranium which are somewhat soluble in the organic phase and are responsible for metal retention, product contamination, and further solvent degradation.

The HDBP complexes of zirconium (Zr-DBP) are believed to be at least partly responsible for the formation of solids at the organic-aqueous interfaces in the Purex process. If these Zr-DBP complexes can be broken apart by complexing ligands which form water-soluble, nonextractable zirconium complexes, the zirconium will be scrubbed out of the organic phase. Ideally, the complexing ligand should not contain any alkali or alkaline earth ions which might complicate the subsequent handling of the waste stream. If an organic acid such as citric acid is used, the citric acid replaces HDBP in the organic phase and thus effectively scrubs out the HDBP which has been freed from the Zr-DBP complexes. Previously [STEINDLER-1978A], tracer amounts of ^{95}Zr in the presence of macro amounts were used, and it was found that after one-minute stirring with an equal volume of 1M citric acid, 95% of the zirconium was removed from HDBP in 30% TBP/70% nDD. However, it was not determined whether stirring with citric acid would be effective in the short residence times expected for centrifugal contactors.

The preliminary results of two sets of experiments are reported. Both experiments were designed to ascertain the effectiveness of various scrubs used to remove zirconium from solutions of 10^{-3}M di-n-butyl phosphoric acid (HDBP) in 30% tri-n-butyl phosphate (TBP) and 70% n-dodecane (nDD). Both experiments were performed using a single-stage mini centrifugal contactor operated at 7000 rpm and total flow rates of 5 mL/min to 20 mL/min (approximate contactor residence times of 14 to 4 s in the mixing zone).

In both sets of experiments, a zirconium-laden organic solution was prepared by stirring 0.01M $Zr(NO_3)_4$ solution in 3M HNO_3 with twice the volume of 10^{-3}M HDBP in 30% TBP/70% n-DD for 1 h at 60°C. The two layers were separated, and the organic layer was used in the experiments. The zirconium organic solutions were prepared 24 h before the scrubbing experiments. The HDBP was prepared from an Eastman reagent grade mixture of 55% HDBP and 45% monobutyl phosphoric acid (H_2MBP) by dissolving the mixture in ether, washing the ether with distilled water to remove the H_2MBP, and evaporating the ether. The HDBP was then reacted with a solution of sodium carbonate until all of the HDBP was in solution. This aqueous solution was then washed with ether to remove butyl alcohols, reacidified with HNO_3, and extracted into ether. The ether was washed with distilled water and then evaporated to produce the purified HDBP.

The zirconium-laden organic phase contained both Zr-DBP and Zr-TBP complexes. The Zr-TBP complexes can be removed by scrubbing with 0.01M HNO_3. The first experiment was designed to investigate the removal of zirconium from the organic phase with both Zr-DBP and Zr-TBP expected to be present. In the second set of experiments, the organic phase was first washed with an equal volume of 0.01M HNO_3 to remove the Zr-TBP complexes so that the behavior of Zr-DBP alone could be studied.

In the first set of experiments, the unwashed zirconium-laden organic phase was divided into four parts. The individual parts were each contacted with an equal volume of scrubbing solution in the mini-centrifugal contactor at flow rates that resulted in 4 s residence time in the mixing zone. The four scrubs used were: distilled H_2O, 0.01M HNO_3, 1M citric acid, and 2.5% Na_2CO_3. This is outlined schematically in Fig. 12. Samples of the initial solution and of each scrub and organic phase that had passed through the contactor were sent to the Analytical Chemistry group. (The analyses will be described and discussed in more detail below.) The results indicate that both water and 0.01M HNO_3 removed some of the zirconium, but that 1M citric acid and 2.5% Na_2CO_3 removed much more of the zirconium. Citric acid appeared to remove all of the zirconium (1 µg/mL is the approximate limit of detectability for the analytical technique used).

In the second set of experiments, the zirconium-laden organic solution was stirred with an equal volume of 0.01M HNO_3 for 5 min and the two phases were then separated. This washed organic solution was then divided into 15 parts. Sets of three parts were scrubbed respectively with five different solutions in the contactor at three different residence times. The five scrub solutions were: distilled H_2O, 0.01M nitric acid, 1M citric acid, 0.007M nitrilotriacetic acid (NTA), and 2.5% Na_2CO_3. The three residence times studied were 5, 7, and 12 s. Twelve seconds was approximately the longest practical residence time available in the contactor. The experiments and their results are outlined schematically in Fig. 13.

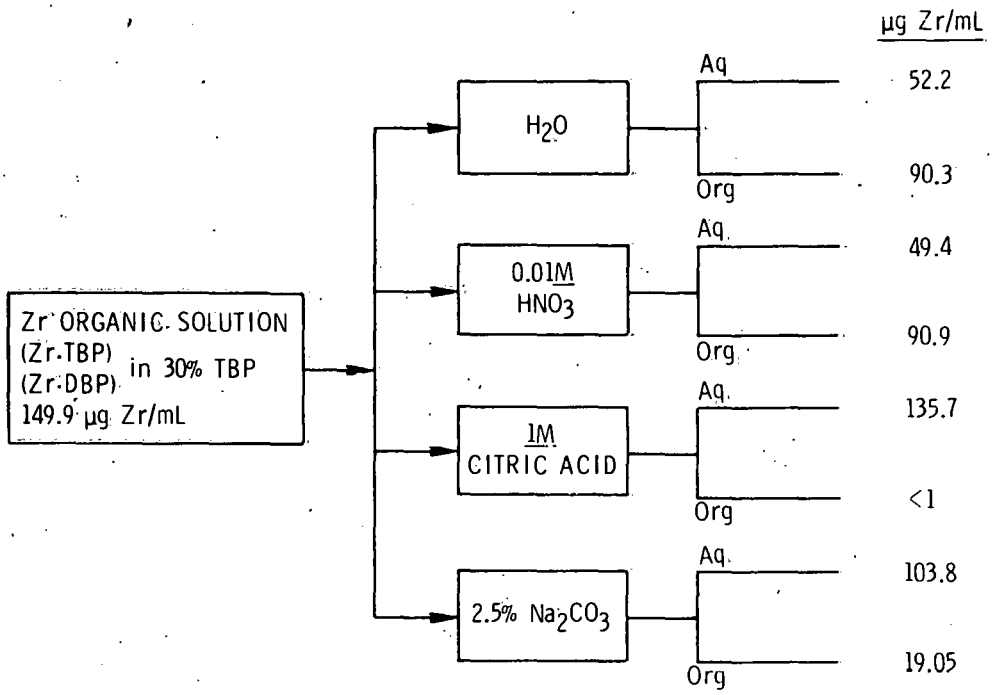

Fig. 12. Contactor Scrubs of Zirconium-Laden Solution of HDBP in 30% TBP/70% nDD

In general, the separations achieved by the contactor were very good. However, in the second set of experiments, the scrubs done with 0.01M HNO_3 produced a cloudy organic layer which formed a small amount of white precipitate after standing overnight. The sodium carbonate scrubs in the second set of experiments produced very cloudy organic solutions, and for the 7 s and 14 s residence times, the organic layers formed a slightly yellow-brown emulsion after standing overnight.

It is obvious from the results (especially the results of the second set of experiments) that the material balances appear to be very poor. The difficulty may lie in the analytical techniques used rather than in the contactor experiments themselves. Flow rates of process solutions to the contactor could be controlled within ±4% at 10 mL/min. The analytical method used by the Analytical Chemistry Group relies upon the colorimetric analyses of HDBP complexes of zirconium. However, the presence of HDBP and the complexing agents that were used to scrub zirconium out of its HDBP complexes can introduce inaccuracies in both aqueous and organic samples. Additionally, zirconium solutions are known to form polymers upon standing, especially at low-acid conditions, when HDBP and TBP are present. These polymers, if not broken down during the analytical procedure, can also add to the inaccuracies of the results. (New analyses of the old samples by neutron activation will be performed by the Analytical Chemistry Group.)

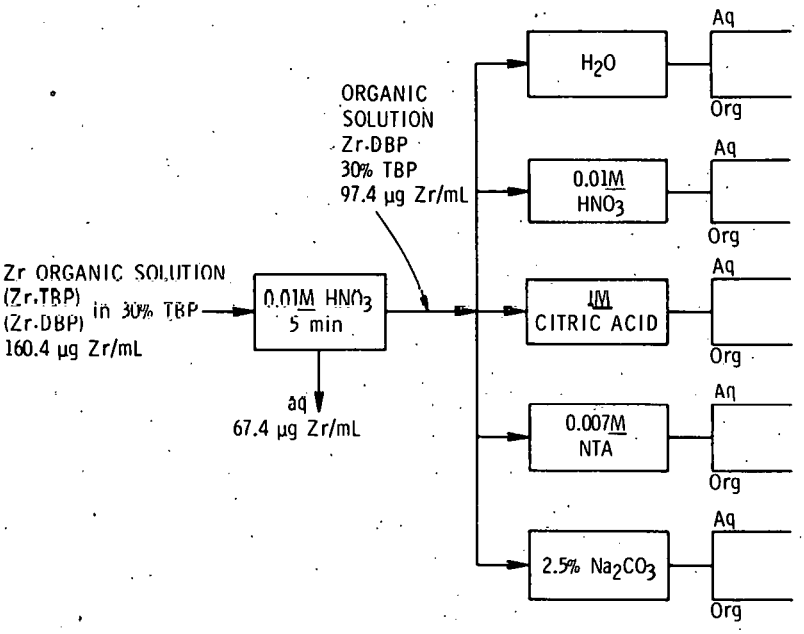

µg Zr/mL		
5.5 s Residence Time	7 s Residence Time	12-14 s Residence Time
2.7	3.2 (2.8)*	4.1
102.5	(96.0)*	96.1
15.6	20.2	27.7
4.7	26.3	8.9
78.8	90.5	72.9
<1**	1.3	1.7
30.1	38.4	36.8
17.4	15.4	33.6
103.6	105.7	90.9
2.9	1.8	1.3

*In these experiments, we used twice the volume of water to organic.
**The approximate limit of detection.

Fig. 13. Results of the Contactor Scrubs of a Washed Zirconium-Laden Solution of HDBP in 30% TBP-70% nDD

The uncertainties and inaccuracies of the available analytical results preclude any quantitative evaluation of the effect of scrubbing on Zr-DBP complexes. Hwever, several judgments can be made: Water and dilute nitric acid were not effective in removing zirconium from the Zr-DBP solution; and sodium carbonate solution appears quite effective in removing zirconium--even from Zr-DBP solutions.

Other experiments have been performed to study the effect of the presence of Zr(IV) on the hydrolysis rate of TBP and HDBP. Analytical results of these experiments are not yet available.

II. ENVIRONMENTAL EFFECTS (ACCIDENT ANALYSIS METHODOLOGY FOR FUEL REPROCESSING PLANTS)

(W. B. Seefeldt and W. J. Mecham)

A. Background and Overview

The purpose of this program is to develop a systematic and coherent body of knowledge as a basis for predicting accident consequences in LWR fuel-reprocessing facilities, for estimating source terms of radioactive releases, and generally for assembling information useful for developing means of further reducing the consequences of accidents, if such be needed. The objectives and scope encompass (1) determination of source terms for postulated accidents in reprocessing plants, including the physical and chemical properties of airborne materials in primary dispersion mechanisms; (2) identification of property modifications of airborne materials under the conditions of transport to the first stage of an air-cleaning system; (3) estimation of the quantitative penetration of radionuclides through the confinement and air-cleaning systems; and (4) identification of properties of airborne products of accidents as released into the atmosphere at the stack or into the environment at the boundary of the plant.

The principal types of accidents identified for study are explosions, fires, and criticality events. Explosions were given initial emphasis because of the relative difficulty of obtaining results in this area consistent with program objectives.

In the previous quarterly report [STEINDLER-1978C], an analysis was made of reported test data in the explosive dispersion (for military purposes) of an organic liquid by high explosives. From the analysis the maximum mass of airborne liquid as a function of the energy of the explosion was calculated. The analysis assumed a lognormal particle size distribution for the calculation of the mass of any size fraction. The analysis is summarized in Fig. 14.

The maximum amounts of liquid and energy in the tests were estimated from the dimensions of the "bomblets," which each consisted of an inner sphere of explosive (maximum 5-cm or 2-in. diameter) surrounded by liquid which was confined by the outer spherical casing (maximum 10-cm or 4-in. diameter). The explosives had detonation energies of 0.78 to 1.36 kcal/g, the mass ratios of liquid to explosive were in the range of 0.4 to 10.

The liquid was bis (2-ethylhexyl)hydrogen phosphite, $(C_8H_{17})_2HPO_3$, described as nonvolatile (at ambient temperature) and having a density of 0.92 g/cm^3. Although exact properties are not available, a compound of this type would be expected to have a viscosity slightly greater than that of water, a surface tension somewhat less than that of water, and a boiling point of about 250°C. It would be subject to thermal decomposition above 400°C. As described in the preceding quarterly report [STEINDLER-1978C], the tests showed tht the fraction of respirable particles (<10 μm) increased from about 1% to a maximum of about 50% as the ratio of energy to liquid increased from about 60 cal/g to 400 cal/g. At energy ratios higher than 400 cal/g, the <10 μm fraction decreased, reportedly because of decomposition of the organic liquid.

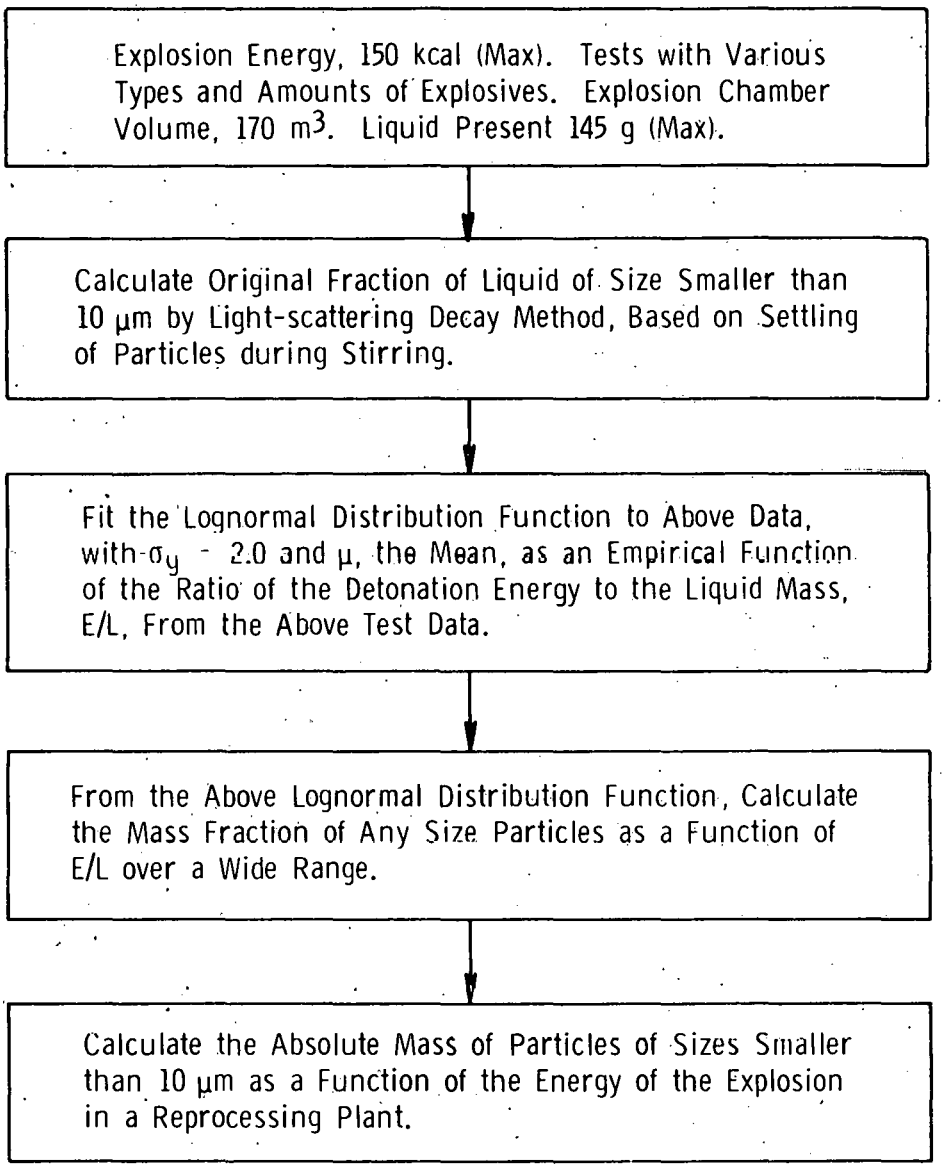

Fig. 14. Steps in the Analysis of Test Data for Explosive Dissemination of Liquid

In the above determination of the small-size fraction of particles, a light-scattering method was used for determining particle concentration in the test volume over a period of time after the explosion [DIMMICK]. This method uses gentle stirring with a fan to keep the concentration homogeneous; simultaneously, particle settling takes place according to the Stoke's velocity, which is proportional to the square of the particle diameter. The result is that the concentration of airborne particles of a given size "decays" exponentially with time. This allows the particle size at time zero to be estimated by calibration or calculation.

Particles suspended in air in a chamber of fixed volume V_o will tend to settle downward at the Stoke's velocity $U_s = \frac{g\ \rho D^2}{18\ \mu}$ where g is the gravitational constant, μ is the viscosity of air in mass units, ρ is the density of the particle, and D is the diameter of the (spherical) particle. The settling velocity is thus directly proportional to the square of the particle diameter. If C is the (homogeneous) concentration of particles in the chamber, C is a function of time t, and $-\frac{d\ln C}{dt} = \frac{U_s}{H_o} = \frac{g\rho}{18\mu}\ \frac{D^2}{H_o}$, where Ho is the vertical dimension of V_o. Thus, $C = C_o \exp -\frac{g\rho D^2 t}{18\mu H_o}$ and the fraction (C/C_o) of material remaining airborne at time t is an exponential decay function of t with D^2 as a factor in the exponential rate constant. (The above analysis pertains only to particles of one size, but it may be generalized for a range of particle sizes using the method employed in analyzing the radioactive decay of a mixture of radioactive species. More important, however, agglomeration and inertial impaction effects in the stirred settling chamber must be considered.)

In the present report period, further consideration was given to this analysis of explosive dispersion of liquid in relation to conditions applicable to reprocessing plant accidents. In particular, an alternative size-distribution function, possibly more appropriate, was compared with the log-normal distribution function used previously as described in Fig. 14.

Also reviewed were some basic mechanisms for subdividing liquids and solids and for dispersing the resulting particles sufficiently to have a practical degree of stability in air transport. The energies required for these mechanisms were calculated as a function of particle size for future comparison with conditions in tests or in plant accidents.

A preliminary review of test data and basic mechanisms relevant to fires is also reported here. Test data on entrainment of process material in fires and application to fabrication plant accidents by the Pacific Northwest Laboratory was summarized. Basic conditions and mechanisms pertaining to reprocessing plants were also examined, including the calculation of forces determining particle entrainment as a function of particle size.

B. Estimation of Amounts of Small Particles Under Plant Accident Conditions

In the preceding quarterly report [STEINDLER-1978C], the amounts of small particles from a given explosion energy were derived from test data for ratios of detonation energy to liquid mass in the range of about 600 to about 120 cal/g. As the energy to mass ratio decreases, the mass median particle diameter increases, as indicated in the correlation of test data using the lognormal distribution described previously. When the energy to mass ratio falls to about 10 cal/g liquid, the mass median is estimated to be about 200 μm. In a postulated reprocessing plant accident, the energy ratio would be less than 10 cal/g liquid, which indicates that the mass median size would be much larger than at the test conditions; the particle size of major interest would remain small ($D < 10$ μm). Thus, the accuracy of the distribution function (particularly the value of the standard deviation, σ) is important since estimates for reprocessing plant accidents are extrapolated by use of this distribution function.

The lognormal distribution has been found to describe most particle-size distributions, and most observed values of σ_g are in the range of 1.6 to 3.0. For a given value of σ_g, the fraction of particles with diameters smaller than a given diameter D can be determined from the cumulative particle size distribution by first calculating the number of standard deviations from the median diameter D_M to (1) to the given diameter as follows:

$$\text{number of standard deviations} = \frac{\ln\left(\frac{D}{D_M}\right)}{\ln \sigma_g} \qquad (1)$$

For example, for D_M = 256 μm and σ_g = 2.0, a particle of 1μm is eight standard deviations from the median diameter, and the cumulative fraction (of particle number or mass) for all particles smaller than 1μm is 6.3×10^{-16}, a number that is very difficult to verify experimentally. This extrapolation of eight standard deviations from the lognormal median, predicts a very small quantity of airborne material of an inhalable size. This may need further confirmation, a point that is further discussed later in this section.

A property of the lognormal distribution is that the frequency of the particle mass (and number) approaches zero as the diameter is reduced without limit. Although this behavior is generally well confirmed in nature (mainly because of the high agglomeration rate of very small particles), the absence of supporting evidence for the extrapolation from the median (as described above) suggests the use of an alternative size distribution function which does not have the property of reducing the particle frequency for small particles to zero. Such an alternative distribution function may be considered to offer "an assured upper limit" to the small-size fraction and therefore may seem less in need of direct supporting data than the estimate based on the lognormal function.

The alternative distribution function proposed is here termed the semi-log distribution. It has been used for some comminution products and can match the lognormal function quite well for mass distributions within three standard deviations of the median on the smaller particle size side. (There is a match only with the mass distribution, not for the particle number distribution.)

1. Semilog Distribution

The semilog distribution (based on particle number) is described as follows:

$$\frac{dN}{dD} = Ke^{-mD} \qquad (2)$$

where N = number of particles

D = particle diameter

dN = number of particles in the size interval, D to D plus dD

m, K = constants

Thus, the characteristic of this distribution is that the number of particles as a function of diameter increases as D becomes smaller and does not approach zero (as does the particle number in the lognormal distribution).

However, the semilog distribution of mass as a function of diameter does approach zero as the diameter is reduced without limit. The semilog distribution of mass is the practical case and one for which the semilog can be considered an alternative to the lognormal distribution.

When Eq. 2 is converted to volume (which is proportional to mass), one obtains

$$\frac{dV}{dD} = \frac{\pi K}{6} D^3 e_{-mD} \tag{3}$$

By integrating Eq. 3 for diameters between 0 and ∞, the total volume of the particles is obtained.

$$V_T = \frac{K\pi}{m^4} \tag{4}$$

Dividing Eq. 3 by Eq. 4, one obtains

$$\frac{dV/V_T}{dD} = \frac{dF}{dD}$$

$$= \frac{\pi K\ D^3\ e^{-mD}}{6} \cdot \frac{m^4}{K\pi}$$

$$= \frac{m^4 D^3\ e^{-mD}}{6} \tag{5}$$

where $F = \frac{dV}{V_T}$ = fraction of total volume in the interval, D to D plus dD

Converting Eq. 5 to a semilog form compatible with that used for the lognormal distribution, we obtain

$$\frac{dF}{d(\ln D)} = \frac{(mD)^4 e^{-mD}}{6} \tag{6}$$

The equivalent expression for the lognormal distribution is

$$\frac{dF}{d(\ln D)} = \frac{1}{\ln \sigma_g \sqrt{2\pi}} \exp - \left[\frac{1}{2} \frac{(\ln D - \ln \overline{D})^2}{\ln \sigma_g} \right] \tag{7}$$

2. Cumulative Fraction of Mass for Particles of Size Smaller than Diameter D

Cumulative fractions of airborne material for diameters smaller than the mode, as calculated from the lognormal and semilog distributions, are compared in Table 9. The cumulative fractions for the two functions were calculated by integrating Eqs. 6 and 7 after the parameters (σ_g, $\bar{D}$, and m) were evaluated for the given value of the mode (256 μm).

Table 9. Comparison of Cumulative Fractions of the Mass of Airborne Material for Lognormal and Semilog Size Distributions. Reference: Modes for both distributions are assumed to be 256 μm.

Upper-Limit Particle Diameter, D, Defining a Range, μm	Lognormal Distribution, σ_g = 2.0		Semilog Distribution
	s[a]	p[b]	p[b]
<256	0	0.500	0.566
<128	1	0.159	0.143
<64	2	0.0228	0.0190
<32	3	1.35×10^{-3}	1.75×10^{-3}
<16	4	3.17×10^{-5}	1.33×10^{-4}
<8	5	2.87×10^{-7}	9.21×10^{-6}
<4	6	9.90×10^{-10}	6.05×10^{-7}
<2	7	1.29×10^{-12}	3.88×10^{-8}
<1	8	6.28×10^{-16}	2.45×10^{-9}
<0.5	9	1.14×10^{-19}	1.542×10^{-10}
<0.25	10	7.77×10^{-24}	9.67×10^{-12}

[a]Number of standard deviations from mode.

[b]Cumulative fraction for size range shown in column 1.

In Fig. 15 are plots of equations 6 and 7 showing the mass frequencies of both distributions with both peaks positioned at a diameter of 256 μm. In Fig. 16 are plots of the integrated forms of equations 6 and 7, showing the cumulative mass fractions to the left of the peaks extended out to the equivalent of ten standard deviations. The two curves reflect the similarity within an equivalent of three standard deviations at the left of the peaks. However, Fig. 16 also illustrates the increasing disparity between the two distributions at the smaller particle sizes.

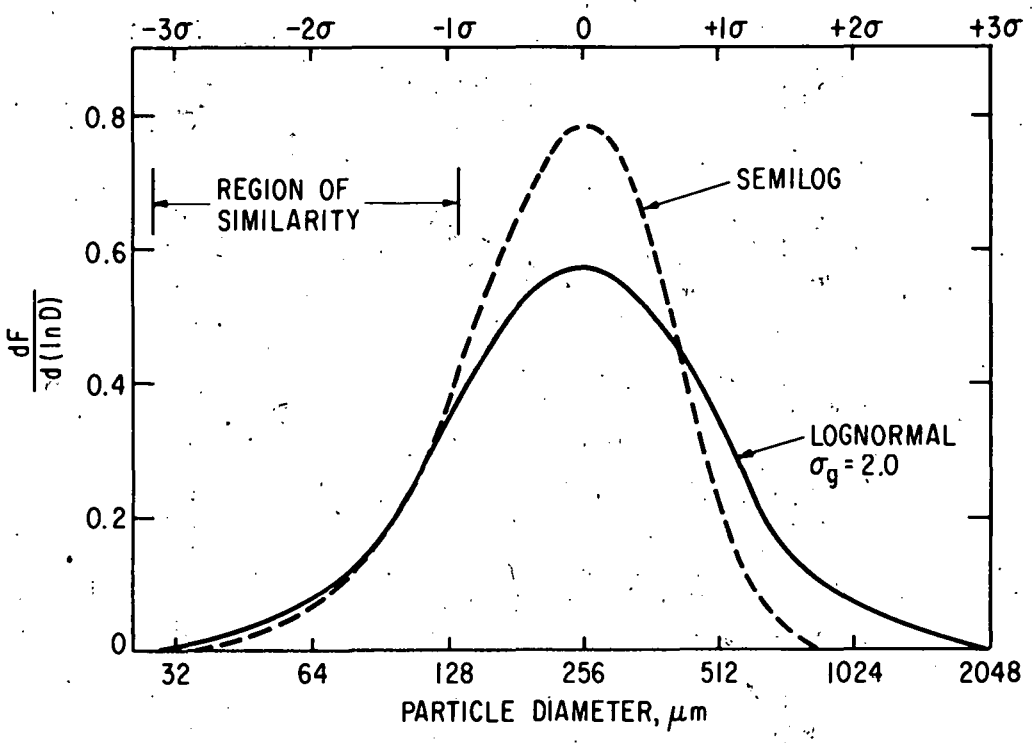

Fig. 15. Comparison of Probability Frequencies for Lognormal and Semilog Distributions

The choice of a model for extrapolation purposes poses some difficulty, in the absence of the needed experimental confirmation. The lognormal model yields cumulative fractions (in the seven to ten standard deviation range) so low that inhalable quantities can be considered nil. The semilog model yields fractions that are small but nonetheless several orders of magnitude larger than the fractions yielded by lognormal. Intuitively, it would appear that the semilog yields values that represent upper limit values since the characteristic of this model is that the number of particles continues to increase without limit as the particle size approaches zero.

It is the intention in this program to apply the results obtained in these excercises to the explosive dispersal data reported earlier [STEINDLER-1978C] and to estimate the absolute quantities of inhalable material produced.

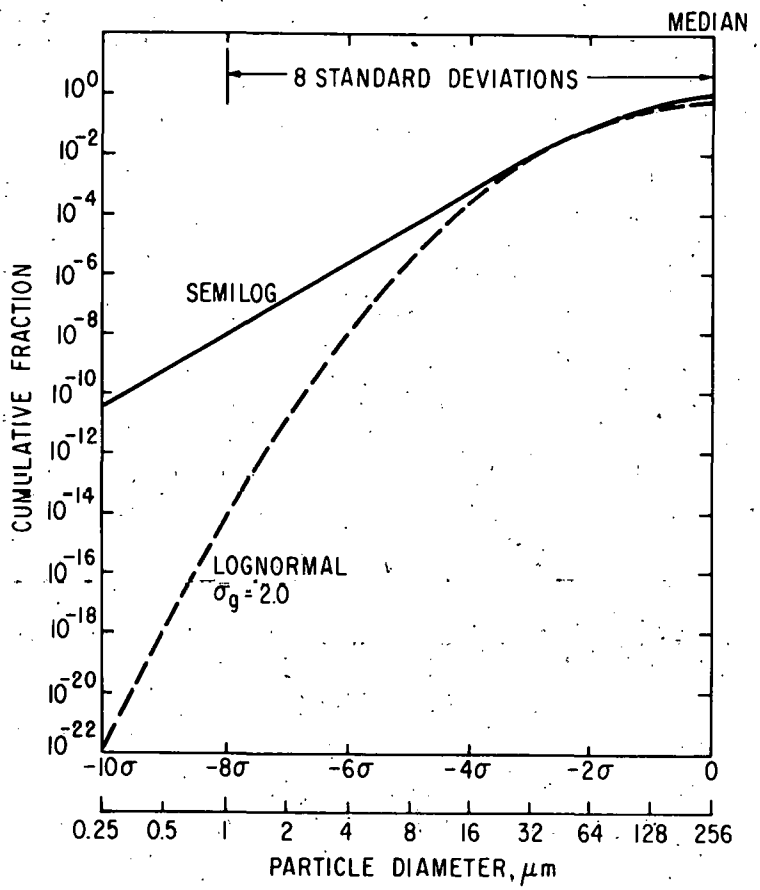

Fig. 16. Comparison of Cumulative Fractions for Lognormal and Semilog Distributions

C. Mechanical Energy Requirements for Basic Mechanisms of Subdividing and Dispersing Liquids and Solids in Air

In this section, the mechanical energy requirements are calculated for basic dispersion processes consistent with explosive dispersion of nonvolatile liquids as discussed above (i.e., excluding vaporization-condensation phenomena). Energy is required for the subdivision of liquid and solid material and for its dispersion in air, as a result of fluid motion such as occurs in explosions and fires.

The mechanical energy requirements are calculated from the interfacial surface energy and viscosity of liquids, from the modulus of elasticity and modulus of rupture of solids, and from the aerodynamic drag of particles of either a liquid or a solid moving relative to the air around them.

The resulting dispersion is an aerosol, which is metastable but always undergoing agglomeration and settling (even if these process rates are low, as they are for small particles at large interparticle distances). The energy to achieve such subdivision and dispersion is not simply related to the total or source energy, as in an explosion, because the source energy may dissipate in paths other than those which result in dispersion. Nevertheless, the calculated mechanical energy requirement is a minimum local energy intensity for dispersion. Conditions facilitating or preventing energy transfers will determine the type and extent of dispersion.

1. Atomization of Liquid in a Hydraulic Jet: Surface Energy and Viscous Force in Liquids

The interfacial surface tension of a liquid droplet in air has a definite energy (mechanical work) associated with the formation of interfacial surface. The surface tension σ is defined as the work (in dyne-cm) to form 1 cm^2 of new liquid surface. The total surface area, S, of N spherical droplets of liquid of density ρ and diameter D has a total mass M and a total volume of droplets such that

$$V = \frac{M}{\rho} = \frac{\pi D^3}{6} N$$

and

$$S = \pi D^2 N$$

If E_m is the surface energy per unit mass, $E_m = \frac{\sigma S}{M} = \frac{6\sigma}{\rho D}$, in consistent units. Typical aqueous solutions at temperatures of interest have σ = 70 dynes-cm and ρ = 1 g/cm, within ±30%; the resulting $E_m = \frac{420}{D(cm)} \frac{(dyne\text{-}cm)}{g} = \frac{0.100}{D(\mu m)} \left(\frac{cal}{g}\right)$, where the units obtained for E_m result from substitution of the units of diameter D, as noted. The calculated surface energies per unit mass of particles are plotted as a function of particle diameter in Fig. 17. (Other energies from other mechanisms, discussed below, are also plotted in Fig. 17 for comparison, and the relationship of these symbols is given in Table 10.)

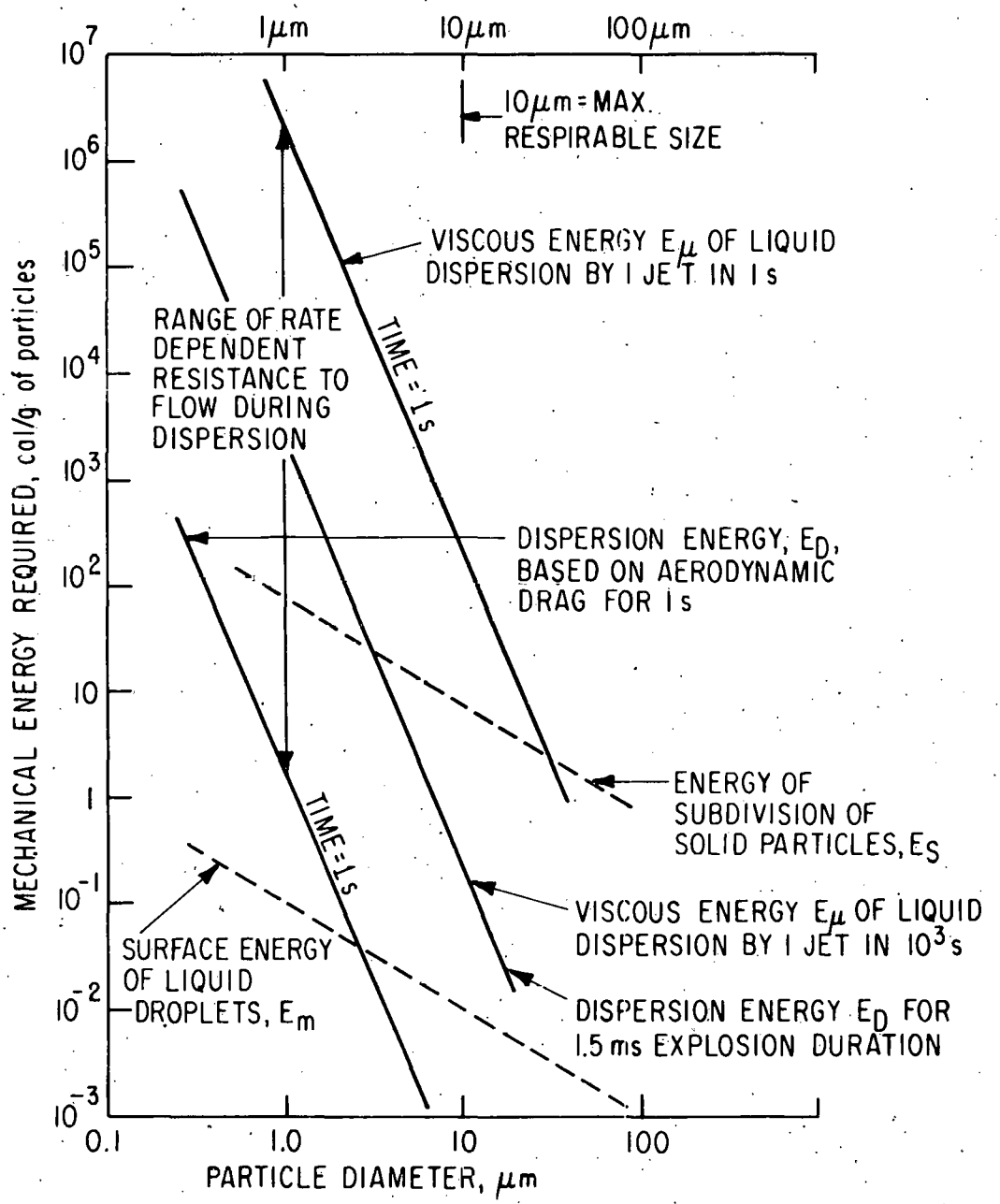

Some Reference Energy Ratios, cal/g

1000:	Detonation energy of TNT
540:	Vaporization of water
400:	Ratio above which organic liquid decomposes
67:	Adiabatic work to compress air to 10 atm
13:	Kinetic energy at speed of sound (330 m/s)

Fig. 17. Energy Requirements for Subdivision and Dispersion of Liquid and Solid

Table 10. Symbols for Theoretical Energies of Mechanisms of Subdivision and Dispersion of Liquids and Solids (Relationship of Symbols in Fig. 17)

	Liquid	Solid
Surface energy (unit mass) E_m	E_m	Not applicable
Viscous energy (unit vol.) E_μ	E_μ	Not applicable
Subdivision energy (unit vol.) E_S	Not applicable	E_S
Dispersion energy (unit mass) E_D	Not applicable (included in E_μ)	E_D
Total energy for airborne material of diameter, D	E_μ	$E_S + E_D$
Other relationships for D in respirable range	$E_m << E_\mu$	$E_m << E_D$

In metric terms, the viscosity of a liquid is the force in dynes to establish a velocity of 1 cm/s between two parallel planes, 1 cm apart, each of 1 cm^2 surface area; viscosity is thus in units of $(dyn \cdot s)/cm^2$ or the mass equivalent $g/(cm \cdot s)$. The poise is numerically equal to 1 $g/(cm \cdot s)$. Viscosity becomes energy when multiplied by cm^3/s. Such a rate-dependent energy exists when a fast-moving jet of liquid is the method for dispersing liquid droplets in air.

Because of fluid deformation, bulk liquid cannot be subdivided like solids by applying tensile stress to the point of rupture. Instead, liquids are subdivided or atomized by accelerating the liquid as fast-moving small-diameter filaments (or thin sheets) and projecting such jets into static air, whereupon the unstable jets break up into droplets whose mean size is determined by the diameter of the jets (or the thickness of the sheets).

The practical aspects of atomization of liquids has been summarized by W. R. Marshall [MARSHALL]. The surface energy of droplets formed by jets amounts to less than 1% of the total energy requirement of efficient hydraulic nozzles. The energy associated with the maximum jet velocity (kinetic energy) has the same order of magnitude as the surface energy, but the largest energy component is that required to overcome viscous forces in achieving a high volumetric flow rate through a small orifice to form a small-diameter jet.

The magnitude of this viscous energy requirement E_μ has been calculated for a reference case of a conical orifice jet by G. W. Monk [MONK]:

$\frac{E_\mu}{V} = \frac{8\mu d_1^2}{3\pi d_2^4} \frac{V}{t} \frac{1}{L}$ where $\frac{E_\mu}{V}$ is the energy, E_μ (in dyne-cm) per unit volume to form a single filament of diameter d_2 for liquid at the volumetric flow rate $\frac{V}{t}$ cm^3/s through a conical nozzle of length L (cm), where d_1 is the inlet orifice diameter in cm and d_2 is the exit diameter in cm. The viscosity of the liquid, μ, is given in poises, where one poise is numerically equivalent to the force in dynes to establish a velocity of 1 cm/s between planes of 1 cm^2 surface area and separated by a distance of 1 cm. The above formula gives $\frac{E_\mu}{V}$ in dyne-cm/cm^3; the energy in joules is 10^{-7} E_μ and in calories is 2.39×10^{-8} E_μ. In the above formula, $\frac{E_\mu}{V}$ is proportional to volumetric flow rate, $\frac{V}{t}$, for multiple jets; E_μ is proportional to the number of jets times the flow, $\frac{V}{t}$, for each jet. Since E_μ is inversely proportional to the fourth power of d_2, which is the approximate mean size of resulting droplets, the viscous energy to produce 1 g of water droplets of 1-μm diameter from one jet in 1 s is 2.0×10^6 cal, while an energy of 200 cal is required for 1 g of 10-μm size droplets from one jet in 1 s, assuming that L = 1, d_1 = 1 cm, and V = 1 cm^3. The specific energy requirement for 1 g of particles is time-dependent. Energy per gram is plotted as a function of diameter for 1 and 1000 jet-seconds in Fig. 17.

This viscous energy, like kinetic energy, is dissipated in aerodynamic turbulence in the breakup of the jet into droplets. (Aerodynamic drag energy is discussed below.)

2. Energy to Subdivide a Solid by Brittle Rupture

Common ceramics having good mechanical strength, such as glass or sintered magnesia, have a modulus of rupture (S_R) of about 1.0×10^5 kPa (1.5×10^4 lb/sq in.) and a modulus of elasticity (K_E) of about 2.1×10^7 kPa (3.0×10^6 lb/sq in.). They rupture in the brittle mode; that is, under tensile stress of 1.0×10^5 kPa they rupture without plastic deformation at an elastic strain of not more than about 0.1% elongation.

The constancy of the modulus of elasticity K_E is generally observed, if K_E is stated in terms of continuous "true" stress and "true" strain, defined as a continuous mathematical function for the linear dimension L:

$$\text{true strain} = \int \frac{dL}{L} = \Delta(\ln L);$$

$$\text{true stress} = \sigma(L)$$

$$K_E = d\sigma/d(\ln L).$$

For a ceramic body of original length L_0 and uniform cross-sectional area subject to axial tensile stress, the rupture stress σ_R is associated with axial rupture strain = $\Delta L_R = L_R - L_0$

where L_0 is the original length and L_R is the length at rupture. From the above definition of K_E,

$$\frac{\sigma_R}{K_E} = \ln \frac{L_R}{L_0}.$$

The energy of rupture, E_R, of a bar of original length, L_0, and original cross-sectional area, A_0, can be found as the integrated product of force, F, times elongation dL over the total A:

$$E_R = \int_{L_0}^{L_R} F dL$$

$$= \int_{L_0}^{L_R} A\, S dL,$$

with F, A, and S all functions of L. The area function A(L) is defined by the typical Poisson ratio of ceramics, 0.60:

$$A(L) = A_0 \left(\frac{L_0}{L}\right)^{0.6}$$

When the above equation for E_R is integrated by parts,

$$\frac{E_R}{A_0 L_0} = 2.5\, S_R \exp\left\{0.4\left(\frac{S_R}{K_E}\right)\right\} + 6.25\, K_E \left[1 - \exp\left\{0.4\left(\frac{S_R}{K_E}\right)\right\}\right]$$

Since $A_0 L_0 = V_0$, the original volume, the above E_R is a function only of S_R and K_E for a single cleavage of the volume. For a typical ceramic, $\frac{E_R}{V_0} = 6.2 \times 10^{-3}$ cal/cm^3 for a single cleavage.

Multiple binary cleavages in each of the three dimensions can reduce an original cube with sides of length D_0 to particles of any size D. The corresponding volumes are $\frac{V_0}{V} = \left(\frac{D_0}{D}\right)^3$. The total number of particles N (all of the same size, D) is $N = \frac{V_0}{V}$. The total number of cleavages C_N is then

$$C_N = 3\left(\frac{D_0}{D} - 1\right)$$

$$= 3\,\frac{D_0}{D} \text{ for large values of } \frac{D_0}{D}$$

$$= 3\left(\frac{V_0}{V}\right)^{1/3}$$

$$= 3N^{1/3}$$

The energy of subdivision to size D, E_S, is given by

$$E_S = C_N\left(\frac{E_R}{V_O}\right)V_O$$

$$= \left(3\,\frac{D_O}{D}\right)\cdot\left(6.2 \times 10^{-3}\,\frac{cal}{cm^3}\right)\cdot\left(D_O{}^3 cm^3\right)$$

$$= 1.9 \times 10^{-2}\,\frac{D_O{}^4}{D}\ cal$$

For 1 g of material of density 2 g/cm^3: $V_O = 0.5$ cm^3, $D_O = 0.794$ cm, and the energy per gram $E_1 = \frac{7.5 \times 10^{-3}}{D(cm)}$ cal/g. The energy of subdivision is inversely proportional to the particle diameter; for a diameter of 1 μm, it is 75 cal/g. The energy of subdivision is not rate-dependent; it is plotted as a function of particle diameter in Fig. 17.

3. Energy to Disperse Particles to Interparticle Distances at which Agglomeration Rate is Low

In order to form a dispersion of particles with inter-particle distances large enough that the agglomeration rate is low in practical terms, the particles must move apart, through the air, from an original location as a consolidated solid or liquid. For small particles, the aerodynamic drag force F_p for motion of one spherical particle in air is given by the Stoke's equation for viscous flow at small Reynolds number, viz., $F_p = 3\pi\mu DU$; F_p is in dynes when μ is the viscosity of air in poise, D is the particle diameter in cm, and U is the particle velocity in air in cm/s. The viscosity, μ, of atmospheric air is about 2.0×10^{-4} poise. We need to establish a mean velocity $\bar{U}$ for the above equation, such that $\bar{U} = \frac{\bar{X}}{\Delta t}$, where $\bar{X}$ is the mean distance traveled by a particle from its original location and Δt is the time for the movement. As shown above,

$$F_p = 3\pi\mu DU = 1.9 \times 10^{-3}\ D\ \frac{\bar{X}}{\Delta t}$$

in the appropriate units of dynes, cm, and s.

From the basic rate equation for agglomeration of particles, the higher the concentration of particles (i.e., the number of particles per cm^3 of air), the higher is the rate of agglomeration. For spherical particles of one size, the time (t_h) for one-half of the particles to agglomerate is given by the equation

$$t_h = \frac{2}{k_o N_O},$$

where t_h is the half-time in seconds, N_O is the initial particle concentration in particles per cm^3, and k_o is a coagulation constant which is a function of particle size [ZEBEL]. For a particle diameter of 2.0 μm, k_o is

6.44×10^{-10} cm^3/s. For smaller particles and for particles of mixed sizes, k_o is larger, indicating shorter half-times for coagulation for a given concentration. For present purposes, a half-time criterion of 10 s is adopted along with $k_o = 6.0 \times 10^{-10}$ cm^3/s, regardless of particle size; this is a reasonable stability criterion--that the particle concentration is to be no greater than 3×10^8 particles/cm^3, or $\frac{N}{V_a} \leq 3 \times 10^8$ cm^{-3}, where V_a is the volume of air. Since particle volume, V_p, is given by $V_p = \frac{\pi}{6} D^3$, $N = \frac{V_o}{V_p}$, where V_o is the total volume of all particles. For 1 g of particles, V_o = 1 cm^3 and V_a (cm^3) $\geq \frac{6 \times 10^{-9}}{D^3}$. The mean distance between particles, $\bar{X}$, for a sphere of volume V_a is $\bar{X} = 0.02(V_a)^{1/3}$ or $\bar{X}$ (cm) $= \frac{1.82 \times 10^{-3}}{D}$. The total number of particles, N, is $2/D^3$.

The energy of dispersion, E_D, is given by

$$E_D = NF_p\bar{X}$$

$$= \left(\frac{2}{D^3}\right)\left(1.9 \times 10^{-3} D \frac{\bar{X}}{\Delta t}\right)\left(\bar{X}\right)$$

$$= \left(\frac{3.8 \times 10^{-3}}{D^2}\right)\left(\frac{1.82 \times 10^{-3}}{D}\right)^2 \frac{1}{\Delta t}$$

$$= \frac{1.26 \times 10^{-8}}{\Delta t\, D^4} \frac{\text{dyne-cm}}{\text{g}}$$

or $E_D = \frac{3.0 \times 10^{-16}}{\Delta t\, D^4}$ cal/g, where D is in cm and Δt is in s.

Thus, E_D is rate dependent and a strong function of particle diameter. For D = 1 μm = 10^{-4} cm, E_D = 3 cal/g for a dispersion time of 1 s. This rather low energy requirement was based on an agglomeration constant of k_o = 6.0×10^{-10} cm^3/s and an agglomeration half-time of 10 s. For a polydisperse aerosol, k_o for very small particles is very much larger and a longer half-time might also be appropriate. Also, for a detonation, the primary expansion is complete in the order of a few milliseconds. In Fig. 17, two curves are shown for dispersion energy, E_D, one for a dispersion time of one second, the other for 1.5 ms (corresponds to the time of completion of the primary expansion of a detonation). Note that the latter curve is identical to the viscous energy curve (liquid dispersion) for 10^3 s. For a given mass and diameter of particles, the energy requirement at the shorter time interval is three orders of magnitude greater.

4. Discussion of Overall Energy Requirements for Subdivision and Dispersion of Liquid and Solid (Fig. 17)

In Fig. 17 are shown the amounts of mechanical energy to subdivide and disperse 1 g of liquid or solid material originally in consolidated form. The mass-specific energy of subdivision (fragmentation of solid and surface generation of liquid) is inversely proportional to particle diameter and is

not a function of the rate of work. The dispersion energy to achieve an interparticle distance sufficient for a stable dispersion is inversely proportional to the fourth power of the diameter and is also proportional to the time rate at which the work of dispersion is applied. These effects combine to make it very difficult to produce particles smaller than 10 μm at a rapid rate--say at a rate of 1000 g in 1 s (as from a single jet from a pressurized vessel) or at a rate of 1 g in 1 ms (as in a single detonation of TNT). At this high a rate, particles can be formed that are larger than 10 μm, but to form smaller particles requires such intense application of energy that the material will be vaporized or decomposed rather than dispersed. Thus, a single explosion or a single pressure jet cannot have a high yield of respirable particles by the mechanisms described here. The absolute amount of particles of respirable size is determined by the time rate of energy release and by the confinement time and volume of the particles produced. To establish the yield quantitatively requires that the specific conditions of fluid dynamics and energy dissipation be determined.

Purely calculational models are complicated and are not convincing in the absence of direct experimental demonstration; however, they may be used to design tests that are highly realistic and relevant to safety analyses.

D. Potential Mechanisms Whereby Airborne Material Would be Generated in Accidental Fires in Fuel Reprocessing Plants

Data on airborne material in fires were reviewed to reveal conditions and mechanisms effective in rendering radioactive materials airborne.

Fission products and actinides enter and leave a reprocessing plant in the form of aqueous nitrate solutions or solid oxides. The actinides pass through a TBP-kerosene phase in solvent extraction. In practical terms, the process steps do not involve high pressures or temperatures or highly exothermic reactions. Except for the fuel element cladding, metals are not present as process materials. The only radioactive materials that are significantly volatile at process conditions are fission product noble gases, iodine, and tritium.

Because of the vulnerability of TBP-kerosene to combustion in a plant fire, the chemical state of uranium and plutonium in this organic phase was examined.

Uranium and plutonium in the organic phase may be present in the 3-, 4-, or 6-valence form, but in all cases the metal atoms are incorporated in the phosphate and/or nitrate portions of the organic complex. In vaporization or combustion of an organic solution containing plutonium or uranium, these elements will remain as stable nonvolatile phosphate or oxide residues. Both compounds are stable and nonvolatile to 1000°C. At 2000 K, the vapor pressure of PuO_2 is about 7.2×10^{-2} Pa (7.1×10^{-7} atm) [CLEVELAND].

It was generally found in our review and analysis that uranium in solution and in the form of oxide powder does not readily become airborne in moving air even in the presence of fire from combustible materials. The major condition favorable to entrainment is the distribution of uranium as a thin

surface layer on a nonporous and nonadhesive substrate which is then exposed to rapidly moving air (say 10 m/s or higher speeds). Another entrainment condition is the presence of a combustible substrate; in the course of destruction of the substrate by combustion, uranium oxide particles of high specific surface area are exposed to an air stream.

High-temperature conditions are favorable to dispersion by destroying the adhesive action of liquid or plastic materials, e.g., water, oil, etc. Flame temperatures are not high enough to form uranium or plutonium vapor, however. Thus, fire has only a secondary effect on making process materials airborne. Fire can have secondary effects (1) by destroying combustible confinement structures (to the extent that such exist), (2) by influencing mechanisms of deposition of process materials on surfaces or volumes of the plant structure, (3) by evaporating moisture or liquids which inhibit entrainment, and (4) by increasing the quantity or speed of air movements within the plant.

The principal influence of fires or accidents on source-term releases is via their effects on air-entrainment processes within the plant structure.

E. Review by Battelle Pacific Northwest Laboratories of Airborne Material in Fires and Other Accidents

Estimated source terms for releases of radioactivity from postulated accidents in mixed-oxide fuel reprocessing plants have been reported [SELBY] by Battelle Pacific Northwest Laboratories (BNWL). The source terms from fires, explosions, criticality, and other postulated accidents are presented in [SELBY, Chapter VII], and empirical data relevant to estimation of airborne material are reviewed in [SELBY, Appendix F]. The Appendix F data includes the work of Mishima, which emphasizes measurements of plutonium and uranium made airborne in fires and other accidents.

1. Factors Affecting Release Fractions and Source Terms Explosions

In the case of explosions, the amount of material airborne was determined by [SELBY] from the volume of space in which the explosion was confined and the maximum stable concentration of aerosol, rather than by the amount of material or the energy involved. This estimate [SELBY] does not make use of the empirical data of Mishima [MISHIMA-1968A, 1968B, 1973A, 1973B]. The source term in the [SELBY] estimate was made by identifying the following factors:

(1) the room in which the explosion occurred and in which the explosion products were confined had a volume of 10^4 m^3;

(2) from cited experimental work, the most concentrated plutonium aerosol measured was 71 mg/m^3; therefore, 100 mg/m^3 was taken as the maximum possible concentration in a significant volume a few minutes after the explosion proper;

(3) the maximum amount of plutonium airborne as a challenge to an air-cleaning system is 1000 g, the product of item 1 and item 2.

(4) If it is assumed that the penetration factor is 10^{-3} for one HEPA filter and 10^{-5} for two HEPA filters in series, the source term releases are, respectively, 1 g plutonium (one filter) and 0.01 g plutonium (two filters).

2. Factors Affecting Release Fractions for Fires

The experimental measurements made by Mishima included the burning of uranium or plutonium metal but did not involve temperatures high enough to vaporize a significant amount of the relatively nonvolatile oxide or phosphate compounds. Because the scope of our review does not include plutonium or other fuels (except cladding) in the metallic form, Mishima's data on metals was not reviewed. His work on compounds of interest to us concerned the entrainment of aqueous nitrate solutions or of powdered solids in conjunction with other process materials in a fuel fabrication plant, and under conditions of overheating or combustion as would occur in an accident situation. The factors considered in connection with entrainment are:

(1) the characteristics of the starting material (especially the chemical properties and state of subdivision, if a solid);

(2) thermal stresses applied to material (heating, drying of solutions, combustion of organic materials present, etc.);

(3) speed and direction of air surrounding the material.

In general, qualitative descriptions of entrainment conditions were given along with quantitative measures (total quantity, composition, and particle size) of the initial material and of airborne material sampled at various time periods. The reference events thus were time-dependent for the material, but were steady state for conditions of airflow and thermal stress. Over the total range of air speeds investigated, the fraction of material airborne varied by nearly eight orders of magnitude, and even for the same nominal conditions unexplained variations of two orders of magnitude were not uncommon. Because the measured data were not presented as fully defined quantitative models, the numerical results are indicative rather than definitive, even as to the order of magnitude.

Mishima's analysis does not make explicit reference to the principles of entrainment process mechanisms, and his results do not fully define the system variables that are controlling. On the other hand, his results are generally consistent and confirmatory of what would be expected in entrainment.

Of particular interest was the effect of gasoline fires on the rate of entrainment by moving air of powders (or solid residues from evaporation of solution) from stainless steel surfaces. Mishima [MISHIMA-1973B, pp. 29-33] found that in the presence of a gasoline fire, the entrainment rate was lower than in the absence of a fire. The size distribution of entrained material suggests that the elevated temperature of the fire had reduced the fraction of smaller particles, as indicated by the relative amounts of 1- and 10-μm particles. Thus, fire tends to increase particle size.

One of the results most likely to be used in assessing the effects in fires is a maximum entrainment of particles in the respirable range (i.e., <10 μm) of 0.23 wt % for UO_2 powder in 5 h. This was found in tests under various conditions with both UO_2 powder and UNH solution and an air speed of 1 m/s [MISHIMA-1973B, p. 30]. This maximum value (one order of magnitude higher than the average) was obtained without fire for powdered UO_2 on bare sandy soil. For the residue from UNH solution, the maximum respirable fraction entrained was 0.5% from smooth stainless steel. The highest air speed used, 10 m/s, resulted in great variability in the fraction entrained, 0.06 to 24 wt %, since in the general process in entrainment higher speeds (and optimum direction of air impingement) may increase the fraction entrained. (The parameters of entrainment are considered in a following section.)

Mishima also has reported tests [MISHIMA-1973A] of uranium made airborne during combustion of simulated waste materials, consisting of cardboard, paper, plastic, rubber, rags, and oil, which were packed in a 45-cm by 60-cm (18-in. by 24-in.) corrugated cardboard box.

Uranium was interspersed in this waste in three forms:

(1) UO_2 powder, ball-milled, 0.2 to 20 μm; mass median size, about 1.0 μm;

(2) uranium nitrate solution, 0.51 g U/mL;

(3) the same uranium nitrate solution as in (2), absorbed into paper and air-dried before it was composited in waste.

Three mixture configurations having different degrees of homogeneity were used.

Eleven tests were made in which a waste container was ignited and burned with air inside a stainless steel enclosure of 20 m^3 (710 ft^3), 2.85-m diameter and 2.0-m tall. Although airflows were not reported, average air speeds through the enclosure are presumed to be less than 10 m/s. In each run, 9.1 to 64 g uranium was contained in about 4.5 kg flammable material. The maximum fraction of uranium particles smaller than 10 μm rendered airborne was 0.048 wt %. The average of 10 runs reported was 0.012 wt % and the smallest 0.0024 wt %.

Wall deposits of up to 0.23% of the total entrained material were measured, and an overall material balance was made; the average material balance was 97% of the uranium used.

There is some indication that the largest airborne fraction may have been associated with the most homogeneous interspersion of the uranium. This would be consistent with expectations. The value of Mishima's and similar empirical work is the consistency of its results with general knowledge of elutriation and entrainment processes.

3. Local Fires Estimate of Release Fractions [SELBY]

The occurrence of a fire near nitrate solution blending tanks was considered one of the greatest potentials for the release of plutonium. The estimated consequences [SELBY] of a fire are shown in Fig. 18. Of the several possible paths, the maximum fraction of plutonium airborne is 0.7% for a fire that vaporizes the solution and heats the tank to complete dryness. For 150 kg of plutonium in 1000 L of solution, the primary airborne release would be 1050 g plutonium. (This is greater release than for an explosion for which, as analyzed above, the primary release would be 1000 g plutonium.)

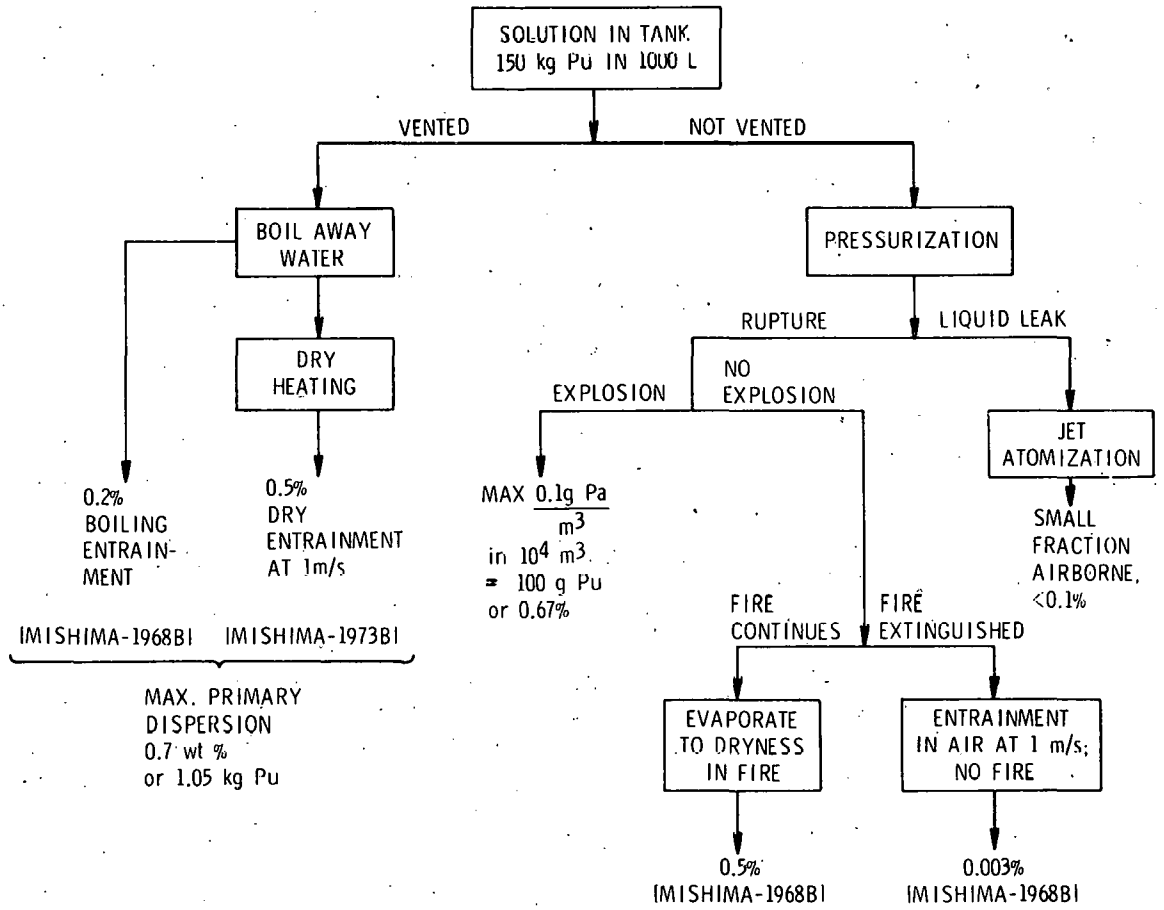

Fig. 18. Accident Analysis: Local Fire Near a Tank Containing an Aqueous Plutonium Nitrate Solution

The source term for a local fire based on the penetration of the HEPA filters then is about the same as for the explosion case (above): 1.1 g plutonium if there is one filter or 0.011 g plutonium if there are two filters.

Note that the energy from a fire must be sufficient to evaporate 1000 L of solution (>5.4 x 10^5 kcal) or have an explosive force great enough to rupture the vessel. Also, the entrainment quantities are based on test values for which the vapor velocities and vessel configuration are much more favorable for entrainment than in an actual case. Thus, the estimated source term is a "worst case" that is larger (probably) by more than one order of magnitude than from any realistic entrainment mechanism.

4. Major Fire Estimate of Release Fractions [SELBY]

Although no realistic scenario for a major fire was identified, it was estimated that a maximum of 1% of the dispersible plutonium inventory would become airborne in a major fire on the basis of: the maximum plutonium inventory (about 200 kg), the maximum fraction in dispersible form (about 50%), and the impossibility of destruction of the final plutonium entrainment barrier. This maximum quantity is about the same as that estimated in the cases described above.

5. Other Accidents [SELBY]

In addition to the accidents of the largest consequences analyzed above, it is appropriate to consider cases with particular plant designs and with smaller releases. Reference "worst case" data from sources identified in [Appendix F, SELBY] are reproduced as Table 11 (Table 16 from [SELBY]).

A further discussion of system parameters fundamentals to entrainment is given next.

6. Basic Entrainment Parameters

As shown in the entrainment summary of Table 11, entrainment is greater for smaller, less dense particles, but most favorable to entrainment are high air speeds and unrestricted airflows. In order to identify the basic conditions under which a particle becomes airborne (or does not), the forces on a single particle can be identified as follows:

(1) gravitational force (per unit mass) of particle, F_G, (volume)x (density) is $\frac{\pi}{6} \rho D^3$, where D = diameter and ρ = density;

(2) aerodynamic drag force on particle, F_D, due to relative speed, U, of particle in air = $\frac{3\pi\mu DU}{g} = F_D$, where μ = viscosity of air (in mass units) and g is the gravity constant;

(3) the contact adhesion force of a particle in contact with a fixed surface, F_C, is equal to KD, where K is an empirical constant (discussed below).

Table 11. Summary of Experimentally Determined and Estimated Airborne Release Fractions of Plutonium Under Various Thermal and Aerodynamic Stresses [Table 16, SELBY]

	Stress Imposed	% of Material Initially Airborne[a]
• Fire		
Dioxide Powder	Airflow less than 100 cm/s	0.5
	Airflow 100 cm/s	1.5
	Airflow greater than 100 cm/s	15
	Mixed with flammable material, natural convection	0.05
	Mixed with flammable material, forced draft	40
Oxalate Powder	Airflow less than 100 cm/s	1.0
Fluoride Powder	Airflow less than 100 cm/s	0.1
Nitrate Solution	Airflow less than 100 cm/s	0.5
	Airflow greater than 100 cm/s	1.0
	Gasoline fire, stainless steel surface, 20 mph airflow (8.8 m/s)	10
	Mixed with flammables, natural convection	0.2
	Mixed with flammables, forced draft	10

• Explosion

Any explosive mechanism of sufficient magnitude to completely destroy the integrity of the containment is assumed to make airborne all of the source material directly involved or to fill the available air space with an aerosol which has a mass concentration of 100 mg Pu/m^3 after 10 min.

• Other

If air at a velocity greater than 10 mph is directed upon or through a finely divided powder (particles smaller than 50 μm AED), 100% of the powder is assumed to be airborne.

[a]The fraction of material at risk that is initially airborne is the maximum airborne material challenging the air cleaning system; the material penetrating the air cleaning system and leaving the plant is the source term for atmospheric dispersion.

The relative values of these forces (in grams) determine particle behavior in entrainment. Ranges of numerical values as a function of diameter (in μm) were calculated. The results are shown in Fig. 19. Settling rates are high, in practical terms, for particles larger than 10 μm. Also, for particles smaller than 100 μm and for air speeds lower than 10^3 cm/s, the contact adhesion force is greater than the drag force. Thus, entrainment at air speeds lower than 10 m/s depends on contact adhesion force being broken by other than simple aerodynamic drag. Once this force is broken, material becomes airborne at speeds lower than 10 m/s, and entrainment is a function of settling rate and other particle removal processes.

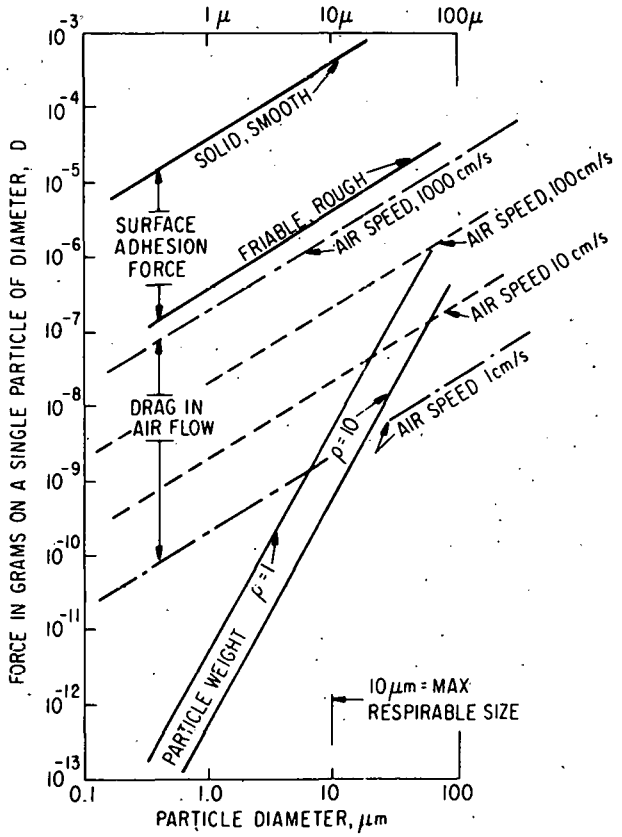

Fig. 19.

Forces on a Particle as a Function of Diameter. Note: Intersection of particle weight with air drag gives settling velocity

Entrainment is a two-step process: (1) an intense local force or acceleration to break the surface contact and to suspend particles momentarily, and (2) a steady air speed sufficient to transport smaller particles. Although Mishima alluded to local air jets and local turbulence in fires and combustion, he did not attempt to define or quantify the contact-breaking step.

The detailed discussion of entrainment in fundamental terms has been given by M. Corn [CORN]. He referred to the lack of available models for calculation of quantitative behavior in entrainment and advised that empirical data cannot be confidently used for a system other than that for which it was measured. Factors determining the contact adhesion force were as follows:

(1) The contact adhesion force, F_C, is at a maximum for a sound, smooth spherical particle on an absolutely flat surface; the maximum measured value was for Pyrex; on other materials, the F_C for a particle of the same diameter can be lower by a factor of 10;

(2) F_C also decreases with increasing surface irregularity: as roughness increases from ±0.015 to ±0.040 μm, the F_C decreases by a factor of two; at roughness of ±10 μm, F_C decreases by more than a factor of ten. (Note, however, that roughness can also protect a particle from aerodynamic drag.)

(3) Liquid or even adsorbed moisture increases F_C. Dry conditions, such as those resulting from a fire, can favor entrainment by reducing adsorbed moisture. (Note, however, that high temperatures tend to sinter particles, increasing their size and reducing entrainment.)

A complete model for entrainment would have to consider all factors identified above in connection with the two-step process of (1) breaking surface contact and (2) stabilizing the aerosol.

7. Discussion of Forces on a Particle as a Function of Diameter (Fig. 19)

Figure 19 illustrates the ranges of forces on particles of various sizes and densities that affect their dislodgement and entrainment in moving air--either by forced draft or by convection currents arising from heat and fires. For particles of any size, air velocities lower than 10 m/s are not sufficient to break the contact adhesion force of a single particle on a stable hard substrate. Additional energy (such as impact or vibration) able to impart an acceleration to the particle equivalent to many gravities is needed before the contact force can be broken. Once contact is broken, particles of sizes smaller than 10 μm are readily carried in air moving at a velocity of more than a few cm/s.

The empirical data from Mishima's tests show that up to 1% of the material is rendered airborne initially in fires or in air having speeds up to 1 m/s. For air speeds of about 10 m/s, entrainment of up to about 20% was observed in some cases. High and variable results were obtained, indicating that the description of conditions, such as vibratory motions, particle size distribution, and changes in the properties of materials being tested is incomplete.

8. Information on Particle Entrainment in the Literature

In an article on resuspension (entrainment) of particles in air in connection with environmental effects, the following statements were made [SLINN, p. 213]:

> "...For resuspension [of particles] from contaminated land, perhaps the best procedure is to use the soil erosion formula developed by agricultural scientists...having an estimate of the erosion rate, however, does not solve the problem...an estimate is needed for the fraction of the erosion flux that is resuspended; most erosion occurs by creep and saltation. Unfortunately, this resuspension fraction is not known at all well...the value 0.1 may not be correct even to within an order of magnitude."

The uncertainty of entrainment of particles was also noted in a review by Hidy, but more attention was paid to the fundamental mechanisms [HIDY, pp. 245-251]. Before a particle can be airborne, its contact with the surface on which it reposes must be broken. Mechanisms of disruption or dislodgment include (a) mechanical concussion or vibration, (b) explosive dislodgment, and (c) aerodynamic dispersement. The particle acceleration imposed by these mechanisms must be sufficient to overcome the contact adhesive force. In addition, the possible presence of electric charge must be taken into account.

In aerodynamic extrainment, the particles first begin to slide or roll, and such movements are likely to reduce the adhesive force. When their speed is sufficient to cause the particles to jump or bounce, this is saltation. The higher the jump, the more likely the particles are to encounter faster-moving air, and a progressive increase in speed may lead to their becoming airborne for longer periods. Rolling of larger particles may also have a disruptive effect on attached smaller particles, which, once detached, are more easily rendered airborne. Local disruption and entrainment can also occur by local air jets or by bubbles of gas passing up through a bed of particles.

The great variability of overall entrainment results from local surface or flow variations influencing the several mechanisms involved and accounts for the lack of quantitative predictability. When all spatial dimensions are fixed and conditions are defined, however, definite ranges of entrainment rates in specific items of equipment can be predicted.

III. PYROCHEMICAL AND DRY PROCESSING METHODS (PDPM) PROGRAM

(Milton Ader, J. K. Bates, C. H. Bean, T. J. Gerding, L. J. Jardine, D. K. Kroeck, Michael Krumpelt, K. M. Myles, B. B. Saunders, Seymour Vogler, and M. J. Steindler)

A. Introduction

A Pyrochemical and Dry Processing Methods (PDPM) Program was established at the beginning of FY 1978 in the Fuel Cycle Section of the Chemical Engineering Division at Argonne National Laboratory (ANL). This program is an expansion of the National Fuel Cycle Program for reprocessing fuel by processes that will reduce the risk of proliferation of nuclear weapons. Argonne has been designated by the U.S. Department of Energy (DOE) as the lead laboratory for PDPM, with various reprocessing developments being performed at other DOE laboratories and by industrial contractors.

The program has been administratively divided into individual work packages, four of which are being done at ANL. Purchase orders have been placed for eight work packages, and a subcontract has been placed for an additional work package. A list of work packages is included as Table 12.

Each work package is being managed for conformance to established statements of work, program objectives, a cost plan, a milestone plan, and a management plan in accordance with Uniform Contractor Reporting Guidelines (UCRG), as required by DOE.

B. Management

(C. H. Bean, K. M. Myles, and Seymour Vogler)

A PDPM Program Review was held at DOE Germantown on May 5, 1978. Presentations were made describing the PDPM Program management and technical program plan. Comments and recommendations were made by DOE staff from the Office of Fuel Cycle R&D and the Technology Branch. No significant redirection of program effort was indicated.

A technical information exchange meeting was held at ANL on May 16 and 17, 1978. Representatives of eight contractors responsible for nine separate work packages, along with individuals responsible for three work packages at ANL, reported on the status of engineering analysis, separations processes, and materials development in support of the PDPM Program. This was the first of a series of meetings that will be scheduled at suitable intervals as the program progresses. These meetings constitute a status review, during which DOE representatives, contractor personnel, and program management are able to assess program progress and to constructively criticize program goals and objectives.

The draft PDPM Program Management Plan was revised May 15, 1978, to reflect revisions to the PDPM Cost Plan and reviewers' comments.

Planned procurement, program schedules, program requirements, and management controls for FY 1979 were reviewed with ANL budget, accounting, procurement, administrative, and quality assurance personnel. The authority and

Table 12. PDPM Work Packages for FY 1978

Work Package Number	Title	Location	Activity No.
00	Program Planning and Program Management	ANL(CEN)	00
01	Materials Development for PDPM	ANL(MSD)	A0
02	Carbide Fuel Processing	ANL(CEN)	B0
03	Th-U Salt-Transport Processing	ANL(CEN)	C0
04	U-Pu Salt-Transport Processing	RI-RF[a]	D0
05	Fabrication of Process-Size Refractory Metal Vessels	RI-RF[a]	E0
06	Aluminum-Alloy Processing of Th- and U-Based Fuels	IRT[b]	F0
07	Chloride Volatility Processing of Th-Based Fuels	B&W[c]	G0
08	AIROX, CARBOX, and RAHYD Processing Systems	RI-AI[d]	H0
09	Molten Nitrate Salt Oxidation Processes	PNL[e]	J0
10	Molten Salt Processes Applied to Ceramic Fuels	ORNL[f]	K0
11	Reprocessing of Thoria-Urania Fuel in Molten Salts Containing $ThCl_4$	AMES[g]	L0
12	Molten-Tin Process for Reactor Fuels	LLL[h]	M0

[a]Rockwell International-Rocky Flats.

[b]IRT Corporation.

[c]Babcock and Wilcox.

[d]Rockwell International-Atomics International.

[e]Pacific Northwest Laboratory.

[f]Oak Ridge National Laboratory.

[g]Ames Laboratory.

[h]Lawrence Livermore Laboratory.

responsibility of individuals representing each of the above was identified. Schedules were set for completing the procurement actions needed to effect the transition to FY 1979 subcontracted effort without delay.

A revised statement of work (SOW) was completed for Work Package 07, Chloride Volatility Processing of Thoria-Based Fuels, and for Work Package 08, AIROX, CARBOX, and RAHYD Processing Systems, to cover effort for FY 1979. Revised SOWs for the remaining 10 work packages are scheduled for completion in July.

C. Engineering Analysis and Separations Processes

In the engineering analysis, prior work will be examined and evaluated. From these evaluations, flow sheets will be devised for each of the prospective reprocessing techniques. It is expected that these prospective flow sheets will reveal gaps in the data which must be filled to provide an operable flow sheet. These gaps will be filled by experimental work carried out under the appropriate separations processes subtasks.

1. Materials Development

(J. Hafstrom,* R. M. Arons,* and J. Y. N. Wang*)

The project involves the anticipation, identification, and scoping of potential materials and fabrication problems associated with the various candidate processes in the PDPM Program. Through analytical and experimental methods, means will be devised to resolve these problems. The fuel state after reprocessing will be considered in terms of fuel refabrication capability.

a. Selection of Materials

A preliminary list of candidate materials for containment was presented at the May 16-17 PDPM information meeting and is shown in Tables 13 and 14. (The metallic materials are listed in the approximate order of preference.) The reference processes for the selection were the various salt transport processes under development at ANL and Rockwell International at Rocky Flats. In addition to the ceramics listed, NbC, Si_3N_4, SiC, and pyrolytic BN will be considered and tested as coatings on inexpensive substrates; their availability and usefulness will be determined after the procurement and testing of samples.

Table 13. Candidate Ceramic Materials for Process Containment for PDPM

Oxides	Nitrides	Borides	Carbides
BeO	HfN	TiB_2	HfC
MgO	ZrN	ZrB_2	ZrC
$MgAl_2O_4$	AlN	HfB_2	TaC
ThO_2	TiN	TaB_2	TiC
ThO_2 with additions[a]			
CaO			
CaO with additions[a]			
Y_2O_3			
Y_2O_3 with additions[a]			

[a]Additions that improve the corrosion resistance of oxides (via Raoults Law)--e.g., $CaO-ZrO_2$ solid solutions.

*Materials Science Division, Argonne National Laboratory.

Table 14. Candidate Metallic Materials for Process Containment for PDPM

W-25 wt % Re
Mo-30 wt % W
Ta-10 wt % W
Mo-0.51 wt % Ti-0.08 wt % Zr
Mo-1.5 wt % Nb-0.5 wt % Ti-0.33 wt % Zr-0.07 wt % C
Ta-8 wt % W-2 wt % Hf
Ta-9.6 wt % W-2.4 wt % Hf-0.1 wt % C
Ta-7 wt % W-3 wt % Re-1.5 wt % Hf
Nb-1 wt % Zr
Nb-5 wt % V-1.25 wt % Zr
Nb-10 wt % W-3 wt % Zr
Nb-28 wt % Ta-10 wt % W-1 wt % Zr
Control Samples: W, Mo, Ta, Nb

b. PDPM Environmental Test Facility (PETF)

The PETF for screening candidate ceramic and metallic materials in simulated PDPM process environments is under construction. Provision has been made for an inert atmosphere, stirring of molten salt and metal mixtures, and careful control of temperature up to 1200°C. Sixteen test samples can be accommodated in one test run.

c. Test Program

(1) Processes

The initial conditions under which candidate materials will be tested are those of the uranium-plutonium and throium-uranium/plutonium salt transport processes. The first environmental tests will simulate the conditions expected in the decladding-reduction vessel in the uranium-plutonium salt transport process.

(2) Metallic Materials

Samples of Mo-30 wt % W and W-25 wt % Re alloys have been received and are being prepared for corrosion testing. Both alloys can be rolled to a thickness of 10 mils. Thus, they offer promise as process vessel liner material. Mo-30 wt % W has been demonstrated [KYLE-1969, BERNSTEIN] (in earlier nonaqueous reprocessing work) to be second to tungsten in corrosion resistance to high-temperature molten metals and salts. However, its thermal stability and weldability have not been conclusively determined. A variety of W-Re alloys (3 to 25 wt % Re) is now available in small quantities. Data on the weldability of these materials and their resistance to PDPM processing conditions are not available. The initial phase of this program will be to evaluate the compatibility with experimental conditions and the weldability of these materials as potential container lining materials for various PDPM

processes. The focal points of this work will be study of the effects of postweld heat treatments and selective microstructural attack due to any metallurgical instability.

The best available materials from commercial sources are being sought for evaluation in the PETF. These will be compared with control samples of high-purity material. Sources for the materials listed in Table 14 have been located, and samples are either on order or have been received. Pretest characterization of metallic samples has been initiated, using optical and electron microscopy.

(3) Ceramic Materials

The fabrication of control samples of ceramic materials is under way. Also, incoming ceramic materials are being characterized by optical and electron microscopy.

(4) Tungsten-Coated Ceramics

Metallized Alumina. Dense (albeit with regions of significant porosity), adherent, tungsten coatings have been achieved on small alumina (with 3 wt % yttria) crucibles and are now being tested for integrity under thermal cycling conditions. It has been found that cofiring the crucible and tungsten coating yields the best results. Vacuum firing of the coating and crucible appears to be as successful as firing in hydrogen. Work continues on determining the optimum particle size and formulation of the tungsten coating slurry aids. Coated crucibles will be evaluated as to their ability to contain PDPM process solutions.

Plasma Spray. An investigation of plasma-sprayed coatings for use on graphite substrates is being initiated. Prior investigations of plasma-sprayed coatings showed them to be permeable to molten salts, allowing the salts to seep through a containment vessel wall. The current investigation seeks methods of reducing interconnected porosity and associated permeability by the use of transition metal sintering aids.

2. Carbide Fuel Processing
(Michael Krumpelt, B. B. Saunders, Milton Ader, and D. K. Kroeck)

a. Flowsheets Involving Bismuth
(B. B. Saunders and D. K. Kroeck)

A preliminary conceptual flowsheet (Fig. 20) has been designed from information in the literature. The principle which is the basis for separation of the fission products from the actinides is the reaction or dissolution of some of the carbides to form bismuthides. The unreacted fission product carbides and bismuthides are lighter than bismuth and are expected to float on the bismuth. Uranium carbide dissociates to a very limited extent (dependent upon the solubility of uranium in bismuth). $PuBi_2$ and $ThBi_2$ are denser than bismuth ($PuBi_2$ = 12 and Bi = 9.8), are of limited solubility in bismuth, and are expected to settle in the bismuth melt along with the unreacted

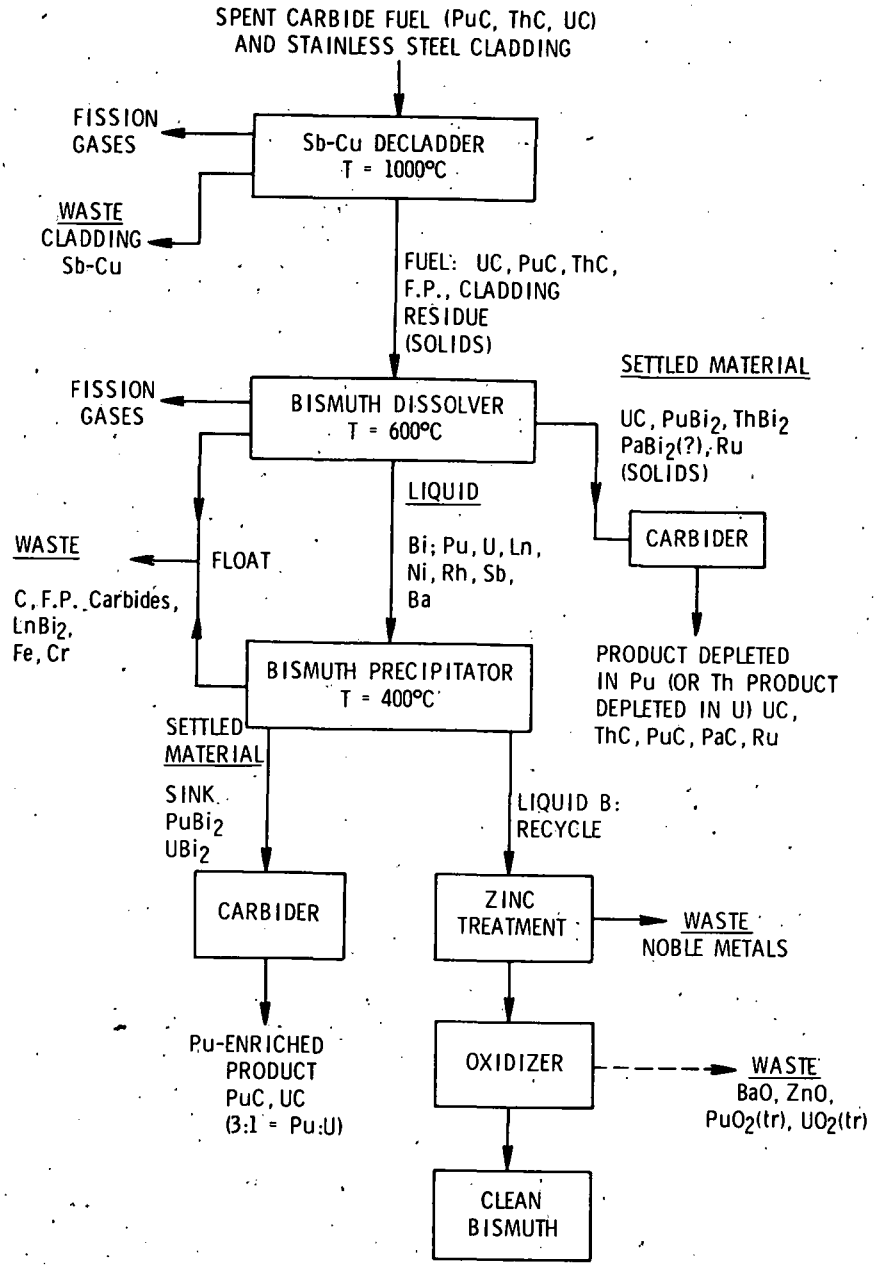

Fig. 20. Bismuth Process for Carbide Fuels.
Ln = lanthanides

uranium carbide. The carbon would float on top of the bismuth. Plutonium is much more soluble in bismuth than is thorium (Fig. 21); the concentration of plutonium can be as high as 3.5% at 600°C. The removal of the dissolved plutonium from the bismuth becomes an important part of proposed flowsheets.

Although uranium carbide does not react appreciably with bismuth, the presence of approximately 10% plutonium or thorium in the carbide fuel may enhance the reactivity of the sintered fuel pellets with bismuth, leading to disintegration of the pellets with release of the fission products.

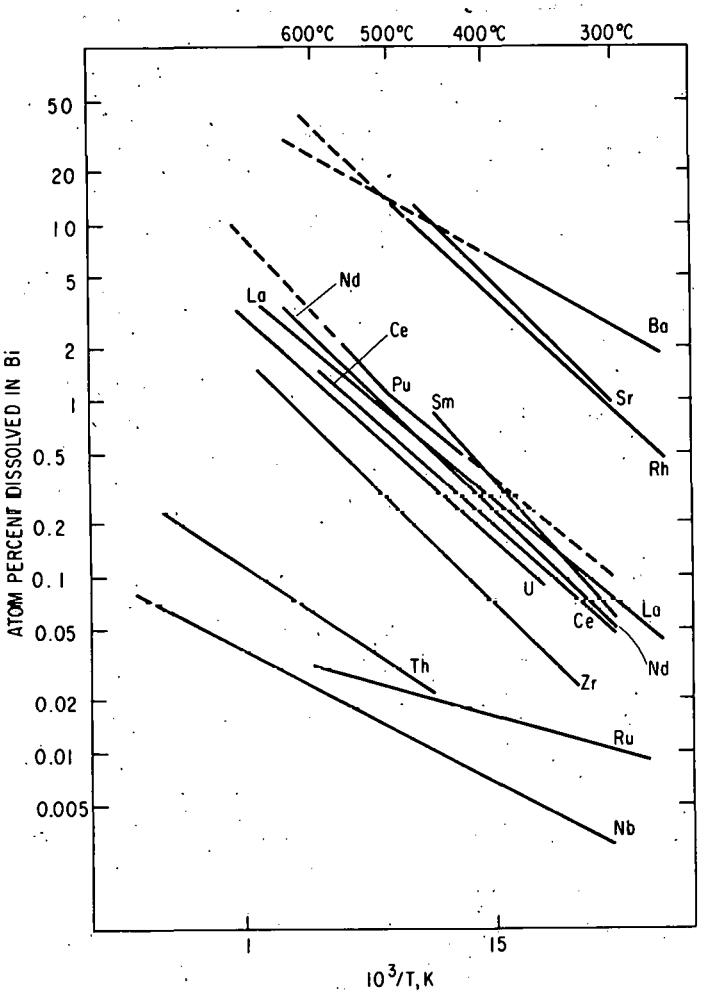

Fig. 21. Solubility of Actinides and Fission Products in Bismuth as a Function of Temperature

(1) Chemistry of the Fission Products in a Carbide Fuel

The chemical forms of the fission products in carbide fuels are not well known. Other workers have published reports describing fission product chemistry on the basis of free energies of formation and some limited experiments [FEE, HOFMAN]. In general, the non-noble metals are expected to be present as carbides (zirconium, niobium, rare earths). Some of the refractory and noble metals may be present as ternary or interstitial carbides with the actinides. These may decompose into actinide carbides and free metal. Some of the noble metals may be present in very stable intermetallics of uranium, plutonium, or thorium (e.g., URu_3). Since the chemical forms of the fission products are not established, their behavior in molten bismuth is a matter of conjecture. However, we can make some reasonable estimates based upon phase diagrams and thermochemical data.

(2) Reactions of the Lighter Fission Products

Carbides of zirconium, niobium, and yttrium (ZrC, NbC, YC) are the most stable carbides and are not expected to react with bismuth. To date, we have not found thermochemical data on any bismuth compounds of zirconium, niobium, or yttrium. These carbides are less dense than bismuth and are expected to float to the surface along with the carbon. The alkaline earth and alkali carbides are not very stable, and the alkali and alkaline earth metals are among the most soluble in bismuth. Consequently, these carbides (BaC_2, SrC_2) and metals (cesium, rubidium) in the spent fuel are expected to dissociate or dissolve in bismuth. The alkali halides, e.g., RbI, CsI, and CsBr, are not soluble in bismuth and will float along with the carbon and unreacted fission product carbides. Some interaction with metals dissolved in bismuth is possible and might reduce the concentration of alkali ions.

(3) Rare Earth Reactions and Separations

The rare earth carbides are generally dicarbides (e.g., LaC_2, SmC_2, CeC_2, NdC_2, PrC_2, and PmC_2) and are of intermediate stability. A recent report in which the bismuth compounds of cerium were studied ($CeBi_2$, Ce_3Bi_5, etc.) [BORZONE] gives the most reliable data for $CeBi_2$; ΔG_f ($CeBi_2$) is -60 kcal/mole at 600°C. This agrees well with values for $NdBi_2$, $LaBi_2$, and $PrBi_2$. Thus, the rare earth carbides can be expected to react with bismuth to form bismuthides. An estimate has been made of the density of $LnBi_2$* based on the fact that $LnBi_2$ has the same crystal structure as $PuBi_2$ (ρ = 12). These estimates suggest that the density of $CeBi_2$ and the lighter rare earth bismuthides is approximately 7 and that thus they would float on bismuth. Smith has studied the interactions of lanthanum, neodymium, and other lanthanides with thorium and bismuth, and finds intermetallics of the probable form, $ThLaBi_2$, with $\Delta G_f(ThLaBi_2)$ = -96 kcal/mole at 600°C [SMITH-1972]. If these compounds should form, they would precipitate and settle along with $ThBi_2$, $PuBi_2$, and uranium carbide. The rare earth metals are somewhat soluble in bismuth--to approximately the same extent as uranium and plutonium. Separation of the rare earths dissolved in bismuth from the plutonium dissolved in bismuth is an important part of the process which will be discussed below.

(4) Noble Metal Separations

Although rhodium is quite soluble in bismuth, ruthenium and molybdenum are almost completely insoluble. After reaction of the fuel pellets with bismuth, ruthenium and molybdenum should collect at the bottom of the bismuth dissolver with UC, $ThBi_2$, and $PuBi_2$. If the molybdenum is originally present in the fuel as Mo_2C, it will probably not react with bismuth and will float on top of the bismuth along with carbon and other unreacted fission product carbides.

The rhodium concentration in the bismuth will regularly increase with reuse, unless it is removed by reaction with zinc as proposed by Dwyer [DWYER]. If a small amount of zinc is added to the bismuth, the noble metals will react with the zinc to form intermetallics which will float

*Ln = lanthanides.

to the surface of the bismuth. The intermetallics can be skimmed off or removed by filtration. Such zinc treatment is known to remove ruthenium, rhodium, niobium, selenium, tellurium, palladium, and technetium from metallic solutions and is a common metallurgical process. Of vital importance is the behavior of the actinides in bismuth in the presence of zinc. This behavior is unknown and will have to be determined experimentally.

(5) The Use of Molten Salts

Most molten metal flow sheets use molten salts and salt transport processes to remove the rare earths and plutonium from the metal. A salt-transport process is really an oxidation-reduction reaction which adds a new metal from the salt to the original metal. The additional cost of cleaning both the metal and the salt for recycling must be offset by the added decontamination obtained by salt transport processes. When decontaminations are to be low, there may be no need for the additional and improved separations that salt processes achieve. If a system can be limited to just one metal and if the use of molten salts is avoided, the volume of wastes and the cost of recycling reagents will be much reduced.

In the initial dissolution step, it may be desirable to put an inert salt cover on the bismuth as an aid to the removal of floating solids and carbon. Some of the halides in the carbide fuel (e.g., CsI) would also be removed by the salt cover. This salt would not be expected to react with bismuth, would be part of the waste, and would not be recycled.

Bismuth is very difficult to distill (boiling point is 1560°C); consequently, it may not be practical to remove additional metals such as magnesium or lithium which have been added to bismuth during salt transfer processes.

(6) Separation and Removal of Rare Earths and Actinides from Bismuth

Instead of a salt transport process, a step in which bismuth is cooled from high temperatures (about 600°C) to lower temperatures (400 to 300°C) is proposed for removing most of the plutonium from bismuth and for separation of the rare earths. The temperature coefficients for the solubility of plutonium, uranium, and the rare earths are very similar (Fig. 21). However, if the rare earth bismuthides float (Fig. 1), they can be separated from both the liquid bismuth and the actinides which settle as $PuBi_2$ and UBi_2. (Thorium is quite insoluble in bismuth and will appear only as a trace amount.) In addition, antimony from a copper-antimony decladding process may react with the rare earths to form antimonides ($CeSb_2$, etc.) [BAYANOV] which would also float.

The heating and cooling cycle will be adequate for separating plutonium from the rare earths if there is no buildup of other metals--either from fission products or from the decladding process. After the bismuth has been used to dissolve a certain amount of fuel, it will have to be cleaned in order to remove metals such as rhodium, palladium, nickel, antimony, and cesium. If these metals are not periodically removed, they eventually will

precipitate along with the uranium and plutonium. The noble metals can be removed by zinc treatment after each cooling cycle, i.e., after most of the uranium and plutonium have been removed from the bismuth, but before it is returned to the dissolver. After zinc treatment, the bismuth is treated with CO or CO_2 to oxidize the fission products but not the bismuth. The clean bismuth is then returned to the dissolver. The bismuth need not be cleaned after each use. An estimate based on dissolving $(U_{0.8}Pu_{0.2})C$ fuel with 10% burnup indicates that after one subassembly is processed, the bismuth is not saturated with the noble metals. Some plutonium and uranium will be lost in the oxidation step, and the extent of that loss as well as the buildup of other metals in each cycle will determine the frequency of cleanup.

(7) Proposed Experiments

Many experiments will be required to test the feasibility of the flowsheets proposed for reprocessing carbides. A lists of problems to be studied is presented in Table 15. In the evaluation of any carbide flow-

Table 15. Aspects of the Reprocessing of Carbides in Bismuth to be Studied Experimentally

1. Solubility of UC, PuC, ThC, and PaC in Bismuth
   a. Kinetics of reaction of sintered pellets having various compositions, e.g., $(U_{0.8}Th_{0.2})C$, $(Th_{0.8}U_{0.2})C$, etc.
2. Behavior of Fission Products
   a. Solubility and the kinetics of reaction of ZrC, NbC, and LnC_2 in bismuth
   b. What are the densities of $LnBi_2$ (lanthanide or rare earth bismuthides)? How quickly will they rise or settle in bismuth?
   c. What is the reactivity of the antimony dissolved in bismuth with the rare earths? What is the density of the rare earth antimonides?
   d. How much of the lanthanides react with thorium (or uranium and plutonium) to produce $ThLnBi_2(s)$ in bismuth?
   e. What happens to alkali halides in bismuth?
3. Behavior of the Bismuth
   a. Does the presence of dissolved metals (especially antimony, nickel, and zinc) change the fission product solubilities or reactions in bismuth?
   b. How will the density and wettability of the bismuth change with buildup of noble metals and cladding residue in the bismuth?
4. Behavior of Zinc in Bismuth
   a. Does the zinc react with uranium and plutonium in bismuth to produce zinc intermetallics floating above the bismuth?
5. Stability of Carbides
   a. Do the more insoluble elements (chromium, molybdenum, iron, etc.) form stable carbides with carbon in bismuth at 600°C?

sheet, it will be necessary to use simulated fuel pellets which have been sintered at approximately the temperatures expected in the reactors. In addition, these simulated pellets must contain approximately 1 to 10 mole % ThC (or PuC) and some of the most abundant fission products in the expected chemical forms. The most crucial fission products include: cerium (as CeC_2), rhodium, ruthenium, molybdenum (as Mo_2C and as Mo), cesium, and zirconium (as ZrC). The behavior of PaC and PuC are unknown and must be determined. There are thermochemical data for PuC and $PuBi_2$ indicating that PuC will dissociate to $PuBi_2$, but there are no corresponding data for protactinium. The kinetics of the dissolution or dissociation of PuC and ThC are critical to the flowsheet and should be studied in one of the first experiments.

(8) Discussion

The reprocessing of spent carbide fuel by the bismuth process outlined in this report has the distinct advantage of avoiding the use of a molten salt. The waste streams are all solids, either oxides or metals and carbides that can easily be converted to oxides. The only cleanup of reagent is the cleanup of the recycled bismuth. The temperature coefficients of solubilities and densities are the keys to the flowsheet. Other advantages of bismuth are that it is one of the least corrosive and most studied metals available for molten metal processing and has the fewest container problems of the metals being proposed for use in the PDPM program.

(9) Equipment for Separation Processes

Work has continued on the design, construction, and purchase of equipment for the bismuth carbide experiments to be performed in an inert atmosphere (argon) glove box. A vacuum sampling system has been built and has been tested outside the glove box.

The safety report for the performance of experiments to determine the solubility of various carbides in bismuth is nearly completed and will be reviewed by the divisional safety committee.

b. Flowsheets Utilizing Immiscible Molten Metals and Molten Salts (Milton Ader)

A conceptual pyrochemical processing scheme employing partitions between immiscible molten cadmium and molten chloride salts has been devised for spent monocarbide fuels. By the use of cadmium (or cadmium/zinc in weight ratios of about 9/1), it is expected that most operations can be carried out below 650°C in readily fabricable container materials such as mild steels and 400-series stainless steels. The low-melting (396°C) eutectic salt composition, 50 mol % $MgCl_2$-30 mol % NaCl-20 mol % KCl, is chosen as the salt phase. Separations of actinides from fission products are achieved by volatilization of fission products, solubility differences in alloy phases, and differences in metal/salt distributions following oxidation-reduction reactions with $CdCl_2$, $MgCl_2$, or magnesium. Essentially similar processes are proposed for Pu-^{238}U, Pu-^{232}Th, and ^{233}U-^{238}U-^{232}Th fuels. Resistance to diversion is achieved by corresponding nonfissile ^{238}U or ^{232}Th with fissile ^{239}Pu or ^{233}U, and by retaining high levels of radioactive fission products in the stream containing the fissile nuclides.

The main steps of the process, as applied to (U,Pu)C, are shown in Fig. 22. Declad fuel is oxidized at about 600°C with excess $CdCl_2$ dissolved in $MgCl_2$-NaCl-KCl. The actinides, zirconium, and FP-2 and FP-3 elements are converted to chlorides, which dissolve in the salt. The elemental carbon that is formed is expected to be wet by and suspended in the salt. Gaseous FP-1 elements are volatilized, and the FP-4 (noble) metals are dissolved or suspended in the molten cadmium produced from the $CdCl_2$. To remove zirconium along with the FP-4 group, a controlled amount of cadmium-magnesium alloy is added to the salt to reduce $ZrCl_4$ to zirconium metal without reducing a significant amount of UCl_3 or $PuCl_3$. The Cd-FP-4 stream is then vacuum-retorted at about 650°C to recover cadmium, which can be recycled as $CdCl_2$ after being chlorinated at about 500°C in the presence of recycled salt.

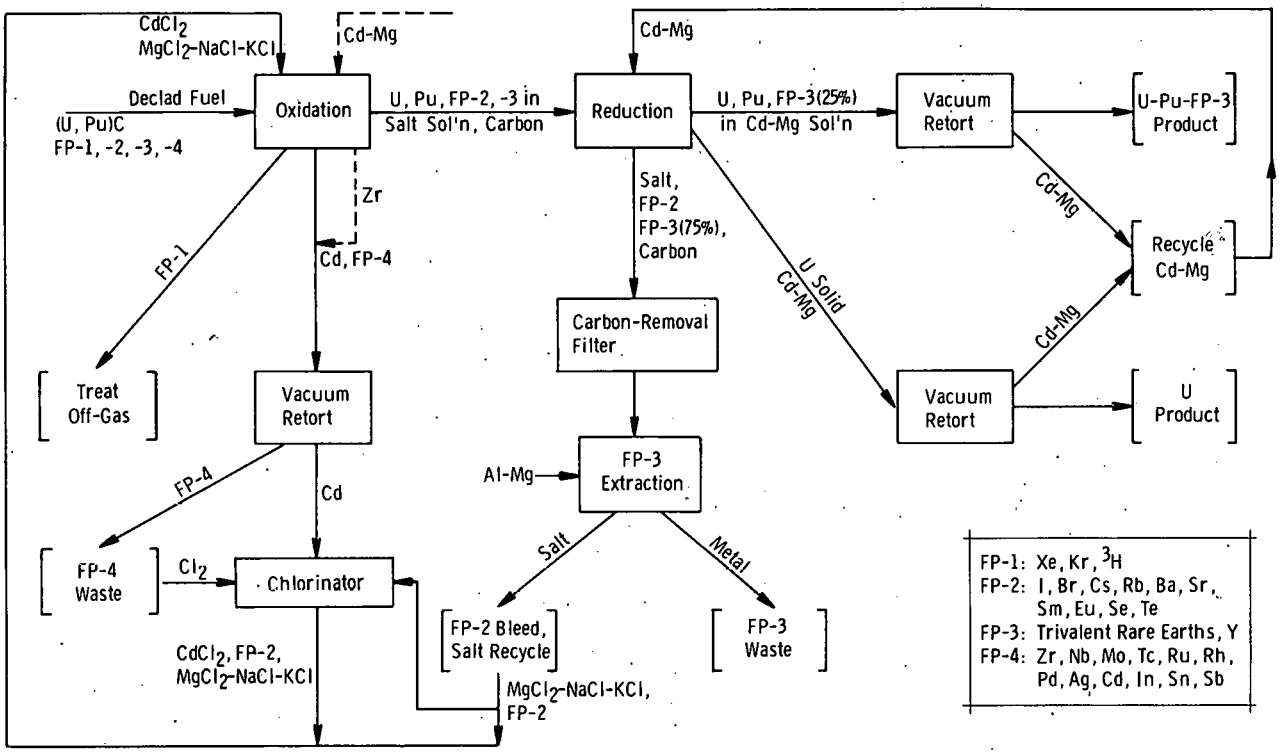

Fig. 22. Conceptual Pyrochemical Process for (U,Pu)C Fuel

Next, the salt stream containing UCl_3, $PuCl_3$, carbon, and FP-2 and FP-3 chlorides is reduced at about 550°C with cadmium-magnesium alloy. The amount of composition of the cadmium-magnesium will be such as to (a) convert all of the UCl_3 and $PuCl_3$ to uranium and plutonium metals, (b) dissolve all of the highly soluble plutonium and part of the moderately soluble uranium in the metal phase, and (c) partition the FP-3 (rare earth) elements about 3/1 in favor of the salt phase. If higher uranium solubility is required, a small amount of zinc can be added to the cadmium-magnesium without introducing serious corrosion problems. The salt phase from this step is a waste stream, but to reduce its volume, a portion is recycled as follows: First, the carbon in the salt is filtered off and the FP-3 fission products are extracted into

aluminum-magnesium, which is discarded. Then a fraction, possibly 10%, of the FP-2-containing salt is bled off and discarded; the remaining 90% is recycled to the $CdCl_2$ oxidation and cadmium chlorination steps.

The metallic phases from the reduction step consist of a cadmium-magnesium-uranium-plutonium-FP-3 solution and solid uranium. The solution can be poured off, combined with magnesium washes of the uranium solid, and retorted at 700 to 900°C to give a uranium-plutonium-FP-3 product. Similarly, the solid uranium and adhering cadmium-magnesium solvent can be retorted to give a uranium product. These products can subsequently be converted to monocarbides by procedures (not shown in Fig. 22) such as hydriding-dehydriding, followed by fluidized-bed reaction with propane. Cadmium and magnesium recovered by retorting are recycled as shown. A possible alternative to retorting of the cadmium-magnesium-uranium-plutonium-FP-3 solution is direct reaction with graphite to form a carbide solid solution. Adjustment of the metal/carbon ratio can be made later during fuel refabrication.

Similar separations are employed for thorium-containing fuels, except that the cadmium-magnesium reductant will be richer in magnesium (about 50 wt %) to render uranium insoluble. Enough cadmium-magnesium solution will be used to dissolve all of the plutonium and about one-half of the thorium. Accordingly, thorium-plutonium-FP-3 and thorium-uranium-FP-3 products will be obtained.

Initial experiments to determine the feasibility of these processing schemes will investigate the reaction of UC and ThC with $CdCl_2$. If the rate of reaction is too low, then the process is impractical. Next, experiments pertaining to the reduction step will be run to find conditions that give the desired combination of reduction, uranium or thorium solubility in cadmium-magnesium (or cadmium-zinc-magnesium), and partition between metal and salt phases.

3. Thorium-Uranium Salt Transport Processing
(Michael Krumpelt, L. J. Jardine, J. K. Bates, and T. J. Gerding)

a. "Conventional" Salt Transport Processes
(J. K. Bates)

The goal of the effort on thorium-uranium salt transport* is to consolidate and adapt previously developed reprocessing methods to meet current nonproliferation criteria which have been established for thorium-based fuels. Fuels to be considered in this program are the thorium-plutonium transmuter and the thorium-uranium breeder types and include both core and blanket elements. The goal is to develop a versatile reprocessing scheme that can be adapted to both metallic and ceramic thorium-based fuels. Oxide fuels

*In the salt transport step, the necessary separations are effected by selective transfer of various fuel constituents from an initial liquid metal donor alloy, to a molten salt transport phase, and to a final acceptor alloy.

would first be reduced and then processed as the metal; thus, any scheme presented for oxide fuels is applicable to metal fuels by omitting the reduction step. Such a process must also be developed under the constraints that it be proliferation-resistant (which requires coprocessed product streams), and that it be diversion resistant (which necessitates both a fission product spike of each stream and remote handling methods).

The flowsheet (Fig. 23), a modification of the salt transport scheme presented in [STEINDLER-1978C, Fig. 38], describes a reprocessing scheme designed to meet the above requirements and is based mainly on work done at Argonne National Laboratory, Ames Laboratory, ISPRA, and Atomics International. The major areas of the flowsheet are (1) decladding, (2) reduction and separation of uranium from plutonium, and (3) plutonium/thorium recovery. The main separation is based on solubility differences of uranium, thorium, and plutonium in magnesium-based alloys. Essentially, solubility offers a method of separating uranium from plutonium.

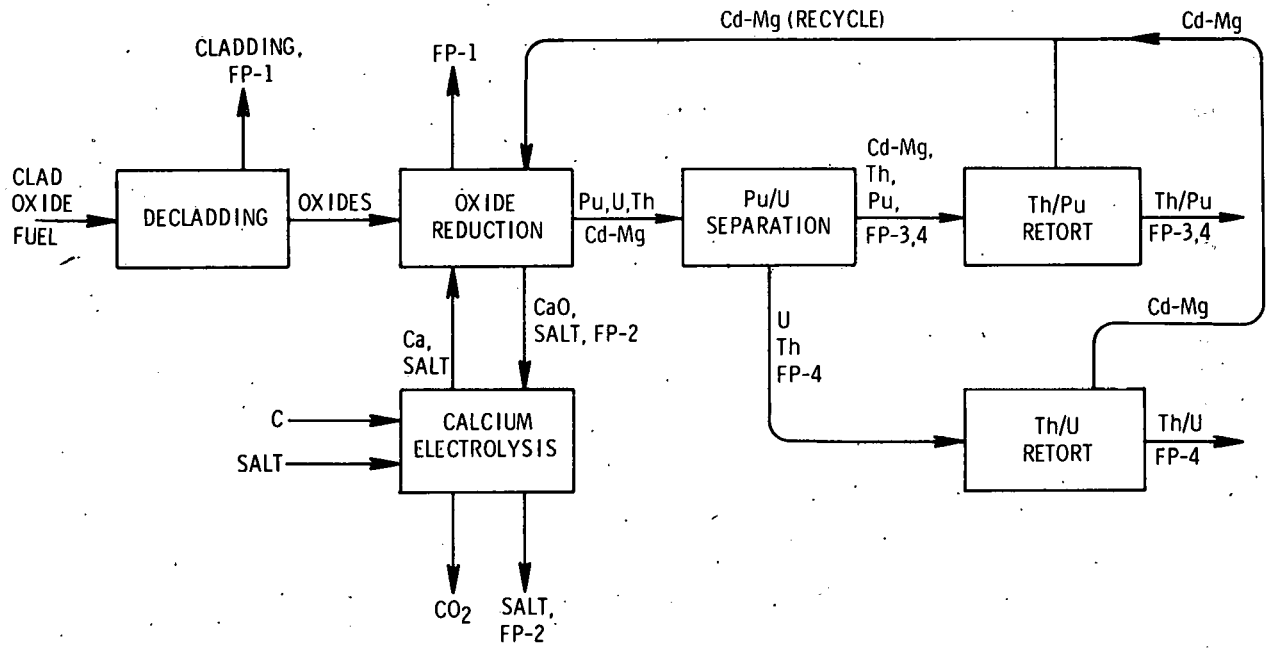

Fig. 23. Flowsheet for Reprocessing Thorium/Plutonium-Based or Thorium/Uranium-Based Fuels. See Fig. 22 for elemental compositions of FP-1, FP-2, FP-3, and FP-4

In an ideal donor alloy, uranium would have a very low solubility and plutonium a high solubility, with the thorium solubility adjustable and intermediate between those of uranium and plutonium. Additionally, the alloy must be compatible with other process steps, including reduction and retorting. Five metals and alloys for which solubility data are available have been considered as donors. These are magnesium, cadmium-magnesium, zinc-magnesium, copper-magnesium, and bismuth-magnesium. Copper-magnesium and bismuth-magnesium are unacceptable due to the high retorting temperatures that would be required, and zinc-magnesium is unacceptable because it has a

relatively large uranium solubility. The solubilities of thorium, uranium, and plutonium in cadmium-magnesium and magnesium are presented in Fig. 24. Initially, 50 wt % cadmium-50 wt % magnesium has been chosen as the alloy because it has a larger range of thorium solubilities than does magnesium, and may add an additional driving force in the reduction step due to intermetallic formation.

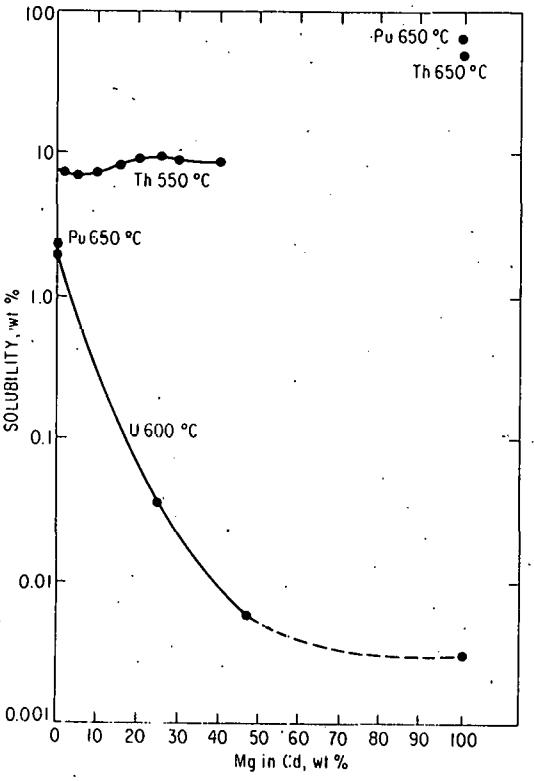

Fig. 24.

Solubilities of Thorium, Plutonium, and Uranium in Cadmium-Magnesium

It being assumed that decladding is accomplished by a satisfactory method, the oxide fuel would next be reduced. The proposed method is to use calcium (a stoichiometric amount) in cadmium-magnesium, with a cover salt of $CaCl_2$-5 at. % CaF_2-10 at. % $MgCl_2$. Results [AMECKE] indicate that thoria reduction with calcium in copper-magnesium proceeds faster than does reduction with just zinc-magnesium. The cover salt serves to reduce the amount of cadmium vapor present, to extract the CaO produced during reduction, to act as a medium for subsequent electrolysis of CaO to regenerate the calcium, to take up the FP-2 elements, and to extract 75% of the FP-3 elements. The salt represents the only waste stream in the process, but it need not be renewed every batch extraction because the CaO is removed by electrolysis and the FP-3 elements are transferred to a zinc-magnesium acceptor alloy. The $MgCl_2$ concentration in the salt and the composition of the acceptor alloy are chosen so that only 75% of the FP-3 can be removed from the process stream. It will be necessary to have a salt bleed to prevent FP-2 buildup in the salt unless another method of FP-2 control can be developed.

During the reduction, uranium is precipitated together with FP-4 and a selected amount of thorium. Thorium precipitation is controlled by the composition and amount of cadmium-magnesium alloy. After precipitation, the salt and the reduction alloy are separately transferred from the solid, which is then retorted to remove any residual alloy.

One problem always associated with precipitation processes is liquid-solid separation. In the present process, it is proposed that the reduction, the precipitation, and the separation occur in the same vessel. This could be accomplished and has been partially demonstrated [CHILTON], using a crucible-within-a-crucible technique. During the reduction step, the inner crucible contains the oxide, and both crucibles are filled with reduction alloy and covered with salt. The metals that precipitate during reduction are contained in the inner crucible. The salt and reduction alloy are removed by pressure siphoning, and the inner crucible containing the thorium/uranium/FP-4 is removed for final product recovery.

After the reduction/precipitation step, thorium/uranium/FP-4 have been isolated, FP-1, -2, and 75% of the FP-3 have been removed in the salt, and plutonium/thorium/FP-3,4 remain in the alloy. The plutonium/thorium/FP-3,4 are recovered from the alloy by retorting, and the cadmium-magnesium is recycled to the reduction step.

The recovery of plutonium/thorium/FP-3,4 may also be accomplished using a hydriding step. The feasibility of this process was recently reviewed, and the results are summarized here. The rare earth and actinide hydrides generally are classified as metallic hydrides and can be formed exothermically by direct contact of metal and hydrogen gas. These compounds are generally designated as dihydrides, although in most cases the compounds are not stoichiometric and their formulas are indefinite. From a process standpoint, the goal would be to precipitate a stable hydride from a liquid metal solvent by contacting the solution with hydrogen. The ideal solvent would be an alloy that is unreactive toward hydrogen and has a relatively low melting point because hydride stability decreases with temperature.

The degree of hydride formation will depend on ΔG° for the reaction

$$M(s) + H_{2(g)} \rightarrow MH_2(s)$$

Factors that will affect the reaction free energy are the temperature, the hydrogen pressure, and metal activity in solution. The relationship between temperature and hydrogen pressure for hydride formation is shown in Fig. 25. Below the line for each metal, the hydride will dissociate; and above the line, the hydride is stable.

Hydriding is proposed as a method of recovering thorium from either a cadmium-magnesium or copper-magnesium donor alloy and of recovering plutonium from a zinc-magnesium acceptor alloy. With a donor alloy, ThH_2 is predicted to precipitate together with some refractory (i.e., zirconium) metal hydrides. Separation of thorium from the alloy, noble metals, and some refractory metals would be achieved. If an acceptor alloy is used, PuH_2

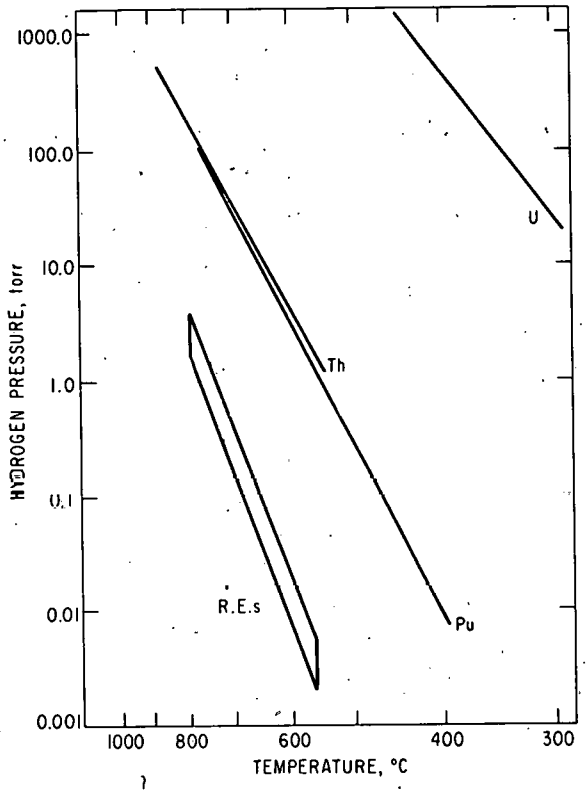

Fig. 25.

Dissociation Pressures of Metal Hydrides. 1 torr = 0.133 kPa

together with the rare earth hydrides should precipitate if the a_{Pu} is large enough. Hydriding of thorium and plutonium under various conditions has been verified [CHIOTTI; CHILTON; LAWROSKI-1962, p. 50]. The data suggest that both ThH_2 and PuH_2 can be separated from magnesium and magnesium-based alloys. However, complicating factors exist for each process.

In thorium separation, ZrH_2 and possibly other refractory metal hydrides would coprecipitate with ThH_2. However, density variations should permit further separation. In either a cadmium-magnesium or a copper-magnesium alloy with a density of about 6 to 7, ThH_2 should settle in the alloy while the refractory metal hydrides should remain on the surface. The ThH_2 can then be separated and either heated under vacuum to yield thorium metal or oxidized to form thoria.

A problem with the plutonium separation can be predicted from the data in Fig. 25. Thermodynamic data indicate that when a solution containing plutonium and the rare earths is hydrided at 700 to 750°C with a hydrogen pressure of 0.665 to 1.33 kPa (5 to 10 torr), the rare earth hydrides should be stable while PuH_2 should be unstable. The precipitated rare earth hydrides could be removed and then PuH_2 precipitated at higher hydrogen pressures. In practice, such a procedure may not work since the reaction kinetics at low hydrogen pressures are not established and careful control of the hydrogen pressure would be necessary.

The advantages to metal recovery through hydriding are the simplicity of the operation and the small amounts of wastes generated. The drawbacks are obvious--hydrogen, ThH_2, and PuH_2 present potential safety

hazards. The metal hydrides are pyrophoric, and hydrogen in concentrations of 4.1% to 74.2% by volume in air forms an explosive mixture. Although full-scale hydriding of liquid metal solutions has not been demonstrated, two reports [DeGRAZIO, CHILTON] contain useful information.

For plutonium recovery, Rocky Flats [DeGRAZIO] has developed a method involving hydriding of solids. The method has been used to recover plutonium from (a) reusable equipment, (b) plutonium scrap, (c) plutonium-coated tools, and (d) plutonium melts from tantalum and tungsten crucibles. The process involves combining hydrogen 66.5 kPa (500 torr) with plutonium at about 400°C and has been operational for several years.

The second report [CHILTON] describes a series of experiments done to demonstrate the feasibility of thorium-uranium reprocessing using uranium precipitation and thorium hydriding. As described in this report, ThH_2 was recovered (101.3 kPa H_2), as was predicted by [CHIOTTI-1964], although the fission product distribution in irradiated samples was not reproducible.

To further evaluate the hydriding alternative, the reaction kinetics should be studied as a function of temperature, hydrogen pressure, and alloy compositions.

As a summary of the entire thorium fuel reprocessing scheme, the location of each fuel constituent and the control which can be exercised over it during the process are listed below.

FP-1 elements - are removed during decladding and reduction and are treated as off-gases.

FP-2 elements - are removed during the reduction step by extraction into the salt phase. There will be accumulation of FP-2 in the salt, which will be controlled by a continuous salt bleed. For processing of 1000 kg of fuel, 2000 kg of salt is required. To keep a constant level of 10% FP-2 in the salt, a bleed of 200 kg of salt per batch is necessary.

FP-3 elements - are soluble (about 15%) in Cd-50 wt % Mg and are removed by selective extraction into the salt during reduction. This is a salt transport step and is used as a method of controlling the FP-3 concentration in the process stream and of consolidating the FP-3 for waste handling. A nominal amount of FP-3 remains in the plutonium/thorium stream for diversion resistance.

FP-4 elements - are slightly soluble (<1%) in Cd-50 wt % Mg, and thus will partition between the plutonium/thorium and uranium/thorium streams. The process offers no method of FP-4 removal, and presumably an unwanted increase in these products would occur if the fuel were to be recycled. This problem should not exist for the thorium/plutonium transmuter fuel since it is not recycled. However, to separate thorium/plutonium from FP-4, either a hydriding or redox step could be added--during either reprocessing or refabrication.

Uranium - is very insoluble in the alloy chosen for reduction, and less than 0.1% of the uranium in the fuel will be in the plutonium stream. Uranium does not transfer into the salt either, and so total uranium losses will be negligible.

Plutonium - is very soluble in the cadmium-magnesium alloy; only through coprecipitation will any be lost to the uranium stream. There will be some plutonium loss during FP-3 extraction, but the loss should be less than 0.4 % with proper choice of alloy and salt.

Thorium - will not be transported in the salt and will be partitioned by solubility equally between the plutonium and uranium streams.

The flowsheet is based on established solubility and distribution data and has been tested, in part, at a limited process level [CHILTON]. The following additional information is required to refine process parameters:

(a) Solubility of thorium in cadmium-magnesium. It is necessary to establish thorium solubility in 40 to 100 wt % magnesium at various possible operating temperatures.

(b) Reduction of ThO_2 and UO_2 fuels. The rate of reduction of ThO_2 by calcium needs to be determined in relation to temperature, stirring rate, calcium loading, salt and alloy composition, and fuel type.

(c) FP-4 solubility and coprecipitation during the reduction step.

(d) Coprecipitation of plutonium with uranium/thorium during the reduction step.

(e) Demonstration of liquid-solid separation.

(f) Distribution measurements to determine the proper conditions for FP-3 removal.

To assess the practicality of the reference flowsheet, experiments are planned to examine each of the above points, with initial emphasis on thorium solubility in cadmium-magnesium alloy and thoria reduction rate.

b. Waste Stream Analysis--Accumulation of CaO in Molten Salt
(L. J. Jardine and T. J. Gerding)

Several flowsheets under development in the PDPM Program for reprocessing oxide fuels employ a reduction step utilizing calcium metal, together with a metal alloy (i.e., cadmium-magnesium, zinc-magnesium, copper-magnesium) and a cover salt containing $CaCl_2$. The basic reduction in the flowsheets is of the type

$$MO_2 \text{ (alloy/salt)} + 2Ca \text{ (salt/alloy)} \rightarrow 2CaO \text{ (salt)} + M \text{ (alloy)} \qquad (1)$$

where M = uranium, thorium, plutonium, etc. One of the reduction reaction products, CaO, concentrates in the $CaCl_2$ cover salt because of the high (about 18 mol % at 835°C) CaO solubility in $CaCl_2$. In many flowsheets, calcium fluoride is typically added to the $CaCl_2$ salt to (a) lower the melting point of the cover salt and (b) increase the wetting of the oxide fuel by the molten alloy and salt during the reduction.

Periodically, when the cover salt becomes saturated with CaO, it must be purified of CaO or discarded as a waste. Howeverr, since the alkali and alkaline earth fission products (i.e., FP-2 group) and perhaps also iodine are collected in the cover salt during the reduction, the salt must be classified as a high-level radioactive waste if discarded. This form of solid waste is highly dispersible by either aeolian or hydraulic means and will probably require further processing to satisfy future waste management criteria for waste forms.

The reduction portion of a flowsheet is shown in Fig. 26 with the estimated mass balances for Eq. 1. The initial objective of this task is to examine concepts for reducing the waste volumes associated with the reduction step. Three alternatives for handling the salt streams containing the

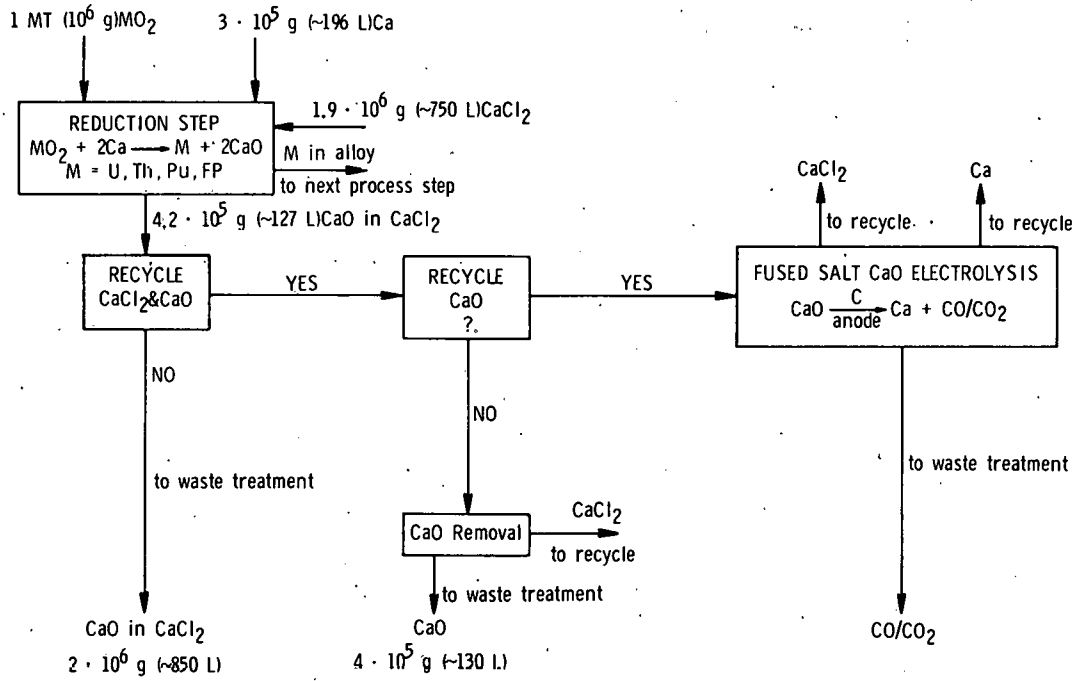

Fig. 26. Alternatives for Removing CaO from the Major Waste Streams Originating in the Reduction of Oxide Fuels with Calcium

reduction product are shown in Fig. 26. If the option of discarding the entire salt stream of CaO dissolved in $CaCl_2$ is elected, the estimated volume of the solid waste is about 850 L per metric ton of fuel reduced. This volume may be compared with the volume of the high level waste from the Purex process--40 L per metric ton of fuel processed if handled as a solid calcine waste or 70 L if converted into a glass waste form [JARDINE]. Thus, this alternative is not very desirable if employed for pyro flowsheets, since the waste volume generated for this single process step would be an order of magnitude larger than for a Purex flowsheet.

Essentially two other basic alternatives for handling this salt waste stream are denoted in Fig. 26. One is to physically or chemically remove (i.e., separate from the chloride salt by some method, e.g., by filtration/settling) all CaO as a solid waste, ideally permitting total recycle of the $CaCl_2$. If such a method could be developed, the volume of solid CaO is estimated as 130 L per metric ton of fuel reduced. This volume, however, also is larger than the volume of high level waste from the Purex flowsheet.

Another alternative, the most appealing, is recycle of all of the $CaCl_2$ and all CaO by converting the CaO back to calcium metal. Such a process would eliminate a large solid waste volume of CaO and also reduce the requirement for calcium chloride.

A method of achieving recycling is based on the fused salt ($CaCl_2$) electrolysis of CaO. The cathode reaction generates calcium metal for recycle. The anode reaction, if carbon is used, yields oxygen which reacts *in situ* with the anode to generate CO/CO_2. The net electrolysis cell reaction is:

$$CaO\ (salt) + C\ (anode) \rightarrow Ca\ (salt/alloy)_{cathode} + CO\ (g) \qquad (2)$$

This cell reaction regenerates calcium metal for recycle to the reduction vessel and essentially removes the oxygen from oxidic fuels as CO/CO_2 which can be scrubbed and cleaned for release as a common gas--not as a large volume of solid waste. Chlorine is not generated with this cell as would be the case if $CaCl_2$ were electrolyzed; this should reduce some of the concern about acceptable materials of construction.

This concept was demonstrated on a laboratory scale [THREADGILL]. In that work, gram-size quantities of calcium metal were successfully produced by electrolysis of fused $CaCl_2$ containing 0.3 to 2 wt % CaO at 786 to 816°C. Current densities of about 30 to 50 A/cm^2 were used with a graphite anode. No chlorine was detected from the anode (checked qualitatively only), which indicated that the CaO was being electrolyzed rather than $CaCl_2$.

For electrolysis, the following relation holds:

$$m = \frac{i\ t}{n\ F} \qquad (3)$$

where m = mass of element electrolyzed, mol
i = current into the cell, A
t = duration of cell operation, s
n = charge number, equiv/mol (2 for calcium)
F = Faraday constant, 96 496 coulombs/equiv.

The current, i, is the integrated current density times the electrode surface area.

From this equation, it may be calculated that for a current density of 30 A/cm^2 and an electrode area of 929 cm^2 (1 ft^2), approximately 14 h would be required to generate 3 x 10^5 g calcium (the amount required to reduce one metric ton of UO_2) at 100% cell efficiency. For a higher current density or larger surface area, the time to produce the required amount of calcium would be correspondingly less.

These ranges of current densities, electrode surface areas, and time requirements appear to be within a practical range. It is concluded that this concept has the potential for production-scale operation and merits further laboratory-scale examination.

A small laboratory-scale cell is being designed and an inert-atmosphere glove box readied for verifying the feasibility of the concept. This initial cell design will attempt to use a molten metal cathode (cadmium), which will also serve to collect the calcium metal reduction product. Such an alloy (cadmium-calcium) could be bled off and used in the reduction step of a typical pyrochemical flowsheet, thereby avoiding the need for physical recovery of the solid calcium metal for recycle. The graphite anode will be consumed during operation of the cell.

Experiments are being planned to examine the sensitivity of the variables in cell operation. Variables under consideration are electrolyte composition (e.g., effect of CaF_2 and CaO concentrations in $CaCl_2$), current density, electrode configuration, and cell temperature. A concept for the direct electrolytic dissolution of oxide fuels based on the above principles is also being examined.

4. U-Pu Salt Transport Processing
(J. Knighton,* C. Baldwin,* W. Averill,* M. Boyle,* T. Santa Cruz,* A. Younger,* and J. Zoellner*)

a. Introduction

The purpose of this work package is to develop pyrochemical processes and associated hardware to coprocess uranium and plutonium contained in spent LWR and FBR reactor fuels. The primary objective is to develop a process capable of producing a proliferation-resistant product suitable for reactor use. This proliferation resistance can be accomplished by coprocessing and/or by producing fission product-contaminated plutonium. In addition, waste management of products and by-products, for both interim and ultimate disposal, will be explored.

*Rockwell International-Atomics International.

The technical goals of this work package are (1) to develop a viable flowsheet for producing by pyrochemical means a proliferation-resistant product suitable for reactor use--either through coprocessing or producing a partially decontaminated plutonium product, (2) to identify key problems and conduct early proof-of-principle experiments on key problems that challenge the feasibility of the flowsheet, (3) to prepare a process description and design criteria for a conceptual Pyrochemical Processing Facility (PPF), and (4) to evaluate containment of fission products and management of waste products.

b. Engineering Analysis

During the third quarter of FY 1978, three pyrochemical process flowsheets for processing spent LWR and FBR fuels were selected for consideration. A matrix was constructed to identify the processing options being examined (see Table 16). Thus far, material balances have been completed around three of the process options.

Table 16. Matrix of Fuel Types and Pyrochemical Options. The numbers shown in the matrix indicate the order in which we will evaluate the options.

Fuel	Coprocessing by Pyroredox	Coprocessing by Salt Transport	U-Pu Separation by Salt Transport
LWR	7	6	8
FBR Core and Axial Blanket	4	1	2
FBR Radial Blanket	9	3	5

Efforts have also been devoted to abstracting the literature for the various steps in the overall U-Pu salt transport processing operation. In addition, reference LWR and FBR spent fuel elements were selected to facilitate material balance calculations being conducted around selected flowsheet options. The free energies of formation for the common oxides, fluorides, and chlorides of the elements were tabulated, as well as the vapor pressures of most elements. The areas investigated thus far are summarized below:

(1) Process Evaluation

Three pyrochemical processes are being considered for the processing of LWR and FBR fuels. In the first process (Fig. 27), the salt transport process is used to coprocess the uranium and plutonium. In the second process (Fig. 28), the pyroredox process is used for the coprocessing of uranium and plutonium. These two processes are applicable to LWR, FBR core and associated axial blanket, and FBR radial blanket fuel. Proliferation and diversion resistance is provided by coprocessing. In the third process (Fig. 29), another salt transport process, uranium and plutonium are separated. This process is likewise applicable to the LWR, FBR core and associated axial blanket, and FBR radial blanket fuel.

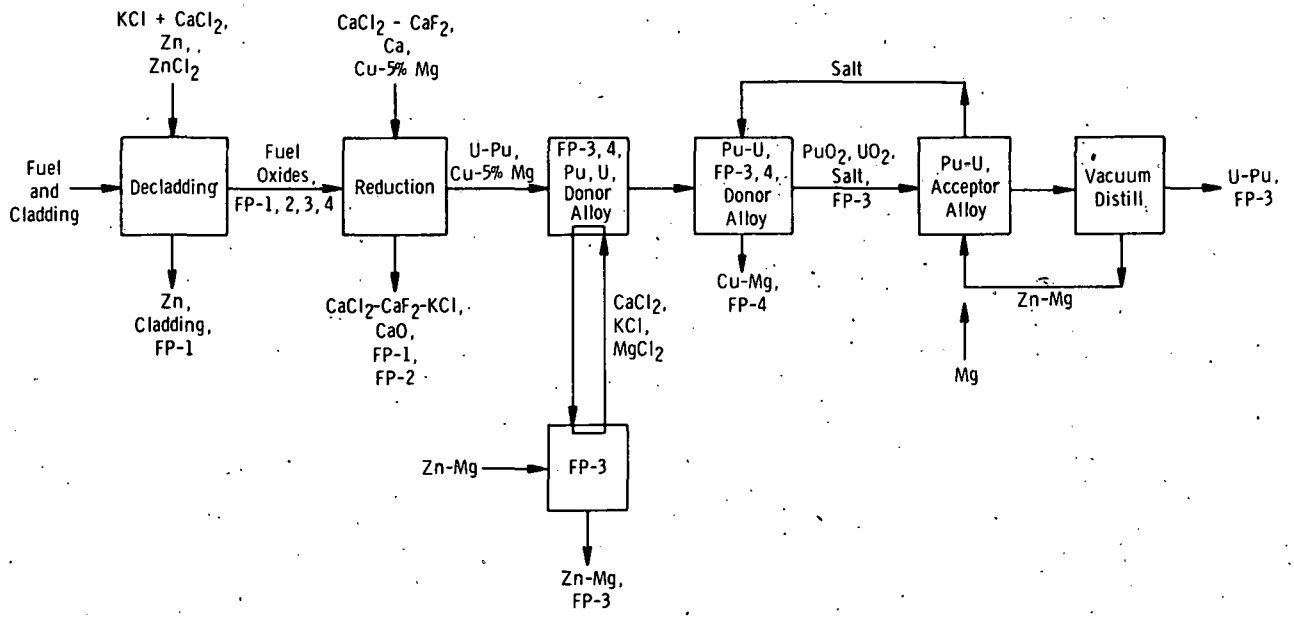

Fig. 27. Coprocessing of Uranium Oxide and Plutonium Oxide by the Salt Transport Process. See text for elements in FPs.

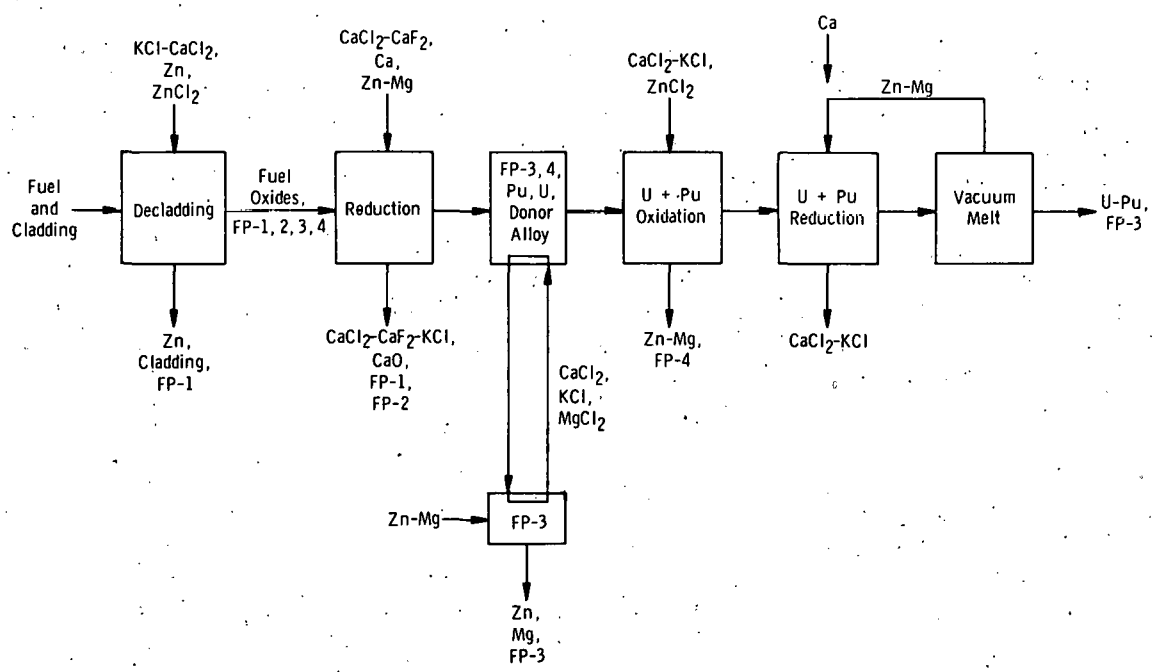

Fig. 28. Coprocessing of Uranium and Plutonium by Pyroredox Process

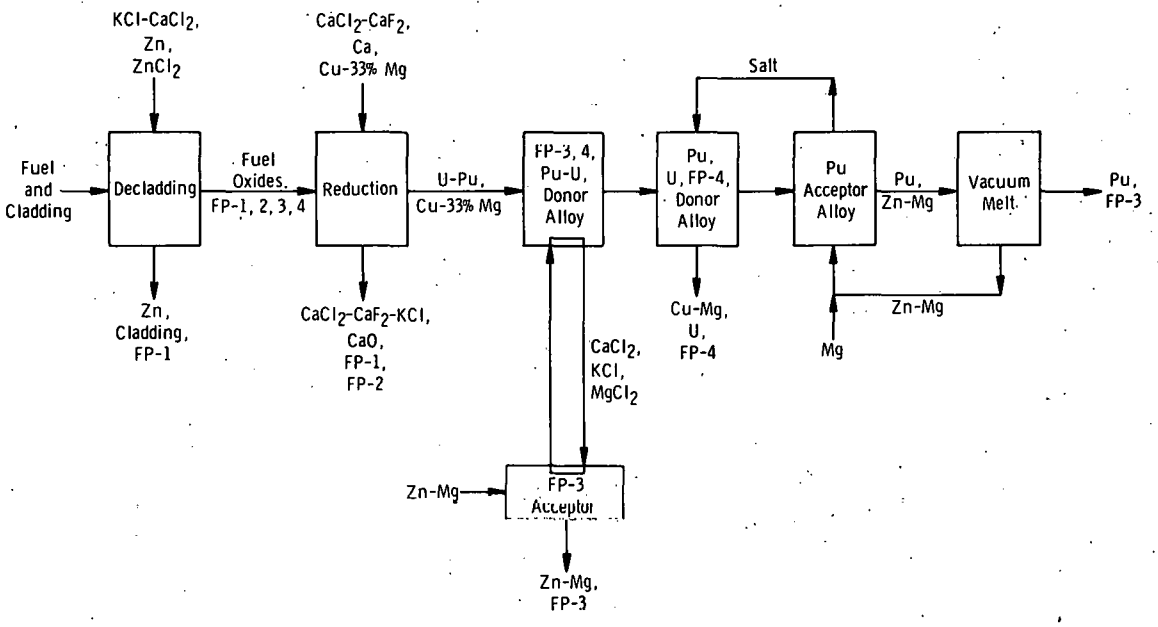

Fig. 29. Plutonium Separation from Uranium by the Salt Transport Process

For convenience, the fission product elements are divided into four groups: FP-1, FP-2, FP-3, and FP-4. Elements in each group have a similar behavior in the process.

FP-1 fission products are volatile and consist of tritium, Xe, and Kr. FP-2 fission products are I, Br, Cs, Rb, Ba, Sr, Sm, Eu, Se, and Te. FP-3 fission products are the rare earth elements that form +3 chlorides--Y, La, Ce, Pr, Nd, Pm, Gd, and Tb. FP-4 fission products are refractory and noble metal elements--Zr, Nb, Mo, Tc, Ru, Rh, Pd, Ag, Cd, In, Sn, and Sb.

In all three processes, diversion and proliferation-resistance is enhanced by incomplete removal of the rare earth (FP-3) fission products. If incomplete removal of the FP-3 fission products is considered an adequate diversion- and proliferation-resistant feature, LWR fuel, FBR core and associated axial blanket fuel, and FBR radial blanket fuel can also be processed by the third process.

Coprocessing by Salt Transport: After the cladding material, FP-1, FP-2, and part of the FP-3 have been removed, uranium and plutonium in the donor alloy are oxidized by magnesium chloride and are taken up by a salt which is transported to an acceptor alloy. The FP-4 elements remain in the donor alloy. The actinides are reduced by magnesium and taken up by the acceptor alloy.

Uranium-Plutonium Separation by Salt Transport. After the cladding FP-1, FP-2, and part of the FP-3 have been removed and with the proper donor alloy, plutonium is selectively oxidized by magnesium chloride, leaving uranium and the FP-4 elements in the donor alloy. The resultant

plutonium chloride is taken up by a salt which is transported to an acceptor alloy (Zn-Mg) where the plutonium is reduced by magnesium and taken up by the acceptor alloy. The uranium and FP-4 fission products (contained in the donor alloy) can be stored with uranium recovery deferred. Residual FP-3 elements will accompany the plutonium for proliferation resistance and diversion resistance.

Coprocessing by Pyroredox. After the cladding, FP-1, FP-2, and part of the FP-3 have been removed, uranium and plutonium are oxidized by zinc chloride. The resultant actinide chlorides are taken into a salt phase, which is then separated from the zinc-solvent metal and FP-4 alloy. After the separation, they are reduced by calcium and taken up into a volatile solvent metal phase.

The volatile solvent metals are removed from the actinide by vacuum melting and may be recycled.

The final phase of the process is to convert the actinide metal into products (metal, oxide, carbide) suitable for refabrication.

Oxide conversion can be initially accomplished by burning metal or by hydriding metal followed by oxidation. Further treatment may be necessary to produce a physically compatible product for fuel fabrication.

Methods for conversion to carbides and nitrides will be evaluated in this program.

The matrix given in Table 16 depicts the three processing options for pyrochemical processing of LWR and FBR core and blanket fuel. The numbers shown in the matrix indicate the order in which we will evaluate the options. Coprocessing of FBR radial fuel may not be an attractive option because a high plutonium enrichment is required in core fuel.

The output from our evaluation studies will (a) provide a basis for selection of a reference flowsheet and (b) identify key problems which challenge the feasibility of the process. In these evaluation studies, we will (a) prepare a process description, (b) conduct a material balance around each operation, (c) determine the process size for each operation, (d) identify peripheral operations, (e) identify problem areas for each operation, and (f) structure an experimental program.

The following material balances should not be considered final and complete. The balances around the uranium-plutonium coprocessing of LMFBR core fuel by the Salt Transport Method, for example, did not rely on the ORIGEN code for input, as do the following process option evaluations. By the use of the ORIGEN code and a computer model being generated, all calculations will be refined. The initial process evaluation material balance calculations were necessary, however, (a) to provide the technical basis for developing the computer model, (b) to define key problems that challenge the feasibility of the process, and (c) to establish process volumes for determining full-scale crucible development requirements.

(2) Process Evaluation of Coprocessing of Uranium and Plutonium from FBR Core Fuel by the Salt Transport Method

To provide a basis for a process evaluation, the core fuel subassembly [AI, Vol. IV] was selected as the reference FBR fuel. This selection is tentative, and a new reference FBR fuel will be selected when firm designs are established for FBR fuels. We do not anticipate major problems in updating the process to accommodate changes in FBR fuel designs.

During this report period, the process evaluation of coprocessing uranium and plutonium from FBR core fuel by the salt transport method was started. Ground rules established for this study include: (a) coprocessing of uranium and plutonium from FBR core fuel, including axial blanket, to enhance proliferation resistance, (b) plutonium content of at least 20% in the plutonium-uranium product for recycle to the FBR core, (c) 75% removal of rare earth (FP-3) fission products, (d) retention of 25% of FP-3 elements with the plutonium-uranium product to enhance diversion resistance, (e) near-quantitative removal of the other fission products (FP-1, FP-2, and FP-4), (f) 99+% plutonium recovery, and (g) 95+% uranium recovery. A preliminary material balance has been conducted on each major process operation. From these preliminary material balance calculations, the size and composition of each feed and product stream are determined (Fig. 30), the process stream volumes are estimated, and the fission product heating associated with each process product is estimated (Table 17).

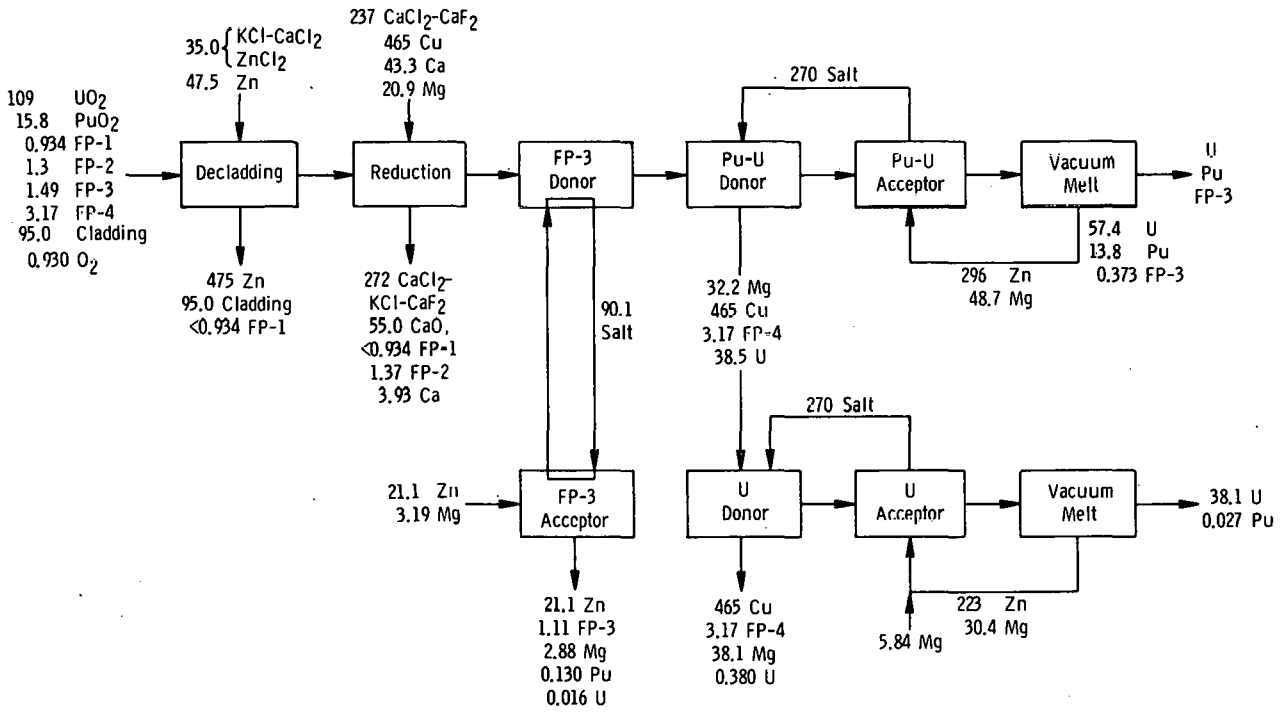

Fig. 30. Material Balance for the Salt Transport Process for Coprocessing Uranium and Plutonium Oxide FBR Core and Axial Blanket. All numbers indicate kilograms.

Table 17. Fission Product Loadings and Power Densities after Coprocessing Uranium and Plutonium from One Reference FBR Core Fuel Subassembly (based on 10% burnup and 30-day cooling)

Assumptions

1. 100% FP-1 removal
2. 100% of FP-2 in the reduction salt
3. 75% of FP-3 to FP-3 acceptor, 25% to U-Pu acceptor
4. 100% of FP-4 to Cu-Mg donor

Process Stream	Total wt, kg	FP Stream	FP, kg	Stream Vol. (STP),[a] L	Fission Product Power Density, W/kg	Total W	Power Density,[a] W/L
Volatiles	0.934	FP-1	0.934	161.55	63.96	59.74	0.370
Zn and Cladding	516.0	--	--	70.70	--	--	--
Calcium Reduction Salt	332.642	FP-2	1.368	146.29	1224.85	1675.59	11.45
FP-3 Acceptor	115.42	FP-3	1.118	4.82	4598.79	5141.45	1066.69
U + Pu Donor (spent) (after 7th pass)	541.81	FP-4	3.171	73.30	3723.56	11807.41	161.08
U + Pu Acceptor	416.22	FP-3	0.373	73.24	4598.79	1715.35	23.42
U Donor (spent)	506.348	--	--	75.43	--	--	--
U Acceptor	291.500	--	--	50.72	--	--	--

[a]Does not consider recycle of process solvents.

Assumptions

Ten percent burnup of FBR core fuel; 30 day cooling.

Pu breeding ratio in core fuel (core + axial blanket) = 1.0.

Feed to the Process

One core subassembly [AI, Vol IV, p. 97]

Cladding

95 kg 316 stainless steel associated with the fuel section.

Irradiated Fuel

Mixed oxides-UO_2, PuO_2, oxides of fission products (FP) = 132.5 kg.

UO_2 (U)	108.81 kg (95.91 kg)
PuO_2 (Pu)	15.80 kg (13.93 kg)
O_2 (as UO_2 and PuO_2)	14.77 kg
O_2 (as FPO_2)	0.93 kg
FP	6.964 kg

Fission Product Weight, kg/subassembly

FP-1	0.934
FP-2	1.368
FP-3	1.491
FP-4	3.171
Total	6.964

This material balance calculation will be updated in the near future, using the fuel description from the ORIGEN code.

(3) Process Evaluation of Coprocessing of Uranium and Plutonium from FBR Radial Blanket Fuel by the Salt Transport Method

Ground rules for coprocessing FBR radial blanket fuel are: (a) coprocessing uranium and plutonium from FBR radial blanket fuel, (b) plutonium content of at least 20% in plutonium-uranium product for recycle to the FBR core, (c) FP-3 elements will follow plutonium through the process, (d) near-quantitative removal of the other fission products (FP-1, FP-2, and FP-4), (e) 99+% plutonium recovery, and (f) 95+% uranium recovery.

A preliminary material balance was made on each major process operation. From these preliminary material balance calculations, the size and composition of each feed and product stream were determined (Fig. 31), the process volumes were estimated, and the fission product heating associated with each process product was estimated (Table 18).

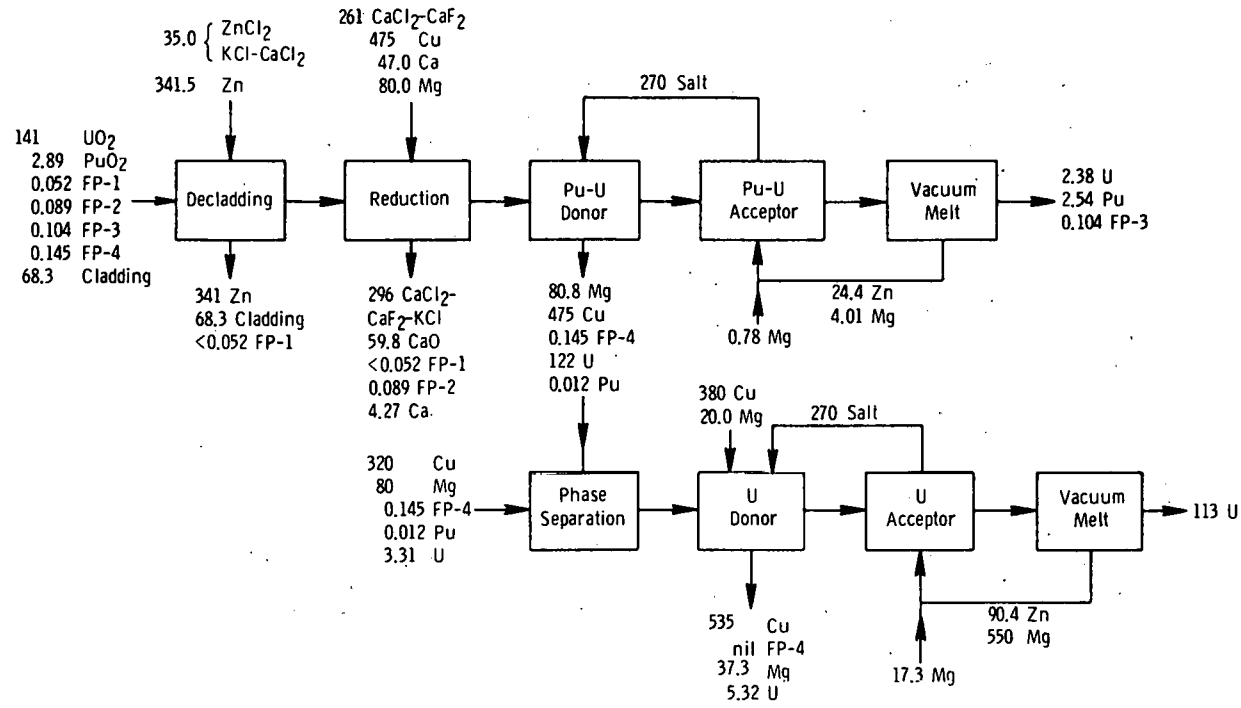

Fig. 31. Conceptual Process for Coprocessing UO_2-PuO_2 FBR Radial Blanket. All numbers indicate kilograms.

Feed to the Process

One radial blanket subassembly [AI, Vol. IX, p. 97] which contains:

Cladding

68.3 kg 316 stainless steel associated with active section.

Active Section

Mixed oxides (UO_2, PuO_2, and oxides of fission products = 144 kg).

UO_2	140.69 kg (124.014 kg U)
PuO_2	2.89 kg (2.550 kg Pu)
O_2 (as UO_2 amd PuO_2)	17.064 kg
FP	0.390 kg

Table 18. Fission Product Loadings and Power Densities after Coprocessing Uranium and Plutonium from FBR Radial Blanket Fuel by the Salt Transport Method (based on 10% burnup and 30-day cooling)

Process Stream	Total wt, kg	FP Stream	FP, kg	Stream Vol. (STP),[a] L	Fission Product Power Density,[b] W/kg	Total W	Power Density,[a] W/L
Volatiles	0.052	FP-1	0.052	9.0	63.96	3.326	0.37
Zn and Cladding	341.50	--	--	46.78	--	--	--
Calcium Reduction Salt	360.04	FP-2	0.089	40.35	1224.85	109.01	2.70
U + Pu Donor (spent)	403.90	FP-4	0.145	82.41	11807.41	1712.07	20.78
U + Pu Acceptor	33.4	FP-3	0.104	6.01	4598.79	478.27	79.58
U Donor (spent)	573.33	--	--	82.15	--	--	--
U Acceptor	753.36	--	--	134.93	--	--	--

[a]Does not consider recycle of process solvents.

[b]Obtained from Martin Kyle, Argonne National Laboratory, private communication.

Fission Product Weight, kg/subassembly

FP-1	0.052
FP-2	0.089
FP-3	0.104
FP-4	0.145
Total	0.390

The fuel description is based on the ORIGEN code: Power = 2.13 MW, Burnup = 2923 MWd/MT, Flux = 5.15E + 14N/cm^2-s, 30-day cooling.

(4) Process Evaluation of Uranium-Plutonium Separation from FBR Core and Axial Blanket Fuel by the Salt Transport Method

Ground rules for the separation of uranium and plutonium are: (a) plutonium separation from uranium while processing FBR core and axial blanket fuel, (b) 75% removal of the rare earth (FP-3) fission products, (c) 25% of the FP-3 elements will stay with the plutonium to enhance diversion resistance, (d) near-quantitative removal of the other fission products (FP-1, FP-2, and FP-4), (e) 99+% plutonium recovery, and (f) 95+% uranium recovery.

A preliminary material balance was made on each major process operation. From these preliminary material balance calculations, the size of each feed and product stream was determined (Fig. 32), the process volumes were estimated and the fission product heating associated with each process product was estimated (Table 19).

Feed to the Process

One core and axial blanket subassembly [AI, Vol. IV, p. 97] which contains:

Cladding

103.3 kg 316 stainless steel associated with the fuel section.

Active Section

Mixed oxides (UO_2, PuO_2, and oxides of fission products = 132.5 kg).

UO_2 (U)	115.41 kg (101.73 kg)
PuO_2 (Pu)	12.73 kg (11.22 kg)
O_2 (as UO_2 and PuO_2)	15.187 kg
O (as FPO)	0.675 kg
FP	3.685 kg

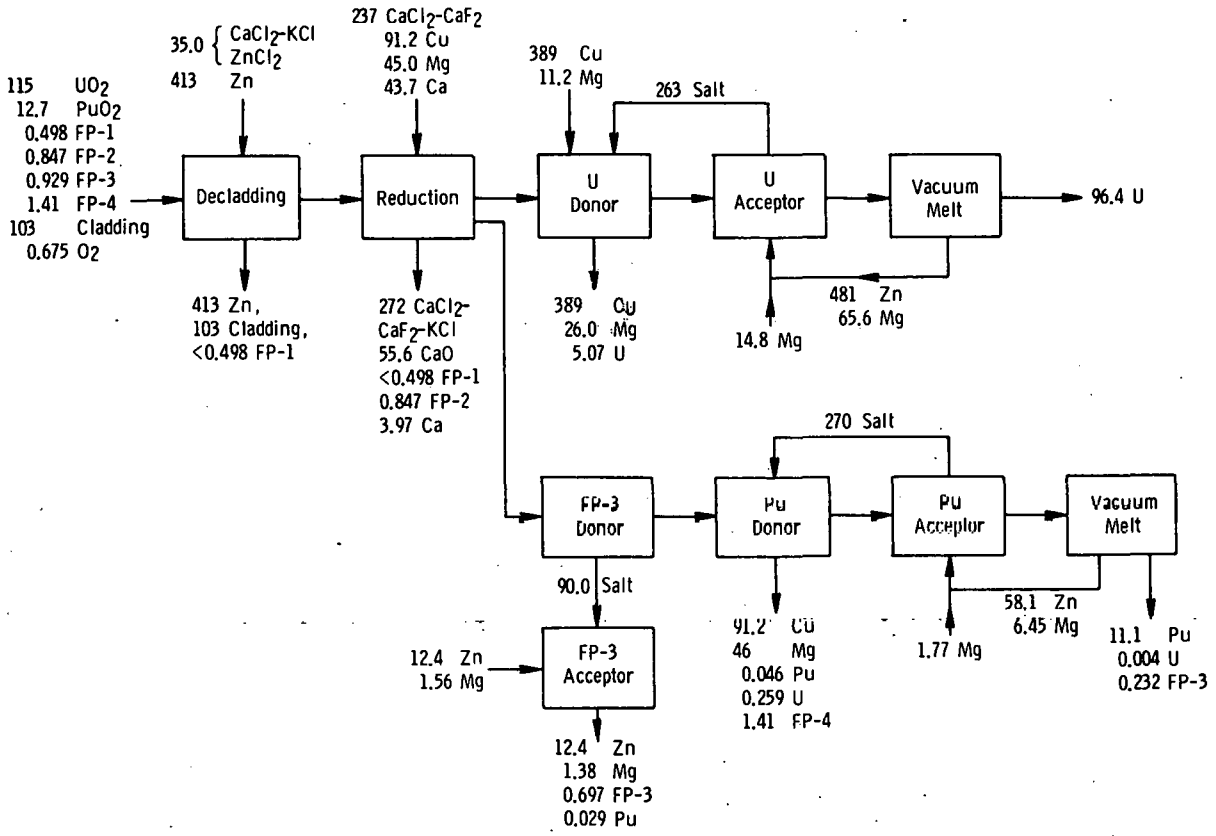

Fig. 32. Conceptual Salt Transport Process for Separation of Uranium from Plutonium, FBR Core and Axial Blanket Fuel. All numbers indicate kilograms.

Fission Product Weight, kg/subassembly

FP-1	0.498
FP-2	0.847
FP-3	0.929
FP-4	1.411
Total	3.685

The fuel description is based on the ORIGEN code: Power = 92.25 MW, Burnup = 50 506 MWd/MT, Flux = 4.17E + 15N/cm^2-s, 30-day cooling.

(5) Selection of Reference Spent Fuel Elements

Work is completed on selection of reference fuel assemblies for pyrochemical reprocessing of LWR and FBR fuels. These assemblies will form the basis for the material balance calculations being performed on the salt transport process operations. The FBR reference core subassembly is described in Tables 20 and 21, and is a 1000-MW(e) fast breeder design [AI]. The LWR reference fuel assembly is described in Tables 22 and 23 and is a hybrid of

Table 19. Fission Product Loadings and Power Densities after Separation of Uranium from Plutonium by the Salt Transport Process

Process Stream	Total wt, kg	FP Stream	FP, kg	Stream Vol. (STP),[a] L	Fission Product Power Density,[a] W/kg	Total W	Power Density, W/L
Volatiles	0.498	FP-1	0.498	87.472	23	11	0.131
Zn and Cladding	516.0	--	--	70.7	--	--	--
Calcium Reduction Salt	332.716	FP-2	0.847	149.477	805	682	4.566
FP-3 Acceptor	14.570	FP-3	0.697	2.65	3262	2274	857.993
Pu Donor	139.846	FP-4	1.411	37.31	2987	4215	112.979
Pu Acceptor	75.90	FP-3	0.232	12.47	3262	757	60.09
U Donor	419.84	--	--	58.75	--	--	--
U Acceptor	642.67	--	--	110.07	--	--	--

[a]Does not consider recycle of process solvents.

Table 20. FBR Reference Reactor

Power Level	1000 MW(e)
Mixed Oxide Fuel in Core	80% UO_2, 20% PuO_2
Depleted UO_2 in Blanket	100% UO_2
Burnup of Core Fuel	10%
Breeding Ratio of Subassembly	1.0
Designer	Atomics International

Table 21. FBR Reference Hexagonal Fuel Subassembly [AI]

Thickness	14.4 cm (5.667 in. across flats)
Fuel Pins Per Subassembly	217
Length of Subassembly	457 cm (180 in.)
Weight of Subassembly	330.9 kg
Length of Hardware Above the Active Section	157 cm (61.66 in.)
Length of the Active Section	170 cm (66.84 in.)
Length of Hardware Below the Active Section	123 cm (48.5 in.)
Length of a Fuel Pin	281 cm (110.5 in.)
Length of the Upper Blanket	30.5 cm (12.0 in.)
Length of Core Fuel	109 cm (42.84 in.)
Length of Lower Blanket	38.1 cm (15.0 in.)
Length of Gas Plenum	∿99 cm (∿39 in.)
Weight of UO_2-PuO_2 in Core Section	79.0 kg
Weight of UO_2 in Blanket Section	53.5 kg
Type of Cladding Material	316 SS
Weight of Cladding Associated with the Active Section	95 kg
Fuel Pin OD	0.56 cm (0.220 in.)
Cladding Wall Thickness	0.44 cm (0.175 in.)

Table 22. LWR Reference Reactor

Power Level	1000 MW(e)
Oxide Fuel in Core	UO_2; max ^{235}U, 3.85 wt %
Burnup of Core Fuel	33,000 MWd/MTU
Conversion Ratio	0.6
Designer	Westinghouse

Table 23. LWR Reference Square Fuel Assembly [RESAR-3]

Thickness	21.4 cm (8.426 in. on a side)
Fuel Rods Per Assembly	264
Length of Assembly, Overall	448 cm (14.7 ft)
Weight of Assembly	648 kg (1428.12 lb)
Length of Hardware Above the Active Section	∿50 cm (∿20 in.)
Length of the Active Section	366 cm (144 in.)
Length of Hardware Below the Active Section	∿6.9 cm (∿2.7 in.)
Length of a Fuel Pin	386 cm (152 in.)
Length of Gas Plenum	16.0 cm (6.3 in.)
Weight of UO_2 in Core Assembly	523.4 kg (1154 lb)
Cladding Material	Zircaloy 4
Fuel Rod OD	0.95 cm (0.374 in.)
Cladding Wall Thickness	0.06 cm (0.0225 in.)
Weight of Grids Per Assembly	4.68 kg (10.32 lb)
Grid Material	Inconel 718
Weight of Zircaloy Per Assembly	119.6 kg (263.8 lb)

the most conservative parameters from modern PWR and BWR fuel subassembly designs. Application of these parameters will result in a process design capable of handling most FBR and LWR fuel assemblies.

(6) Decladding of Spent LWR and FBR Fuel Assemblies

The following nonaqueous decladding methods have been investigated as possible headend processes for treatment of spent fuel: melt decladding, AIROX oxidative decladding, copper-antimony decladding, zinc chloride decladding, and liquid zinc decladding. In comparison with alternative decladding methods, the liquid zinc decladding method has advantages that make it one of the best decladding options.

The liquid zinc decladding operation consists of immersing the fuel assembly in molten zinc at 800°C. Stainless steel dissolves in zinc up to a loading as high as 26 wt %; however, only mixtures with loadings no higher than about 20 wt % [ANL-1970] are pourable.

During initial dissolution of the cladding, tritium and the gaseous fission products (xenon, iodine, and krypton) are released to the molten metal. The decladding operation is performed in a sealed furnace, and the tritium, xenon, and krypton gases can be retained in the furnace atmosphere and stored in pressurized gas cylinders.

The elemental iodine released from the fuel forms zinc iodide by reaction with molten zinc. A molten salt phase (calcium chloride-potassium chloride-zinc chloride) covers the liquid zinc in the crucible. Upon contact with the salt layer, the zinc iodide reacts with potassium chloride as follows [ANL-1970]:

$$ZnI_2 + 4KCl = K_2ZnCl_4 + 2KI$$

The iodine is retained in the cover salt, which is subsequently discarded as a dry waste. The cover salt prevents excessive zinc evaporation. The zinc chloride in the cover salt oxidizes residual uranium, plutonium, and magnesium (which may be in the crucible as a donor alloy heel) and any residual sodium (which may be entrained from fast breeder fuel assemblies).

Once the cladding has completely dissolved, the molten zinc-cladding alloy is separated from the fuel oxides. This can be effected by high-temperature pumps or by siphoning through electrically heated transfer tubes [ORNL-1970]. This allows use of the vessel for subsequent operations. The advantages of liquid zinc decladding include:

Control of Fission Gases. Liquid zinc decladding can be performed in a sealed enclosure, which permits the collection and storage of fission gases.

Decay Heat Dissipation. With liquid zinc decladding, removal of decay heat may not be a problem when shorter-cooled fuels are processed.

Control of Sodium and Iodine. With liquid zinc decladding, control of sodium and iodine should not be a problem since sodium is oxidized by zinc chloride, and iodine forms zinc iodide. The chloride and zinc iodide formed are taken up by the cover salt.

Mechanical Operations Reduced. Mechanical disassembly is avoided with zinc decladding and chopping or piercing of the fuel rods is not necessary. Transfer of fuel oxide to a reduction crucible is also avoided.

Reduced Temperatures. Zinc decladding takes place at 800°C, which is lower than the temperatures required for melt decladding (1450-1600°C) and for copper-antimony decladding (900-1000°C).

Liquid zinc decladding also has disadvantages:

High Metal/Cladding Ratio. A high zinc to cladding ratio must be maintained for complete and rapid dissolution; thus, there are significant quantities of zinc to be recycled.

Materials of Construction. Containers of the molten metal solvent must be fabricated of refractory metals. Construction of full-size containers will be difficult.

The molten zinc method of decladding spent reactor fuels provides a viable technique for solving decladding problems associated with both LWR and FBR fuels.

(7) Oxide Reduction Operation

An important operation in the pyrochemical reprocessing of spent nuclear fuel is the oxide reduction operation. This operation interfaces with the decladding operation and with the following processes of pyrochemical separations. A product of the decladding operation is the oxide fuel pellet. A variety of reducing agents such as alkali metals, alkaline earth metals, aluminum, and others have been used to reduce the halides and oxides of uranium and plutonium to the elemental metallic state [ANSELIN, BAKER, BOWERSOX, GITTUS, JENKINS, KNIGHTON-1961, -1963, -1965A, -1965B, -1969, SHARMA, STEUNENBERG-1967A, STEUNENBERG-1969B]. However, the most satisfactory reducing agent is calcium. The choice of calcium is based on several factors, including thermodynamics, cost, and ease of handling. The chemical reactions for reduction of uranium and plutonium oxides by calcium metal are:

$$UO_2 + 2Ca \rightarrow U + 2CaO \quad (1)$$

and

$$PuO_2 + 2Ca \rightarrow Pu + 2CaO \quad (2)$$

The thermodynamics for these reactions are very favorable. At 1000 K, the free energies of reaction in kilocalories per mole of oxide are -36.1 and -21.9, respectively, for Eqs. 1 and 2.

The oxide reduction operation is accomplished in a sequence of process steps. There is added to the reaction vessel, which contains the oxide fuel pellets and molten cover salts from the liquid zinc decladding operation, a blended charge of molten calcium chloride-calcium fluoride salts. To this, the calcium metal is added and blended with an alloy of either copper-magnesium or zinc-magnesium. The products of these reactions are uranium and plutonium metals, which are dissolved in the liquid alloy phase along with the FP-3 and FP-4 fission products. Calcium oxide and the FP-2 fission products are taken up into the salt phase. Next, the salt phase is separated from the liquid alloy phase.

A calcium chloride-calcium fluoride salt is used in oxide reduction for a number of reasons. The first is the ability of the salt to wet the oxide fuel pellet [KNIGHTON-1961, -1963, -1965A, 1965B, WENZ-1966]. This wetting enhances the rate of reduction of the oxide fuel pellets. Other reasons for the choice of calcium chloride-calcium fluoride salt are that both calcium metal and calcium oxide are soluble in the salt. This enhances the rate of reduction of the oxide fuel pellets.

The prescribed composition of the calcium chloride-calcium fluoride salt is yet to be specified. Factors which will be used in the determination are: operating temperature, maximum solubilities, the effect of the $^{19}F(\alpha, n)^{22}Na$ reaction, and the capability of recovering the waste salt.

The waste stream from the oxide reduction operation is the calcium chloride-calcium fluoride salt, which is burdened with calcium oxide and the FP-2 fission products. To minimize the amount of waste products generated during reduction of fuel oxide, methods for removing calcium oxide from the reduction salt need to be developed. There are unexplored possibilities of filtering out significant amounts of FP-2 elements by cycling the waste through heating and cooling sequences.

In an earlier report, a method was proposed for the removal of the calcium oxide [BALDWIN]. The proposed method was based on a report describing the preparation of uranium dioxide by reacting calcium oxide with uranium tetrafluoride in fluoride melts [GORBUNOV]. The same reaction may be used to remove calcium oxide from the reduction salt by the addition of uranium tetrachloride.

$$2CaO + UCl_4 \rightarrow 2CaCl_2 + UO_2$$

The resultant uranium dioxide is insoluble in the calcium chloride-calcium fluoride reduction salt and is separated by taking advantage of density differences. Uranium tetrachloride may be formed for this step by reacting uranium oxide with carbon tetrachloride.

$$UO_2 + CCl_4 \rightarrow UCl_4 + CO_2$$

The choice of the liquid alloy solvents is dependent on the following process operations: If the salt transport scheme is to be followed, a copper-magnesium alloy is used. If the pyroredox scheme is to be followed, a zinc-magnesium alloy is used. The solubilities of uranium and plutonium in the above alloys have been determined [KNIGHTON-1966, -1969A,

KNOCH, STEUNENBERG-1968A, 1968B, VOGEL-1968A, 1968B]. The solubility of calcium oxide in calcium chloride-calcium fluoride salt has been determined [WENZ-1969].

(8) Fuel Refabrication

After processing of spent fuel, the uranium-plutonium metal must be converted to a form suitable for use in a reactor.

For the preparation of the mixed oxide type of reactor fuel (MOX), the metallic alloy can be oxidized by a procedure similar to the skull oxidation step of the EBR-II skull reclamation process [WINSCH-1969] and then reduced with hydrogen to form a uranium oxide-plutonium oxide mixture. The oxidation is carried out at 700-800°C at 1.33×10^4 - 6.65×10^4 pascals (100 to 500 torr) of pure oxygen [JOHNSON, ANL-1965, BARR]. This oxidized mixture is reduced in 4×10^4 pascals (300 torr) of hydrogen at 600-800°C to obtain a uranium oxide-plutonium oxide mixture. This mixed oxide powder is then mechanically pressed into pellets, sintered, and loaded into fuel rods. The entire process must be done remotely in hot cells due to the radioactivity of the plutonium and fission products.

A fluidized-bed technique has been developed for the preparation of uranium-plutonium monocarbide. The process has been demonstrated at Argonne National Laboratory [PETKUS]. In these runs, uranium-plutonium metal was hydrided at about 250°C to produce fine particles which were then reacted with a hydrogen-methane fluidizing gas mixture at 550 to 800°C and $2.03\text{-}4.05 \times 10^5$ pascals (2-4 atm) pressure. The powdered product was suitable for pressing and sintering into fuel pellets.

Mixed uranium-plutonium carbide powders have also been prepared by the reaction of finely divided metal with propane at 645-745°C [BROWN]. The product was a fine powder suitable for pressing and sintering. Carbide powder is pressed at 7.03×10^7 kg/m^2 (50 tsi) and sintered in argon at 1600°C.

Remote fabrication of uranium-plutonium metallic alloy was extensively studied at Argonne for the EBR-II fuel cycle. A precision casting operation was develolped [ANL-1966]. The product of the pyroredox or salt transport coprocessing methods is already in a metallic state and ready for fabrication into metallic fuel elements.

(9) Miscellaneous

ORIGEN Code. Effort has been devoted to establishing the ORIGEN computer code at Rocky Flats. The fission products to be expected in a LWR spent fuel assembly have been calculated and will be used as the basis for the mass balances for the three LWR spent fuel processing options.

INFCE Study. A request was received from ANL during the quarter to provide descriptive flow sheets, material balances, and cost estimates for conceptual facilities for pyrochemical processing of uranium-plutonium core, uranium blanket, and thorium blanket spent reactor fuel by

salt transport. This information was compiled and will be forwarded to the U.S. International Fuel Cycle Evaluation Support Group for inclusion in their International Fuel Cycle Studies Report.

Computer Modeling of Selected Flowsheets. A computer program being constructed for use in modeling of selected pyrochemical flow sheets is near completion. The program will be used to calculate a material balance around each step in the flowsheet. Ultimately, the desire is to interface an upgraded version of the program with the ORIGEN code as a tool to optimize process conditions and to minimize process operations.

Corrosion. In the pyrochemical reprocessing of nuclear fuels, the container for reprocessing becomes a major consideration because the process chemicals are extremely corrosive. A failure of the container during reprocessing operations could result in a radioactive spill that would be most difficult and expensive to rectify.

The container materials under consideration for this project include tungsten, molybdenum-30 wt % tungsten, and tantalum. The corrosive fluids to be contained are in two phases: the salt phase and the metal phase. The salt phase will generally contain some proportion of calcium, magnesium, and potassium chlorides and calcium and magnesium fluoride. Zinc chloride will also be present in the salt phase and is of particular interest since it causes tantalum embrittlement [NELSON]. The metal phase consists of some proportion of zinc, copper, magnesium, and calcium. The temperature will range from 750 to 850°C, and the atmosphere will be inert gas.

Currently, 30 journal articles and reference books are being reviewed for information related to the corrosion of tungsten, molybdenum-30 wt % tungsten, and tantalum by molten zinc, halides, uranium, and plutonium at high temperatures. These substances seem to cause most of the corrosion in uranium-plutonium salt transport processing.

The three container materials have all been extensively tested with liquid zinc in the 750 to 850°C temperature range. Tantalum cannot handle molten zinc because a zinc-tantalum intermetallic forms and there is separation at the grain boundaries caused by embrittlement [DE KANY, NELSON]. Since project specifications call for zinc-12 mol % magnesium and since other tests have shown tantalum to be a resistant container for zinc-magnesium alloys [HODGE, NELSON, KNIGHTON-1965B, -1969A, -1969B, -1965C, KYLE-1965], tantalum should still be considered a resistant container for this project. Tantalum has shown no corrosion with as little as 5 wt % magnesium in zinc at 750°C [DE KANY].

Molybdenum-30 wt % tungsten is rated superior to the tantalum and has performed well at 800°C and 1000°C for 400 to 500 h. The corrosion that does take place is by molybdenum leaching at 800°C to a depth of four to eight mils and then by intergranular corrosion at 1000°C to a depth of 2 to 8 mils [NELSON]. However, tungsten shows the greatest resistance to molten zinc and halide salt systems. At 800°C, less than 1 mil of intergranular corrosion occurs. At 1000°C, there is about 2 to 4 mils of pitting and intergranular attack [NELSON].

In addition to the uniform corrosion of one material with another, consideration should be given to the size, shape, and operation of the assembly to determine any special problems with crevice, erosion, or stress corrosion. The agitator will be subject to stress and erosion corrosion. These types of corrosion seem to especially threaten a metal with a protective coating. Tantalum forms an oxide coating which is a good electrical insulator. However, apparently tantalum is chemically inert and does not depend on its coating for corrosion resistance [HAMPEL]. Weld decay, a form of intergranular corrosion, is a problem in fabricating a tungsten crucible by welding [WINSCH]. Even though no specific reactions have been identified that will corrode the assembly, with such unusually corrosive fluids and with the project being designed for a much larger scale than has been previously tested, some corrosion seems inevitable. Keeping the crucible rounded on the bottom would help avoid crevice corrosion, and keeping the bends in the transfer lines as rounded as possible would help avoid erosion corrosion.

Because of easier machinability, molybdenum-30 wt % tungsten seems to be the choice for agitators and transfer lines for which replacement of parts would not be a major problem [WINSCH]. There is evidently some evidence that the alloy is stronger than elemental tungsten [LI, WINSCH]. Generally, though, pure metals are not supposed to be nearly so susceptible to stress corrosion as are alloys. The use of molybdenum-30 wt % tungsten for carrying molten zinc has been proved in the zinc industry, where (3/4-in.-dia) shafts have given several years of service [BURMAN].

Much of the direct research on reprocessing of nuclear fuel elements done by Argonne National Laboratories was doen in tantalum containers with tantalum agitators [KNIGHTON-1965B, 1969A, 1969B, 1965C], but their research suggests that tantalum will not be satisfactory for large-scale operations [WINSCH-1967].

Tungsten crucibles have been successfully fabricated and used for pyrochemical nuclear fuel reprocessing in sizes up to 25.4-cm (10-in.) ID, 30.48-cm (12-in.) OD and 50.8-cm (20 in.) high. Three methods of fabrication were successful, and two methods failed. The successful methods were (1) pressing and sintering, (2) shear forming, and (3) plasma spraying of free-standing shapes.

The unsuccessful methods were unfortunately those most useful for large crucibles: (1) arc welding and (2) plasma spraying on a substrate. The arc-welded crucible developed cracks because of residual stresses remaining after the welding operation. Crucibles of tungsten plasma sprayed on 410 stainless steel, silicon carbide, and graphite substrates have been fabricated. The tungsten coating adhered well to the silicon carbide and the graphite substrates. It cracked and peeled on the stainless steel [LAWROSKI-1962, VOGEL-1964A, 1964B].

The only true corrosion problem with tungsten seems to be its ready oxidation in air at 400°C. After oxidation, it spalls or exfoliates easily [LI]. Molybdenum behaves similarly at temperatures above 650°C [ARCHER].

Vapor Pressures. Data on the vapor pressures of most elements was compiled within the temperature range of 800 to 1400 K in increments of 200 K [HULTGREN, MARGRAVE, SMITHELLS]. See Appendix A. Tables of vapor pressures of the associated chlorides, fluorides, and oxides are being prepared. These vapor pressures will provide a method of predicting potential problems associated with the volatilization of the different salts and/or elements. Volatilization of these salts and/or elements could cause plugging of equipment due to buildup of condensates.

c. Separations Process

(1) Salt Purification Laboratory

Work is under way to establish a salt purification laboratory. Major equipment to be installed in the laboratory includes a Varian Cary Model 17DH UV-Vis-NIR spectrophotometer which will be used for high-temperature analysis of molten salts, a laser Raman spectrometer, an inert-atmosphere glovebox, furnaces and controllers, and assorted electrochemical equipment. Almost all equipment has been selected and ordered. The facility should be operational during the fourth quarter of FY 1978.

A suitable site has been located for the expanded salt purification laboratory and for depleted uranium pyrochemical experimental work. Final approval for use of the site should be obtained soon.

(2) Proof of Principle Experiments

The outline of the experimental program which will be conducted to investigate the key problems that challenge the feasibility of uranium-plutonium salt transport processing has been completed. This outline includes schedules for timely completion of the proposed tasks.

Work has begun on the modification of equipment to be used in the proof-of-principle experimental work.

5. Fabrication of Process-Size Refractory Metal Vessels
(C. Edstrom,* C. Baldwin,* R. Corle,* and L. Johnson*)

a. Introduction

The pyrochemical processing of nuclear fuels requires crucibles, stirrers, and transfer tubing that will withstand the temperature and the chemical attack from the molten salts and metals used in the process. The capability of fabricating the necessary hardware is critical to pyrochemical processing. For economics and safety in the pyrochemical process, a crucible large enough to contain the entire fuel rod is needed. Tungsten, the material known to withstand the temperature and chemical attack, is presently not available in a sheet size large enough to provide the surface area of large crucibles. This indicates that joining, coating, and/or forming processes must be developed to achieve the desired shape and size.

*Rockwell International-Rocky Flats.

b. Engineering Analysis

(1) Survey of Tungsten Suppliers

Contacts made through visits or by telephone with tungsten sheet suppliers produced the following capability summary:

> GTE Sylvania can supply tungsten sheet in 30.48 cm (12-in.) widths down to 0.15-cm (0.060-in.) thickness.
>
> Wah Chang starts with a 1.6-cm (5/8-in.) by 15.24-cm (6-in.) by 30.48-cm (12-in.) sintered ingot and can supply 30.48-cm (12-in.) wide tungsten to a minimum thickness of 0.15 cm (0.060 in.). For desired forming characteristics tungsten should be hot-worked with 60% minimum reduction. This indicates we would not want to buy plate thicker than 0.635-cm (1/4 in.) from Wah Chang.
>
> Metallwerk Plansee has a rolling mill which can roll 101.6-cm (40-in.) wide tungsten; however, all related handling equipment limits the available tungsten sheet width to 60.96 cm (24 in.). This can be provided in thicknesses as small as 0.013 cm (0.005 in.).
>
> AMAX Specialty Metals supplies tungsten 0.10-cm (0.040 in.) thick in widths to 60.96 cm (24 in.). For 0.013-cm-0.099-cm (0.005 to 0.039-in.)-thick tungsten, the maximum width is 30.48 cm (12 in.).

The capability of tungsten suppliers is important to the program because it controls some of the fabrication options for making the required 283 L (10 ft^3) tungsten crucible.

GTE Sylvania's capabilities lie in tungsten powder production; therefore, they favor the production of large crucibles by sintering. GTE Sylvania feels they possess the technology to make a 50.8-cm (20-in.) diameter by 121.9-cm (48-in.) -high by 2.54-cm (1-in.)-wall sintered crucible with 92% density. Such a crucible would weigh approximately 1090 kg (2400 lb).

AMAX supports a joining approach because they know that tungsten becomes more formable as the thickness decreases.

Metallwerk Plansee proposes that the large crucible be made by roll forming and riveting. The riveted joints would be plasma spray coated with tungsten. Metallwerk Plansee has had experience in making molybdenum vessels by this method. In cooperation with Crucible Steel, they made a 137-cm (4 1/2 ft-dia by 427-cm (14-ft) -high molybdenum crucible for Battelle. Fred Bydash of Metallwerk Plansee also praises their plasma spray quality. They use a Swiss-made gun which gives twice the velocity of the American-made guns and improves the density of the coating.

(2) Literature Search

Most of the literature search material has been received and abstracts are being prepared. The abstract is scheduled to be complete July 1.

(3) Fabrication Techniques

Tungsten Crucible Spinning. The attempt on April 21, 1978, to spin a 12.7-cm (5-in.) ID tungsten crucible 27-cm (10 1/2 in.) high failed. Spinning practice was discussed with people at AMAX and GTE Sylvania, Fred Bydash of Metallwerk Plansee, and Dieter Bauer of Super Temp. The consensus was that spinning could be improved by using a tight mandrel-to-tungsten-cup fit. In the first spinning attempt, the inside diameter of the tungsten cup was 0.635 cm (1/4 in.) larger than the mandrel. Beyond this recommendation, opinions on how to achieve improvement varied. AMAX thought that the drawn cup should be partially recrystallized before spinning and that the tungsten crucible should be removed during the spinning operation for a stress-relieving operation. Both Messrs. Bydash and Bauer of Metallwerk Plansee felt that the spinning temperature of 1150°C is high enough that stress relieving is not required. GTE Sylvania felt the drawn cup should be fully recrystallized before spinning.

Both GTE Sylvania and AMAX suggested contacting Curt Staub for tungsten spinning recommendations. Staub could not be located; however, Dieter Bauer, an engineer who worked with Staub and authored two reports on spinning tungsten, was contacted. Arrangements are now being made to hire Mr. Bauer as a consultant.

Joining. Currently, brazing seems to be the best choice for joining tungsten. The literature indicates that electron beam welding provides joints with strengths 40% that of the parent metal [DMIC REVIEW]. Diffusion bonding requires some interface metal such as niobium or molybdenum-niobium and high pressure (6.89×10^7 pascals) at 925°C (1700°F) [COLE]. The required pressure presents a severe alignment problem for crucible wall bonds, and the interface metal leaves a path for corrosion. Brazing development focuses on selection of a brazing alloy that will bond below the recrystallization temperature, yet remain strong at the service temperature of 850°C [BRITISH PATENT, GTE SYLVANIA]. Also, some corrosion resistance to the molten salts and metals is desired, even though the joints will be plasma-sprayed with tungsten. Reactive brazes present the best hope for some corrosion resistance [METCALFE].

Chemical Vapor Deposition (CVD) Coating with Tungsten. Chemical vapor deposition of tungsten on a substrate offers promise as a method for fabricating a full-size crucible. Deposition of tungsten from tungsten hexafluoride is preferred to using tungsten hexachloride as a source of tungsten because of increased coating ductility. The problems with any CVD tungsten coating lie with the presence of columnar grains, which present corrosion concerns [BLOCHER]. Grain refining techniques need to be investigated. Dick Corle and George Mah's visit to Lawrence Livermore Laboratories, Chemetal, and Ultramet the week of June 6, 1978, provided some very encouraging information.

Grain refining is accomplished commercially by coating at a low temperature (approximately 350°C). The method of wire brushing during coating (seen in the literature) needs extensive development before it can be applied to crucible fabrication [BLOCHER]. All three contacts recommended coating a molybdenum substrate. High-density graphite works, but Chemetal questioned the availability of a 50.8-cm (20-in.)-dia by 122-cm (48-in.)-high graphite crucible suitable for coating.

The most encouragement comes from Chemetal, who believe that after the process had been developed, production costs for coating a 50.8-cm (20-in.)-dia by 127-cm (50-in.)-high crucible, would be approximately $5000.

All three felt that a free-standing CVD tungsten crucible would not be practical.

Chemetal also stated that they can CVD-coat tungsten onto tungsten substrates, molybdenum transfer tubes, pump parts, and stirring hardware.

c. Separation Processes

(1) Spinning Tungsten Crucible

Modifications to improve the safety operation of hydrospin are complete. Torches are now easier to turn on and off. Heat shields prevent the roller grease from catching on fire. Plans to spin the one remaining tungsten cup into a crucible are made for the week of June 26, 1978. The spinning procedure will incorporate the recommendations of tungsten suppliers. The drawn cup has been stress-relieved 30 min at 1300°C to obtain a partially recrystallized grain structure. Refer to photomicrographs (Figs. 33-38) which show the recrystallization data generated on a drawn cup.

(2) Sintered Crucible

A sintered crucible is on order from GTE Sylvania. This crucible will be used in the service life test.

(3) Service Test Furnace Modification

Instruments to be used in operating the service life furnace 24 h/day are on order and are due to arrive September 1, 1978. The mechanism for tilt-pouring the crucible is being fabricated. The stirring mechanism is still to be ordered.

(4) Brazing

The concept of brazing tungsten liners was demonstrated at the PDPM meeting on May 16, 1978, at Argonne National Laboratory. A crucible was made with existing draw tooling and was brazed with crude fixturing. The NIORO (83% gold and 17% nickel) braze provided a good jointing under less than ideal conditions.

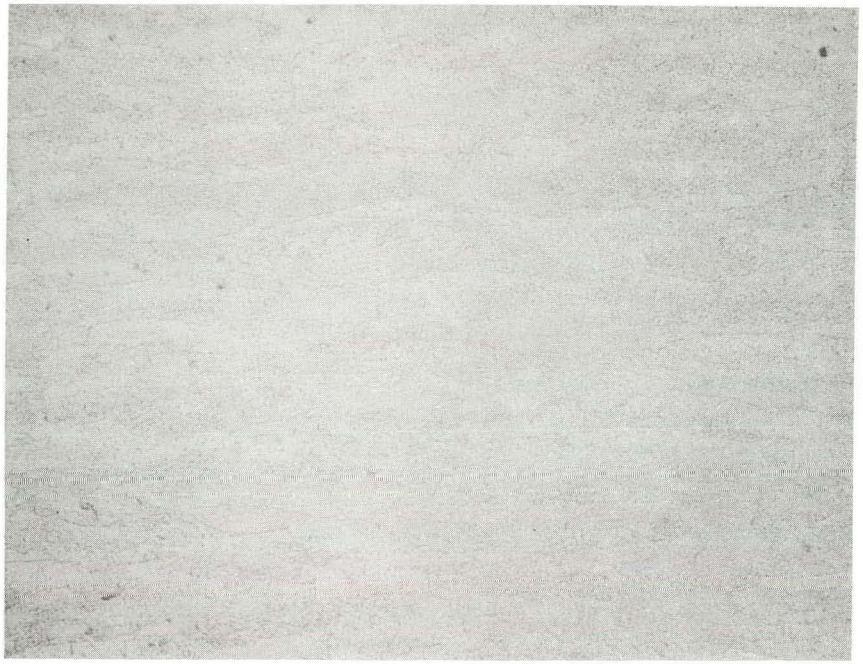

Fig. 33. Recrystallization Data for Drawn Cup. Magn, 100X. Etch: 10% $K_3Fe(CN)_6$

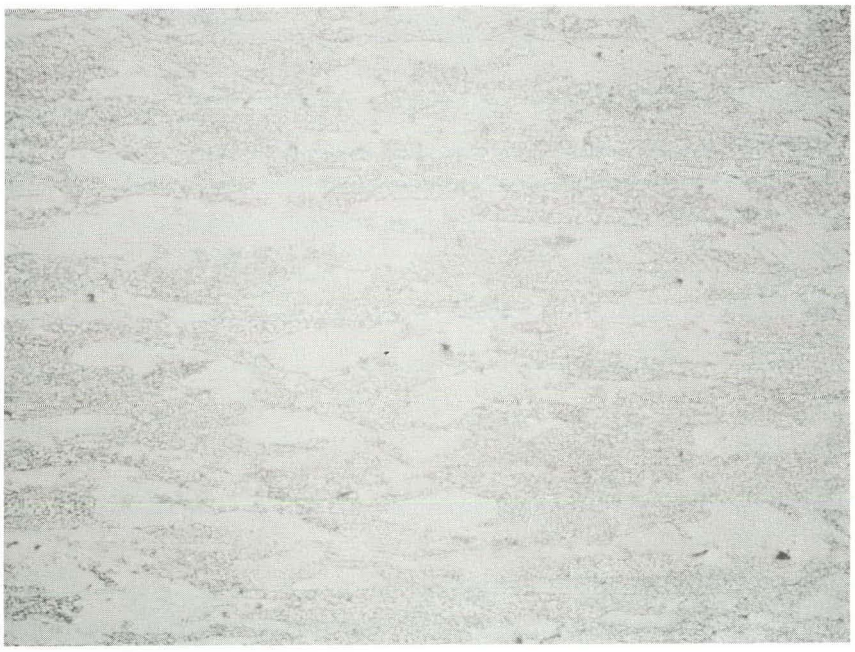

Fig. 34. Recrystallization Data for Drawn Cup. 30-min stress relief at 1250°C. Magn, 100X. Etch: 10% $K_3Fe(CN)_6$

Fig. 35. Recrystallization Data for Drawn Cup. 30-min stress relief at 1300°C. Magn, 100X. Etch: 10% $K_3Fe(CN)_6$

Fig. 36. Recrystallization Data for Drawn Cup. 30-min stress relief at 1350°C. Magn, 100X. Etch: 10% $K_3Fe(CN)_6$

Fig. 37. Recrystallization Data for Drawn Cup. 30-min stress relief at 1400°C. Magn, 100X. Etch: 10% $K_3Fe(CN)_6$

Fig. 38. Recrystallization Data for Drawn Cup. 30-min stress relief at 1450°C. Magn, 100X. Etch: 10% $K_3Fe(CN)_6$

Several types of brazes (NIORO, PALCO, PALNIRO, and PALNISAL) have since been attempted. These joints are being examined metallographically and for corrosion resistance in liquid magnesium-copper alloy and molten calcium chloride-calcium fluoride salt. Metallographic examinations of NIORO and PALCO brazes show good diffusion of the braze with the tungsten; the PALCO braze temperature (250°C) recrystallizes the tungsten (refer to Figs. 39 and 40).

Testing of the compatibility of several conventional brazed strips with molten calcium chloride-calcium-fluoride salt and copper-magnesium alloy began June 21, 1978. In the future, samples of conventional brazes that have been plasma spray coated with tungsten and samples joined by reactive brazes will be tested.

A procedure for three roll bending 0.025-cm (0.010-in.) thick tungsten into 12.7-cm (5-in.)-dia cylinders has been developed. This knowledge hopefully will transfer to forming cylinders with 0.10-cm (0.040-in.) wall thickness. Tungsten sheet 0.10-cm (0.040-in.) thick is on order to make 12.8-cm (5-in.)-diameter by 26.6-cm (10 1/2-in.)-high crucible liners. Tooling for drawing the bottom cap is being fabricated.

(5) CVD Tungsten on Molybdenum Crucible

A contract is being prepared for study of the development by Chemetal of chemical vapor depositions of tungsten on crucibles of molybdenum and tungsten. The substrates provided to Chemetal will include a brazed tungsten crucible of 0.10-cm (0.040-in.)-thick sheet, a joined molybdenum crucible of 0.10-cm (0.040-in.)-thick sheet, and a spun molybdenum crucible. Two types of CVD coating will be examined--low-temperature grain-refined tungsten coating and conventional tungsten coating.

6. Aluminum Alloy Processing of Thorium- and Uranium-Based Fuels (ANL Activity No. FO)

(H. R. Lukens,* D. E. Bryan,* J. K. MacKenzie,* C. A. Preskitt,* D. H. Rock,* W. E. Selph,* G. Smellen,* D. P. Snowden,* and R. J. Teitel†

a. Introduction

The objective of the work is to develop economically feasible, proliferation-proof flowsheets for the reprocessing of thorium- and uranium-based fuels, with aluminum a key solvent element. Included in this objective are such considerations as compatible head-end and finishing steps, materials recycling, fission product disposal, and hot processing. An important goal of the program is to avoid the complete separation of fissile isotopes from nonfissile heavy metals at any point in the process. Demonstration of a suitable process is the final objective of the current project.

---

*IRT Corporation.

†R. J. Teitel Associates.

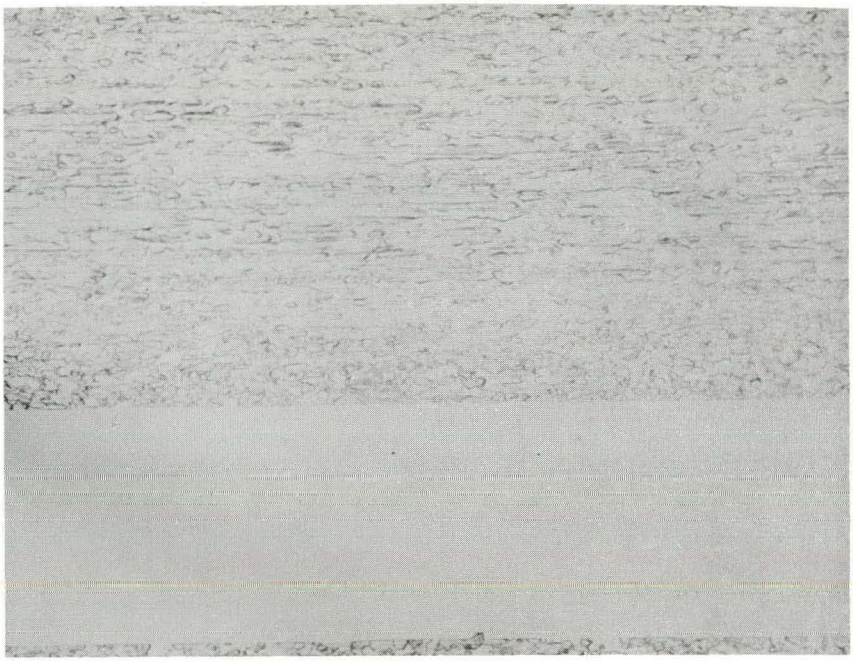

Fig. 39. PALCO Braze of Tungsten Sample.
Etch: 10% $K_3Fe(CN)_6$. Magn, 400X

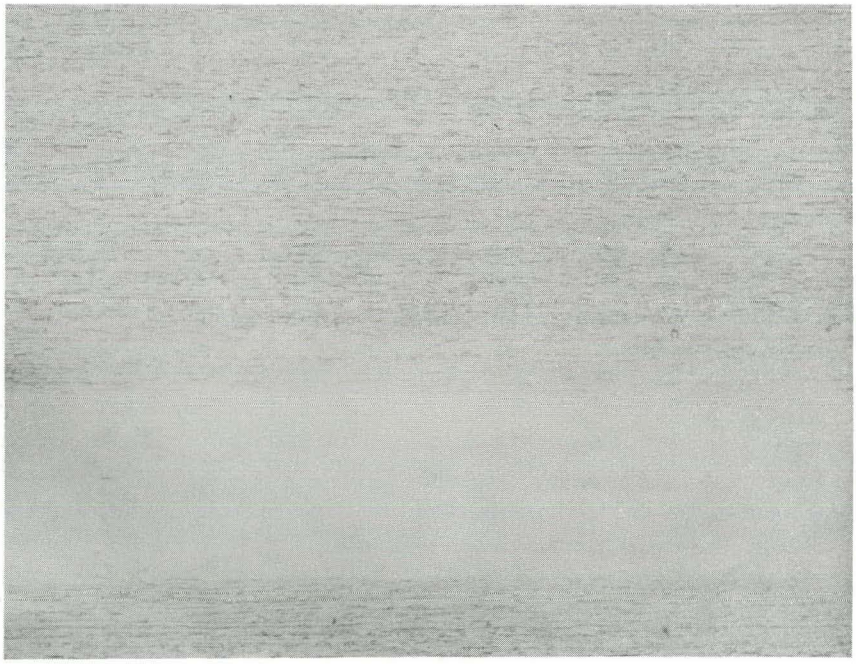

Fig. 40. NIORO Braze of Tungsten Sample.
Etch: 10% $K_3Fe(CN)_6$. Magn, 400X

During the present quarter, several new alternative flowsheets have been formulated that reflect both the contributions of data obtained in an ongoing literature survey and concepts that seem worth investigating with respect to project goals. Also, experimental work is now under way toward the gathering of essential data that is not in the literature.

Previous work on this project has been reported in the preceding quarterly report in this series [STEINDLER-1978C].

b. Engineering Analysis

After several months of steady influx of requested reprints, reports, and other literature, our files now contain about 550 titles. The rate of receipts has now declined, a review of the literature is well under way, and a first draft topical report based on this review is in preparation. The topical report will utilize process flowsheets to highlight the more important contributions of the literature to the project. Also, the data that are needed for the project but which are not in the literature will be identified by flowsheet analysis.

As of this writing, the behavior in aluminum of material having the compositions of spent thorium-based fuels has not been found in the literature. Thus, the initial impression that this would be a major focus of experimental work has been sustained.

Among the literature quite relevant to this project are the works of [TEITEL-1960A], the phase diagram collections of [HANSEN, ELLIOTT, and SHUNK], and [GLASSNER's] collection of free energies of formation. These references contain data regarding solubilities of certain metals in aluminum and of certain intermetallic compounds of aluminum and/or thermodynamic data important to understanding the role of aluminum in alloys and mixtures of aluminum alloys and fluxes.

A work of considerable usefulness is Hildebrand and Scott's The Solubility of Nonelectrolytes [HILDEBRAND], which provides a rule, based on thermodynamics, for estimating the miscibilities of metals. For example, this rule helped us to design an experiment to ascertain which of two different values for the solubility of molybdenum in aluminum is correct. According to one article [FEDER-1958], the value at 700°C is over 20 wt %, while it is reported elsewhere [TEITEL-1960A] to be about 0.16 wt % at that temperature. The Hildebrand-Scott rule indicates poor miscibility of these metals, and therefore our experiment was directed toward testing the latter value rather than the former.

Numerous helpful approaches are suggested by reports on other processes. For example, Lawroski and Burris [LAWROSKI-1964] have described the reduction and removal of noble fission products prior to the reduction of oxidized uranium in the EBR-II skull reclamation process. It may be possible to use an analogous sequence in the aluminum alloy process. Another example is provided by [CAFASSO], who shows that the partition of palladium, rare earths and uranium between molten cadmium and aluminum phases at 680°C is such

that the solutes reside mostly in the cadmium phase. This result is in agreement with the Hildebrand-Scott rule for the rare earths. However, the rule is violated with respect to palladium and uranium--probably due to the formation of compounds with cadmium.

The review of literature pertinent to strictly metallurgical process operations is essentially complete. In general, the literature concerning aluminum-magnesium-zinc processes emanates primarily from two sources: (1) the Argonne National Laboratory [KNIGHTON-1957, STEUNENBERG-1967B, 1969A, and FEDER-1961] fast breeder reactor fuel cycle project and (2) Dow Chemical Company [TEITEL-1958, 1959, 1960A, 1960B, 1962, 1963, 1964A, 1964B, 1964C, 1964D, 1964E, and LAYNE-1963, 1965] fuel cycle studies on solid fuels. Most of the information available from these projects pertains to uranium-plutonium fuel cycles. Phase diagrams, intermetallic compound identification, solubility of uranium and plutonium, separation of mixtures of fission products from uranium, and process flowsheet evaluations of fuel cycles are reported in the above-cited references.

Very little of the available information pertains to the Th-U or Th-Pu fuel cycles, which are important objectives of the current program.

Information on thorium-aluminum pyrometallurgical processes can be summarized as follows:

(1) The melting points of solvent metals alone are fairly well known. The binary alloy systems appear in [HANSEN, ELLIOT, and SHUNK]. Ternary phase diagrams for Al-Mg-Zn alloys and Cu-Mg-Al alloys have been reported in [GUERTLER].

(2) The solubility of Th in Al, Cu, Zn, Mg, individually, and the identification of binary intermetallic compounds have been reported [CHIOTTI-1961]. In summary, thorium is considered to be highly soluble in Al, Cu, and Mg. Thorium is not very soluble in zinc at temperatures near the melting point of zinc. The solubility of thorium in a 67% Mg-Al alloy was reported by R. J. Teitel and G. S. Layne [TEITEL-1960A]. Similarly to uranium, the thorium solubility in the Mg-Al alloy is low. This was unexpected since thorium is highly soluble in both Al and Mg. No other fuel solubility data was found on ternary or higher component systems.

(3) Except for binary diagrams for the solvent metals and individual fission products, there is little information on fission product phase diagrams. J. H. N. Van Vucht [VAN VUCHT] investigated the ternary system, Th-Ce-Al. He identified intermetallic compounds in the system. Al-Ce-U intermetallic compounds were identified and reported. No data was found on the separation of fission products from thorium, Th-U, or Th-U-Pu fuels by the use of Al, Mg, Zn, Cu, and Ca alloy solvents.

c. Separation Processes

(1) Process Solvent Alternatives

As a result of the literature search, the metallic solvent constituents to be studied for the initial dissolution step have been extended to include zinc, cadmium, and copper in addition to aluminum and magnesium. Calcium is being considered as a chemical reducing agent and copper as an additional solvent constituent for metallic fuels.

Figure 41 illustrates the probable metal solvent compositions for the basic steps of the aluminum pyrometallurgical processes to be developed in the course of the current project. Although this diagram is based on information concerning uranium fuels, it provides a starting point for the development of thorium-uranium fuel cycle processes.

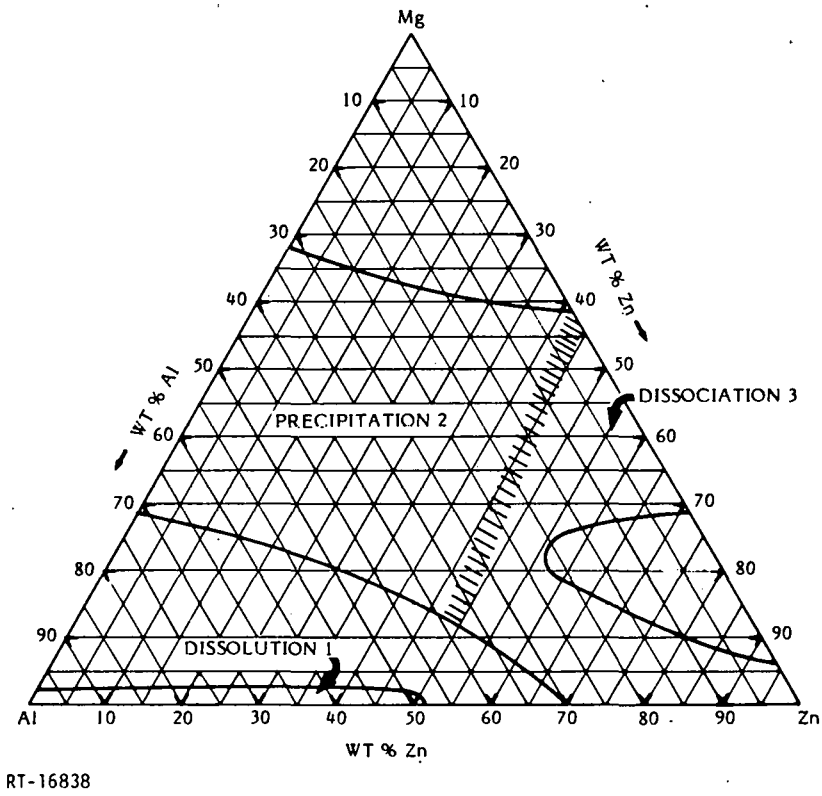

Fig. 41. Solvent Compositions for Aluminum Alloy Processes [LUKENS]

The diagram shown in Fig. 41 is a ternary plot of three metal phases. Aluminum alloys containing copper and calcium as alloy constituents appear at one corner. Magnesium and zinc are at the other corners. The compositions are expressed in weight percent Al, Mg, and Zn, as indicated. Compositions of calcium and copper are known only qualitatively.

Three areas of solvent composition have been designated in Fig. 41. Compositions in "dissolution 1" are good candidates for the dissolution step of the process. Solvent compositions included in "precipitation 2" will serve the fuel intermetallic compound precipitation step. Solvent compositions included in "dissociation 3" will be involved in the intermetallic compound dissociation step. The final solvent constituents will be low Mg-Zn alloys. Alloys of aluminum, copper, and to some extent zinc form solvent alloys in which typically the three fuels (U, Th, Pu) have a high solubility [TEITEL-1960A, FEDER-1961].

Copper forms low-melting alloys with aluminum, magnesium, and zinc [HANSEN, ELLIOTT, SHUNK, and CHIOTTI-1961]. According to [HANSEN] and [TEITEL-1964B], the nuclear fuel constituents (U, Pu, Th) are highly soluble in copper, as in aluminum. Calcium forms no intermetallic compounds with uranium and plutonium. No information has been found on calcium-thorium reactions. In the proposed process, the addition of calcium to the solvents will probably be limited to a low concentration. Both calcium and magnesium are chemical reduction agents that can be used to reduce fuel oxides directly into liquid metal solvents [GLASSNER, LAWROSKI-1964, TEITEL-1963, 1964E].

Magnesium and zinc additions lower the melting point of the solvent and reduce the solubility of U, Th, and Pu except in high-magnesium alloys and magnesium. Thorium and plutonium have a high solubility in the latter, but uranium has a low solubility; formerly magnesium was proposed for processes to separate uranium from plutonium and thorium [LAWROSKI-1964]. In a proliferation-resistant fuel processing cycle, it will not be desirable to fully separate fuel constituents. As a result of the above considerations, the solvent composition in the precipitation operation will be in "precipitation 2" of Fig. 41.

Zinc and magnesium additions convert solvent metal-fuel intermetallic compounds to metallic fuel, magnesium compounds, or zinc compounds. This operation has been successfully demonstrated for uranium processes by R. J. Teitel and G. A. Layne [TEITEL-1960A]. Both magnesium and zinc may be removed by distillation [TEITEL-1960A, LAWROSKI-1964, STEUNENBERG-1967B, 1969A].

(2) Head End Considerations

As discussed in the preceding quarterly report, use of both calcium and magnesium for reducing heavy metal oxides is under consideration. In addition, establishing conditions whereby aluminum is used to sequentially reduce noble fission products first and then to reduce heavy metals may be possible on the basis of work of [MOORE] and by the chloride stability data in [GLASSNER]. Thus, three main alternatives for head end steps for nonmetallic fuels are under consideration. These approaches, plus the simple case of dissolving metal fuels, are shown in Fig. 42 as they relate to the main aluminum-alloy processes, up to the step wherein heavy metals are precipitated. The dotted line of Fig. 42 separates the head-end steps from the main process steps. The question marks in Fig. 42 identify requirements for data (to be obtained experimentally).

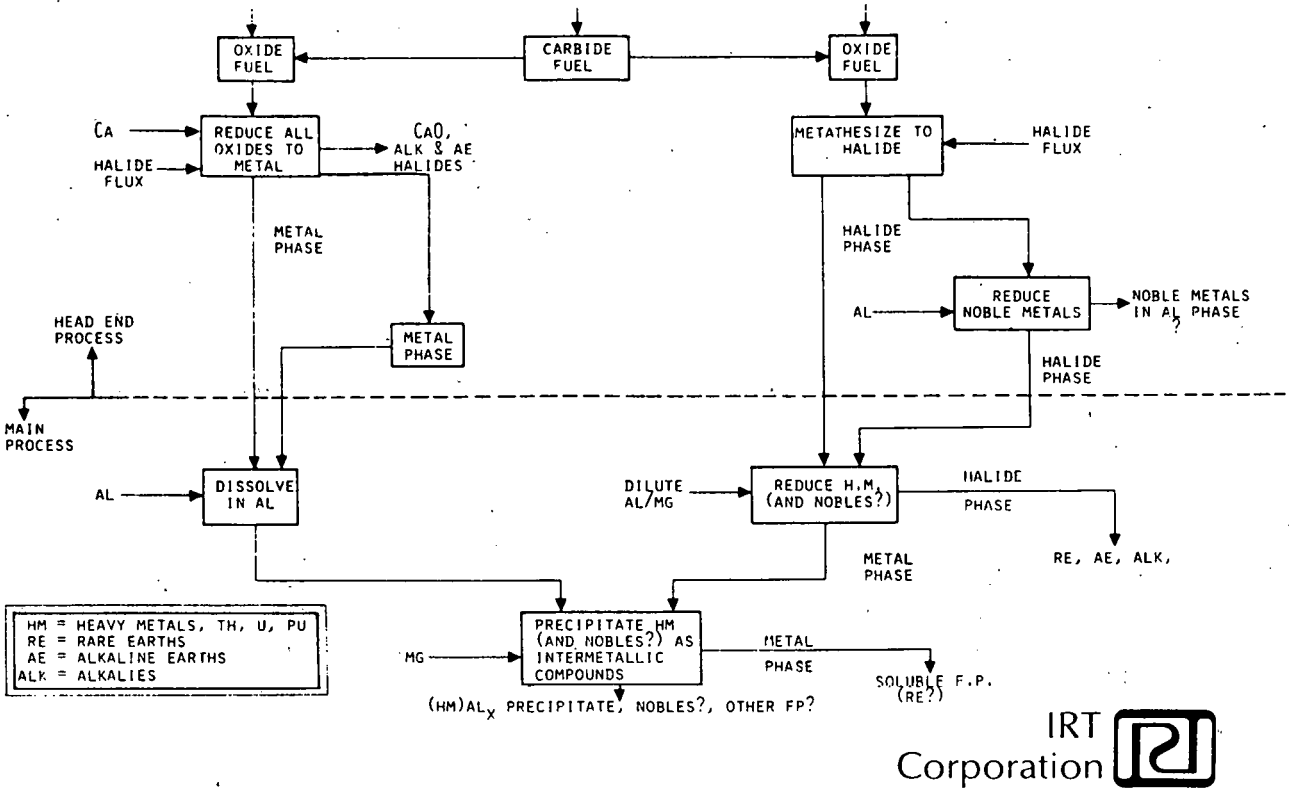

Fig. 42. Preliminary Selection of Process Alternatives Through Heavy Metal Precipitation Step [LUKENS]

(3) Main Process Alternatives

Fission product separation from the heavy metals in the dissolution step is limited by the differing solubilities of fuel and fission products in the solvent metal and copreciptation of the fuel with the insoluble fission product. The separations in this step may be enhanced by adding insoluble constituents (scavengers) that will selectively coprecipitate fission products and not fuel.

The removal of strontium from an aluminum-uranium melt by additions of zirconium [TEITEL-1960A, p. 139] is an example. Zirconium is very insoluble in aluminum and forms the intermetallic compound $ZrAl_3$. Strontium apparently was coprecipitated to a large extent with the zirconium compound. Uranium remained in solution, effecting separation. On the other hand, where partial removal of zirconium is desired, this may be achieved by scavenging with carbon [SCHRAIDT].

An example of an undesirable extractant is molybdenum added to a uranium-aluminum melt [TEITEL-1958, LAYNE-1963]. It was found that the solubility of uranium is reduced and that uranium is coprecipitated in the form of a ternary compound with molybdenum. Addition of copper, zinc, or both to the aluminum melt may prevent formation of the ternary intermetallic compound and make it possible to consider molybdenum a scavenger addition.

Yamagishi's work [YAMAGISHI] suggests that Al_2O_3 may be used to scavenge Zr, Nb, and Ru.

Another modification of the process being studied for metal fuels is direct corrosion of metallic fuel in the molten solvent. It has been demonstrated that direct corrosion of metallic fuel (in the example, uranium) will give the same separation from fission products as when the fuel is first dissolved and then precipitated [TEITEL-1960A]. Further, it has been demonstrated that thermal treatments which cause the insoluble intermetallic compound particles to grow can assist in the attainment of chemical equilibrium [TEITEL-1960A, pp. 138-142]. This is not surprising since the mechanism for particle growth is one of dissolution of small particles and precipitation onto large particles.

Uranium intermetallic compounds formed with aluminum-magnesium-zinc solvent alloys (Fig. 43) have been identified and reported [TEITEL-1960A]. In general, the uranium-aluminum compounds appear to be the most stable. This information, combined with the data on the Al-Mg-Zn system [GUERTLER], allows the speculation that compositions in the "precipitation 2" area of Fig. 41 may be desirable for investigations on direct corrosion and grain growth separation.

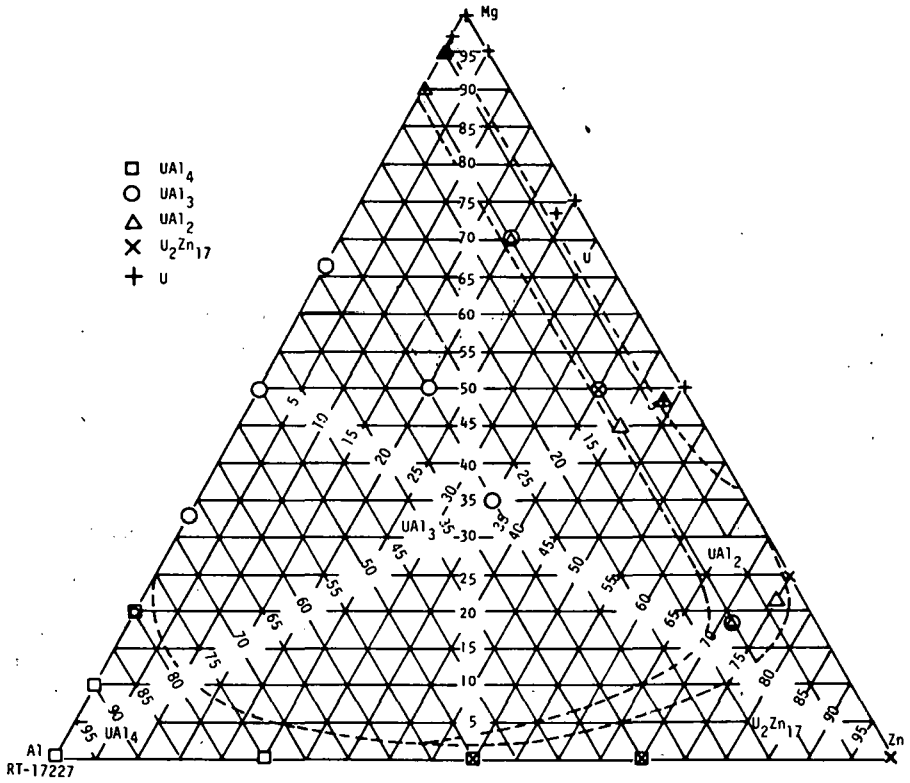

Fig. 43. Uranium Compound Formed from Al-Mg-Zn Alloys [TEITEL-1960A]

The process operation described above suggests that fission product separations may be made in the solid state and thereby significantly reduce the quantity of process metals required. It suggests a countercurrent, multiple-stage operation. Conceivably, particles can be grown as the liquid metal solvent is percolated through a bed of particles. The fresh solvent would drive the transfer. This concept has been demonstrated stepwise for the extraction of uranium from $ZrAl_3$ [TEITEL-1958, p. 133].

Figure 44 illustrates three alternatives for proceeding from a solution of heavy metals to precipitates of intermetallic compounds of aluminum and heavy metals, which may then be dissociated for purposes of recovering heavy metals free of aluminum. The three alternatives are: (1) proceed directly from precipitation of $(HM)Al_x$ to dissociation, (2) use grain growth to enhance the removal of fission products and to minimize solvent volume, and (3) use scavenging to enhance the removal of fission products. Of course, it is possible that both scavenging and grain growth could be used in a single process.

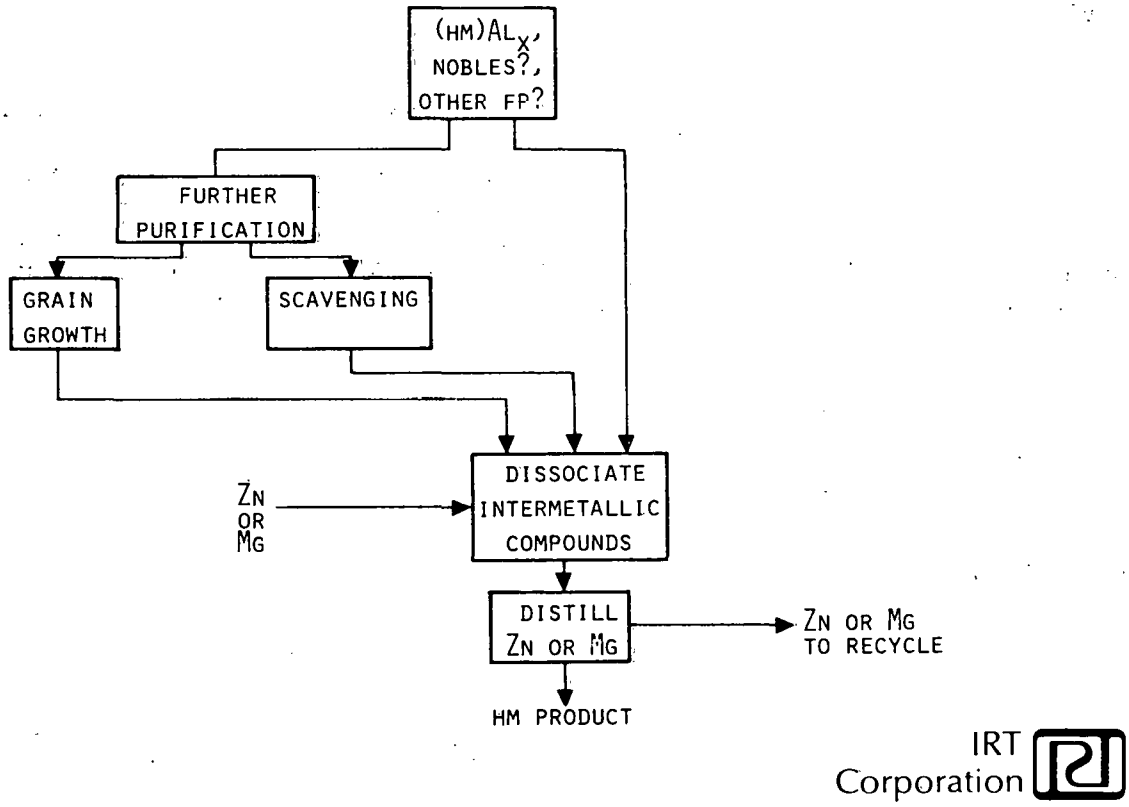

Fig. 44. Preliminary Selection of Process Alternatives Following Heavy Metal Precipitation [LUKENS]

It is worth noting that the alternatives considered above, including head-end steps, have the potential of single-vessel processing. Dissolution of heavy metals in aluminum alloy would occur in the same vessel as head-end reduction steps, provided that head-end side streams (shown in Fig. 42) were first removed from the vessel. Then, formation of $(HM)Al_x$, including grain growth and/or scavenging steps, followed by dissociation and retorting could occur in the same vessel.

(4) Experimental

The laboratory equipment has been brought to the point where experiments are being carried out. The apparatus for preparing melts has been used to prepare several melts. Two melts have been prepared with molybdenum and ruthenium in aluminum and several with a simulated spent fuel containing Th, U, Zr, Mo, and Ru dissolved in aluminum. Samples have been taken from the latter melts at measured temperatures. The filtered samples and the unfiltered melts have been examined by energy-dispersive X-ray fluorescence (XRF) spectrometry. Acquisition of comparator standards for quantification of elements identified by XRF is under way.

(a) Equipment

The overall apparatus in which melts are prepared was shown in the preceding quarterly report [STEINDLER-1978C]. Graphite crucibles and sampling cups, as shown in Fig. 45 and Fig. 46, are used as containers for the melts.

The heart of the XRF equipment is the Nuclear Data ND-660 multichannel analyzer shown in Fig. 47. A lithium-drifted silicon detector is coupled to the ND-660. X-radiation is stimulated in the sample or a secondary X-ray source with an extrinsic americium-241 source and is measured with the Si(Li) detector. The analyzer includes a minicomputer, which was described in the preceding quarterly report, and most of the programs necessary for XRF data reduction have been loaded into the minicomputer. Programming for reduction of gamma ray spectra, acquired with the Ge(Li) detector, was supplied with the ND-660.

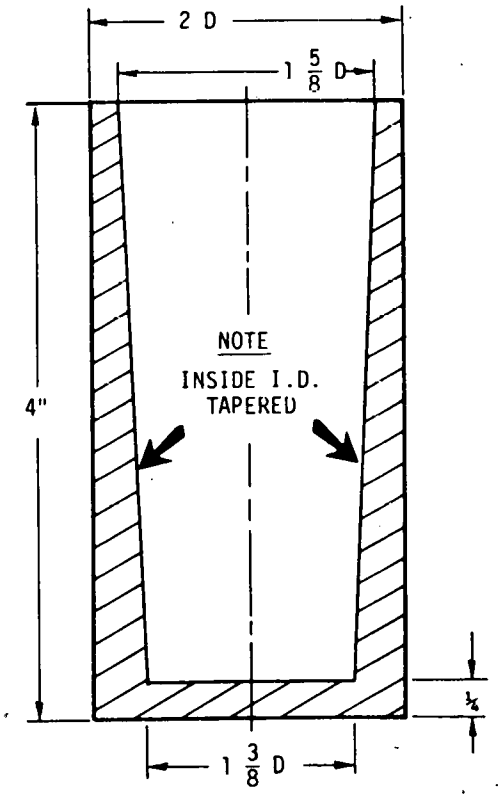

Fig. 45.

Crucible Constructed of Dense Graphite (dimensions in inches)

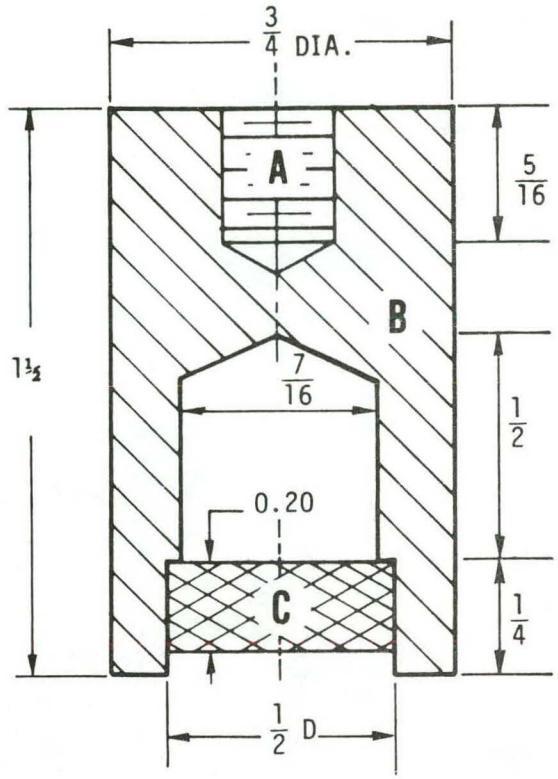

Fig. 46. Sampling Cup (dimensions in inches)

(b) Results

The two experiments were carried out with 0.11 wt % Mo and 0.04 wt % Ru in aluminum. In the first experiment, the metals were heated to 720°C for 3 h under a vacuum of 9.3 pascals (70 x 10^{-3} torr), and in the second experiment, the metals were heated for 4 h at 740°C under a vacuum of 6.7 pascals (50 x 10^{-3} torr). After cooling, the metal discs were examined for Mo and Ru with dysprosium X-rays generated by excitation by the ^{241}Am source. The disc from the first experiment had top to bottom concentration ratios of 0.01 for Mo and 0.1 for Ru. The ratios for the other disc were 0.04 for Mo and 0.24 for Ru. There was a relatively poor vacuum in these experiments which may have reduced the solute solubilities due to the formation of oxide films. These results suggest that it may be possible to suppress the dissolution of some noble metals in aluminum.

Among other experiments there was one in which the mixture consisted of 36.7 g of Al, 6.69 g of Th, 5.47 g of U, 37.6 mg of Zr, and 24.2 mg of Mo. The mixture was kept at 2.6 x 10^{-3} pascals (2 x 10^{-5} torr) and 750°C for 2.5 h, during which time a filtered sample was taken. The ratios of concentrations of the elements in the filtered sample to the concentrations in the melt were Th-0.70, U-0.61, Zr-0.15, and Mo-0.57. These results indicate that the solubilities of these elements (when in the described mixture at the described conditions) are as follows (relative to the weight

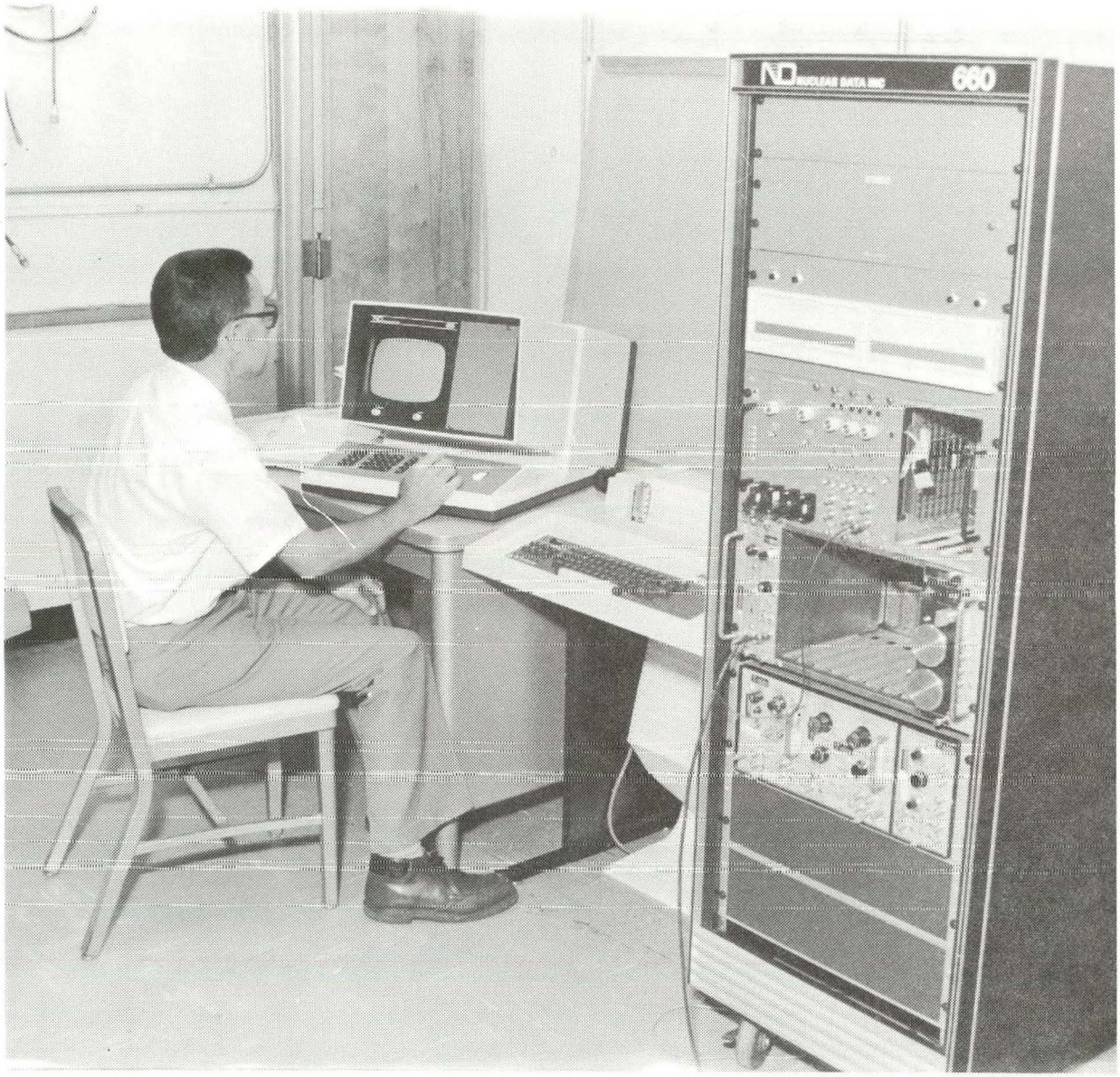

Fig. 47. ND-660 Multichannel Analyzer

of aluminum): Th-12.8%, U-9.1%, Zr-0.015%, and Mo-0.038%. Again, there is some possibility of solubility suppression due to oxide films, since the metals were exposed to air prior to melting. This experiment is of interest because it gives an indication of the amount of aluminum required to dissolve the described mixture of spent fuel. Also, it demonstrates a complete sequence of basic steps in solubility experiments--melting under a fairly hard vacuum and taking filtered samples at temperatures indicated by a thermocouple in the sampling cup.

7. Chloride-Volatility Processing of Thorium-Based Fuels

(R. L. Bennett*)

a. Introduction

The objective of the research and development being conducted for this contract is to determine the feasibility of a chloride volatility coprocess for recovery of irradiated thorium-based fuels. In this process, the thorium-uranium fuel is reacted with Cl_2 and CCl_4 to form volatile heavy metal chlorides which are thereby separated from some fission products and are then separated from some other fission products by fractional condensation. An evaluation of prior work has been performed to obtain data and information about the current technology. This data and information has been organized to provide a block diagram (not included here) of the chloride volatility process. A report is being prepared which describes the existing data and information and the conceptual block diagram. The report will be organized to permit evaluation of technical feasibility, safety, and nonproliferation attributes of the chloride volatility process. Tests are being conducted with simulated fuel to establish technical feasibility and to provide bases for cost estimates.

b. Engineering Analysis

(1) Summary of Work Accomplished During this Quarter

A review of Chemical Abstracts, Energy Research Abstracts, and Nuclear Science Abstracts was completed. The bibliography prepared by Oak Ridge National Laboratory [MCDUFFIE] was reviewed. Hundreds of references were identified, and copies were ordered. Most of these references have been received and reviewed.

Visits were made to Argonne National Laboratory (ANL), Idaho National Engineering Laboratory, Oak Ridge Gaseous Diffusion Plant (ORGDP), Oak Ridge National Laboratory (ORNL) and Pacific Northwest Laboratory. A representative also attended the American Ceramic Society Convention in Detroit on May 9 through 11, 1978. Much valuable information was gained from these visits. There appears to be a wealth of information available at each of these facilities that has not been previously published.

Extensive information has been found on the hydrochlorination of zirconium-uranium alloy fuel, Zircaloy-clad uranium dioxide fuel, and Zircaloy hulls. Work done at ANL, Brookhaven National Laboratory (BNL), Oak Ridge Gaseous Diffusion Plant (ORGDP), Fontenay-aux-Roses (FAR), and ORNL produced data on reaction rates, hydrogen chloride utilization, and uranium losses. Some of the major results, agreed upon by all the organizations mentioned above, are:

---

*Babcock & Wilcox.

(a) Acceptable reaction rates of Zircaloy with hydrogen chloride can be attained at temperatures ranging from 350 to 500°C. The reaction rates range from 0.034 kg zirconium/h for bench-scale studies [REILLY] to 2.4 kg zirconium/h for semiworks-scale studies [BOURGEOIS].

(b) Of the alloying components of Zircaloy, tin will be almost completely removed with the zirconium, while iron, chromium, and nickel will, for the most part, remain with the fuel.

(c) The reaction rate of Zircaloy with hydrogen chloride increases with increasing temperature, hydrogen chloride concentration, and superficial gas velocity. Hydrogen chloride utilization increases with increasing temperature, but decreases with increasing superficial gas velocity. The reaction rate and hydrogen chloride utilization are large at the beginning of a decladding experiment, but drop off rapidly as the reaction proceeds to completion. This makes a multiple-charging technique attractive.

(d) Uranium losses, usually incurred by the entrainment of fines or the volatilization of small quantities of uranium tetrachloride, can be reduced below 0.1% by proper filter design and control of the reaction and filter temperatures.

(e) If the fuel matrix is destroyed, the fission products niobium and zirconium will form volatile chlorides and will be removed from the fuel, and antimony, molybdenum, technetium, and tellurium will form small quantities of volatile chlorides and will be partially removed from the fuel. Ceramic uranium dioxide clad with Zircaloy generally remains intact and so the elements mentioned above are not substantially removed from the fuel during hydrochlorination.

Some problems have been identified with hydrogen chloride decladding that have not yet been solved. Five of the most important problems are listed below:

(a) Sintered metal filters downstream from the hydrochlorination vessel are unsatisfactory for reducing the entrainment of fines and for capturing volatile uranium compounds because they plug during exposure to decladding conditions. Sintered metal filters have been preferred over packed-bed filters because they offer easier scale-up, simpler installation, and reduced maintenance.

(b) The behavior of thorium oxide during decladding has not been determined.

(c) The roles of heat transfer, mass transfer, and reaction kinetics in the reaction of Zircaloy with hydrogen chloride need clarification.

(d) A better grasp of the behavior of fission products during decladding is needed.

(e) Zirconium oxychloride formation has been reported to limit the completeness of reaction of Zircaloy. The mechanism of oxychloride formation should be studied more carefully in order to develop the capability of controlling it.

Knowledge about chlorination of uranium-based fuels appears to be spotty, and knowledge about chlorination of thorium-based fuels is almost nonexistent. The feasibility of uranium dioxide chlorination has been proved experimentally in a number of laboratories--primarily in the United States, Germany, India, and Japan. Chlorination of thorium dioxide-uranium dioxide fuels has been emphasized in India and Germany. Some major results are:

(a) Increased surface area of the solid fuel causes the reaction rate to be substantially increased. Crushing and pulverization to smaller than 0.25 mm is adequate to ensure suitable reaction rates [BOHNENSTINGL].

(b) A mixture of chlorine and carbon tetrachloride is the most efficient chlorinating medium [SOOD-1967].

(c) A temperature greater than 650°C is necessary to provide volatile thorium tetrachloride along with volatile uranium tetrachloride [ISHIHARA].

Two major technological problems are yet to be resolved before commercial nonproliferable chlorination is achieved:

(a) The optimum temperatures to covolatilize thorium and uranium chlorides while yielding minimum corrosion must be determined.

(b) Materials of construction for chlorination systems that have high corrosion rates at chlorination conditions.

Only a few references have been found that relate directly to oxidation of thorium chlorides and uranium chlorides. Investigations were conducted at ORNL [PATTERSON] and at Karlsrule [KANELLAKOPULOS]. All of these investigations were bench-scale and produced limited thermochemical data.

The individual sections of the topical report which discusses decladding, chlorination, fuel oxidation, materials evaluation, ash oxidation, and off-gas treatment have been written. Editing and assembly of the report is under way, and portions of the report have been typed.

(2) Work Plans for the Next Quarter

During the next quarater, work will be done to complete the topical report.

(3) Problem Areas

This task is about six weeks behind schedule. The work effort required to provide a contribution to the INFCE studies delayed completion of the report by about two weeks. The remaining slippage has been caused by underestimation of the effort needed to summarize the extensive literature found during the review of reports.

c. Separations Processes

(1) Summary of Work Accomplished during this Quarter

A drawing for a corrosion tester was sent to International Nickel Company (INCO) in April; INCO originally offered to supply the material for construction of the tester. They have reevaluated the testing conditions and no longer believe they have suitable alloys, and so they have retracted their offer. Because of the loss in time, we now plan to perform the corrosion tests in one of our experimental systems and accept the risk of sacrificing some of the reactor wall thickness.

All equipment and supplies needed for this work have been ordered. Approximately 90% of these materials have been received. Construction of the hood for the main experimental system has been completed. Assembly of the system has been started.

A report was issued which describes the experimental plan, experimental apparatus, and safety procedures and precautions. This report was reviewed by the B&W safety review committee. They requested additional information as well as revisions of some safety procedures. These have been completed, and we expect their approval by July 15.

Design of experiments continued and is about 75% complete. Fuel oxidation experiments were started in June and so we have met the milestone set for that task. A modified pyrohydrolysis apparatus was installed for these tests.

Three preliminary runs were conducted to evaluate the apparatus for oxidation of uranium tetrachloride. A known volume of air was drawn by vacuum through a constant-temperature (95°C) steam generator. This gas mixture then passed over the uranium tetrachloride sample. Gaseous reaction products and unreacted steam passed through a condenser where samples were collected. Preliminary condensate and product analyses indicated that the product was uranium oxide. Additional analyses are necessary to determine the actual composition of the product. Quantitative analyses indicate that the apparatus is functioning properly.

Thoria powder has been purchased from Tennessee Nuclear Specialty, Inc. Physical characterization measurements have been completed. Fabrication of pellets has been completed. Pellets of LWR geometry (weighing approximately 11 g/pellet) and FFTF pellets (weighing about 2 g/pellet) have been made from thorium dioxide, uranium dioxide, and 80% ThO_2-20% UO_2 powders. Thoria pellets made on a hydraulic press sintered to approximately 91% of theoretical density (T.D.) with slight cracking. Hand-pressed pellets sintered to about 93% of T.D. cracked severely upon sintering. All urania pellets, whether made on a hydraulic press or a hand press, sintered to approximately 92% T.D. with excellent surface characteristics. Thorium dioxide-uranium dioxide pellets made on a hydraulic press sintered to approximately 92% T.D. with excellent surface characteristics. Hand-pressed pellets also had excellent surface characteristics, but sintered only to 90% T.D.

(2) Work Plans for the Next Quarter

The design of experiments and experimentation will continue. Assembly of experimental apparatus will be completed.

(3) Problem Areas

We are about four weeks behind schedule on the installation of laboratory apparatus. Delayed delivery of some pieces of equipment has caused this slippage. An effort will be made to recover this lost time by efficient coordination of experiments.

8. AIROX, CARBOX, and RAHYD Processing Systems

(L. F. Grantham* and L. J. Jones*)

a. Introduction

This portion of the program is an extension of fuel reprocessing technology previously undertaken at AI and consists of gas-solid fuel reactions to (a) release gaseous fission products, (b) pulverize the fuel, and (c) separate the fuel from the cladding. These reactions are multiple oxidation-reduction cycles of oxide fuels (AIROX), multiple hydride-dehydride cycles of metal fuels (RAHYD), and multiple oxidation-reduction cycles of carbide fuels (CARBOX). These processes meet the nonproliferation criteria by (a) retention of solid radioactive fission products in the fuel and (b) nonseparation of fissile isotopes such as plutonium and uranium-235 from the fertile isotopes of uranium. During GFY 1978, only oxide fuels and the AIROX process will be studied.

Funding for this portion of the program was released in mid-March 1978. Subaccount Work Authorizations for all phases of FY 1978 activities were released. Capital equipment funds were released in mid-June, and preparation of specifications and purchase orders for the individual equipment items has been initiated.

AIROX and CARBOX Unit Operations Summary Data and Process Cost Estimates for ANL's use in the INFCE (International Fuel Cycle Evaluation) studies were submitted.

b. Engineering Analysis

(1) Proliferation Resistance of Fuel Cycles Utilizing Dry Processing

(L. F. Grantham*)

Until recently, reprocessing of spent fuel was aimed at extracting high-purity, highly decontaminated fissile material for recycle to the reactor by aqueous reprocessing. Recently, emphasis has been placed on

*Rockwell International-Atomics International.

the importance of positive antiproliferation and safeguarded approaches to the nuclear fuel cycle. Two positive approaches are (1) maintenance of a lethal complement of radioactive fission products with the fissile material and (2) avoidance of the separation or utilization of high-purity fissile material in the fuel cycle.

One fuel cycle approach which utilizes these positive antiproliferation and safeguarded considerations is the "dry reprocessing" fuel cycle. Dry reprocessing consists of pyrochemical reprocessing techniques which rely on spent fuel gas-solid or solid-solid oxidation-reduction reactions at elevated temperatures to reprocess the fuel and prepare the reprocessed fuel for enrichment adjustment prior to refabrication and recycle to a nuclear reactor.

Dry-reprocessing fuel cycles have been developed for the uranium-plutonium and thorium-uranium fuels in the LWR, FBR, and the combined LWR-FBR fuel cycles. These fuel cycles will be illustrated with oxide fuels since these are the most highly developed. The reprocessing portion of a typical oxide fuel cycle is the AIROX process, which utilizes air as the oxidizing agent and hydrogen (about 20 vol %) in nitrogen as the reducing agent. Uranium dioxide (UO_2) is oxidized to triuranium octaoxide (U_3O_8) with air, and the U_3O_8 is reduced to UO_2 with hydrogen, as shown in Fig. 48. This cyclic oxidation-reduction reprocessing accomplishes the following:

(a) It expands the fuel (about 30%), which ruptures the punched cladding,

(b) It pulverizes the fuel so that it falls free of the cladding and can readily be reenriched for recycle to the reactors,

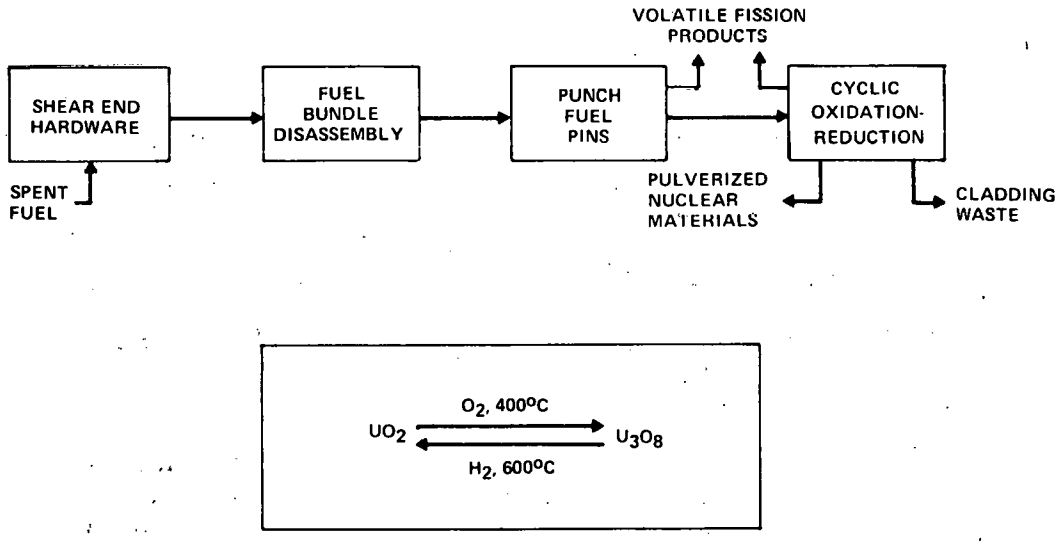

Fig. 48. Flow Diagram for Dry Processing of Oxide Fuel

(c) It releases the entrapped volatile fission products (tritium, krypton, xenon, and iodine) from the pulverized fuel, eliminating the potential of these fission products to cause cladding rupture in recycled fuel, and

(d) It restores the fuel to the original chemical form so that it can be reenriched and recycled to the reactor.

Dry-reprocessing reactions similar to the AIROX process and applicable to reprocessing of other fuels are shown in Table 24.

Table 24. Dry Reprocessing Reactions

	Basic Reactions	
Fuel Type	Uranium-Based Fuels	Thorium-Based Fuels
Oxide	$UO_2 \underset{H_2,\ 600°C}{\overset{O_2,\ 400°C}{\rightleftharpoons}} U_3O_8$	Not Applicable
Carbide	$UC \underset{C,\ 1500°C}{\overset{O_2,\ 400°C}{\rightleftharpoons}} U_3O_8$	$ThC \underset{C,\ 1500°C}{\overset{O_2,\ 400°C}{\rightleftharpoons}} ThO_2$
Metal	$U \underset{Heat}{\overset{H_2}{\rightleftharpoons}} UH_3$	$Th \underset{Heat}{\overset{H_2}{\rightleftharpoons}} ThH_2$

An LWR fuel element is designed so that it reaches its integrity limit about the same time as it reaches its minimum permissible reactivity contribution. Conventional reprocessing is aimed at retrieving as much of the residual fissile material as possible--both the unburned uranium-235 and the bred plutonium or uranium-233. If these considerations are extended to breeder driver and blanket fuels, we note that the integrity limit of these fuels is not reached when the minimum permissible reactivity contribution is achieved.

In the case of the driver, the integrity limit is due to fuel swelling, neutron-induced swelling of cladding, or fission gas limitations. In the case of the blanket, the integrity limit is additionally somewhat coupled with heat-removal limitations as the bred fissile content increases. Since reprocessing techniques for breeder fuel are direct extensions of technology evolved from weapons systems and LWR fuel, the same approach of achieving separate high-purity fissile material and minimizing residual radioactivity levels has been followed.

One aspect of the fuel cycle reevaluation has been a reconsideration of partial reprocessing techniques developed in the early 1960's at Atomics International. These reprocessing approaches were initially aimed at minimizing the complexity and the cost of reprocessing by eliminating to some extent the solvent extraction and high-purity separation steps--that is, except after extensive reuse of the fuel. In other words, the reprocessing was aimed at both satisfying the integrity limits of the fuel and deferring the ultimate high purity reprocessing as long as was economically practicable. These early studies were aimed at the LWR only; however, their results are even more suitable and possibly more desirable for an integrated breeder reactor-LWR cycle. In essence, the fuel is reprocessed through a cycle called "dry" reprocessing to perform the decladding function and to extract the volatile fission products. These rather simplified steps, all conducted in dry thermal-chemical cycles, return a basic raw material properly comminuted for enrichment and pelletizing. Enrichment in the case of the early LWR studies was obtained from the usual fresh uranium-235 sources; for breeders, enrichment was obtained by partial uranium-plutonium separation in the reprocessing of the driver core material.

Fuel cycles capable of utilizing this reprocessing technique were developed to determine if this approach to recycling fuel in a proliferation-resistant manner is feasible. One of the first questions which must be answered is what effect recycled fission products have on the reactor neutronics.

Preliminary computer analyses of the effects of recycled fission products were made using a modified AIMFIRE Code for the LWR analysis and the CEASAR Code for the fast reactor system. These analyses indicated that, indeed, fission product recycle is feasible. In the LWR, the major effect of recycling of fission products is that the recycled fuel eventually requires 115% of the fissionable material otherwise needed to maintain the fuel reactivity and to overcome the parasitic neutron absorption by the fission products. In the FBR, the major effect of recycled fission products is that the fission products displace fertile material, which leads to a corresponding decrease in breeding ratio. The effect on breeding ratio can be significant if breeder core fission products are retained beyond a few cycles (about 10 wt % fission products produced per cycle) for the FBR. Therefore, as discussed later, after a number of dry reprocessings, the driver core fuel is generally further processed by aqueous or pyrochemical means to minimize the impact on breeding ratio.

With AIROX reprocessing, an enrichment stream is required that will bring the fissile content of the AIROX product up to the desired value. The enrichment stream for LWR converts would be provided by virgin uranium enriched to about 17%, which is below the enrichment required for effective weapons production. Alternatively, a low-decontamination pyrochemical or modified aqueous reprocessing plant not capable of completely separating plutonium from uranium or fission products could be used. Dry reprocessing could be used as the head-end decladding step in these processes.

In Fig. 49, a schematic of a combined AIROX-aqueous reprocessing plant is shown. Note that conventional aqueous process front-end steps--chop and voloxidation--are shown in Fig. 49; however, AIROX could

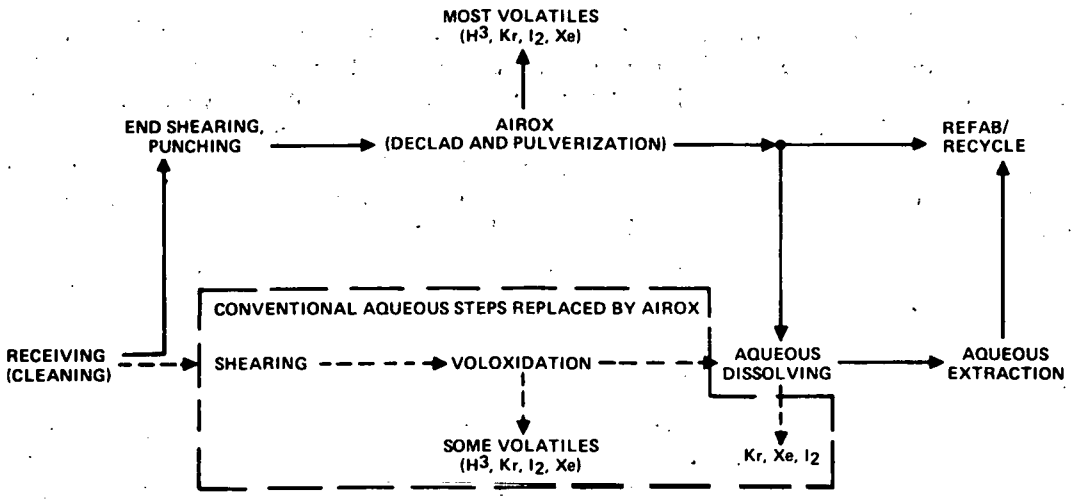

Fig. 49. AIROX Process Use as the Sole Reprocessing Method or as a Head-End System for Conventional Aqueous Reprocessing

completely replace these front-end steps and simplify the overall cycle. This combined reprocessing plant would be small, since only a fraction of the fuel would be processed further than AIROX. Thus, it could be colocated with the refabrication system at a nuclear site. This would enhance fuel security by maintaining the fuel in a secure area and minimizing the amount of plutonium-rich material available onsite at any one time.

(a) LWR Fuel Cycle

One LWR fuel cycle which could utilize dry processing is shown in Fig. 50. In this cycle, the enrichment stream is virgin uranium enriched to about 17% uranium-235; this concentration of fissile uranium-235

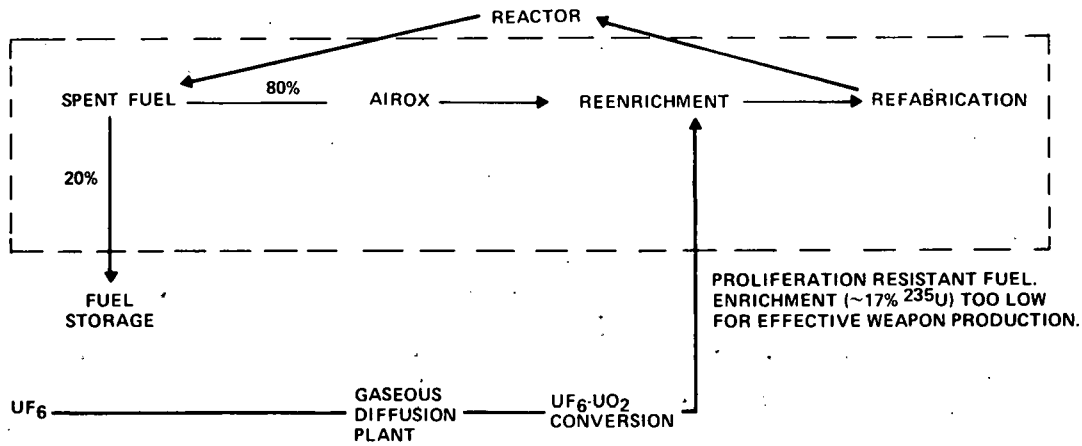

Fig. 50. Proliferation-Resistant LWR Fuel Cycle with Maximum Uranium Utilization. Proliferation resistance provided by leaving fuel highly radioactive with no uranium-plutonium separation

in uranium-238 could not be used to produce an effective weapon without further enrichment. Under these conditions, about 80% of the spent fuel would be recycled after AIROX processing. Since residual plutonium remains in the AIROX processed LWR fuel material, only about 80% as much virgin uranium (assuming that uranium tails are reduced to 0.3% uranium-235) would be required to refuel the reactor if this fuel cycle were used than if no fuel recycle were utilized. Thus, our uranium reserves could be extended about 20% by utilizing the residual recycled plutonium to produce energy instead of an equivalent amount of virgin uranium-235.

(b) FBR-LWR Combination

The fuel management scheme shown in Fig. 51 is particularly attractive for an FBR-LWR combination cycle. In this fuel management scheme, a 1000-MWe breeder would breed enough surplus fissile material to operate a 400-MWe LWR converter, and the LWR enrichment requirements (3 to 4 wt % fissile) could be bred into the fuel in the FBR blankets. The enriched fuel would be withdrawn from the FBR blanket, AIROX processed, and refabricated into LWR fuel. The next FBR driver core would be enriched with the fissile material in spent LWR fuel and the spent driver core fuel after AIROX processing and additional reprocessing. After AIROX processing only, a large fraction (about 40%) of the blanket material is recycled to the LWR or the FBR blanket as (1) the subsequent LWR fuel, (2) the subsequent FBR driver fuel, or (3) subsequent axial blanket material. In the FBR-LWR fuel cycle shown in Fig. 51, a small amount of additional enrichment material would be required for the initial startup of the LWR; after the first 3-y cycles, the enrichment material would be obtained from the spent LWR fuel and the internal blanket.

For an LWR to operate off a breeder island site and still satisfy current proliferation-resistance trends, it would have to operate on the thorium-uranium fuel cycle with the breeder breeding uranium-233 from thorium in the blankets.

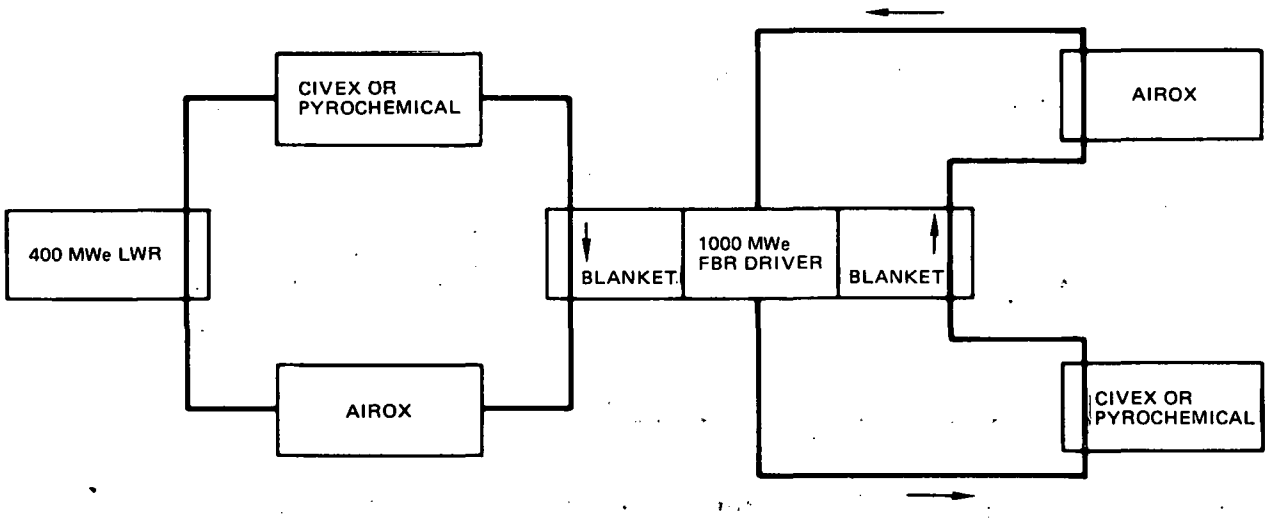

Fig. 51. Fuel Cycle in which a 1000-MWe FBR Drives a 400-MWe LWR

Therefore, in a bullseye core FBR, all of the internal blanket and about one-third of the external blanket would be thorium while the axial blanket and the remainder of the external blanket would be uranium. The fuel flow schemes would be similar to those shown in Fig. 51 except (1) the material flowing between the FBR blanket and LWR would be thorium containing the bred uranium-233 and (2) the material flowing from the LWR to the breeder blanket and driver, respectively, would be thorium and plutonium. About 40% of the fuel could be recycled after dry processing only.

(2) Nuclear Analysis
(P. W. Twichell*)

(a) Work Plan

Objectives. The primary objective of the nuclear analysis activities for GFY 1978 will be to perform scoping fuel cycle analyses of a typical large PWR which uses the AIROX fuel reprocessing method. A secondary objective will be to determine the decay heat and radiation levels for spent fuel during and after AIROX fuel reprocessing.

Approach. To meet these objectives, an analysis of the buildup and burnup of the major fission products and actinides will be performed for a multicycle system. The relative importance of individual fission products will be determined. Fuel cycle parametrics will be conducted to establish an optimum reference fuel cycle with respect to cost. Fuel cycle cost comparisons will be performed for a once-through cycle, a Purex reprocessing system, and the reference AIROX reprocessing system.

Fission Product Buildup and Importance. Because AIROX is a partial-decontamination fuel reprocessing technique, the importance of individual fission products must be quantified in order to determine the multicycle fuel enrichment requirements, and ultimately to evaluate the overall fuel cycle costs. The preliminary step-by-step approach to determine individual fission product importance is shown in Fig. 52. The following is a short description of the 14 steps in Fig. 52.

Steps

1 and 2	- Fission product cross-section libraries will be added to the HAMMER Code. The fission product cross sections and yields in the AIMFIRE Code will be updated to agree with the national Evaluated Nuclear Data File (ENDF/B-IV).
3,4, and 5	- The reactor parameters for the reference LWR will be obtained and organized for proper input into all three computer codes.

*Rockwell International-Atomics International.

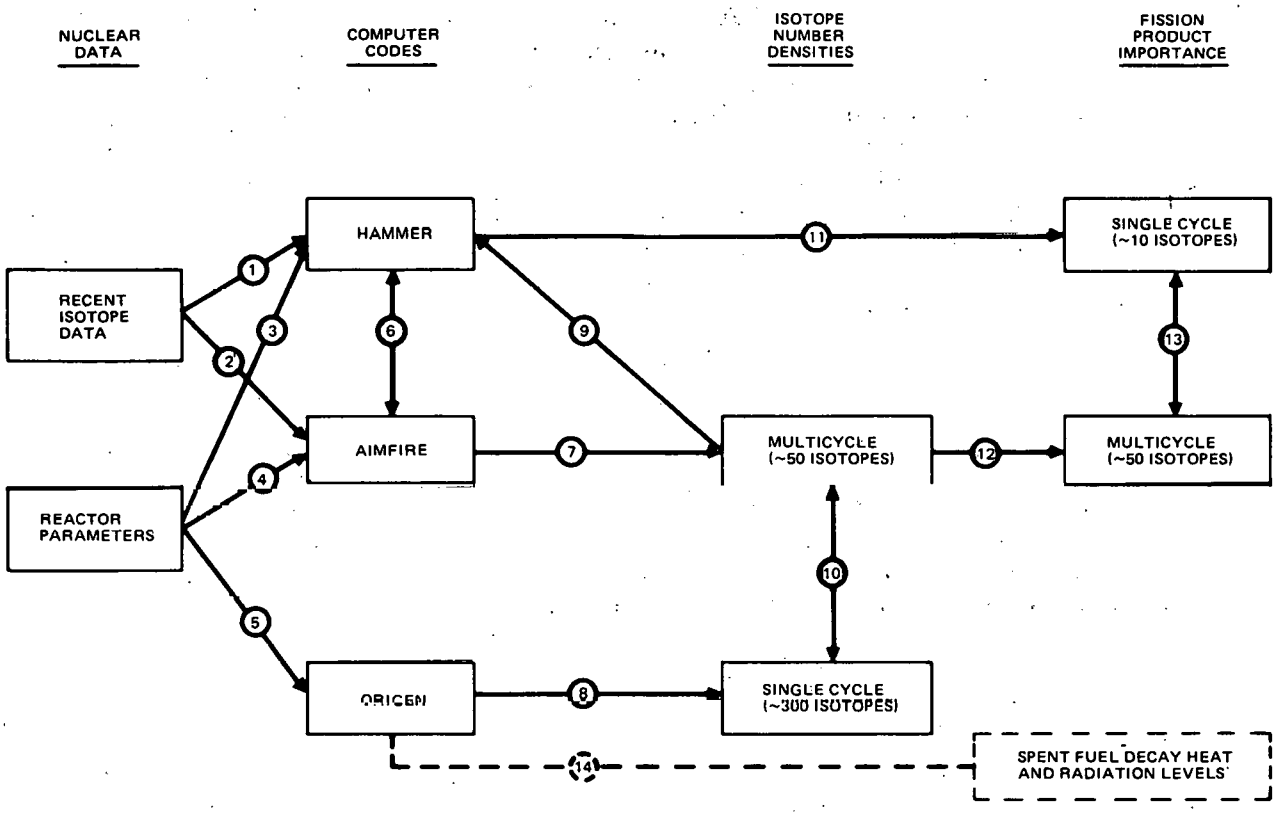

Fig. 52. Procedure for Determining Fission Product Distribution after Multiple Cycles

6 - Physics data (e.g., diffusion constants, cell disadvantage factor, individual non-I/V cross-section factors, etc.) which are needed as input in the AIMFIRE Code will be obtained via the HAMMER Code. Some physics data will be obtained by several interactions between the two codes at different burnups.

7 - The output of AIMFIRE yields isotope number densities for approximately 50 fission products and actinides at the beginning and end of each cycle for a specific multicycle system.

8 - The output of the ORIGEN Code yields isotope number densities of more than 300 nuclides at the end of a single cycle.

9 and 11 - The number of densities of the major fission products from AIMFIRE will be fed into HAMMER to calculate fission product importance.

10 - The number densities obtained from AIMFIRE and ORIGEN will be compared and evaluated.

12 - Fission product importance will be obtained from AIMFIRE.

13 - The fission product importance from HAMMER and AIMFIRE will be compared and evaluated.

14 - Spent fuel decay heat levels and radiation levels as a function of time after reactor shutdown will also be obtained from ORIGEN.

The Yankee Core 1 will be evaluated first to test the codes before a large reference PWR is analyzed. Since there is much available experimental and theoretical nuclear analysis on Yankee Core 1, this analysis should be a good test case for these codes and this method of analysis.

Optimum Fuel Cycle. Scoping analysis will be performed to obtain a fuel cycle that is optimal with respect to cost. Fig. 53 shows the preliminary flow path for fuel cycle cost optimization. The fuel cycle

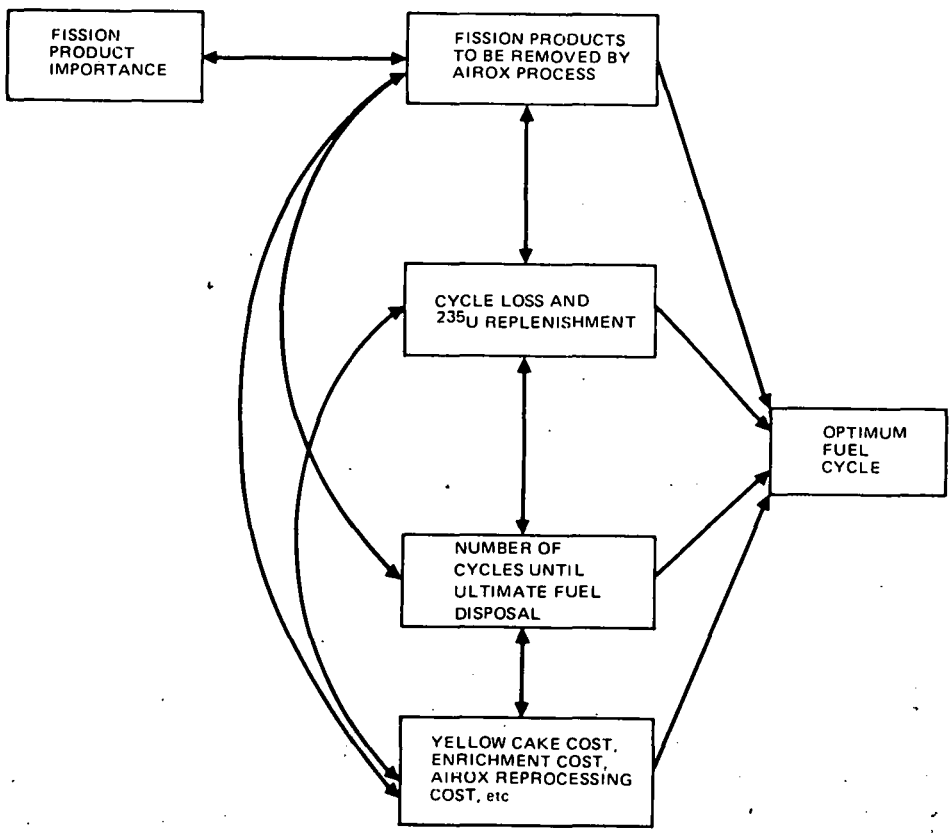

Fig. 53. Flow Path for Fuel Cycle Cost Optimization

cost is a function of four factors: (1) fission products which will be removed by the AIROX process, (2) cycle loss and uranium-235 enrichment between cycles, (3) number of cycles until ultimate fuel disposal, and (4) costs of AIROX reprocessing, yellow cake, enrichment, etc. An optimum fuel cycle will be selected by performing sensitivity analyses of these four factors. The AIMFIRE Code, which was developed specifically for this purpose, will be used to perform this analysis.

Comparison of Fuel Reprocessing Alternatives. Fuel cycle cost comparison of the reference AIROX process, an aqueous process (e.g., Purex process), and a once-through fuel cycle system will be made. Cost sensitivity will be applied to the AIROX reprocessing method. These three fuel cycle alternatives will also be compared with respect to their fuel utilization characteristics, subject to the constraint of a fixed uranium resource base.

Spent Fuel Decay Heat and Radiation Levels. Decay heat and radiation levels as a function of time after reactor shutdown and cycle number will be determined by use of the ORIGEN Code. This information will be needed to characterize the thermodynamic processes and to assess shielding requirements for AIROX reprocessing.

(b) Accomplishments

Code Development. Three codes have been made operational on Atomics International's computing system for the purpose of performing the nuclear analysis. AIMFIRE is a multicycle fuel inventory reprocessing economics code which calculates the burnup and buildup of fission products and actinides, fission product importance, and fuel enrichment requirements. The HAMMER Code performs static neutronic calculations for a specific reactor configuration. The HAMMER Code is used to determine reactor criticality and to calculate certain physics data which are needed as input for the AIMFIRE Code. ORIGEN is a point depletion code which will be used to determine decay heat and gamma radiation levels for spent fuel during and after reprocessing.

Both the AIMFIRE and HAMMER Codes have been modified to better perform the fuel cycle analysis for the AIROX fuel reprocessing technique. The fission product chains used in the AIMFIRE Code have been improved. The new fisison product chains are similar to the 12-chain library contained in the EPRI-CINDER Code. The fission product cross section and yield library in AIMFIRE has been revised to conform with the most recent values. A fission product cross-section library has also been added to the HAMMER system.

Preliminary Analysis. Preliminary analysis of the Yankee Core 1 was conducted using the AIMFIRE and HAMMER Codes. This analysis was a good test case for these codes and the method of analysis. Preliminary results, such as fuel burnup length, are in good agreement with documented Yankee Core 1 performance. The Yankee Core 1 analysis also highlighted the necessary code modifications, e.g., revision of the fission product chain, before fuel cycle analysis of a more complex large (3411-MWt) reference PWR.

The decay heat and radiation levels for fuel burnup to 33,000 MW/MT for a large (3411-MWt) PWR have been successfully calculated using the ORIGEN Code. The decay heat and radiation levels for fuel burnup greater than 33,000 MW/MT, i.e., after AIROX reprocessing, will be calculated with the ORIGEN Code when the isotope-removal fractions and uranium enrichment requiremens have been calculated by the AIMFIRE and HAMMER Codes discussed above.

(3) Literature Review
(R. C. Hoyt*)

The following is a summary of the AIROX literature review, which is still in progress.

(a) AIROX Pyrochemical Process

The AIROX pyrochemical process is a low-decontamination dry process [BRAND] which is applicable to UO_2, UO_2-PuO_2, and possibly UO_2-ThO_2 fuels. Prior to dry processing, the fuel rods are punched at regular intervals of about 1.27 cm (about 1/2 in.) to facilitate fuel-gas interaction and to facilitate fuel decladding by serving as stress points which initiate cladding rupture as the fuel expands.

This reprocessing method utilizes a cyclic pyrochemical technique to simultaneously declad the fuel, pulverize the fuel, remove volatile fission products, and restore the fuel to the proper chemical form for reenrichment and recycle to the reactor. The UO_2 (density 11.0 g/cm^3) is oxidized to U_3O_8 (density 8.3 g/cm^3) in oxygen at 400 to 500°C and then reduced back to UO_2 in hydrogen at 600 to 850°C. During these reactions, the UO_2 phase undergoes a volume change of about 38%; the resulting internal stresses are relieved by pellet cracking and pulverization to a powder. Repeated oxidation-reduction cycling pulverizes the fuel to a very fine powder, allowing both entrapped fission gas and volatile fission products to be released and the fuel to be completely separated from the cladding. The pulverized fuel is then blended with enriched UO_2, refabricated into pellets, and recycled to the reactor.

A flowsheet for the AIROX cyclic pyrochemical process is shown in Fig. 54. The principal piece of equipment is an atmosphere- and temperature-controlled furnace having conventional materials of construction which can withstand oxygen atmospheres at up to 500°C and hydrogen atmospheres at up to 850°C.

(b) Review of Previous AIROX Pulverization and Decladding Investigations

The AIROX process was investigated by Atomics International from 1959 to about 1965 to determine whether lower fuel cycle costs could be achieved by low-decontamination reprocessing. They performed a series

*Rockwell International-Atomics International.

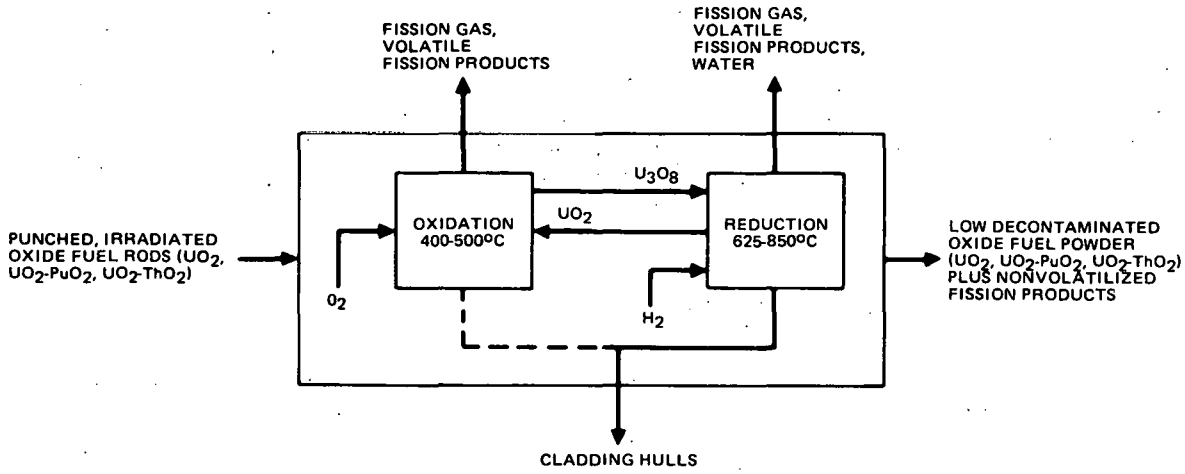

Fig. 54. AIROX Cyclic Pyrochemical Process

of small-scale pulverization experiments to investigate the oxidation and reduction conditions of unirradiated UO_2 [STRAUSBERG-1959] and unirradiated UO_2-1% fissia (UO_2 with simulated fission products equivalent to 1% total burnup) [STRAUSBERG-1960]. Results of these experiments (Tables 25 and 26) indicate that oxidation at temperatures 375 to 400°C yields the highest degree of pulverization and that the addition of 1% fissia to the UO_2 does not significantly affect pulverization.

Table 25. UO_2 Pellet Comminution by AIROX Process[a]

Temperature, °C	305	375	375	520	700
Oxidizing Time, h	3	2	2	1	1
Oxidizing Medium	Air, 1.01×10^5 Pa (1 atm)	O_2, 2.13×10^4 Pa (160 mm Hg)	Air, 1.01×10^5 Pa (1 atm)	Air, 1.01×10^5 Pa (1 atm)	O_2, 2.13×10^4 Pa (160 mm Hg)
Mesh Size	Weight Percent				
+10	7.5	0.1	0	12.0	0.6
-10 +20	4.2	0.4	0	2.1	2.5
-20 +40	1.7	0.6	0	0.8	11.3
-40 +100	1.4	2.4	0	0.7	32.2
-100 +200	0.8	5.9	0.3	5.0	24.4
-200 +325	3.7	9.4	4.4	8.4	10.0
-325	80.6	81.2	95.2	71.1	19.0
	99.9	100.0	99.9	100.1	100.0

[a]Data taken from [STRAUSBERG-1959].

Table 26. Comparison of Pellet Oxidation Comminution for UO_2 and UO_2-1% Fissia [STRAUSBERG-1959]

	UO_2-Fissia		Pure UO_2	
Number of Pellets	1	5	1	10
Pellet(s) Weight, g	11.18	54.92	5.78	58.09
Air Pressure, pascals x 10^5	1.01	1.01	1.01	1.01
Temperature, °C	370-390	375	370-400	375
Time at Temperature, h	1 1/2	3	1 1/4	2
Mesh Size				
+50, wt %	0.8	0.9	0.5	0
-50 +400, wt %	5.5	4.4	3.8	4.7
-400, wt %	93.6	94.7	95.7	95.1
	99.9	100.0	100.0	99.8
U_3O_8 (Calculated), %	95	84	100	93

In work not presented in a graph or table, thermal reduction of the oxidized powders at 1100 to 1200°C proved undesirable because at this temperature, sintering of the UO_2 particles reduced the quantity of particles that were smaller than 400 mesh by more than 45%. Reduction in hydrogen at temperatures of 590 to 725°C, however, did not change the particle size distribution of the powders.

A series of experiments [STRAUSBERG-1962] was carried out to investigate the effect of fission product buildup on the AIROX process during multicycle operation. In these experiments, simulated fission product buildup was accomplished by mixing processed powder with 2% fissia (Table 27) prior to each experiment, fabricating the blender powder into pellets, and AIROX processing these pellets through three oxidation-reduction cycles. Fissia was added five times, (Runs ETB-II through ETB-VI), simulating a total burnup of 100,000 MWd/MTU. Particle sizes of the processed powders, shown in Table 28, demonstrate that the accumulation of fission products equivalent to a burnup of 100,000 MWd/MTU does not significantly affect pulverization of the UO_2 pellets.

Small-scale decladding experiments [HANSON] were conducted on 10- to 15-cm sections of stainless steel tubes and Zircaloy tubes containing UO_2 pellets. Scaled-up experiments [BODINE-1964] were then conducted on 28- to 91-cm sections of stainless steel tubes containing UO_2 pellets. These investigations indicated that if the fuel rod is punctured at 2.5-cm intervals, the cladding will split as the fuel expands during the

Table 27. Relative Composition of Stable Isotopes in UO_2-2% Fissia, Simulating Burnup of 20,000 MWd/MTU [STRAUSBERG-1962]

Fission Product	Fission Product Compound	Parts of Compound/1,000,000 parts UO_2
Ba	$BaCO_3$	963
Ce	CeO_2	2,112
Cs	Cs_2CO_3	1,470
La	La_2O_3	803
Mo	Mo	1,800
Nb	Nb_2O_5	63
Nd	Nd_2O_3	2,137
Pr	Pr_6O_{11}	811
Ru	Ru	961
Sm	Sm_2O_3	291
Sr	SrO	881
Y	Y_2O_3	423
Zr	ZrO_2	3,240
	Total	15,955[a]

[a]Approximately 1.6 wt % fissia.

oxidation of UO_2 to U_3O_8. Decladding rates of the punched fuel elements were three to ten times greater than those for fuel rods with their ends cut off but unpunched. It was demonstrated that a 91-cm-long fuel rod could be completely declad in oxygen at a pressure of 9.80×10^4 pascals (737 mm Hg) at 400 to 425°C. The pulverized fuel contained no cladding corrosion products, and sieve analysis showed that 20 to 24 wt % of the particles were smaller than 37μm diameter.

A multicycle experiment on a 100-g scale was carried out, using remote methods. The fuel was clad in stainless steel and had been irradiated to 5,700, 18,000, and 21,000 MWd/MTU; it was processed through AIROX, using three oxidation-reduction cycles [GUON-1962]. The powder from this work was then refabricated and reirradiated for an additional 10,000 MWd/MTU GUON-1964], then reprocessed and refabricated a second time [BODINE-1965]. Decladding tests from these studies indicated that the decladding rate for irradiated UO_2 is similar to that of unirradiated UO_2 and that the optimum conditions for decladding is in the oxygen pressure range of 5.05×10^4–8.45×10^4 pascals (380- to 635-mm Hg) and in the temperature range of 440

Table 28. Summary of Multicycle Reprocessing of UO_2-Fissia [STRAUSBERG-1962]

	Run ETB-1	Run ETB-II	Run ETB-III	Run ETB-IV	Run ETB-V	Run ETB-VI
Starting Material	MCW UO_2	Pellets from ETB-I	Pellets from ETB-II	Pellets from ETB-III	Pellets from ETB-IV	Pellets from ETB-V
Powder Product						
No. oxidation-reductions	3	4	3[a]	3	4	3
-400 mesh, %	91.9	98.0	97.3	98.0	98.3	96.7
Mean part. size, μm	1.2	1.2	1.5[a]	1.2	1.4	1.4
O/U ratio	2.0	2.0	2.6 [a]	2.0	2.0	2.0
Simulated burnup (%)	0.0	2.0	4.0	6.0	8.0	10.0
Green compacts						
Density[b] (% TD)	58.2 ± 0.5	57.4 ± 0.6	61.8 ± 0.7[a]	56.1 ± 0.8	57.0 ± 0.6	60.3 ± 0.3
Diameter, cm	1.123	1.123	1.123	1.120	1.123	1.123
Height, cm	1.125	1.125	1.102	1.171	1.077	1.097
Sintered Pellets						
Density [c] (% TD)	95.7 ± 1.4	93.2 ± 1.6	91.0 ± 1.2	98.4 ± 0.7	98.8 ± 0.3	100.3 ± 0.3
Diameter, cm	0.973	0.975	0.886	0.991	0.922	0.935
Height, cm	0.942	0.945	0.879	0.917	0.914	0.922
Sintering weight loss, %	2.06 ± 0.04	2.03 ± 0.03	8.63 ± 0.34[a]	2.59 ± 0.14	2.78 ± 0.02	3.93 ± 0.09
Product weight, kg	2.1	1.8	1.5	1.3	1.0	0.9

[a] Pyrophoric product of three oxidation-reduction treatments was refabricated as U_3O_8.

[b] Percent of theoretical density, determined by geometric method.

[c] Percent of theoretical density, determined by water-displacement method.

to 515°C. No differences were noted in oxidation-reduction processing of unirradiated or highly irradiated UO_2, except that approximately 2% of the highly irradiated powder would not pulverize to smaller than 200-mesh.

(c) The Chemical and Physical States of Spent Oxide Fuel

In order to determine the behavior of actinide and fission product compounds during AIROX processing, it is first necessary to establish the physical and chemical states of spent oxide fuels prior to dry processing. The fuel must be characterized as to fission product compounds,

fission product and actinide distribution, and pellet grain structure. These characteristics, along with process conditions, ultimately determine the degree of pellet pulverization and the extent of fission gas and volatile fission product release.

Oxide fuel undergoes significant restructuring during irradiation [DEHALAS, CHRISTENSEN-1969 and -1970]. The center of the fuel pellet may melt during initial irradiation, and within a few hours, the pellet will be restructured through void migration caused by the high-temperature gradient. Voids near the central portion of the pellet migrate up the thermal gradient by a fuel evaporation-condensation mechanism, resulting in a central void surrounded by large columnar grains. Equiaxed grain growth occurs adjacent to the outer radius of the columnar grain zone and adjacent to the central void because of high temperatures and lower thermal gradients in these regions. However, the equiaxed grain growth region near the central void is not always noticeable because of its replacement with columnar grains resulting from the continued, but much slower, migration of voids. Grain growth does not occur in the outer, cooler regions of the pellet. The net result of this fuel pellet restructuring is the formation of a heterogeneous grain structure which influences the particle size distribution during AIROX processing because irradiated UO_2 fractures along grain boundaries [NEWKIRK, HAIRE]. This is not the case for unirradiated UO_2, which has been reported to fracture predominantly by transcrystalline cleavage [NEWKIRK. Consequently, the particle size distribution obtained from pulverization of unirradiated UO_2 is not limited by its grain size distribution.

As burnup increases, the accumulation of fission products affects the dimensional and chemical stability of the fuel, in addition to reactor neutronics. The chemical form and distribution of these fission products are major factors in determining the difficulty of their removal during fuel reprocessing. Neglecting, for the moment, fission product distribution, the fission products may be divided into three groups shown in Table 29: (1) those that are stable as a metal, (2) those that are stable as a vapor, and (3) those that are stable as an oxide or other compound. Fission products which are stable as metals may form various metallic inclusions within the fuel matrix. Some of the reported compositions of these inclusions are listed in Table 30. A few of the elements may exist as both a metal and a vapor, depending on their location in a pellet and hence the temperature they are exposed to. Upon removal from the reactor, however, these elements would exist in their solid metal states because of the lower fuel temperature.

It is difficult to predict the behavior of specific fission products because this depends on many variables: (a) the birth location of the fission product in the fuel pellet, (b) the fission product concentration, which increases with burnup, (c) the temperature distribution and hence thermal conductivity of the fuel, which continuously changes with burnup and fuel restructuring, (d) the O/M ratio, which increases with burnup and affects the thermodynamic properties of some fission products, and (e) the large number of compounds and metallic inclusions which are possible because of the large number of different fission products. Redistribution of the fission products results in the formation of gas bubbles, inclusion phases, and solid solutions with the UO_2 matrix. It has been observed,

Table 29. Stability of Fission Products Found in Irradiated Oxide Fuel

	Element or Compound	Reference				
		[O'BOYLE-1969]	[EWART]	[LEITNAKER]	[DAVIES]	[KLEYKAMP]
Metals	Mo	x	x	x	x	x
	Ru	x	x	x	x	x
	Tc	x	x	x	x	x
	Pd	x	x	x	x	x
	Rh	x	x	x	x	x
	Ag	x		x		
	Cs		x		x	
	Te		x		x	
	Fe		x			x
	Cr		x			
	Ni		x			x
	Sn		x			x
Vapors	Xe	x		x	x	
	Cs	x			x	
	Te	x		x		
	Kr	x		x	x	
	I	x				
	Rb	x			x	
	Cd	x		x		
	Sn	x				
	Se	x				
	Sb	x				
	Br	x				
Oxides and Other Compounds	ZrO_2	x		x	x	
	MoO_2	x			x	
	NdO_2 or Nd_2O_3	x		x	x	
	CeO_2 or Ce_2O_3	x		x	x	
	LaO_2 or La_2O_3	x		x	x	
	PrO_2 or Pr_2O_3	x		x	x	
	YO_2 or Y_2O_3	x		x	x	
	SmO_2 or Sm_2O_3	x		x	x	
	PmO_2 or Pm_2O_3	x		x	x	
	EuO_2 or Eu_2O_3	x		x	x	
	GdO_2 or Gd_2O_3	x		x		
	NbO_2			x	x	
	Nb_2O_3	x				
	SrO	x		x	x	
	BaO	x		x	x	
	Rb_2O			x		
	Cs_2O			x		
	$BaZnO_3$				x	
	CsI			x	x	
	CsBr				x	

Table 30. Composition of Metallic Inclusions Found in Irradiated Oxide Fuel

Fuel	Inclusion Composition, at. %													Reference
	Mo	Cs	Ru	Tc	Te	Rh	Pd	Zr	Ba	Ce	Sn	U	Pu	
UO_2[a]	60	--	24	16	--	--	--	--	--	--	--	--	--	[BRADBURY]
UO_2[a]	54	--	23	17	--	6	--	--	--	--	--	--	--	[JEFFERY]
UO_2[a]	33	--	13	9	--	--	--	17	22	6	--	--	--	[JEFFERY]
UO_2[a]	--	--	--	--	--	--	--	34	11	55	--	--	--	[JEFFERY]
$PuO_{1.7}$[b]	27	--	26	14	--	13	20	--	--	--	--	--	--	[DAVIES]
PuO_2[b]	5	--	17	8	--	17	33	--	--	--	--	--	--	[DAVIES]
$U_{0.8}Pu_{0.2}O_2$	--	--	1	--	--	15	59	--	--	--	--	18	8	[KLEYKAMP]
$U_{0.8}Pu_{0.2}O_2$	21	--	48	17	--	12	2	--	--	--	--	--	--	[O'BOYLE-1970]
$U_{0.85}Pu_{0.15}O_2$	44	--	32	15	--	7	2	--	--	--	--	--	--	[BRAMMAN]
$U_{0.85}Pu_{0.15}O_{1.94}$	--	--	--	--	--	--	74	--	--	--	--	15	11	[EWART]
$U_{0.85}Pu_{0.15}O_{1.94}$	37	--	37	10	--	11	5	--	--	--	--	--	--	[EWART]
$U_{0.85}Pu_{0.15}O_{2.15}$	--	--	62	9	--	20	9	--	--	--	--	--	--	[EWART]
$U_{0.85}Pu_{0.15}O_{2.15}$	--	--	--	--	22	--	74	--	--	--	--	4	--	[EWART]
$U_{0.85}Pu_{0.15}O_{2.15}$	--	--	--	--	30	--	60	--	--	--	--	10	--	[EWART]
$U_{0.85}Pu_{0.15}O_{2.023}$	--	-6	--	--	14	--	74	--	--	--	3	3	--	[EWART]
$U_{0.85}Pu_{0.15}O_{2.023}$	--	-1	--	--	21	--	70	--	--	--	5	3	--	[EWART]

[a] These inclusions were also reported to contain from 12 to 40 wt % uranium.

[b] Inclusions were not well formed and had entrained fuel material.

however, that cesium migrates to the cooler, unrestructured region of the fuel and accumulates predominantly at the grain boundaries [OI-1965]. Both ruthenium and niobium are frequently found at high concentrations near the fuel center and at the periphery of the columnar grain zone, and at intermediate concentrations in the equiaxed grain zone [POWER, OI-1964]. There is also a tendency for americium, neodymium, and curium to concentrate at the periphery of the pellet [MEGERTH].

Some of the fission products have considerable mobility particularly krypton, xenon, iodine, and tritium, as well as the elements which form volatile oxides depending upon the O/M ratio such as cesium and to a much lesser extent niobium [TURNBULL, STEHLE, FINDLAY, FROST]. A dynamic equilibrium exists between the gas bubbles, which remain very small and at very high pressure, and the gas which is dissolved in the fuel matrix. The fission

gas produced in the cooler, unrestructured zone of the pellet remains intragranularly dispersed in the fuel matrix. However, in the region where the temperture is high enough for equiaxed grain growth to occur, the bubbles migrate toward the grain boundaries where they accumulate and may interlink, forming a connecting path to the exterior of the pellet and escaping into the gas plenum. Gas bubbles in the higher temperature, columnar grain zone migrate up the temperature gradient by a fuel evaporation-condensation mechanism and reach the gas plenum through the central void. This transport of gas bubbles through the fuel matrix is dependent upon the diffusion coefficient of the fission gas, which has been shown to be a function of both temperature and grain size [KLIMA].

Based upon the above information, it is possible to understand the relationship between the degree of fuel restructuring, the amount of fission gas released, and the particle size distribution obtained during pellet pulverization. As the amount of restructuring increases, the amount of fission gas released during pulverization increases because of the increased fission gas accumulation at the grain boundaries. It also follows that increased fission gas accumulation at the grain boundaries will result in more fission gas being released to the gas plenum through interlinking. Consequently, more fission gas will be released from the fuel rod during AIROX punching and decladding operations.

If relatively little restructuring occurs during irradiation, the majority of the fission gas remains intragranular and is not released upon pellet pulverization. It would also be expected that if no fuel pellet restructuring occurs during irradiation and if the original microstructure of the fuel pellet was homogeneous, the particles obtained upon pellet pulverization would be small and have a narrow size distribution. However, if the pellet had been restructured such that the grain structure is significantly heterogeneous, one would expect to obtain both large and small particles during pellet pulverization. One would also expect that smaller particles would be obtained upon pulverization of unirradiated UO_2 fuel pellets than upon pulverization of any irradiated pellets.

These relationships have been observed experimentally and reported in the literature. Increased fission gas release to the gas plenum when the amount of fuel restructuring increases is shown in Table 31, and the increase in particle size which results from pulverization of fuels with increased burnup and, hence, increased fuel restructuring, is shown in Table 32. Additional results from voloxidation studies, [GOODE-1970A and -1970B], have shown that during oxidation of UO_2 to U_3O_8, krypton gas is released more completely from portions of the fuel where restructuring has occurred (more fission gas has accumulated at grain boundaries) than from regions where the fuel was not restructured (more fission gas intragranularly dispersed in the fuel matrix).

Table 31. Dependence of Fission Gas Release on Grain Growth[a]

Percent of Fuel Pellet in which there is Equiaxed and Columnar Grain Growth	Percent of Fission Gas Released to the Gas Plenum
9	1.4
30	2.8
38	35.5
52	31.0
81	58.3

[a]Data taken from [BODINE-1965].

Table 32. Effect of Burnup on Particle Size During Oxidative Decladding of Uranium Dioxide

Burnup MWd/MTU	Percent of Particles Smaller than 200 Mesh	Reference
0	95-98	[BRAND]
5,700	91.3	[BODINE-1964]
18,000	78.9	[BODINE-1964]
21,000	71.3	[BODINE-1964]

c. Separations Processes

(1) Fuel Procurement
(J. R. Miller*)

Oxide, carbide, and metal fuels are being obtained by transfer from DOE sources to supply the materials needed for the process verification and process demonstration studies. The status of this effort is shown in Table 33. As the specific fuels are identified, stainless steel and Zircaloy claddings are being ordered so that simulated fuel elements can be assembled. These simulated fuel elements will be used to evaluate the decladding effectiveness of the various processes.

*Rockwell International-Atomics International.

Table 33. PDPM Fuel Procurement

Fuel Type	Burnup	Dia., cm	Quantity	Source	Status
UO_2	0	1.27	1200 g	AI	On hand
UO_2	0	0.51	400 g	HEDL	To be shipped by 7/7/78
UO_2	∿3%	0.94	3 Oconee I Rods	B&W	RFQ[a] out
(U, 0.15 Pu)O_2	0	0.51	75 g	HEDL	
(U, 0.20 Pu)O_2	0	0.51	100 g	HEDL	To be shipped by
(U, 0.25 Pu)O_2	0	0.51	75 g	HEDL	7/7/78
(U, 0.25 Pu)O_2	0	0.51	75 g	HEDL	
U metal	0	0.33	80 EBR II pins	ANL-W	RFQ[a] out
U metal	8%	0.33	50 EBR II pins	ANL-W	RFQ[a] out
	10%	0.33	∿10 EBR II pins	ANL-W	Available 10/1/78
UC	0	0.76	∿200 g	WARD[b]	To be shipped by 1/1/79
(U, Pu)C	0	0.76	∿200 g	WARD[b]	To be shipped by 1/1/79
(U, Pu)C	8%	0.76	∿4 kg	WARD[b]/ LASL	Being negotiated
Th-U metal	0			Nat'l Lead (?)	Still seeking source
Th-1.3 U metal	∿0.2%	6.35 OD, 4.57 ID (tube)	90 kg	SRL	Being evaluated
(U, Th)C	0			Nat'l Lead (?)	Still seeking a source of material
(Th, 20Pu)C	0	0.76	∿300 g	LASL	Being negotiated
(Th, 20U)C	0	0.76	∿300 g	LASL	Being negotiated

[a]Request for quotation.

[b]Westinghouse Advanced Reactors Division.

To establish a standard of comparison for judging the performance of the AIROX processes, a tentative oxide fuel specification is being prepared. This specification will be based on existing standards and manufacturers' product analyses. A summary of the standards and product analyses obtained to date is shown in Table 34.

(2) Process Verification--Uranium Dioxide
(R. G. Clark* and R. C. Hoyt*)

(a) Experimental Approach

(i) Test Parameters and Methodology

The overall AIROX process can be considered in the context of four major steps: (1) decladding, (2) cyclic oxidation-reduction pulverization, (3) blending of processed powder with powder enriched with a fissionable isotope, and (4) fabrication of the blended powder into pellets. The first two process steps are currently under investigation during FY 1978.

Parameter optimization can be considered with respect to three different areas of interest: (1) overall process time, (2) degree of fuel pellet pulverization, and (3) amount of volatile fission products released. The release of volatile fission products will depend upon both temperature and the degree of pellet pulverization; however, any volatile fission products not released during the decladding and pulverization steps will most likely be released during the blending and pellet sintering operations. This is because of the extremely fine particles formed during ball-milling and the high temperatures reached during pellet sintering. Pellet decladding and pulverization steps should be optimized with respect to the release of volatile fission products in order to minimize fission product evolution during subsequent process steps. The degree of pellet pulverization during decladding and cyclic oxidation-reduction pulverization steps is not necessarily a limiting factor, however, since results published in the literature indicate that the processed fuel particles are highly friable, with many of the particles breaking up during normal sieve analysis. Therefore, if a sufficient amount of pulverization is obtained to release fuel from cladding, the ball mill blending operation should easily reduce the particles to the desired 5- to 10-μm size range. The maximum particle sizes suitable for being ball-milled in a reasonable amount of time will have to be determined experimentally.

The most important condition in parameter optimization is overall process time. The literature review has indicated that decladding can be accomplished in a minimum of 2 h, with the resulting reactor fuel particles being about 24 wt % <37μm, and that pulverization of the fuel to about 97 wt % <37μm can be accomplished during one oxidation-reduction cycle or in many oxidation-reduction cycles in a process time of 8 to 10 h. It is felt that processing with the minimum number of oxidation-reduction

*Rockwell International-Atomics International.

Table 34. Typical Fuel Powder Specifications and Characteristics

	LMFBR Specifications			LWR Specification				
Spec. Source	RDT E13-2T	RDT E13-1T	RDT E13-6T	ASTM C-753	LWR Fabrication Data			
User Reactor					Slurry 1 & 2	Zion 1, Region 3	Oyster Creek Cycle 7	Peach Bottom-2 Cycle 2
Fuel Material	UO_2	PuO_2	$(U, Pu)O_2$	UO_2	UO_2	UO_2	UO_2	UO_2
Particle Size, μm, Max.	79	90		850		--	850	--
Avg.	10(max)	10(max)				2.82 to 0.79	6.84	
Surface Area, m^2/g	2.5	2.5				2.80 to 2.10	2.04 to 3.09	--
Bulk Density, g/cm^3				0.75(min)		1.64 to 1.81	2.07 to 2.28	--
Sintered Density, % TD	92(min)[a]	90(min)[a]	90.4 (nominal)	92(min)[a]	93.1 to 96.0	92.9 to 95.4	93.2 to 94.6	94.0 to 96.7

			ASTM C-753	
Spec. Source	E13-2T	E13-1T	Dry	Wet
Binder Type A Addition (max)	4% Carbowax 20-M	0	0	1.5% PVA
Lubricant Addition (max)	Optional	Optional	0	0.4% Sterotex
Pressing Pressure (pascals x 10^7)	20.7 to 34.5	20.7 to 34.5		
Green L/D	1.0 to 1.5	1.0 to 1.5	≥1	≥1
Green Density, % TD	--	--	45 to 55	50 to 60
Sintering Atm	6 to 8% H_2 in Inert Gas	Wet Air or Inert Gas	H_2 or NH_3	H_2 or NH_3
Sintering Temp, °C	1600		1625	1625
Sintering Time, h	2 h 15 min (max)	1 h (min)	4(max)	4(max)
Sintering Density, % TD	92(min)	90(min)	92(min)	92(min)
Theor. Density, g/cm^3	10.97	11.46	10.96	10.96

[a] Sinterability test parameters.

cycles necessary would be desirable because of the additional time required to change temperature and atmosphere during cyclic operations. Experiments are being aimed at optimization of a single oxidation-reduction cycle; future experiments will be aimed at optimization of the second and possibly third cycles.

A review of previous work on the oxidation and reduction of uranium oxides, and in particular past work on AIROX and VOLOXIDATION, has indicated that the important process parameters and their ranges of interest during oxidation are: (a) temperature, 350 to 500°C; (b) oxygen pressure, 1.01×10^4-4.78×10^4 pascals (76 to 360 mm Hg); and (c) water vapor pressure, 0-6.65×10^3 pascals (0 to 50 mm Hg). The important parameters during reduction are: (a) temperature (550 to 850°C), (b) hydrogen pressure 1.0×10^4-4.78×10^4 pascals (76 to 380 mm Hg), and (c) water vapor pressure of 0-6.65×10^3 pascals (0 to 50 mm Hg). Pulverization tests are being performed on about 27-g samples of 1.27-cm-dia cold UO_2 pellets to verify and to optimize process conditions. The effects of pellet diameter will be determined by additional testing on about 5-g samples of 0.51-cm-dia cold UO_2 pellets. Kinetic data is also being obtained from these experiments to determine the effect of process parameters on the oxidation and reduction rates, to determine the completeness of reaction during successive oxidation-reduction cycles, and to provide information on whether or not process conditions should be changed during successive cycles.

It is desirable to accomplish as much of the decladding during the oxidation step as possible prior to the reduction step. For this reason, most of the decladding experiments will be aimed at optimization of the oxidation step, with later experiments to be performed on the reduction step after oxidation has been accomplished under optimum conditions. The parameters to be investigated are the same as those mentioned for the pulverization studies except that during oxidative decladding, the oxygen pressure will be in the range of 2.0×10^4-8.45×10^4 pascals (150 to 635 mm Hg). Process parameters which affect AIROX decladding will be optimized in tests on 61-cm lengths of about 1.27-cm-dia cold UO_2 pellets clad in Zircaloy-II, having a wall thickness of about 0.86 mm. The effectiveness of the AIROX process on smaller pellets clad in stainless steel will be determined with tests on 30.5-cm lengths of stainless steel 304 tubing (wall thickness about 0.38 mm) containing about 0.51-cm diameter cold UO_2 pellets.

(ii) Equipment

Pulverizing and decladding equipment for unirradiated UO_2 and mixed oxides was designed. The construction of two pulverizing systems was completed, and two decladding units are under construction. One of the pulverizing systems was used for the experiments described in this report. The second one is ready for testing.

Pulverizer. A diagram of the pulverizing apparatus is presented in Fig. 55. The pulverizer will be arranged so that the gas supplied by a manifold arrangement can be circulated through the furnace in a closed loop while the pressure in the loop is continuously measured by

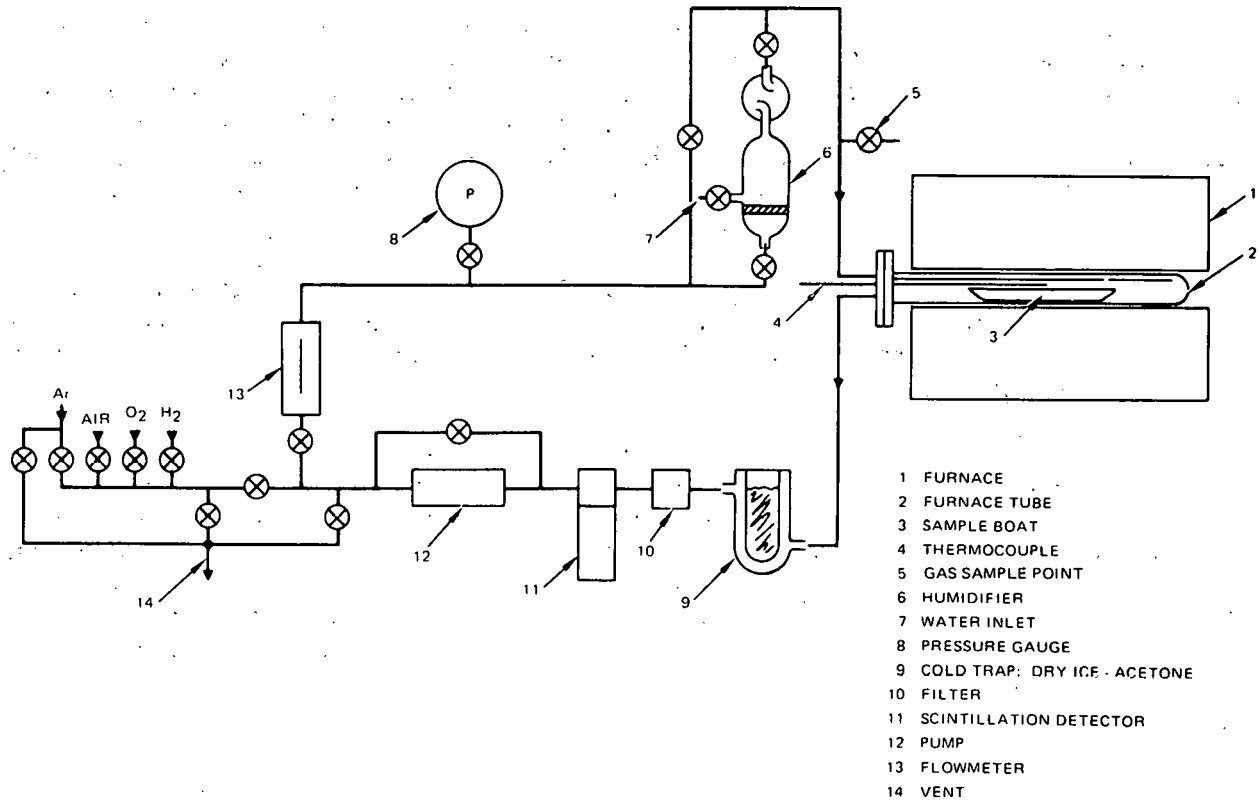

Fig. 55. Dry-Process Pulverization Apparatus

a pressure gauge. The loop will be composed of the following units arranged in series: pump, flowmeter, humidifier furnace, cold trap, filter, and an alpha scintillation chamber-photomultiplier system for counting radon.

Test facilities for the unirradiated UO_2-PuO_2 fuel will be set up in the Nuclear Materials Development Facility (NMDF) and will involve a dry-processing system in a glove box, similar to that shown in Fig. 55. Samples will be placed in a stainless steel boat inside the reaction vessel, the desired atmosphere will be introduced, and the system will be sealed off. The bellows pump will be turned on to circulate the gas during the experiment, and the reaction vessel will be heated to the desired temperature. System pressure will be maintained at a constant value by bleeding in oxygen during oxidative decladding and pellet pulverization and bleeding in of hydrogen during fuel reduction. The cold trap will lower the gas temperature to a range compatible with the HEPA filter. There will be additional filters in the lines entering and leaving the glove box. The scintillation detector will monitor the radon gas released during pellet decladding and pulverization. The water vapor pressure will be maintained by bubbling the gas through the temperature-controlled humidifier and will be monitored with a gas chromatograph. The gas chromatograph will also be used (as a safety precaution) to monitor for the presence of oxygen during reductions with hydrogen atmosphere.

The pressure gauge is a 0-4.14 x 10^5 pascals (0 to 60 psig), 15.2-cm (6-in.)-dia test gauge with 1.38 x 10^3 pascals (0.2-psi) divisions and a 0.25% full-scale reading accuracy. A precision millivolt potentiometer measures the output of an alumel-chromel thermocouple. The thermocouple point is located midway along the fuel charge and immediately above it. The humidifier is included in the loop to supply moisture to the process gas in future experiments.

Decladder. The decladding apparatus is shown in Fig. 56. It consists of a rotatable wire cloth drum mounted above a receiver and contained in a furnace tube. The associated gas-handling equipment is the same as shown in Fig. 55.

A line of 0.17-cm-dia holes about 1.27 cm apart, will be punched through the cladding along the length of a 61-cm segment of clad fuel. The fuel will be placed in the wire cloth drum, and the assembly will be sealed in the furnace tube. As the fuel oxidizes, it will rupture the cladding, and the oxidized (powdered) fuel will fall through the wire cloth into the receiver.The drum is made rotatable to assist in separating the cladding from the fuel. The fuel is left in the receiver during the reduction cycle and during any subsequent redox cycles.

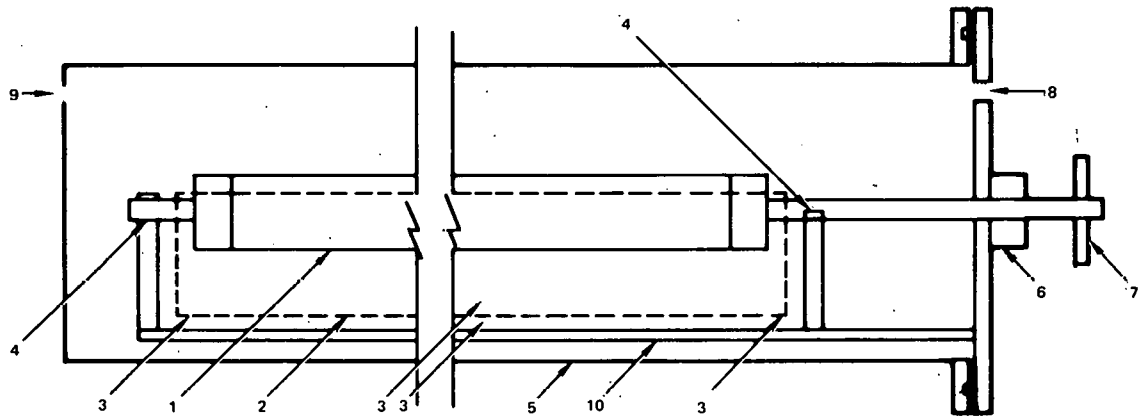

1 WIRE CLOTH DRUM
2 RECEIVER
3 THERMOCOUPLE POINTS
4 BEARINGS
5 FURNACE TUBE
6 SEAL
7 HANDLE
8 GAS INLET
9 GAS OUTLET
10 BASE PLATE

Fig. 56. Dry-Process Decladding Apparatus

(iii) Operating Procedure for Pulverizer

The weighed fuel is placed in the sample boat and the apparatus for operation. Air is flushed through the apparatus at room temperature, with the pump operating and the vent open. The vent is closed, and the pressure is adjusted to 0 psig, with the flowmeter indicating the desired circulating rate. Power is turned on to the furnace, and the radon counting system is turned on simultaneously. The radon counts collected during the run are recrded at 10-min intervals and are totalled for the run. The furnace is heated to operating temperature, and the pressure in the loop is maintained at 1.23×10^5 pascals (3.2 psig) during the run by frequent small additions of oxygen. The time and amount of each oxygen addition are noted. The pressure and temperature in the loop are recorded at regular intervals.

When oxidation is complete, the gas in the loop is replaced with argon, the furnace temperature is adjusted o 400°C, the cold trap is filled with dry ice-acetone, and the average temperature of the circulating argon is equilibrated at the desired circulating rate. Hydrogen is added to the argon to obtain the desired circulating rate. Hydrogen is added to the argon to obtain the desired hydrogen concentration, and the system is re-equilibrated.

The pressure of the argon-hydrogen gas mixture is adjusted so that it is 1.25×10^5 pascals (3.5-psig) at operating temperature. To maintain the 1.25×10^5 pascals (3.5-psig) operating pressure, small amounts of hydrogen are added frequently to the loop as reduction proceeds. The remainder of the reduction procedure is the same as that described for the oxidation cycle. When reduction is complete, the gas in the closed loop is replaced with argon, and the system is cooled to room temperature.

Twenty-, 100-, 200-, and 400-mesh Tyler sieves were used to determine the particle size distribution of the pulverized fuel. The entire fuel charge from each experiment was sieved. The sieves were shaken by hand for 15 min, the fractions were weighed, and the percentage of the charge in each fraction was determined.

(b) Experimental Results

Pulverization. The pulverization experimental conditions are presented in Table 35 and the results of sieve analyses in Table 36. The fuel charge for the first redox cycle of Run V-O-P-3 was 51 g of fragmented pellets. After the cycle was completed, small portions of unreacted fuel were found at each of the sample boat. This was a result of the hot zone of the furnace not extending to the charge ends. These fragments were removed, and the rest of the charge was sieved. Exactly one-half of the powdered fuel on each sieve was reserved as part of the fuel charge for the second cycle. A comparison of the results of sieving after the first cycle with those following the second cycle in V-O-P-3 shows an increase of approximately 25% in the -400-mesh fraction.

Table 35. Pulverization Experiment Run Conditions

Run No.	Form of Charged Sample	Sample Weight, g	Oxidation		Reduction	
			Temp., °C	O_2, Vol %	Temp., °C	H_2, Vol %
V-O-P-3	Fragments	51	400	21	625	4
2nd cycle	Powder	21	400	21	625	4
V-O-P-4	Fragments	25	400	21	625	4
2nd cycle	Powder	25	400	21	625	4
V-O-P-5	Pellet	27	400	21	625	21
V-O-P-6	Pellet	27	400	21	--	--
V-O-P-7	Pellet	27	400	21	625	21
V-O-P-8	Pellet	27	450	21	625	21
V-O-P-9	Pellet	27	480	21	625	21

Table 36. Sieve Analyses

Run No.	Percent of Product				
	+20 Mesh	-20 to +100 Mesh	-100 to +200 Mesh	-100 to +400 Mesh	-400 Mesh
V-O-P-3	18.1	5.7	1.0	2.9	72.4
2nd cycle	1.5	0.9	0.2	1.4	96.0
V-O-P-4					
2nd cycle	0.1	0.3	0.1	2.4	97.0
V-O-P-5	4.4	0.4	0.1	1.7	93.5
V-O-P-6	27.3	0.7	0.2	13.8	58.0
V-O-P-7	0.0	0.3	3.8	9.5	86.4
V-O-P-8	0.0	0.1	6.1	14.3	79.4
V-O-P-9	0.3	2.7	8.2	19.3	69.6

Runs V-O-P-3 and -4 were identical except for the different fuel charge size in the first redox cycle of V-O-P-3 and the absence of product sieving between cycles in V-O-P-4. The particle size distributions following the second cycle of these two runs are very similar.

The fuel charge in each of the remaining runs was a single whole pellet. The reduction gas mixture composition was also changed to argon-21 vol % H_2.

V-O-P-5 and -7 were single-cycle redox experiments made under conditions that were intended to be identical. The probable reason for the difference in particle size distributions is that the two runs were possibly oxidized through different phases, as discussed in a following section on kinetics.

V-O-P-6 was a single oxidation cycle experiment. Oxidation was stopped when a 2.4-O/U ratio was reached to determine the extent of oxidation that had occurred.

Experiments V-O-P-8 and -9 were a continuation of a series of runs, starting with V-O-P-7, in which different oxidation temperatures were employed. When this series of runs is completed, results should indicate if an optimum oxidation temperature exists.

Radon Detection. The alpha scintillation counter (11 in Fig. 55) was included in the closed gas-circulating loop to monitor the progress of the pulverization process by continuously measuring the radon alpha activity released from the fuel into the circulating gas.

The results from monitoring the pulverization of $^{238}UO_2$ fuel in Run V-O-P-6 are presented in Fig. 57. The average net counting rate was about three times the background, and it was essentially constant throughout the run. Thus, the activity from the 3.8-day radon-222

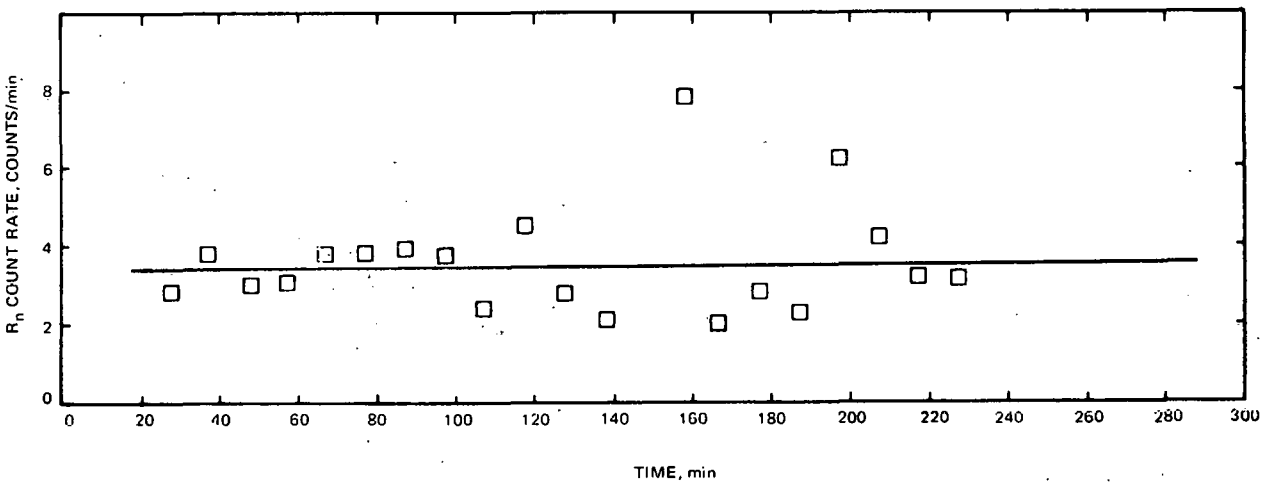

Fig. 57. Radon Count Rate During Oxidation of a UO_2 Pellet. About 27 g sample oxidation in air. 400°C. Run V-O-P-6

associated with uranium-238 is not sufficient for monitoring of the pulverization process. However, the counter will be used to monitor the processing of uranium-235 and thorium-containing fuels from which the 3.9-s radon-233 and 54-s radon-220 isotopes, respectively, are released.

(c) Kinetic Results

Reaction kinetic information for the AIROX process is being obtained by monitoring the required addition of oxygen during oxidation or the required addition of hydrogen during reduction to maintain a constant system pressure. When the system pressure drops to about 3.33×10^3 pascals (about 25 mm mercury), gas is added to return the pressure to the

desired value. This pressure change is converted into equivalent moles of gas, using the ideal gas law, calculated values of the system volume, and the average temperature of the circulating gas within the process system. The mole ratio of oxygen to uranium (O/U) at different times throughout both oxidation and reduction processes is then calculated.

The effect of higher oxidation temperatures on the oxidation rate of UO_2 in air is shown in Fig. 58. In all cases, reaction was not taken to completion but rather was terminated when the reaction rate had significantly slowed down. The data indicate three significant points: (1) the reaction rate changes from an accelerating rate to a decelerating rate at an O/U ratio of about 2.3, (2) as the oxidation temperature is increased from 400°C to 480°C, the oxidation rate increases and the induction time period decreases, and (3) the shape of the oxidation curve for UO_2 at 400°C may vary significantly above an O/U of 2.3.

The variation of the oxidation curve for temperatures near 400°C can be understood by consideration of the uranium-oxygen phase diagram shown in Fig. 59 at temperatures below 600°C. As UO_2 is oxidized at temperatures below 600°C, phase boundaries are crossed at O/U ratios of

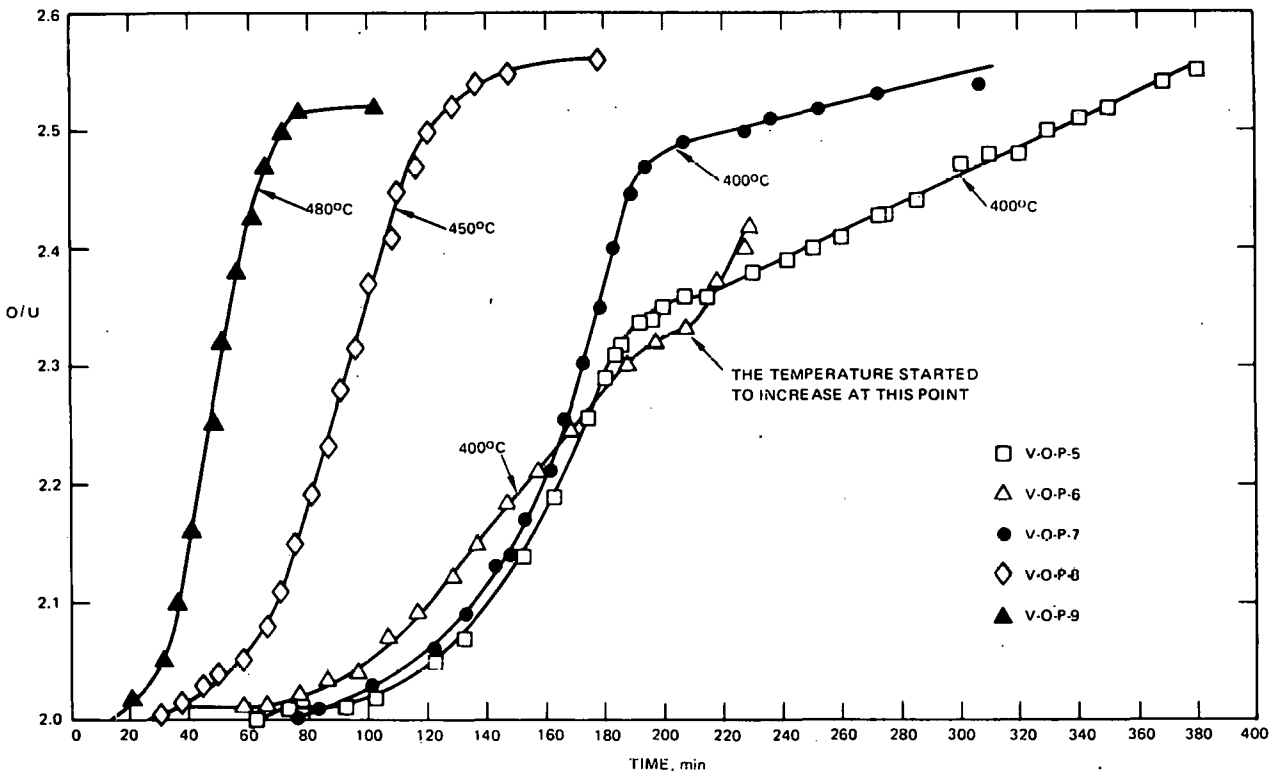

Fig. 58. Effect on UO_2 Oxidation Rate of Temperature. UO_2 pellets about 25 g each, oxidation in air, 925 to 941 mm Hg

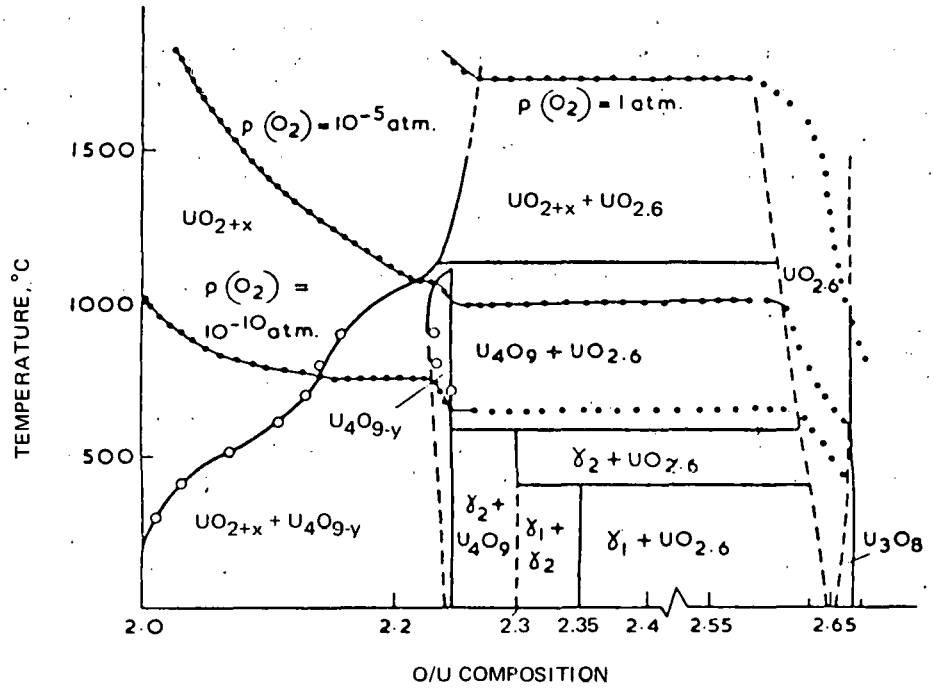

Fig. 59. Portion of Uranium-Oxygen Phase Diagram [RAND]. Reprinted from Thermochemistry and Nuclear Engineering, Proceedings of the Symposium on Thermodynamics, Vienna, July 22-27, 1965, Vol. 1, by permission of Atomic Energy Research Establishment, Harwell.

2.25 and 2.3, and at 2.35 if the temperature is 400°C or less. Oxidation accelerates through the UO_{2+x} + U_4O_{9-y} phase and then slows while passing through the γ_2 + U_4O_9 phase. When the temperature is near 400°C or less, the γ_1 + γ_2 phase is entered, and oxidation slows further. Once oxidation proceeds past on O/U ratio of 2.35, the γ_1 + $UO_{2.6}$ phase is entered and the oxidation rate increases to a constant rate. Oxidation at temperatures between 400 and 600°C is similar to that described above except that the oxidation-inhibiting γ_1 + γ_2 phase is not crossed, and the phase γ_2 + $UO_{2.6}$ is entered at an O/U ratio of 2.3. Since the oxidation reaction is exothermic, it is possible that the internal temperature of the pellet may exceed 400°C during oxidation at this temperature. This would cause the γ_2 + $UO_{2.6}$ phase to be entered rather than the γ_1 + γ_2 phase, which is postulated to have occurred during experiments V-O-P-6 and V-O-P-7. The fact that the shape of the oxidation curve at 400°C for experiment V-O-P-7 is similar to that for temperatures of 450°C and 480°C seems to confirm passage through similar phases.

The oxidation at 400°C during experiment V-O-P-6 was purposely stopped at an O/U ratio near 2.4 to determine the degree of pulverization at this point during oxidation. Sieve analysis (given in Table 36) shows that only 58% of the powder is smaller than 400 mesh, indicating that oxidation to O/U ratios greater than 2.4 is necessary to significantly pulverize the UO_2 to a fine powder. It appears that the γ_2 + $UO_{2.6}$ or γ_1 + $UO_{2.6}$ phase must be crossed to achieve pulverization of the fuel.

The fact that the reaction rate is affected by surface area is shown in Fig. 60, where the oxidation rate for UO_2 fragments is considerably greater than that for a solid pellet. Note, however, that both oxidations still had approximately the same induction period of 70 min before reaction started. This indicates that sample surface area does not significantly affect induction time period, whereas Fig. 58 shows that higher temperatures reduce the induction period markedly.

Future oxidation studies will involve higher temperatures to see if an optimum exists, and then the effect of thermal cycling will be investigated.

Reduction curves for uranium oxide powders reduced in 21% H_2 - 79% Ar at 625°C are shown in Fig. 61. The starting powders for reduction were prepared by oxidations at different temperatures, and had different particle size distributions, as listed in Table 36. These results indicate that the particle size distributions, and hence surface areas, of these powders are similar enough to yield similar reduction rates. These data

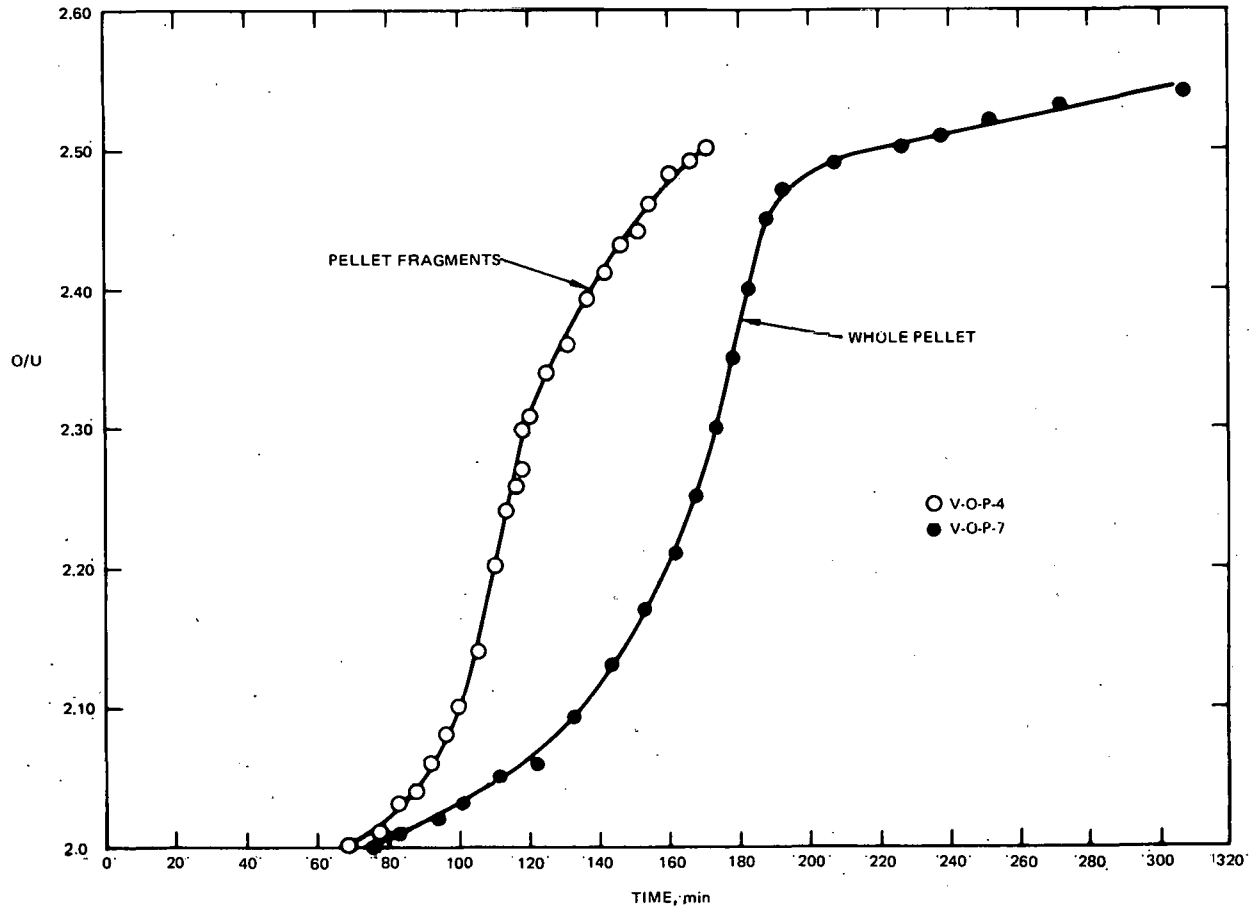

Fig. 60. Increasing UO_2 Oxidation Rate with Increasing Surface Area. Oxidation in air. 400°C, 1.25×10^5 pascals. About 27-g samples

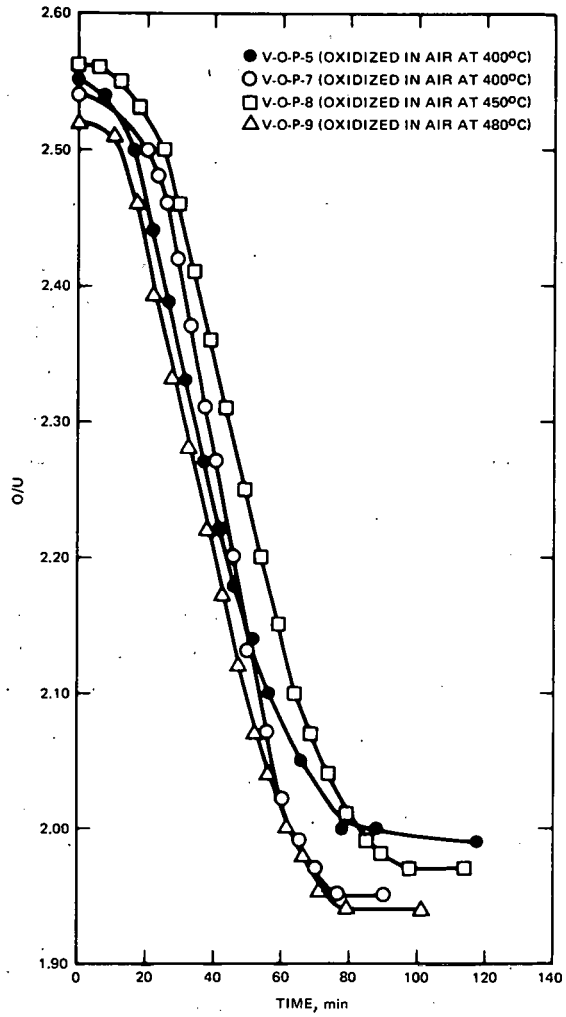

Fig. 61.

Reduction Rates of U_3O_8 Powder from Pellets Oxidized at Different Temperatures. 21% H_2 -79% Ar. 1.25 x 10^5 pascals. 625°C

also give an indication of the reproducibility of obtaining kinetic information by the procedure used in this work. It should also be pointed out that the O/U ratio falls below 2.00 because of the cumulative error that results from determination of the O/U ratio first during oxidation and then during reduction. The starting UO_2 pellets have been assumed to have an O/U ratio of 2.00, and this will be checked by chemical analysis.

(3) Process Verification--Plutonium-Uranium Oxide
(J. R. Miller,* R. Meyer,* W. R. Marsh, * and R. C. Hoyt*)

A previous study at ORNL on voloxidation [ORNL-1973] of mixed oxide fuel has indicated that oxidation of UO_2 may be partially inhibited by the presence of PuO_2 in concentrations above 25 wt %. The oxidation of UO_2 to U_3O_8 occurs in two stages, the first stage being oxidation of UO_2 to U_3O_7 or U_4O_9 and the second stage being oxidation of U_3O_7 or U_4O_9 to U_3O_8. The second stage of the oxidation causes the fuel pellet to pulverize

*Rockwell International-Atomics International.

because of the large change in crystal lattice; it is this portion of the oxidation process that is partially inhibited by high concentrations (15 to 25 wt %) of PuO_2. Verification tests with cold UO_2-PuO_2 will investigate this oxidation-inhibiting effect for fuel containing PuO_2 and will determine if oxidation-reduction cycling enhances the second stage of the oxidation process.

Fuel pellet pulverization tests will be performed on about 5 g samples of about 0.51-cm (about 0.2-in.)-dia UO_2-PuO_2 pellets containing 15, 20, 25, and 30 wt % PuO_2 to determine the effect of nonoxidizable material content and to determine necessary adjustments in the optimum process conditions for UO_2 when high concentrations of nonuranium materials are present.

The effect of nonuranium material content on the effectiveness of the AIROX oxidative decladding step will be investigated with the mixed oxide fuel mentioned above by testing about 15 g samples clad in stainless steel 304 having a wall thickness of about 0.38 mm.

A review of previous work on the oxidation and reduction of uranium oxides and uranium-plutonium oxides has indicated the important parameters and their ranges of interest. During oxidation, the important parameters are: (a) temperature, 415 to 515°C; (b) oxygen pressure, 1.01×10^4-8.45×10^4 pascals (76 to 635 mm Hg); (c) water vapor pressure, 0-6.65×10^3 pascals (0 to 50 mm Hg). During reduction, the parameters are: (a) temperature, 550 to 700°C; (b) hydrogen pressure, 1.01×10^4 to 5.05×10^4 pascals (76 to 380 mm Hg); and (c) water vapor pressure, 0 + 0.65×10^3 pascals (0 to 50 mm Hg).

In the verification tests on unirradiated UO_2-PuO_2 fuel, the optimum values for test parameters at the start of each series of tests will be based upon results from the verification tests with unirradiated UO_2. Process conditions will then be varied to determine the required parametric values to achieve rapid oxidation and reduction when the fuel contains various quantities of PuO_2.

After decladding and pulverization tests, particle size distributions of the fuel will be determined, using standard sieve and subsieve analyses.

The status of test equipment is shown in Table 37.

(4) AIROX Process Demonstration
(J. R. Miller,* R. J. DeMinico,* E. J. Babcock*)

(a) Test Plan

The objectives of the Process Demonstration portion of this program are (1) to demonstrate that the process that will be developed in the process verification studies is applicable to spent fuels and (2) to determine the effects on product quality of off-normal process conditions.

*Rockwell International-Atomics International.

Table 37. AIROX Test Equipment Status for UO_2-PuO_2 Studies

Component	Status
Process System	
Temperature recorder. Max, 1100°C (2000°F)	On hand
Furnace & control	On hand
Retort	Being designed
Boat	Being designed
Cage assembly	Being designed
Cold traps	Design complete
Humidifier	Design complete
Controlled temp bath	On hand
Metal bellows pump	On hand
Tubing	On hand
Fittings	On hand
Valves	On order
Gages	On hand
Thermocouples	On order
Flowmeters	On order
Ar, O_2, and N_2 Bottled Gases	On hand
HEPA filters	On hand
Scrubber & charcoal trap	Being designed
Alpha and beta counters	On hand
Clad puncturing device	Design complete
Heater	On hand
Product Analysis	
Pellet press	On hand
Syntron sieve shaker	On hand
Sieves (1700 to 38 μm)	On hand
Sonic sifter	Ready to purchase
Sieves (20 to 5 μm)	Ready to purchase
Ball mill & jars	On hand

Initial studies will be performed in Cell 1 at the Atomics International Hot Laboratory (AIHL), using unirradiated fuel pellets to verify that the system can duplicate the results obtained in the Atomics International Process Verification System. Next, irradiated UO_2 fuel will be processed. This fuel will be UO_2 pellets (about 0.94 cm dia) clad in about 61 cm sections of 0.038-cm-thick Zircaloy 4 tubing and irradiated to about 27,000 MWd/MTU burnup in the Oconee I reactor. The test parameters optimized in the process verification studies will be initial parameters for the UO_2 demonstrations on spent fuel. The parameters will then be varied to obtain optimized parameters for irradiated fuel and to evaluate process sensitivity.

The test parameters that will be controlled and measured include:

1. System pressure
2. Flow rate of the circulating gas
3. Number of oxidation-reduction cycles
4. Oxygen concentration during oxidation
5. Hydrogen concentration during reduction
6. Temperature
7. Duration of reaction
8. Water concentration in the circulating gas

The test equipment design will be similar to that used for the process verification studies and is shown schematically in Fig. 47. Clad test samples will be punctured at regular intervals to provide a path for the reactant gases and then will be sealed in the reaction vessel in the furnace. The desired atmosphere will be introduced into the furnace tube. The bellows pump will circulate the gas, and the system will be heated to the desired temperature. Makeup gas, either oxygen or hydrogen, will be added during reaction to maintain the system pressure. The system will be flushed with inert gas (nitrogen) between changes in atmosphere (oxidizing and reducing) to avoid an explosive mixture of hydrogen and oxygen. During the experiments, the released fission products and other volatiles will be conveyed in a heated line from the furnace to a cold trap and an absolute filter. The process gas will then be returned to the furnace.

At the completion of a run, the gas will be circulated through the analytic train shown in Fig. 62 to trap the noncondensable fission products. The gas flow will be reduced and circulated until the analytical reactions reach equilibrium. A solution of mercuric nitrate in nitric acid will collect any iodine and cesium not condensed in the first cold trap. A heated copper oxide burner will oxidize tritium and hydrogen to water and the water will be condensed in the second cold trap. The remaining krypton and xenon will be absorbed by cold activated charcoal in the final trap. When equilibrium is reached, the gas will be vented and replaced with an inert gas (nitrogen). The vented gas will be monitored by a multichannel analyzer for alpha activities and by a beta counter for beta activities.

The product powders will be screened for particle size analysis and to separate the fraction to be used for sinterability evaluation. The cold pressing and sintering conditions for these evaluations will be based on ASTM specification C-753 [ASTM] and the final pellet density will be the measure of sinterability and thus, of quality of the product powder.

The "Test Plan to Demonstrate the AIROX Process with Spent Fuel," [RI-AI] has been approved and releasd. A request to dry-process irradiated fuels in the AIHL has been prepared and submitted to the AI Isotopes Committee for approval.

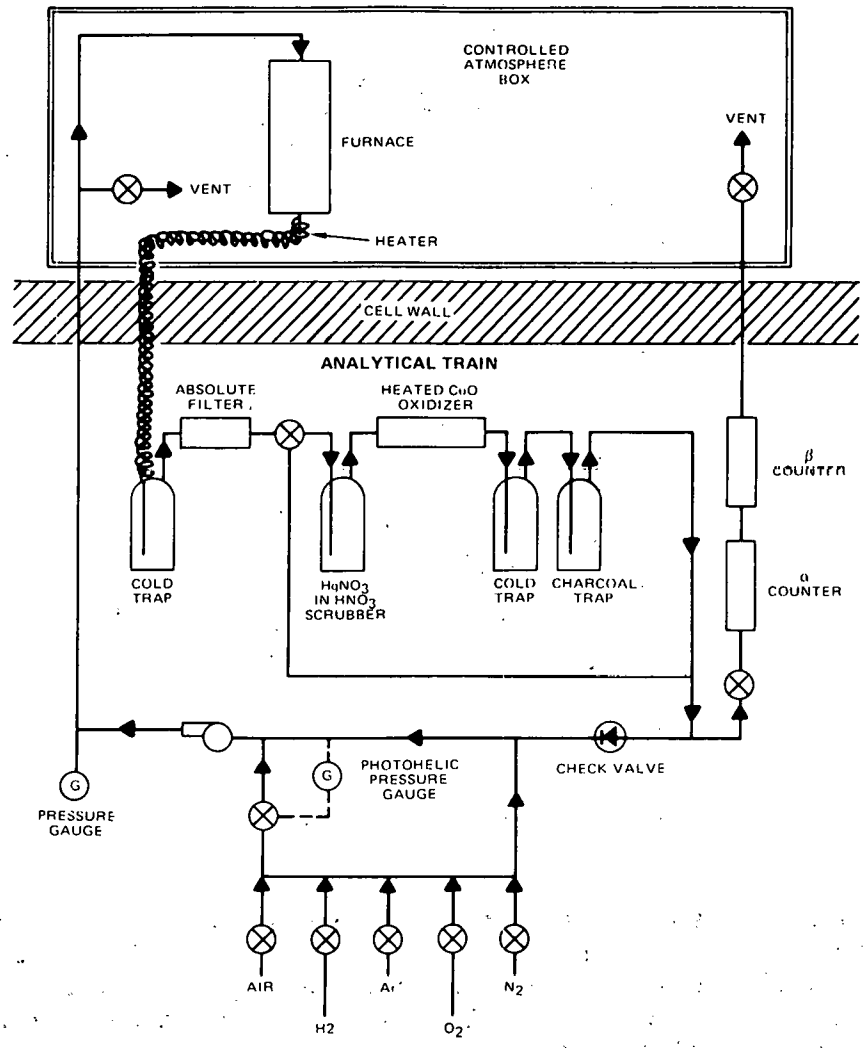

Fig. 62. Schematic of In-Cell System for AIROX Processing

(b) Design and Construction for Glove Box

Processing of carbide and metallic fuels will require the design and construction of a glove box to control the composition of the atmosphere in the working area. The design of the box has been completed, and a fabricator is being sought. The glove box, which is shown schematically in Fig. 63, will be installed in Cell 2 of the AIHL. The box will be 167 cm x 183 cm x 335 cm tall (5 1/2 ft x 6 ft x 11 ft tall). When installed, there will be a 7.6 cm (3 in.) gap between the cell and the box walls. The design will permit almost full utilization of the cell volume served by the manipulators. Holes will be provided in the box walls, floor, and roof for glove ports, windows, manipulators, transfer ports, a fuel storage vault, and lighting. Equipment such as the hydraulic press, Ro Tap sieve shaker, and balance

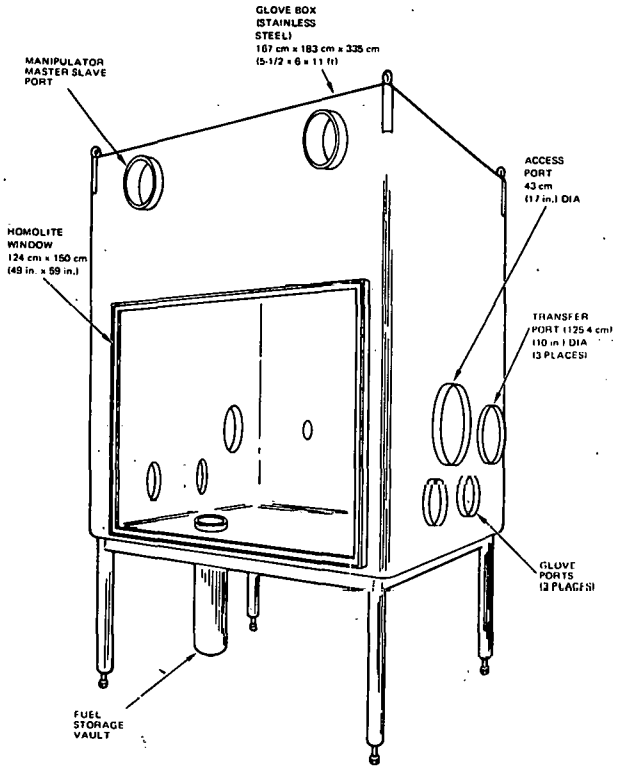

Fig. 63. Hot Cell Glove Box

are being designed so that most of their components requiring maintenance will be outside the box. Only those portions of the equipment that must be in the box to perform their intended functions will be inside. The reaction furnace will be attached to the rear of the box, with the retort and sample boat attached to its door which opens into the box.

The tooling and equipment being fabricated or purchased for the AIROX processing in Cell 1 are being designed so that they can be readily transferred to the glove box in Cell 2 for CARBOX and RAHYD processing. The status of the test equipment components is shown in Table 38. Assembly and checkout of the test apparatus for AIROX should be completed next quarter.

9. Molten Nitrate Salt Oxidation Process

(L. L. Burger,* L. G. Morgan,* and R. D. Scheele*)

The objective of this work is to identify chemically feasible nonaqueous reprocessing methods within the framework of nonproliferation. The study will examine treatment of ceramic fuels by molten salts and will emphasize the use of molten nitrate systems. The incorporation of other nonaqueous steps will be considered, where applicable to the development of a conceptual process.

*Pacific Northwest Laboratory.

Table 38. Status of AIROX Test Equipment for Irradiated UO_2 Studies

Component	Status	Component	Status
Controlled-Atmosphere		AIROX Process System (contd.)	
Glove Box	Design complete	Gages, thermocouples and flowmeters	On hand, being calibrated
Glove ports	Ready for purchase	Temp recorder 1100°C (2000°F)	On hand
HEPA filters	Ready for purchase	Ar, O_2, N_2, and H_2 bottle gases	Ready for purchase
Transfer ports	Ready for purchase	HEPA filters	Ready for purchase
Homolite window	Ready for purchase	Scrubber & charcoal trap	Being designed
Hoist	Being selected	α and β counters	Being selected
Manipulator booting	Ready to order		
Photohelic pressure gage	On order	Clad-Puncturing Device	
Magnatrol valve	On order	Product Analysis	10% fabricated
Vacuum regulator	On order	Ro tap sieve shaker	On hand
Oxygen analyzer	Being selected	Sieves (1700-38μm)	On hand
Blowers (2)	Being selected	Sonic sifter	Ready to order
Plenum control valve	Being selected	Sieves (20 to 5 μm)	Ready to order
		Ball mill and jars	Being selected
AIROX Process System		Pellet press	
Furnace	On hand	AIROX	On hand
Retort	Fabrication to be completed 7/20/78	CARBOX & RAHYD	Design complete
Boat	85% fabricated	Hydraulic pump & hoses for press	On hand
Cage assembly	Design complete	Powder containers	On hand
Cold traps	Design complete	Punch & die set	On hand
Refrigerated-water supply	On order	Sintering furnace	Being designed
Dry ice machine	On hand	TOCCO generator for sintering furnace	Installed
Humidifier	75% fabricated		
Controlled-temp bath	On order		
Metal bellows pump	On hand	General Equipment	
Tubing, fitting and valves	On hand	Balance - 1 kg capacity	Being selected
Heated cell wall feedthrough	On hand	Leak detector	On hand

a. Engineering Analysis

Acquisition and categorization of reference materials pertinent to the topical report entitled "Review of Physical and Chemical Properties of Molten Nitrates Applicable to Nuclear Fuel Processing" was largely completed in the previous quarterly reporting period. Additional references and secondary sources continue to be acquired.

First drafts of several chapters of the topical reports were initiated during the current quarter. The unexpected volume of literature to be reviewed has delayed completion of the report, but no significant problems are foreseen.

No expenditures on this portion of the project were made during June 1978 so that instead, supporting studies on the behavior of actinide oxides in molten alkali metal nitrates could be completed.

b. Separations Processes

Emphasis during this reporting period has been placed on determining the behavior of actinide oxides in molten alkali metal nitrates. Such determinations will clarity existing contradictions in the literature and permit evaluation of conceptual process steps. In support of this goal, the preparation of both a nonradioactive synthetic fission product oxide and a sample of plutonium dioxide with a documented history has been completed. Pertinent analytical methods have been identified, and preliminary analyses are in progress.

(1) Synthetic Fission Product Mixture

A nonradioactive representative fission product mixture has been prepared for use in the determination of fission product behavior in molten alkali metal nitrates. The representative fission product mixture consists of equal masses of the desired elemental metals, not equal masses of the compounds utilized.

An ammonium hydroxide solution was utilized to dissolve molybdenum oxide, MoO_3; this solution was added to an aqueous solution containing the nitrates of cerium, palladium, and rhodium. The resulting mixture was calcined at 500°C for 17 h, after which the temperature was increased to 550°C for an additional 7 h.

The solids resulting from the calcination were powdered and added to a blended mixture consisting of the oxides of antimony, ruthenium, samarium, strontium, yttrium, and zirconium. Cesium was then added as cesium iodide; niobium was added as potassium hexaniobate, $K_8Nb_6O_{19}\cdot 16H_2O$.

The final representative fission product mixture is therefore believed to consist of the oxides of antimony, cerium, molybdenum, palladium, rhodium, ruthenium, samarium, strontium, yttrium, and zirconium; cesium iodide; and potassium hexaniobate. Current analytical tests in progress will provide the exact concentrations of the elements of concern.

(2) Preparation of Plutonium Dioxide

The behavior of plutonium dioxide is highly dependent on the history of the material. Thus, although irradiated plutonium dioxide may differ from unirradiated laboratory samples, it is essential that the history of the latter, used in our experiments, be well documented. A sample has been prepared for which we have a complete history, method of preparation, purity, and sintering conditions. This material will be utilized in our experiments on the behavior of plutonium dioxide in molten alkali metal nitrates.

A plutonium(IV) nitrate solution of approximately 7M nitric acid concentration was purified by loading the plutonium onto Dowex 1-X-3 ion exchange resin in an ion-exchange column at room temperature. The column was washed with 8M nitric acid, followed by elution with 0.35M nitric acid and collection of the purified plutonium(IV) effluent.

A drop of hydrazine was added to the purified plutonium solution, and the Pu(IV) was reduced to Pu(III) by the addition of ascorbic acid. Oxalic acid was added to the Pu(III) solution and the Pu(III) oxalate was precipitated, filtered, and air-dried.

The Pu(III) oxalate was calcined at 750°C to plutonium dioxide in an alumina crucible. Typical calcination temperatures for plutonium dioxide prepared for fuel manufacture are 650°C to 850°C. Our material will not be sintered at higher temperatures, although this is normally done (following blending and pellet formation) in the preparation of mixed oxide fuels.

(3) Behavior of Uranium Dioxide in Molten Alkali Metal Nitrates

In the study of the behavior of uranium dioxide in molten $LiNO_3$-KNO_3 eutectic, rapid attack of our Pyrex reaction vessels was noted. During the current quarter, the decision was made to utilize an equimolar $NaNO_3$-KNO_3 melt instead. The behavior of uranium dioxide containing the synthetic fission product mixture was investigated. The mass ratio of the fission product mixture to uranium dioxide was 1:10; the mass ratio of uranium dioxide to total alkali metal nitrate was 1:100. The total alkali metal nitrate mass was 1 kg in each experiment.

The uranium dioxide initially reacted with equimolar $NaNO_3$-KNO_3 melt at a temperature of 350°C. The reaction was carried to completion at a final temperature of 420°C. Reaction was fairly vigorous, as evidenced by the rate of NO_2 generation, but at no time was it excessive. During this portion of the experiment, an inert-gas (argon) sparge was maintained to aid in agitation of the melt and to sweep out the copious quantities of NO_2 produced. Complete reaction required about 2.5 h at the maximum temperature of 420°C.

After reaction was complete and the inert gas sparge had removed the remaining NO_2, the supernate was clear, with no apparent color. The solids were predominantly reddish brown, although a small amount of denser black solids was visible on the bottom of the reaction vessel. The melt temperature was then lowered to 275°C.

Nitric acid vapor was added when the melt had cooled to 275°C. The nitric acid vapor was carried from a heated vessel containing 100% nitric acid with the inert gas sparge. Transfer lines were heated to minimize condensation. The quantity and transfer rate of the nitric acid were not determined.

Addition of the nitric acid vapor to the melt produced considerable NO_2; this is believed to be due, in part, to decomposition of the nitric acid at this temperature. Addition of nitric acid vapor was continued until no solids were visible on the bottom of the reaction vessel. Cessation of the nitric acid addition and sparge allowed a very small quantity of solids to settle to the bottom of the reaction vessel. It is not known at this time whether these solids represent insoluble material or whether the addition of nitric acid was discontinued too soon.

The melt containing the soluble species was greenish-brown, in contrast to the characteristic yellow uranyl color noted when only uranium dioxide was utilized in the $LiNO_3$-KNO_3 eutectic.

The temperature was slowly increased to 420°C over the period of one hour. The formation of solids was first apparent at 300°C to 320°C. With the formation of solids, a large quantity of NO_2 was produced. Sparging was utilized to remove this gaseous reaction product. When thermal decomposition was complete, the melt was clear and without apparent color.

Samples were taken of the molten phase throughout the total experiment, and the final solids were recovered by aqueous dissolution of the nitrate melt after solidification. Quantitative analyses of the samples for uranium and for the various elements present in the added fission product mixture are currently in progress.

Determination of fission product behavior and the exact uranium chemical forms awaits the analytical results. It does appear, however, that the behavior of uranium dioxide in molten alkali metal nitrates is reproducible.

(4) Behavior of Plutonium Dioxide in Molten Alkali Metal Nitrates

The behavior of plutonium dioxide in molten alkali metal nitrates is an area of major concern. Claims that alkali metal plutonates are formed [AVOGADRO-1972, CEN, HENRION, HEYLEN, WURM-1968] are not substantiated by definitive analytical results. In some cases [CEN, WURM-1968], sodium peroxide was added as an oxidant to either an alkali metal nitrate melt [CEN] or to an alkali metal hydroxide melt [WURM-1968]. If the temperature is high enough (e.g., above 700°C), thermal decomposition of the nitrate melt produces peroxide species.

Other studies concerned with the behavior of plutonium dioxide in molten nitrates [AVOGADRO-1971, BRAMBILLA-1976, GER OFFEN, WURM-1970] do not claim the formation of a plutonate species but only state that an insoluble plutonium-containing compound exists. However, in all the

references cited, these results are given for mixed uranium-plutonium dioxide and definitive analytical results are not given.

Our studies of the behavior of plutonium dioxide in molten alkali metal nitrates were conducted in equimolar $NaNO_3$-KNO_3 without the addition of peroxide. Melt temperatures were low enough so that thermal decomposition would not produce peroxide species. In addition, we studied only the behavior of plutonium dioxide, not the behavior of a uranium-plutonium dioxide mixture.

A mass ratio of plutonium dioxide to nitrate melt of 1:100 was chosen for study. The experiments were performed in a facility designed for containment of high-alpha-activity materials, commonly called a glove box. Changes in the experimental equipment used were necessary to utilize the available facilities without additional expenditures of time or monies.

A standard muffle furnace was used, rather than the pot type furnace equipped with viewing ports that has been utilized in the uranium dioxide work. Use of the muffle furnace necessitated temporary removal of the reaction vessel from the furnace to obtain samples or to add reagents. Frequent opening of the furnace door was necessary for visual observations. Temperatures cited, therefore, undoubtedly exceed the actual temperature of the melt during either sampling or reagent addition.

Plutonium dioxide and equimolar $NaNO_3$-KNO_3 were added to the reaction vessel, and the temperature increased to a maximum of 525°C. The total time that the temperature exceeded 350°C was approximately three hours; the temperature exceeded 500°C for at least one hour. No reaction of plutonium dioxide was noted at any time. The melt remained clear and without apparent color throughout the entire period of time. There was no indication of reaction or change in appearance of the plutonium dioxide. It therefore appears that plutonium dioxide does not react with the alkali metal nitrate melt to produce a plutonate in the temperature range cited ($\leq$525°C).

Next, the temperature of the furnace was reduced to 300°C. Liquid 100% nitric acid was added at intervals to the melt through a small pipet after temporary removal of the melt from the furnace. The actual melt temperature appeared to be just above the melting point at most times. Addition of the nitric acid caused gas bubble to form on the surface of the particulate plutonium dioxide and caused the release of NO_2. The melt appeared to have a somewhat greenish color immediately after the addition of the nitric acid which color would fade with time if no further nitric acid was added.

In an attempt to force the dissolution of the plutonium dioxide, the nitric acid was added as rapidly as was possible without freezing the melt. It could not be determined visually whether all of the plutonium dioxide had dissolved, due to the evolution of NO_2 and the presence of gases in the melt. Allowing the melt to remain in the furnace at 300°C for 1.5 h following the nitric acid additions produced an almost colorless supernate. The solids' color and appearance were unchanged from that of the original plutonium dioxide.

Samples of (1) the melt taken throughout the experiment and (2) the final solids are currently being quantitatively analyzed.

Although exact results must await the analytical determinations, it is apparent that the behavior of plutonium dioxide in molten alkali metal nitrates is not identical to that of uranium dioxide. It should be noted, however, that the behavior of solid solution uranium-plutonium dioxide may differ from that of blended and sintered mixed oxide or of the material used in our experiments.

It did appear likely that at least a portion of the plutonium dioxide was dissolved upon the addition of the nitric acid, but the soluble species probably is not stable in the melt unless an excess of nitric acid is present. If the analytical results verify the dissolution of plutonium dioxide in the melt with nitric acid, the claims [BRAMBILLA-1973, 1976] for this behavior will be supported by our results.

10. Molten Salt Processes Applied to Ceramic Fuels

(H. F. McDuffie,* D. H. Smith,* and G. W. McDonald*)

In the proposed process, the oxide fuel is converted to chlorides and dissolved in LiCl solvent. Next, in the separation step, fissile and fertile materials are extracted into bismuth in the presence of lithium metal. The fissile and fertile materials are next transferred to NH_4AlCl_4. The NH_4AlCl_4 may be volatilized, leaving behind the fissile and fertile chlorides.

a. Progress

(1) Engineering Analysis

Figure 64 shows a zero-level reprocessing flowsheet of the type reported earlier [STEINDLER-1978C], but generalized to include a variety of potential alkali metal halide solvents. At present, LiCl is the preferred solvent and 700°C is the preferred temperature for the separation step, because of the known favorable distribution coefficients shown in Fig. 65 [FERRIS-1971, 1972, MOULTON-1970A, RICHARDSON-1970, 1972, SMITH-1970]. The advantages of these process conditions include (1) coprocessing of all fissiles, fertiles, and their intermediates, (2) recycle also of americium and curium, (3) adaptability to a variety of fuel types, and (4) excellent separation of recycled materials from essentially all of the fission product elements with just one separation stage. Each of these attributes confers important antiproliferation and economic advantages [SELVADURAY].

In principle, sodium chloride, potassium chloride, or a binary or ternary mixture of lithium, sodium, and potassium chlorides could be substituted for the lithium chloride solvent. However, it is expected that the separation factors may be poorer for these other solvents; any economic or process advantages of these other chloride solvents would then be minor in comparison to the advantage of recycle of LiCl in a lithium chloride-based process.

---

*Oak Ridge National Laboratory.

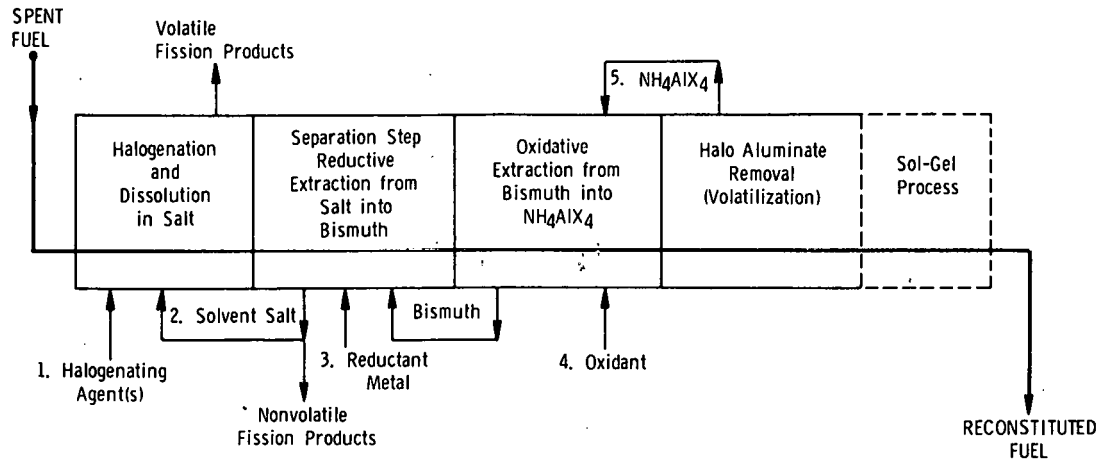

Reagents for Halide-Based Process

1. Halogenating Agent	2. Solvent Salt	3. Reductant Metal	4. Oxidant	5. Salt Reextractant
Chloride System				
CO_2, CCl_4 Cl_2, CCl_4 etc.	LiCl (Li/K)Cl etc.	Li Na etc.	HCl $BiCl_3$ etc.	NH_4AlCl_4
Fluoride System				
HF	(Li/Na/K)F etc.	Li Na etc.	HF BiF_3 etc.	NH_4AlF_4

Fig. 64. Zero-Level Reprocessing Flowsheet Showing both Chloride- and Fluoride-Based Separations Processes

Possible problems in the conversion of irradiated oxide fuels to chlorides have also been considered: for example, if it should prove necessary to use strongly oxidizing chlorinating agents to overcome the inertness of a thoria-containing fuel and change it the chloride, these agents might further oxidize UCl_3 (whose vapor pressure is very low) to UCl_4, UCl_5, and UCl_6, whose vapor pressures (as pure phases) are substantially higher. If these compounds were produced and their fugacities from LiCl were high, there could be process difficulties. An analogous difficulty might occur with UO_2-PuO_2 fuels, for which a small amount of $PuCl_3$ will be chlorinated to $PuCl_4$ [BENZ].

One way to overcome these potential difficulties is to work at a lower temperature, where the higher chlorides are less stable. Although UO_2 apparently does not chlorinate at satisfatory rates below 500°C with Cl_2/CCl_4 or CO_2/CCl_4 mixturs, it has been shown that fuels containing less than 20% PuO_2 can be easily oxidized to U_3O_8-PuO_2 [HARIHARAN]. U_3O_8 can be chlorinated easily at 350°C [SOOD-1969, PRASAD].

However, the activity coefficients of UCl_4 and UCl_5 in LiCl must be substantially less than one. The phase diagram work of Barton et al., indicates the formation of the compound Li_2UCl_6 [BARTON]. UCl_5 is

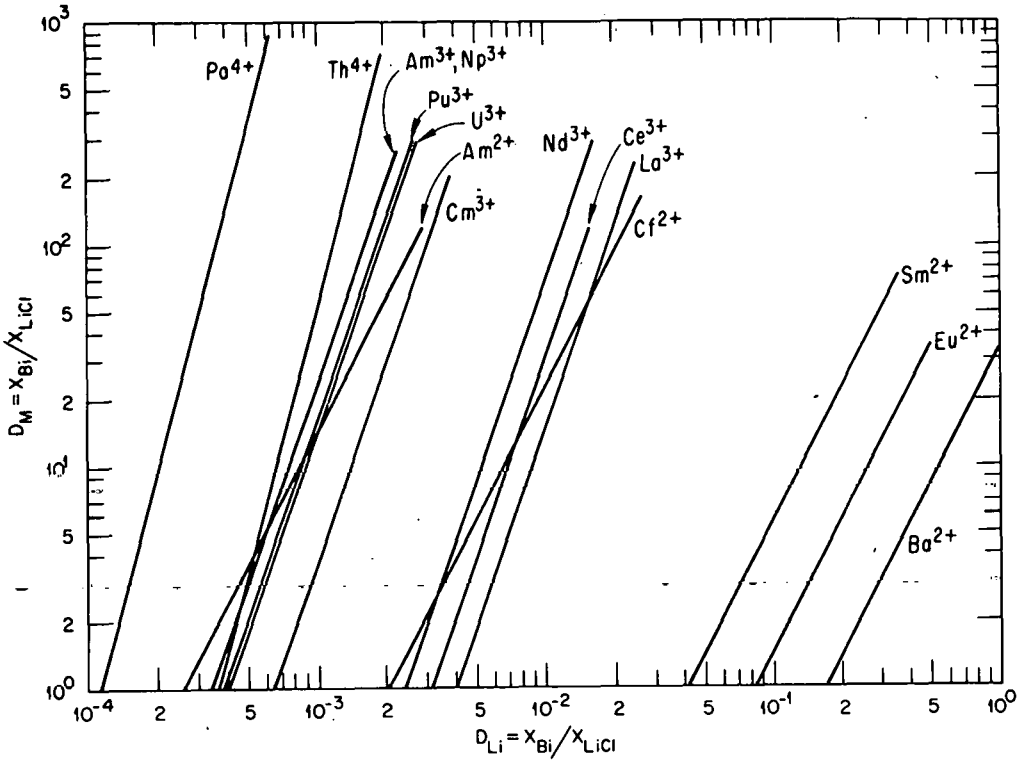

Fig. 65. Redox Distribution Coefficients at 700°C for the Solvent Pair LiCl/Bi, with Lithium Metal as the Reductant. See text for references.

reported to form compounds of the type $MUCl_6$ [HARIHARAN, BAGNAL]. Thus, we believe that the volatilities of dissolved fissile chlorides will be too low to cause process difficulties.

The relative ease of fluorination of irradiated fuel rods with HF suggests the use of a fluoride solvent in place of LiCl. Many distribution coefficient data are available for the solvent pair, $LiF-BeF_2-ThF_4/Bi-Li$ (Fig. 66) [FERRIS-1971, 1972, MAILEN, MOULTEN-1976, RICHARDSON-1970, 1972, SMITH-1971]. However, the handling of beryllium fluoride is difficult, which makes its use unattractive. In addition, the separation factor for thorium is poor with this molten salt solvent.

Examination of the few data extant indicates that the fluoride ion probably complexes the various solutes more effectively than does chloride ion, and that the complexing strength differences between chloride and fluoride are largest for those elements, e.g., thorium and uranium, which have the strongest tendency to distribute from the salt into the metallic phase. If these expectations are true, the distribution coefficients will be smaller from fluoride melts for all solute elements, but the effect will be most pronounced for those elements which we wish to extract from the fluoride melt into bismuth. Thus, the differences between the distribution coefficients will be smaller with fluorides than with chlorides, and the separation factors will be poorer.

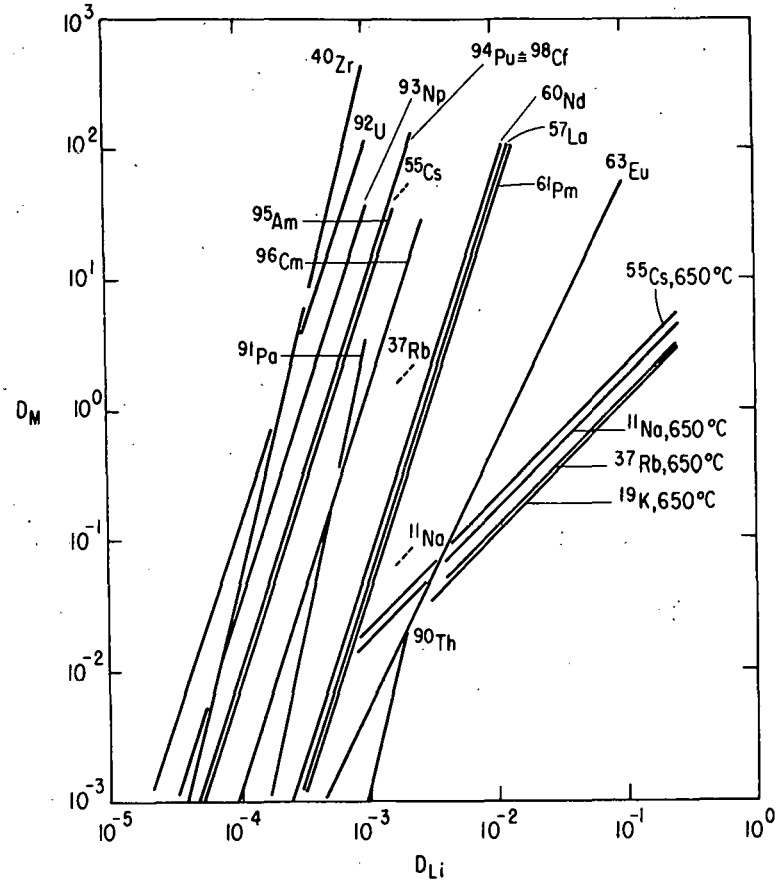

Fig. 66. Redox Distribution Coefficients for the Solvent Pair 72 mol % LiF-16 mol% BeF_2-12 mol % ThF_4/Bi-Li at 600°C. See text for references.

The use of a mixed chloride-fluoride system could combine the anticipated advantages of fuel rod fluorination with the superior separation factors of a predominantly lithium chloride solvent. For example, we have calculated that a uranium-neodymium separation factor of 70 could be achieved with a single reductive extraction step from LiCl-LiF (80-20 mol %) into bismuth [FERRIS-1972, SMITH-1970, 1971]. The thorium-neodymium separation would be even better for lithium reductant concentrations greater than 1 mol % in bismuth. The separation factors of uranium and thorium from the other rare earths would all be greater than 70. This process would require removal of excess fluoride during the salt recycle or else eventual discard of the solvent salt. [GRIMES] has patented a process for substituting chloride for fluoride.

Another way of combining the different advantages of the chloride and fluoride systems might be a two-stage process utilizing reductive extraction from fluoride solvent into bismuth, followed by oxidative extraction of the excess rare earths from bismuth into LiCl, then extraction of the fissile and fertile elements from the bismuth into NH_4AlCl_4.

An indexed, selected bibliography was published and distributed at the May 16-17, 1978, meeting [MCDUFFIE]. This contained citations of use to all work packages in the program, and was based on the ERDA Energy DATA BASE from July 1976.

Similar data bases have been constructed from Nuclear Science Abstracts (covering their citations back to 1971) and from Chemical Abstracts, even-month issues from 1970 through March 1978.

(2) Separations Processes

Since all of our flowsheets utilize an oxidative extraction into ammonium chloroaluminate, we have begun efforts to prepare and characterize this compound. It has been shown that uranium tetrachloride can form a 23.8% solution with this solvent at 350°C [ORNL-1957]. Despite repeated statements to the contrary in the earlier literature, [LAUGHLIN] has shown that the "boiling" of NH_4AlCl_4 at 400°C is actually a decomposition to HCl and NH_3AlCl_3 and has measured the vapor pressures of HCl and the ammine. In addition, small amounts of organic material are invariably present in the starting materials, which react with $AlCl_3$ upon fusion of the salt; and $AlCl_3$ also reacts very quickly with atmospheric moisture under ambient conditions.

Working in a dry box, we have combined sublimed ammonium chloride and (Fluka) aluminum chloride in a 1:1 mole ratio in a 1.27-cm (1/2-in.)-diameter tube, sealed off the tube under vacuum, fused the contents, and zone-refined the reaction product.

Analysis of the zone-refined material for nitrogen, aluminum, and chlorine showed a 1:1:4 ratio throughout most of the tube length, including the bottom portion, which was black due to very finely dispersed carbon (and possibly reduced metal). An X-ray powder pattern (copper radiation) of the refined NH_4AlCl_4 agreed well with the published data [SEMENENKO], as did the melting point of 300°C [KENDALL]. It appears unlikely that composition variations evidenced as slight discolorations of the ammonium chloroaluminate would materially affect the separations chemistry. A small portion of material having excess chloride (Al:Cl = 1:4.3) was found in the zone-refined material.

b. Plans for Next Quarter

Scouting experiments to characterize distribution coefficients of fuel constituents of interest between NH_4AlCl_4 and bismuth will be started this quarter. A summary of the literature relevant to our work package will be made. Efforts to estimate the activity coefficients of solutes in alkali halide melts from data in the literature will be started.

11. Reprocessing of Thoria-Urania Fuel
(P. Chiotti* and L. E. Burkhart*)

These studies involve the separation of fission product elements from simulated spent $(Th,U)O_2$ fuel. Reaction media are to be molten chloride salts and molten metals such as zinc, tin, lead or bismuth or mixtures

* Ames Laboratory.

of these. However, the principal effort will involve KCl-LiCl, KCl-$MgCl_2$ or KCl-NaCl-$MgCl_2$ eutectics and liquid zinc. Two processing techniques will be investigated: (a) conversion of $(Th,U)O_2$ to carbide (a more reactive material), with vaporization of volatile fission products, with or without reconversion to the oxide, (b) extraction of uranium and fission product elements from $(Th,U)O_2$ solid solution.

a. Conversion of $(Th,U)O_2$ to $(Th,U)C_x$
(O. N. Carlson* and L. Shiers*)

Because of the inert character of high-density $(Th,U)O_2$, its conversion to $(Th,U)C_x$ is considered an advantageous first step. Available thermochemical data indicate that a high degree of decontamination can be achieved during this conversion by volatilization under reduced pressure of many of the fission product elements. Elements such as yttrium, zirconium, niobium, molybdenum, technetium, and possibly ruthenium will remain with the carbide, assuming that there is no loss as volatile suboxides. Reconversion of the carbide to the oxide under strong oxidizing conditions may conceivably remove molybdenum as MoO_3.

(1) Experimental

A summary of experiments for the conversion of ThO_2 and ThO_2-UO_2 to carbide is given in Table 39. In each experiment, the oxide powders were thoroughly mixed with graphite powder and pressed into compacts in a 1.91 cm (3/4-in.)-dia steel die at a pressure of 6.895×10^6 pascals (1000 psi). The compacts were heated in a graphite crucible inserted into a cylindrical tantalum susceptor surrounded by several layers of graphite felt insulation.

The first sequence of experiments involved the formation of the dicarbide (runs 14-23, Table 39). Weight change and X-ray diffraction data indicate that almost complete conversion of ThO_2 to ThC_2 is achieved by heating at 2435°C for 15 min. In two of the experiments (runs 20 and 23), fission product elements were added to the initial thoria-carbon mixture in the form of their oxides in concentrations corresponding to those present in a ThO_2-9.3% UO_2 fuel after irradiation to 95,000 MWd/metric ton.

A second series of experiments (runs 25 and 29) was designed to study the possible decontamination, during conversion to the monocarbides, of a ThO_2-10% UO_2 mixture containing the same fission product oxide addition. The carbon content was so controlled that a substoichiometric $(Th,U)C_{0.88}$ composition would be attained. As was shown by the earlier work of [BRAND], this facilitates the removal of some of the less volatile elements such as cerium and plutonium. The reactions were carried out at 2125 to 2275°C, which is well below the melting point of the monocarbide.

Portions of both the monocarbide and dicarbide specimens containing simulated fission product additions (runs 23 and 29) were arc-melted in an argon atmosphere, and sections of each were subsequently electron beam melted at a pressure of 0.01 μm for a period of 20 min. Approximately

*Ames Laboratory.

Table 39. Summary of Experiments on the Conversion of ThO_2 and $(Th,U)O_2$ to ThC_x

Run	Charge	Wt, g	Temp, °C	Time at Temp, min	Pressure, Pascals	Major Product
14	ThO_2, C	18	2435	15	2.7[a]	ThC_2
20	ThO_2, F.P.,[b] C	20	2375	40	2.4[a]	ThC_2
23	ThO_2, F.P.,[b] C	63	2375	50	3.3[a]	ThC_2
25	ThO_2, UO_2,[c] F.P.,[b] C	62	2275	60	27 → 3.7[a]	$(Th,U)C_{0.88}$
29	ThO_2, UO_2,[c] F.P.,[b] C	61	2125	80	17 → 2.7[a]	$(Th,U)C_{0.88}$
36	ThO_2, C	50	2000	50	20 → 2.7[a]	ThC_2
43	ThO_2, C	57	2005	60	73 → 27[a]	$ThC_{0.9}$

[a] Pressure at the end of the heating time.

[b] Fission products added (in wt %): Zr, 1.25; Nd, 1.12; Mo, 0.90; Ce, 0.85; Ba, 0.44; Sr, 0.40; Ru, 0.39; La, 0.36; Pr, 0.35; and V, 0.20.

[c] Weight ratio ThO_2/UO_2 = 10.

20% of each sample was lost by vaporization during the electron beam melting step, including significant amounts of urania and thoria.

Qualitative analyses by emission spectroscopy of samples from runs 20, 23, 25, and 29 showed that strontium and barium are removed almost completely during the carbide conversion step but that the rare earth elements, Ce, La, Nd, Pr, and Y, are only partially removed. The higher melting elements, Ru, Mo and Zr, showed little if any change in concentration from that of the initial charge. Quantitative analyses of these samples by wet chemical methods are still under way. Results currently available show that strontium was decreased from 0.4% to less than 0.05% and that barium was decreased from 0.44% to less than 0.05%. Analysis for the other elements is hampered by difficulties of dissolving the samples. The arc-melted and electron-beam-melted specimens were particularly resistive to chemical dissolution; hence, no results are available for these experiments.

A series of experiments is now under way to determine the optimum conditions for converting the oxides to carbides and particularly the degree of conversion to the monocarbides at 2200°C and 2400°C, using similar heating rates and heating times. The specimens will be analyzed for oxygen content by vacuum fusion and for residual ThO_2 by X-ray diffraction to determine the completeness of the reaction under each set of conditions. Recently, another furnace setup has been placed in operation. Some difficulty has been encountered in attaining temperatures near 2400°C. Modifications of the furnace design are now under way.

A 100-g mixture of ThO_2-10% UO_2 powders was compacted in a 3.2-cm (1 1/4 in.)-dia die and then heated in a tantalum crucible to 2000°C for one hour in an induction furnace under a vacuum. The purpose of this experiment was to produce a homogeneous $(Th,U)O_2$ solid solution for use in future processing experiments. X-ray diffraction patterns taken of the oxide after heating revealed a single $(Th,U)O_2$ phase. This temperature and time are adequate for obtaining complete equilibrium.

(2) Future Work

Monocarbide conversion experiments with $(Th,U)O_2$ solid solution containing selected representative fission products will be done at 2000°C, 2200°C, and 2400°C by heating at a constant rate and holding at temperature for 1 h. These will be evaluated by determining the oxygen content of the carbide and by X-ray diffraction.

Samples from the preceding experiments will be reoxidized in air and oxygen at 800°C to determine if additional removal of fission products as volatile oxides, particularly as MoO_3 and RuO_4, can be achieved.

Experiments on converting the chemically inert sol-gel thoria pellets to the more reactive carbide will be investigated. These pellets were fired at 2800°C for 4 3/4 h during preparation and probably represent the most inert material to be encountered in fuel reprocessing.

b. Reaction of ThC_x with $ZnCl_2$ in Fused KCl-LiCl
(P. Chiotti* and D. Johnson*)

It may be necessary or desirable to remove zirconium and other nonvolatile fission products from ThC before it is reconverted to the oxide for refabrication into fuel pellets. A reaction like that given below might be used in such a separation.

$$ThC_2 + 2ZnCl_2 \rightarrow ThCl_4 + 2Zn + 2C \quad (1)$$

Three experiments have been completed for evaluating the kinetics of this reaction and the kinetics of the reduction step

$$2ThCl_4(\text{in salt}) + 4Mg(\text{in 5 wt \% Mg in Zn}) \rightarrow Th_2Zn_{17}(\text{in Zn alloy}) + 4MgCl_2(\text{in salt}) \quad (2)$$

A typical charge consisted of approximately 900 g KCl-LiCl eutectic salt, 14 g ThC_x, 22 g $ZnCl_2$. At the end of the oxidation reaction, approximately 90 g of Zn-5 wt % Mg alloy was added. In each experiment, the change in composition with time was monitored. The charge was contained in a 8.9-cm dia by 20.3-cm (3.5-in.-dia by 9.0-in.-dia) tantalum can. The charge was heated under an argon atmosphere in a standard 4-in. mild steel pipe, 71 cm (28 in.) long, jacketed with a type 316 stainless sheath and which had a water-cooled flange. The flange cover was equipped with vacuum-tight inlet ports for a 0.635-cm (1/4-in.) stirrer shaft, a 0.32-cm-dia (1/8-in.) tantalum thermocouple well, a gas inlet and a gas outlet, and with a larger port equipped with 1.90-cm (3/4-in.) ball valve for removing samples from the charge or introducing Zn-Mg alloy into the charge. The charge was heated to 150°C under vacuum, and the system was then filled with purified argon and maintained at a pressure about 2.7 pascals (2 cm of mercury) above atmospheric pressure. Upstream from the reaction vessel the argon was passed over titanium sponge and zirconium chips maintained at 580-620°C. The salt temperature was controlled to ±5°C.

The thorium and zinc concentrations in the salt during the first two experiments are shown graphically in Fig. 67. Both were conducted at 500°C. In experiment A, thorium dicarbide from run 14 of Table 39 was ground to pass a 150-mesh sieve and was added to the charge with the other constituents. Consequently, some reaction occurred as the charge was heated above the melting temperature of the salt to the final temperature of 500°C. A sample of the salt was taken when a temperature of 500°C was attained and was labeled time zero. As a result, the solid curves in Fig. 67 do not extrapolate to zero time.

In run B, carbide from run 36 of Table 39 was crushed and the -20 +40 mesh fraction was used. In this run, the $ZnCl_2$ was not added to the charge until the final temperature of 500°C was attained. The thorium and zinc analyses as a function of time are shown as the two broken curves in Fig. 67. While the third sample was being taken, some air was inadvertently

*Ames Laboratory.

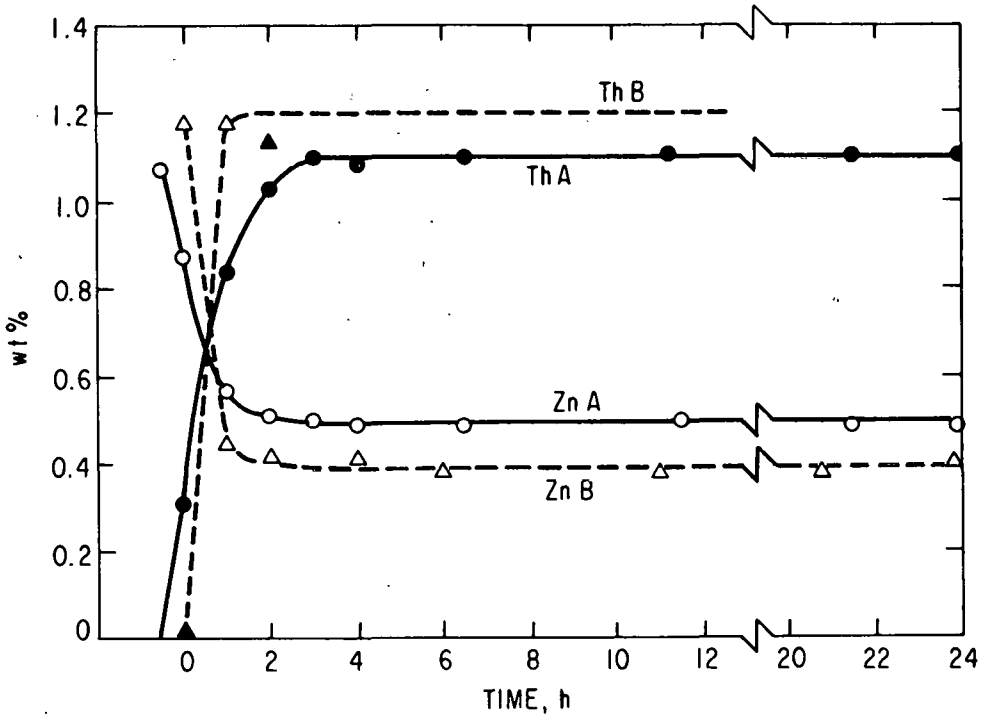

Fig. 67. Thorium and Zinc Concentrations in KCl-LiCl Eutectic Salt during the Reaction, $ThC_2 + 2ZnCl_2 \rightarrow ThCl_4 + 2Zn + 2C$, at 500°C for Experiments A and B

admitted to the system and the oxygen obviously precipitated some of the thorium as ThO_2. Therefore, thorium concentrations of subsequent samples are not plotted. The thorium content of the salt might have increased somewhat above 1.20 wt % if oxygen had not been admitted. If all of the ThC_2 added had been converted to $ThCl_4$, the final thorium concentration would have been 1.39 wt % instead of 1.2 wt %; in experiment A, the final concentration would have been 1.26 wt % instead of 1.11 wt % observed.

After approximately 24 h at temperature, Zn-5 wt % Mg was added. The reduction reaction (Eq. 2) is very rapid. In experiment A, the thorium concentration of the salt was reduced to 48 ppm in 40 min and to 7 ppm in 2 h. The final zinc concentration in the salt was reported to be approximately 20 ppm. Thermodynamic data indicate that the final concentration of thorium and particularly of zinc in the salt should be below detectable limits. Almost identical results were obtained in experiment B except that in 2.5 h the zinc in the salt was below detectable limits.

The third experiment was conducted at 450°C with monocarbide from run 43 of Table 39. Analytical data are not yet available.

(1) General Observations and Conclusions

(a) The kinetics of reaction 1 are not highly sensitive to the particle size of the thorium carbide but appear to be sensitive to the temperature of preparation of the carbide, as indicated by the initial slopes

of curves A and B in Fig. 67. Previous data reported by [IVERSON] for a similar experiment, conducted at 500°C with fused ThC_2-C eutectic which had been pulverized to -20 +325 mesh, showed much slower oxidation and reduction. His oxidation data are shown in Fig. 68. The fact that he used fused carbide is probably not the main reason for the lower oxidation rate. He does not describe his apparatus in detail in his thesis, but a review of his laboratory notebook indicates that the carbide was in a small separate tantalum container immersed in a salt which was in a larger container. The stirrer rod passed through and was welded to the center of this container bottom. The stirrer blade was about 4 cm below the bottom of the container holding the carbide. Although the bulk of the salt was well stirred, the salt in the inner container was not. The reaction rate was presumably controlled by the diffusion of $ZnCl_2$ into the container to the carbide particles and the rate of outward diffusion of the product $ThCl_4$.

In any case, the kinetics of the oxidation reaction (Eq. 1) or the reduction reaction (Eq. 2) are not expected to present any special problems in the application of this step to fuel reprocessing.

(b) It was observed in experiments A and B that 10-13% of the thorium in the carbide was not converted to $ThCl_4$ even though an excess of $ZnCl_2$ was employed in each experiment. Some oxygen (air) may have entered the reaction vessel during sampling; however, results obtained during experiment A show that there was no significant decrease in the thorium content on continued sampling of the salt after the maximum thorium concentration was attained (Fig. 67). It may be concluded that access of air to the

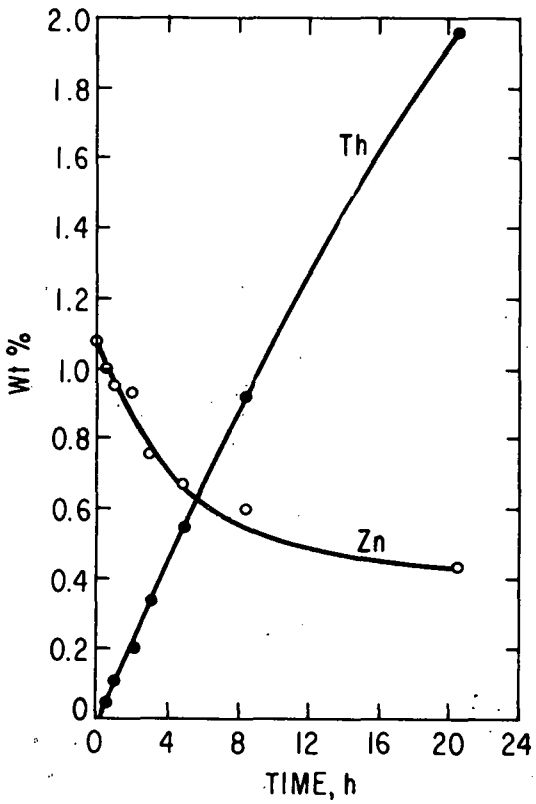

Fig. 68.

Change in Thorium and Zinc Concentrations in KCl-LiCl Eutectic Salt During the Reaction $ThC_2 + 2ZnCl_2 \rightarrow ThCl_4 + 2Zn + 2C$ at 500°C as Reported by [IVERSON]

reaction vessel during equilibration was negligible except in experiment B. Residual moisture or oxygen in the purified salts was also believed to be negligible. Consequently, there must be a significant concentration of oxygen in the thorium carbide. Oxygen analyses of the carbide are not yet available. It has been estimated that the solubility of oxygen in ThC_xO_{1-x} may be as high as 20 mol % ThO, if it is assumed that the solid solution is ThO dissolved in ThC. The solubility of oxygen in ThC_2 is not known.

It is not known whether the unconverted thorium is concentrated at the salt-zinc interface or dispersed in the zinc phase. If ThO_2 is dispersed in the zinc phase, it would follow that the noble fission products would concentrate in the zinc and be discarded. In the reprocessing of $(Th,U)C_x$ fuel material, some of the uranium would follow the thoria and its discard would represent an unacceptable fuel material loss. Recovery of uranium and thorium would require an additional reprocessing step.

(c) Salt samples taken during the oxidation cycle were observed to be gray and to contain finely divided carbon. It is not known whether all or only part of the carbon produced by reaction 1 remains suspended in the salt. However, after addition of the Zn-5% Mg alloy to the charge, the salt samples were observed to be milk-white, indicating no suspended carbon. Chemical analyses of the zinc-rich phase showed an excess of magnesium and a quantitative reduction of the thorium.

c. Reaction of the ThC_x with Zinc-Titanium Solution (J. T. Mason* and F. Chu*)

Previous work has shown that neither ThC_x nor UC_x reacts with zinc to form the respective intermetallic zinc compounds. In the case of UC_x, current thermodynamic data indicate that the reaction is not favorable. However, current data, which are believed to be reasonably valid, indicate that ThC_x should react with zinc at temperatures below 850°C. The reaction of ThC_x with zinc may be inhibited by the formation of a carbon film around the carbide particles. On the basis of this supposition, the following reaction

$$2ThC_x + 17Zn + xTi \rightarrow Th_2Zn_{17} + xTiC$$

was considered, it being hoped that TiC would tie up the carbon and not itself form an adherent film on the carbide particles. It was considered reasonable to expect the carbides of zirconium, niobium, and molybdenum (fission products) to concentrate in the relatively large amount of low-density TiC phase produced and to float to the surface while the more dense $(Th,U)_2Zn_{17}$ would settle to the bottom of the liquid zinc-rich phase.

The carbide $(Th,U)C_x$ (with x = 0.88) containing the above-mentioned fission products was equilibrated with a zinc-titanium solution by the following procedure: The reactants were sealed in a tantalum crucible which was enclosed in a welded stainless steel jacket and equilibrated in a

*Ames Laboratory.

rocking furnace for 24 h at 700°C, then for 2 h at 500°C, and furnace cooled. The microstructure of a vertical section of the zinc billet showed no concentration of a carbide phase at the surface. Microprobe analyses of the phases near the bottom of the billet indicated the presence of $TiZn_{15}$, $(Th,U)C_x$, and a third phase containing approximately 15 wt % zinc, 50 wt % thorium, and 20 wt % titanium, in addition to the zinc-rich matrix. A second experiment in which a similar charge was equilibrated for approximately four days also showed no carbide phase near the top of the billet. Microprobe analyses are not yet available. In any case, this procedure does not appear promising and will be discontinued.

d. Extraction of Uranium and Fission Product Elements from $(Th,U)O_2$ (J. T. Mason* and F. Chu*)

The purpose of the current effort is to elucidate the chemistry and kinetics involved in the reaction of $(Th,U)O_2$ solid solution in molten salts containing $ThCl_4$ and thorium metal chips to produce uranium metal and decontaminated ThO_2. The noble fission product (NFP) elements will concentrate in the uranium, and the more reactive fission product elements will concentrate in the salt. Separation of fission product elements from the uranium or the salt can be achieved by previously developed methods. The principal advantage of this procedure is the retention of the bulk of the fuel as ThO_2. The limiting factor is the kinetics of the reactions of $(Th,U)O_2$ in the fused salt, particularly in the case of high density $(Th,U)O_2$ produced by the sol-gel process. The possible anodic decomposition of $(Th,U)O_2$ as described in [STEINDLER-1978C] is also being considered.

(1) Experimental

Previous experiments on the reaction of UO_2 in a $(Th,U)O_2$ solid solution with thorium metal chips in a $KCl-LiCl-ThCl_4$ salt to produce UCl_3 and uranium metal have shown that the reaction may be too slow to be practical. Some later experiments have been conducted in a controlled-atmosphere glove box having a residual oxygen content of 10 to 100 ppm of oxygen in the argon atmosphere. Recent experiments have shown that this oxygen level can have a significant effect on the reactions occurring in open containers, in which reaction times of more than several hours are involved. Consequently, a different glove box has been put into operation in which a helium atmosphere is circulated through a molecular sieve to remove moisture and successively through zirconium chips and titanium sponge (both at 650°C) to remove trace amounts of oxygen, nitrogen or other reactive gases. This glove box is also equipped with a furnace chamber extending through the floor into an external furnace. This arrangement permits heating of larger charges to temperatures up to 1000°C without excessive heating of the glove box atmosphere. Kinetic experiments are under way in this new facility.

The slow step in this reaction is believed to be the formation of $ThOCl_2$ and the exposure of UO_2 to the reaction media. Experiments for abrading the surface of the $(Th,U)O_2$ particles during reaction have been

*Ames Laboratory.

designed. Initial results appear promising with $(Th,U)O_2$ that contains 10% UO_2 and had been prepared by sintering of the mixed oxides at 2000°C. Chemical analyses are not yet available. Experiments with $(Th,U)O_2$ produced by the sol-gel process are planned.

(2) Electrolytic Decomposition of $(Th,U)O_2$

An alternative method for the decomposition of the $(Th,U)O_2$ solid solution involves anodic dissolution of an oxide-carbon mixture, as outlined in [STEINDLER-1968C]. Initial results indicate that the overall cell reaction can be rather complex. To obtain some insight on the basic reactions involved, pure UO_2 was employed as the anode in a KCl-LiCl-5.7 wt % $ZnCl_2$ salt at 500°C. As expected, the UO_2 was deposited at the cathode. With a ThO_2-carbon mixture as the anode, gas evolution (presumably CO_2) was observed and some transport of ThO_2 to the cathode was also observed. With $(Th,U)O_2$ and carbon as the anode, the cathode deposit was observed to be a $(Th,U)O_2$ solid solution. These electrode reactions will be investigated further in the new glove box facility.

e. Engineering Analysis
(L. E. Burkhart* and D. Rehbein*)

A preliminary flowsheet has been prepared for what now appears to be the most promising reprocessing scheme for thoria-urania fuels. The flowsheet, shown in Fig. 69, gives the material requirements for a 10-kg fuel charge which initially contains 9.3% uranium and has been irradiated to an exposure of 94,271 MWD/MT at a power of 65 MW and a flux of 8×10^{13} neutrons/cm^2-s. This is a higher exposure and lower power than is typical but gives a reasonable neutron fluence. The 10-kg charge was chosen as a convenient basis for a possible bench-scale process. If one considers a single LWR with a fuel loading of about 130 tons and replacement of one-third of the core per year, then for 300 d/y operation, a minimum continuous capacity of about 144 kg/d would be required. For a breeder reactor operated under similar conditions, a core of about 20 tons would require an average minimum reprocessing capacity of about 22 kg/d.

In the flowsheet in Fig. 69, the fuel is first converted to monocarbides in a 100-kW induction furnace (T-1) according to the reaction,

$$(Th,U)O_2 + 3C \rightarrow (Th,U)C + 2CO$$

The reaction is carried out at 2000°C or higher under a dynamic vacuum of approximately 20 μm. Current vapor pressure data indicates that under these conditions, the volatile fission products, VFP (all except zirconium, niobium, molybdenum, technetium, and ruthenium) , should distill out of the fuel. These five elements constitute only 21% of the total fission products in the fuel, and so significant purification is achieved. Conversion to the monocarbides is preferable to conversion to the dicarbides since more effective volatilization of fission product is achieved and only one-half as much free carbon is

*Ames Laboratory.

released in the subsequent step to act as a possible contaminant. The volatile fission products are collected on a cold plate at the top of the furnace and are sent to a high-level waste disposal facility. The off-gases go to a radioactive gas cleanup system. An acceptable physical form for the radioactive gases is yet to be determined. Also, if the fuel is reprocessed after only a short radioactive cooling period, some arrangement may have to be made for continuous removal of the heat generated by radioactive decay of fission products.

After the fuel has been rendered more reactive by conversion to carbide, it is converted to $ThCl_4$ and UCl_3 by the following reaction with $ZnCl_2$ in a LiCl-KCl medium:

$$ThC + 2UC + 5ZnCl_2 \rightarrow ThCl_4 + 2UCl_3 + 5Zn + 3C$$

The reaction is carried out in a 50-L resistance-heated stirred vessel (T-2). This reaction vessel, and those used for subsequent steps in the process, must be inert to liquid zinc and should probably be made of tungsten or have a tungsten liner.

Since the $ThCl_4$ and UCl_3 are soluble in the LiCl-KCl fused salt bath, they will be drawn up into the salt phase and away from the remaining noble fission products as the reaction proceeds. The fission products form

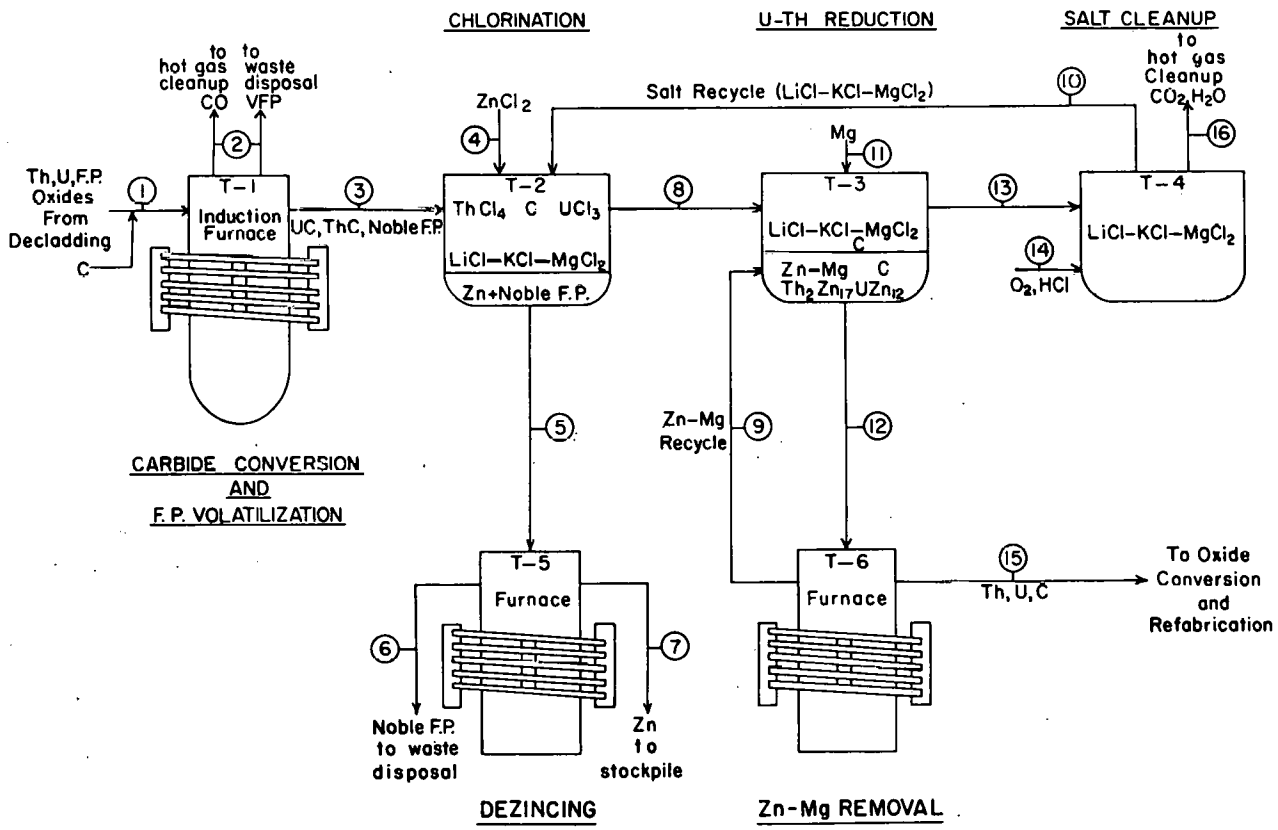

Fig. 69a. Preliminary Flowsheet for Reprocessing $(Th,U)O_2$ by Carbide Conversion, Chlorination, and Reduction to Metal

Line Number		1	2	3	4	5	6	7	8	9	10	11	12	13	14	15	16
Process Material		Feed														Product	
Mass	(gm)	11295	2781	8514	9085	4599	241	4358	119349	264603	106348	1621	271500	112777	216	8193	297
ThO_2	(gm)	8394															
UO_2	(gm)	556															
NFP	(gm)	241		241		241	241										
VFP	(gm)	790	663														
C	(gm)	1314							407				326*	81*		326	
CO	(gm)		2118														
ThC	(gm)			7758													
UC	(gm)			515													
Zn	(gm)					4358		4358		251963			232683				
LiCl-KCl	(gm)								100000		100000			100000			
$MgCl_2$	(gm)								6348		6348			12696			
$ZnCl_2$	(gm)				9085												
$ThCl_4$	(gm)								11885								
UCl_3	(gm)								709								
Mg	(gm)									11640		1621	11640				
Th_2Zn_{17}	(gm)												25041				
UZn_{12}	(gm)												2106				
Th	(gm)															7377	
U	(gm)															490	
H_2O	(gm)																
O_2	(gm)														216		
HCl	(gm)																
CO_2	(gm)																297

* Based on estimated 80%-20% carbon distribution between Zn-Mg and salt.

Fig. 69b. Process Stream Flows Based on 10-kg Charge

intermetallic compounds with the molten zinc produced by the reduction of $ZnCl_2$. It is known experimentally that a layer of liquid zinc containing these fission products forms in the bottom of the reaction vessel. When reaction is complete, the vessel can be cooled to 420°C to solidify the metal phase, and the salt phase, which freezes at about 355°C, can be decanted off. Optimum reaction time and temperature for this step is still under study. Two potential engineering problems which remain are possible zinc fog formation in the salt phase and an increase in the freezing point of the salt mixture as $MgCl_2$ builds up during recovery and recycle of the salt.

Possible solutions to a zinc fog problem, if it exists, are filtration through an inert filter medium or centrifugation. The rise in freezing temperature of the salt with $MgCl_2$ buildup may determine the number of cycles the salt may be recycled before it must be discarded and replaced.

The $ThCl_4$ and UCl_3 are treated with Zn-Mg in reaction vessel T-3 in order to reduce the Th and U according to the reaction:

$$2ThCl_4 + 2UCl_3 + 7Mg + 41Zn \rightarrow Th_2Zn_{17} + 2UZn_{12} + 7MgCl_2$$

As this reaction proceeds, the Th-Zn and U-Zn intermetallics precipitate out as solids--probably as the solid solution $(Th,U)_2Zn_{17}$. In order to facilitate their removal from the reaction vessel, sufficient reactants are added to provide a slurry containing 10% solids (by weight). The amount of magnesium used was calculated to provide an initial alloy of 5% magnesium in zinc, although further work may show that less magnesium can be used. The $MgCl_2$ formed during the reaction will remain in the salt. There will thus be a continual buildup of $MgCl_2$ in the fused salt bath, which will cause the salt composition to change from an initial equimolar LiCl-KCl mixture to an equimolar LiCl-KCl-$MgCl_2$ bath after five cycles. Again, the salt phase can be decanted off after cooling the vessel to the freezing point of the liquid metal phase.

The salt is cleaned in reaction vessel T-4 between processing cycles by bubbling oxygen through the bath to remove carbon left from the reduction of ThC and UC. Anhydrous HCl is then bubbled through the bath to dry it, removing any residual oxygen or hydroxide.

A furnace (T-6) is used to remove zinc and magnesium from the zinc-magnesium-thorium-uranium alloy obtained by the reduction of $ThCl_4$ and UCl_3. This alloy should be essentially independent of the fuel composition since the alloy is more than 95% zinc and magnesium. Consequently, the dezincing heat cycle should be the same regardless of the fuel being processed. The heating cycle for furnace T-6 is:

(a) Heat to 650°C and hold for 2 h

(b) Heat to 850°C at 100°C per hour and hold for 1 h

(c) Heat to 1100°C at 100°C per hour and hold for 1 h.

The total heating time per cycle is 8.5 h.

A single furnace could be used for T-5 and T-6 because of the small charge from T-2 in each cycle. The charge capacity of a 50-kW furnace is approximately 34 kg, and so dezincing of the fission products from T-2 is necessary only after every sixth cycle. On the other hand, the charge to T-6 from each cycle is 271.5 kg and so with a 50-kW furnace, eight heats must be made for each 10 kg of fuel charged to the process. In a production-scale process, a larger furnace would be used in order to reduce the time required to remove the zinc and the magnesium.

At this point in the development work, it appears that the solid intermetallics in the Zn-Mg solution are too finely dispersed to allow gravity settling and decanting of any of the Zn-Mg solution in order to reduce the distillation load on furnace T-6. However, two other possibilities exist for shortening the time required to recover the products. First would be filtration of the intermetallic products from the Zn-Mg solution. A possible filter medium has been ordered and will be tested. A second rather interesting possibility is the use of a centrifuge for increasing the settling rate of the precipitate, allowing decantation of much of the Zn-Mg solution.

The free carbon released during chlorination in T-2 remains suspended in the salt phase, but when the $ThCl_4$ and UCl_3 are reduced by Zn-5% Mg in T-3, much of the carbon appears in the metal phase. It is present as graphite rather than combined with the thorium and uranium as the carbide. In the flowsheet, the estimate is that 80% of the carbon will collect in the metal phase.

New material inputs and losses for the system for a single cycle are shown in Table 40.

Table 40. Single-Cycle Material Balance for Proposed Process

Material	Constituents of Input Streams, kg	Amount Lost, kg
Carbon	1.314	
Volatile F.P.		0.663
CO		2.118
$ZnCl_2$	9.085	
Noble F.P.		0.241
Magnesium	1.621	
Oxygen	0.216	
CO_2		0.297

Consideration has also been given to a reprocessing scheme whereby a portion of the fission products is allowed to remain in the fuel. In this option, the fuel would be converted to carbide in T-1 and subsequently re-oxidized and fabricated into fuel elements. Information is now being sought on the equilibrium levels of these elements under continuous recycle in order to estimate the effect on neutron economy, refabrication, and in-core effects during irradiation.

12. Molten Tin Process for Reactor Fuels
(R. Borg*)

A new investigation to identify chemically feasible pyrochemical nuclear fuel reprocessing methods within the general frame of nonproliferation systems is directed to the reprocessing of spent fuel elements by the precipitation of thorium nitride, uranium nitride, and plutonium nitride from molten tin solvent. Separation of fission product elements and other impurities by volatilization and selective precipitation of intermetallic compounds is also under study.

Lawrence Livermore Laboratory will provide program management, studies and analyses, development of a fuel reprocessing flow sheet, and general support for the research and development of molten tin processes for the removal of fission products and other impurities from spent uranium-plutonium and thorium-uranium (plutonium) fuels in oxide, metal, or carbide form. Initial effort will be on oxide fuel, with metal and carbide fuels to be studied later.

Effort in FY 1978 will include calculations of relevant thermodynamic data and experimental studies of process chemistry with simulated fuel in order to determine process parameters.

Effort will be expanded in FY 1979 to determine the technical feasibility of a selected process flowsheet and to prepare for small-scale process demonstrations with irradiated fuel specimens. Hot laboratory experiments will be performed with small test specimens.

a. Studies and Engineering Analysis

(1) Thermodynamics

The three major objectives of this task for FY 1978 are:

(a) To review relevant thermodynamic literature

(b) To review relevant kinetic data

(c) To prepare a tentative process flowsheet for the molten tin-nitrogen (MTN) process.

The form of the last objective will rely heavily upon revelations when pursuing objectives (a) and (b). In order to determine the relevant chemical reactions, it is first necessary to establish the approximate concentrations of fission products, residual uranium, and transuranic elements. Appendix B lists the pertinent initial fission yields in spent LWR fuel; these values are in general agreement with those calculated by the ORIGEN code for 33,000 MWd/MTU (LWR). Other fuel cycles will be considered in the future.

---

*Lawrence Livermore Laboratory (LLL).

There are three or perhaps four distinct process streams which can contain fission products, viz.

(a) off gases

(b) liquid Sn solution

(c) UN solid phase

(d) cladding phase

The cladding, category (d), is a variable whose effect will depend on the details of the process. Nevertheless, at some stage, the cladding must be separated from the solvent tin and the nitride precipitate; hence, it may scavenge some fission product activities.

As the MTN research progresses, we will attempt to estimate the nature and concentration of radioactive species in each of the four process streams. The easiest to estimate is the off gases; Table 41 lists the initial approximations of the relative volatilities of the more important (i.e., hazardous) fission products. These values will become more quantitative and reliable if our search of the literature yields better data. Streams (b) and (c) are currently being studied.

Table 41. Estimated Volatilities of Fission Products from Liquid Tin Solutions at 1873 K

A.	Very high,	1.01×10^{4} to 1.01×10^{1} pascals (10^{-1} to 10^{-4} atm) I, Br, Cd, Cs, Rb, and Se
B.	Moderate,	1.01 to 0.1 pascals (10^{-5} to 10^{-6} atm) Sb and Te
C.	Low,	1.01×10^{-3} to 1.01×10^{-5} pascals (10^{-8} to 10^{-10} atm) Ba, Eu, Sm, Sn, and Sr
D.	Very low,	1×10^{-6} to 1×10^{-12} pascals (10^{-11} to 10^{-17} atm) Ce, Gd, La, Mo, Nd, Pd, Pm, Pr, Rh, Ru, Tc, Y, and Zr

The degree to which the nonvolatile fission products would partition between the solvent and nitride phases is a major unanswered question. It is doubtful that sufficient data exists to resolve this problem, and almost certainly, laboratory measurements will eventually be required. Table 42 lists the lattice parameters and decomposition temperatures for several refractory nitrides formed with major constituents of fuel, cladding, and fission products. With the exception of Mo_2N, all have the rock salt (f.c.c.) crystal structure and lattice spacings of similar magnitude to UN. Several have decompositon temperatures higher than that of UN, suggesting even greater thermodynamic stability. This is shown in Table 43, which lists

Table 42. Physical Constants of Selected Nitrides

Compound	a_o (f.c.c.), A	ρ, g cm^{-3}	Decomposition Temp. (T_d), K
UN	4.880	14.32	2800
PuN	4.805_5	14.23	2563-3043
ZrN	4.537-4.562	7.35	3253
ThN	5.144	11.50	2903
Mo_2N (hex)	a_o = 5.725 c_o = 5.608	9.16	873
YN	4.79	5.89	>2950
GdN	5.00		
SmN	5.05		
LaN	5.30	6.90	--
CeN	5.01	8.09	--
NdN	5.15	7.70	

standard enthalpies of formation for several of the same nitrides. This information suggests that several fission products may dissolve in the nitride phase. The partitioning of each element is governed by the requirement that the chemical potential, at equilibrium, be equal in both the solid and liquid phase. Consequently, if the activity in the liquid phase is extremely low, i.e., if the activity coefficients are much less than unity, the solubility in the nitride phase may be severely limited. Whenever sufficient data exists, the relative chemical potentials can and will be estimated by a semiempirical method.

A search of the literature for pertinent thermodynamic data is in progress. We have received a bibliography from the ORNL data base, and an in-house effort by the LLL Technical Information Division is under way. The available data tends to fall mostly into two categories, viz, the thermodynamic properties of the pure monometallic nitrides, and binary phase diagrams having tin as one of the components. While some data have been found which deal with the thermodynamics of molten metals, few, if any, describe nitride-molten metal systems. A preponderance of the pertinent references are written in Slavic or Japanese and will require translation.

(2) Kinetics

The literature search for kinetic data has been initiated, but none of the ordered reports have been received.

Table 43. Thermodynamic Data for Nitrides of Interest

	$\Delta H^{\circ}_{f,298}$, kcal/mol	S°_{298}, cal/K mol
1/2 Ba_3N_2	-43.4 ± 4.0	(18.2 ± 1.0)
CeN	-78.0 ± 6.0	
EuN	-46.5 ± 2.8	
GdN	-73.4 ± 5.0	
LaN	-71.5 ± 4.0	
Mo_2N	-16.6 ± 0.5	(21.0)
Nb_2N	-61.1 ± 1.0	
NbN	-56.8 ± 1.5	
PuN	-70.2 ± 1.5	
SmN	-77.2 ± 3.7	
1/2 Sr_3N_2	-46.7 ± 2.5	(14.8 ± 1.2)
ThN	-90.6 ± 3.0	
1/4 Th_3N_4	-77.5 ± 1.2	(10.7)
UN	-70.4 ± 1.0	(13.0 ± 1.5)
YN	-71.5 ± 5.0	
ZrN	-87.3 ± 0.5	

(3) Process Flowsheet

A preliminary process flowsheet has been constructed and once revised (Appendix C). Major improvements in this initial scheme will require a more exact knowledge of:

(a) fission product partitioning

(b) the amount of tin occluded in the nitride salt

(c) a method of reclaiming tin from $ZrSn_2$.

Upon solution of the above problems, our attention will shift to the next set of problems. The project is too new for a second category of foreseeable problems to have developed, but questions of optimization of throughput and economics might arise at this stage.

b. Separations Processes

Apparatus is being assembled to conduct a variety of high-temperature experiments. The essential features are an induction-heated graphite crucible contained in a water-cooled quartz jacket. A dynamic vacuum or inert gas atmosphere can be maintained within the jacket, allowing simple vacuum melting or study of nitriding reactions. Special components of the vacuum system have been designed and committed to fabrication. Orders have been placed for commercially made components.

Also designed and under construction is equipment necessary to test the feasibility of filtering UN precipitate from molten tin.

IV. ENCAPSULATION OF RADIOACTIVE WASTES IN METAL

(L. J. Jardine, K. F. Flynn, and R. E. Barletta)

The major objectives of this task are to identify the advantages and disadvantages of encapsulating solidified radioactive waste forms in a metal matrix for storage in geological formations. The net attributes of metal encapsulation are to be identified by comparisons of the properties and fabrication methods of this waste form with those of other well-developed solidification alternatives (i.e., calcination and incorporation in glass monoliths in the special case of high-level radioactive wastes). In progress are laboratory-scale investigations specifically aimed at generating data required to further assess probable or unresolved problem areas. Experimental studies during this reporting period have focussed on the leach rates of (1) a simulated waste form encapsulated (dispersed) in a metal matrix, (2) Zircaloy and aluminum-12% silicon alloy, and (3) simulated high-level waste glass containing uranium. The leaching media were distilled water and saturated sodium chloride solutions.

A. Determinations of Leach Rates of Simulated Waste Forms

1. Introduction

A major factor affecting the successful isolation of radioactive waste is the rate of release of the radioactivity from the solid waste to the environment. A very probable mechanism for this release from waste stored underground is leaching of the solid waste with groundwater. Measurements of leach rates are necessary to evaluate the rates at which specific hazardous radionuclides will migrate from the waste if the waste form comes in contact with groundwater.

2. Experimental Procedure and Results

These experiments have been conducted using relatively simple laboratory equipment. The room temperature (25°C) quiescent water leaching tests were done in either simple Florence flasks (Fig. 70) or beakers (Fig. 71). These tests were performed with stagnant water since it is felt that samples immersed in quiescent water most closely approximates the conditions expected in geologic storage. Leaching tests at about 100°C are in progress using a Florence flask equipped with a water-cooled condenser (Fig. 72). In the tests at about 100°C, there is significant agitation since they are performed at the boiling point of the medium. The gamma-ray analyses* of the dry samples were accomplished using a standard lithium-drifted germanium (GeLi) apparatus combined with a computer programmed spectrum analysis [STEINDLER-1978A].

A neutron activation analysis (NAA) technique [FLYNN] was used to evaluate leach rates for elements of specific interest to nuclear waste management.

---

*Performed by E. Huff of Analytical Laboratory, Chemical Engineering Division.

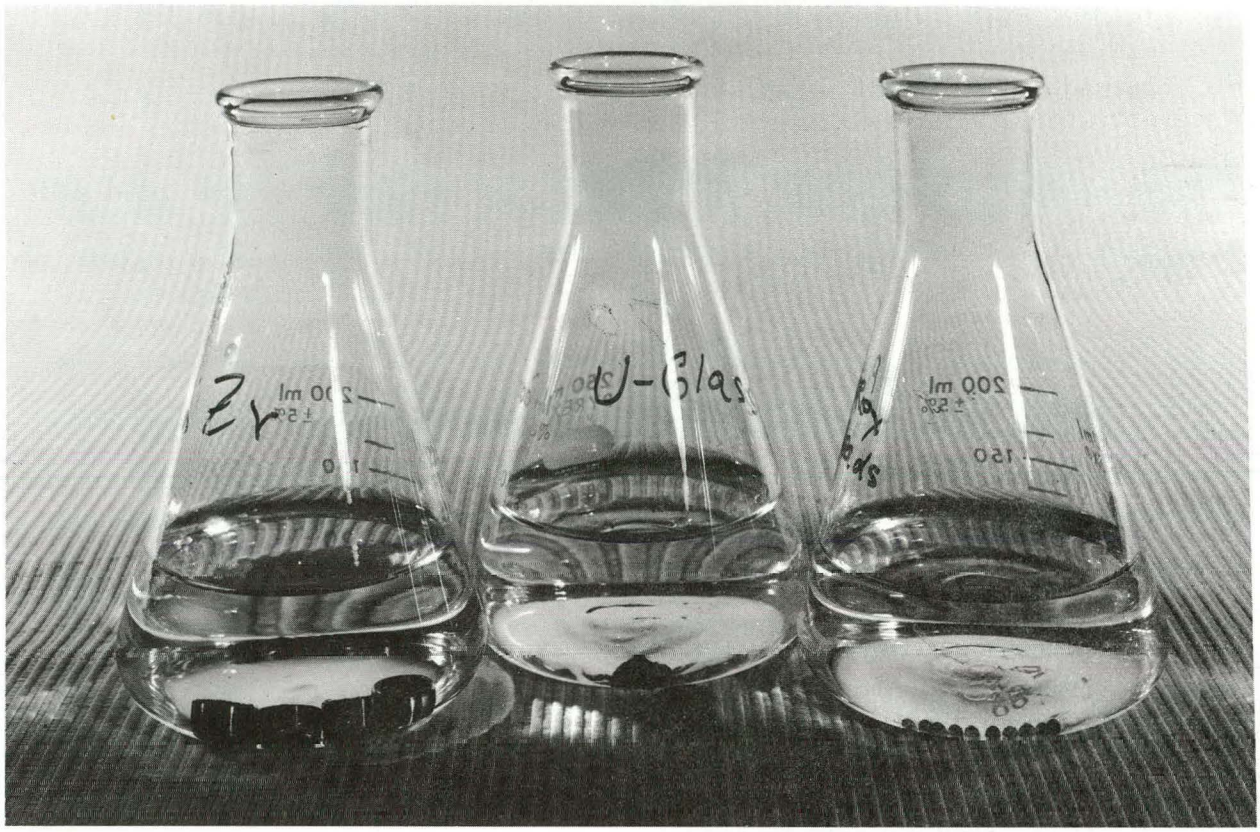

Fig. 70. 25°C Leach Test of Zircaloy, PNL 76-68 Glass, and Pyrex Glass Beads. ANL Neg. No. 308-78-348

Neutron irradiation of simulated high-level waste produces activation products which can be readily measured by radiochemical and/or instrumental methods. For example, gamma ray analysis of neutron activated material before leaching and of leachant after leaching provides an assay of the various gamma-emitting isotopes leached. This technique has been applied successfully to numerous proposed waste forms in a spectrum of potential storage environments. Additional background information on these studies can be found in previous reports in this series [STEINDLER-1976 and 1978A].

a. Leachability of Reaction Products of Waste Pellets with Molten Lead

Compounds of $Pb_3RE_6(SiO_4)_6$, (RE = rare earth) were identified as the major component of the reaction zone which resulted from the reaction at about 700°C between (1) simulated solidified high-level calcine waste pellets containing 10 wt % SiO_2 and (2) molten lead [STEINDLER-1978C].

In order to determine whether or not formation of these compounds within the waste matrix would cause any appreciable change in dispersibility as a result of increased solubility of the rare earths and/or the matrix material, two such compounds, $Pb_3La_6(SiO_4)_6$ and $Pb_3Nd_6(SiO_4)_6$, were prepared in the laboratory.

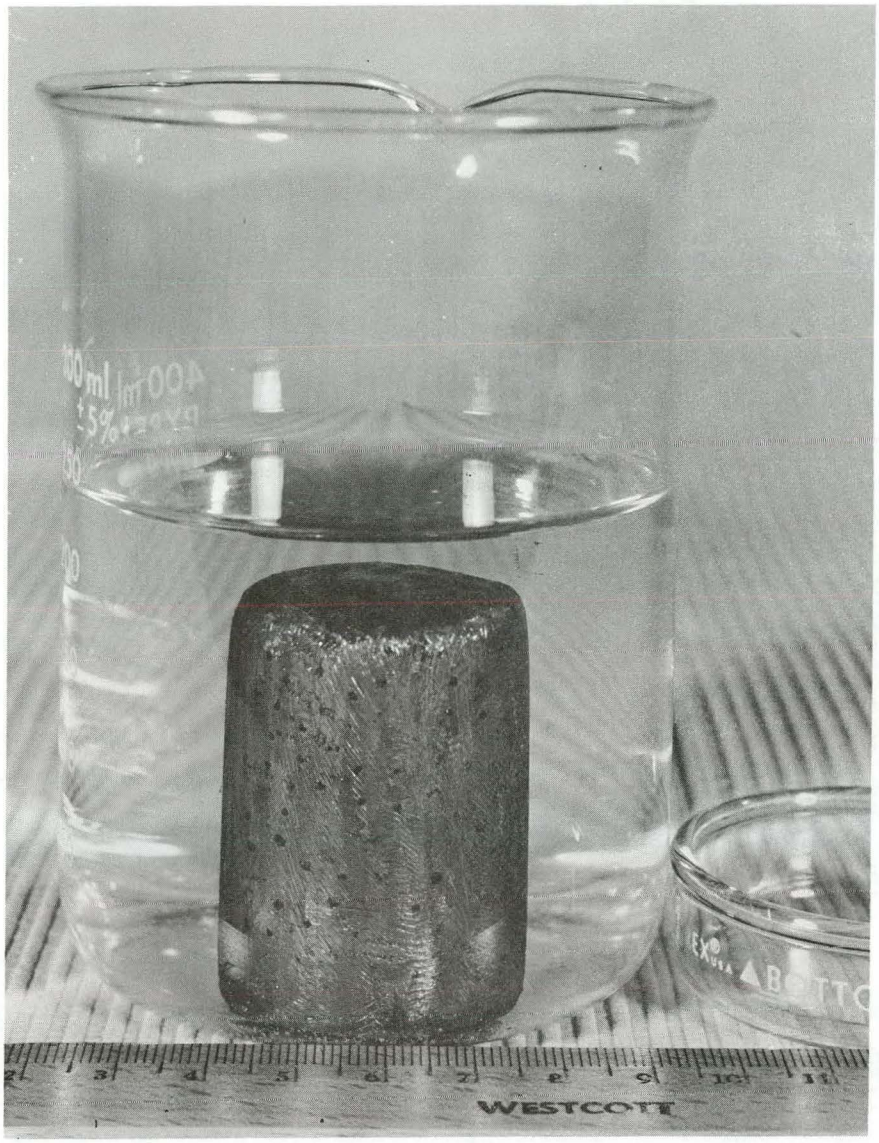

Fig. 71. 25°C Leach Test of a Small-Scale 2839 Lead Metal Encapsulated Composite. ANL Neg. No. 308-78-344

These compounds were irradiated in the isotope tray (flux of about 6×10^{12} n/cm^2s) of the Argonne National Laboratory (ANL) CP-5 Research Reactor for 24 h. The surface area of each sample was estimated from BET measurements. Two sequential leach tests were then performed on each of these compounds, using room temperature (about 25°C), quiescent distilled water. The measured leach rates, together with other pertinent information, are summarized in Table 44. The activation products of the rare earth nuclides (^{140}La and ^{147}Nd) were used to make these measurements radioanalytically [STEINDLER-1978A].

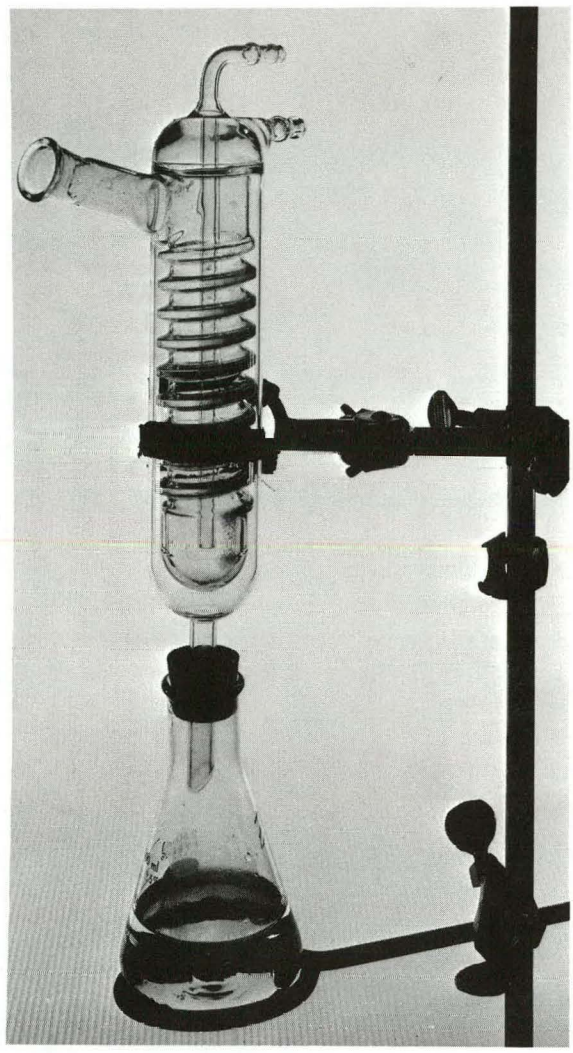

Fig. 72. Leaching Apparatus for about 100°C Measurements. ANL Neg. No. 308-78-344

The results show that these compounds are extremely insoluble; leach rates are less than 10^{-7} gram (equivalent) per square centimeter of surface area per day, compared with 10^{-6} g/cm^{2}d for typical glasses. Hence, these compounds should not be detrimental to the overall leaching characteristics of metallic lead-encapsulated waste forms if they are formed in any significant concentration in actual waste.

Table 44. Leach Rates of Reaction Zone Compounds[a] in Quiescent Distilled Water at 25°C

Compound	Leach No.	Sample Wt, mg	BET Surface Area,[b] m^2/g	Leach Time, days	Leach Rate, g/cm^2d
$Pb_3Nd_6(SiO_4)_6$	1st	57.2	0.54	5.81	3.9×10^{-8}
	2nd			21.0	8.8×10^{-9}
$Pb_3La_6(SiO_4)_6$	1st	25.6	0.27	0.95	1.4×10^{-7}
	2nd			7.02	1.6×10^{-9}

[a]Compounds observed to form in the reaction zone between calcine waste pellets and molten lead at about 700°C [STEINDLER-1978C].

[b]Surface areas were established by R. Malewicki of the Analytical Laboratory.

b. Leach Rates of Zircaloy and Aluminum-Silicon

Leach rate studies of Zircaloy and aluminum-12% silicon alloys have been concluded. Zircaloy was studied because of the current waste management concepts advocating interim and geological storage of spent fuel. The leach rate for Zircaloy in 25°C stagnant distilled water was determined to be 2×10^{-9} g/cm^2d (grams per square centimeter of surface area per day), whereas the leach rate in 110°C solution (boiling) saturated with sodium chloride was 2×10^{-8} g/cm^2d. These measurements by the NAA technique [FLYNN] were based on the fraction of the radioactive activation product ^{95}Zr found in the leaching medium compared with the ^{95}Zr present in the solid Zircaloy matrix. We were not able to determine any decrease in leach rate with time during the 100 days these tests were performed.

The leach rate for aluminum-12% silicon alloy (proposed as a metal matrix material) in 25°C distilled water was determined to be less than 3×10^{-6} g/cm^2d; at 100°C, the leach rate was 5×10^{-6} g/cm^2d. These measurements were based on the activation products, ^{59}Fe and ^{60}Co. Both iron and cobalt are present as trace metals in the alloy. Because of the small size of the sample used, it was only possible to assign a maximum to the 25°C distilled water leach rate.

No further testing of Zircaloy and aluminum alloy is planned at this time.

c. Leach Rates of Sintered Waste Forms (Encapsulated in Lead or Unencapsulated)

Leach rate studies are continuing on metal-encapsulated composites consisting of sintered waste form (SWF) granules* encapsulated in a lead matrix. Results from three 1.5-cm-dia ingots ranging in height from 0.4 to 1.5 cm have been reported [STEINDLER-1978C]. A description of these composites, together with a description of the experimental procedures used and the rationale for the measurements, can be found in [STEINDLER-1978B]. The results of these leach tests have indicated that the metal matrix has little if any effect on the leaching characteristics of the dispersed SWF. Leach rates were determined for six different radioisotopes present in the SWF granules, and each leached at approximately the same rate as it did in the absence of any metal matrix.

Since these ingots were rather small [see STEINDLER-1978C], a larger ingot (i.e., a 283-g ingot with a smaller surface area to volume ratio) was produced to see if the effect (or lack thereof) of the metal matrix is a function of ingot size. The larger size also helps to decrease the uncertainties due to surface effects. A cylindrical ingot (3 cm in diameter by 5 cm) containing about 54 g of neutron-activated SWF granules* close - packed in a matrix of about 230 g of lead metal was fabricated by casting. The radioactivity of each isotope in the ingot was determined by gamma-ray analysis (lithium drifted germanium [GeLi] detector) of one SWF granule (0.163 g) and multiplying this result by the weight ratio of the total beads (54.2 g) to the one bead (0.163 g). The external surface area (apparent geometric surface) of the ingot was about 64 cm^2.

Sequential leach tests using 300 mL of distilled water (25°C) for each test were performed (in the apparatus shown in Fig. 71). Leach rates were determined for eight different radioisotopes. The results are summarized in Table 45. The tabulated values are in units of "fraction (of the specific radionuclide) leached per day." There is a marked variability in the leach rates of the various radionuclides. As in the case of other determinations with this SWF, the cesium had a relatively high leach rate [STEINDLER-1978A, 1978B]. This attribute of cesium in these SWF granules makes it particularly attractive for studying the shielding effect of the metal matrix in the composite waste forms. Any shielding effect by the metal matrix should result in a dramatic drop in the fraction of cesium leached per unit time as the surface to volume ratio of the ingot is decreased. A comparison of the cesium leach rate (as a function of time) for composites of various sizes (i.e., surface to volume ratios) is made in Table 46.

---

*These sintered waste form (SWF) granules were obtained from PNL. They were not optimized for leach resistance but were provided to develop the activation analysis technique for determining leach rates. They were prepared with a disc pelletizer by agglomerating 85 wt % PW-7a [BONNER] spray calcine and 15 wt % glass frit, followed by sintering for 1 h at 1000°C.

Table 45. Leach Tests for the Large (283-g) Ingot in Quiescent Distilled Water at 25°C

Isotope Analyzed	Incremental Leach Rate, fraction leached/day						
	1st (2.9 d)[a]	2nd (10.2 d)[a]	3rd (6.8 d)[a]	4th (13.8 d)[a]	5th (17.0 d)[a]	6th (21.0 d)[a]	7th (32.0 d)[a]
^{51}Cr	3.7×10^{-2}	1.5×10^{-2}	7.1×10^{-3}	5.4×10^{-3}	7.1×10^{-4}	4.4×10^{-3}	3.0×10^{-3}
^{60}Co	6.1×10^{-7}	1.5×10^{-6}	7.4×10^{-7}	6.5×10^{-8}	2.9×10^{-8}	2.1×10^{-7}	4.3×10^{-8}
^{65}Zn	6.6×10^{-6}	5.9×10^{-6}	4.2×10^{-6}	2.3×10^{-7}	7.8×10^{-8}	9.7×10^{-7}	1.7×10^{-7}
^{75}Se	6.2×10^{-3}	2.0×10^{-3}	1.2×10^{-3}	7.3×10^{-4}	4.8×10^{-4}	3.8×10^{-4}	2.5×10^{-4}
^{124}Sb	1.6×10^{-5}	5.5×10^{-6}	4.2×10^{-6}	3.0×10^{-6}	8.9×10^{-7}	1.4×10^{-6}	9.0×10^{-7}
^{134}Cs	1.0×10^{-2}	3.4×10^{-3}	1.8×10^{-3}	1.2×10^{-3}	1.4×10^{-3}	6.1×10^{-4}	4.0×10^{-4}
^{141}Ce	4.5×10^{-7}	2.7×10^{-6}	1.2×10^{-6}	5.4×10^{-7}	1.1×10^{-7}	2.3×10^{-7}	5.7×10^{-8}
^{152}Eu	1.1×10^{-7}	3.3×10^{-7}	5.2×10^{-7}	2.3×10^{-7}	1.6×10^{-7}	1.6×10^{-7}	8.5×10^{-8}

[a]Length of time (in days) for each sequential leach test.

Table 46. Cesium Leach Rates in Lead Matrix Composites in Quiescent Distilled Water at 25°C

Ingot No.	Wt, g	Surface Area, cm^2	Volume, cm^2	Surface to Volume Ratio	^{134}Cs Leach Rate, fraction leached/day				
					10 d[a]	20 d[a]	30 d[a]	40 d[a]	50 d[a]
7[b]	7.55	6.1	1.06	5.8	1.1×10^{-2}	---	1.0×10^{-3}	0.8×10^{-3}	---
23[b]	23.36	10.6	2.65	4.0	2.1×10^{-2}	---	4.0×10^{-3}	3.8×10^{-3}	1.3×10^{-3}
283	283.0	63.8	37.74	1.7	3.4×10^{-3}	1.8×10^{-3}	1.2×10^{-3}	---	1.4×10^{-3}
SWF granule		---	---	---	4.7×10^{-2}	1.1×10^{-3}	---	---	---

[a]Integrated time of leaching in days (approximate).

[b]These data were previously reported in [STEINDLER-1978C].

Cesium leach rates for the unencapsulated and rather porous SWF granules have been included for comparison purposes. As can be seen from this table, there is little if any shielding effect by the lead matrix for this range of surface to volume ratios, using the relatively leachable waste forms of this type. These data have been plotted in Fig. 73. Although there is some spread in the leach rates initially, they very rapidly converge.

The incremental leach rates for five of the isotopes studied from the large ingot (283-g) have been plotted as a function of time in Fig. 74. Data points are plotted at midpoint of the time span for each measurement. As can be seen from this figure, the leach rates (after the initial 20 days) for all of the isotopes studied follow the same trend of a decreasing leach rate with time, even though the absolute leach rates of the different isotopes vary by four orders of magnitude. Leach rates decrease by about one or two orders of magnitude during the first 100 days of leaching. Further studies are required to determine if the leach rate levels off or continues to decline at a lower rate. A brief, but small, rise in leach rate (e.g., for ^{152}Eu and ^{141}Ce) during the first few days of testing is attributable to the time necessary for the leachant to thoroughly permeate the relatively large ingot. The mechanism of penetration is attributed to the high porosity of the individual SWF granules, which are in contact with each other. The experimental data show some scatter around the smooth curves drawn, but this scatter is well within the experimental uncertainties (i.e., about a factor of 2) of the measurements. The wide range of leach rates for the various isotope studies has been interpreted previously [STEINDLER-1978A].

As part of this experiment, a sample of lead (about 7 g) was taken from the cast ingot (283) and was analyzed for the radioisotopes originally present in the irradiated SWF granules. This was done in order to determine if any significant fractions of the radioisotopes were "leached" into the lead matrix during the casting process. The results indicated that the fraction "leached" varied between 1×10^{-5} (10 ppm) for cesium (the

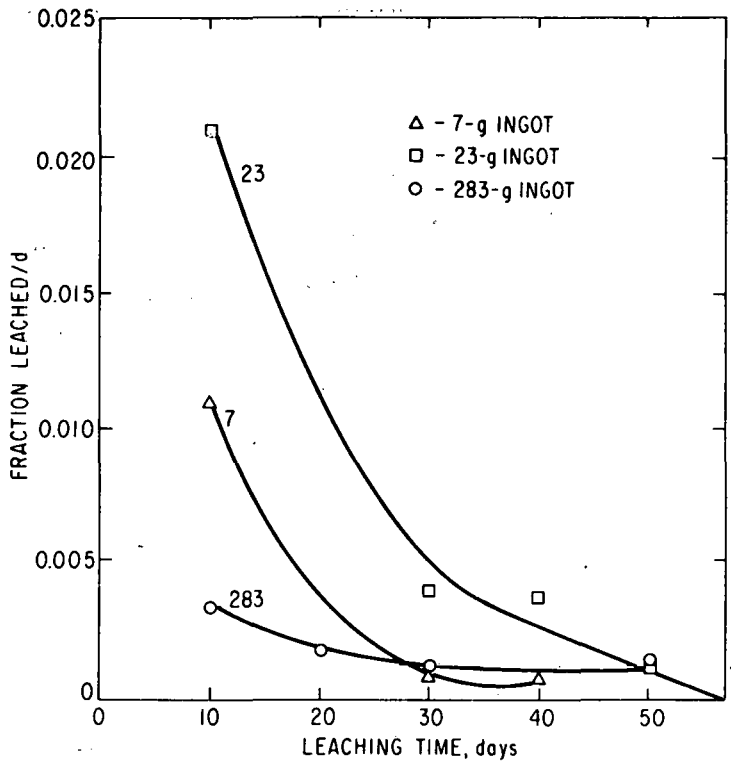

Fig. 73. Leach Rates in Quiescent Distilled Water at 25°C for Various Size Ingots as a Function of Time. Based on data for cesium-134, the most leachable element.

most leachable element) and 2 x 10^{-7} (0.2 ppm) for cerium (among the least leachable elements). These results suggest that there may be some, but probably not a significant, problem of dispersal of the radioactive waste into the metal matrix during the fabrication process. These results may be very dependent upon the specific dispersed waste form and casting conditions.

d. Preliminary Leaching Tests with Pyrex Encapsulated in Lead

An experiment has been planned in which Pyrex (i.e., borosilicate glass) beads will be used as the substitute waste form to be activated and incorporated in a lead matrix. Since the total porosity for the Pyrex beads is very low (particularly when compared with the relatively porous SWF granules used in the current studies), there should be a significantly smaller pathway for the leaching medium to penetrate to the interior of the ingot. Results from this experiment may establish whether or not the metal matrix exhibits a shielding effect for composites containing low-porosity waste forms. Preliminary tests indicate that ^{134}Cs (resulting from activation of cesium in the Pyrex) might be a satisfactory activation isotope for making these measurements.

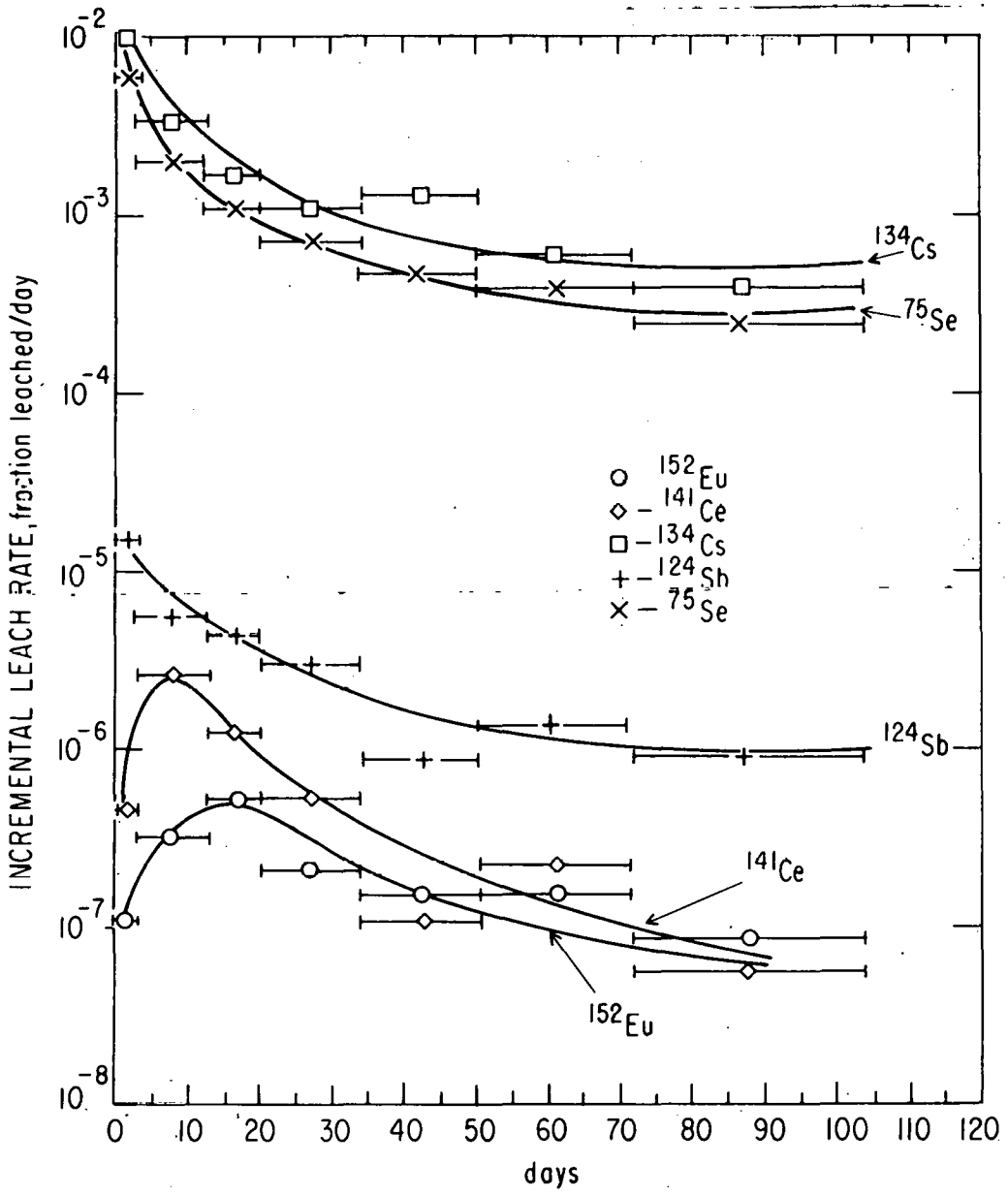

Fig. 74. Incremental Leach Rate from a Large (283-g) Composite in Quiescent Distilled Water at 25°C vs. Time for Various Elements (Lead Matrix).

e. Leaching Tests with Simulated High-Level Waste Glass Containing Uranium

A small sample (about 6 g) of simulated high-level waste glass containing uranium was obtained from Battelle Pacific Northwest Laboratories (PNL). This glass was composed of PW-8a-3 calcine and 76-68 glass [McELROY] and had been previously characterized by the Battelle group. A slice of this glass (0.5 g) was irradiated in the ANL-CP-5 research reactor and was subjected to leach testing in stagnant distilled water, using the activation technique previously described [STEINDLER-1978A, FLYNN].

Results of the first leach tests (5.8 days) are shown in Table 47. They include several isotopes with short half lives. The results of three additional sequential leach tests of the same glass specimen covering a time period of about two months are given in Table 48. The leach rates for all nine of the radioisotopes studies were within one order of magnitude, indicating a relatively uniform waste form matrix. Because of their short half lives (^{237}U at 6.8 d and ^{239}Np at 2.4 d), it was not possible to determine the leach rates for uranium and neptunium beyond the first leach test (i.e., 5.8 days). However, since leach rates generally do not increase with time for stable waste forms, these initial values may represent conservative upper limits for the leach rates on a geological time scale. No significant increases in leach rate with time have been observed thus far in our studies. However, additional testing is necessary before any definitive statements can be made.

The indications are that the 76-68 PNL glass is a particularly good waste material in terms of leach resistance (i.e., leach rates were of the order of 10^{-6} g/cm^{2}d) under the conditions tested; there was only one order of magnitude spread between the most leach-resistant and the least leach-resistant isotopes. Further testing of this waste form using alternative leaching media (e.g., 100°C saturated brine, etc.) are in progress.

Table 47. Leach Rates for PNL Glass[a] in 25°C Stagnant Distilled Water for Initial 5.8 days

Isotope Analyzed	Leach Rate		
	Fraction/day	Fraction/cm^{2}day	g/cm^2 day[b]
^{22}Na	8.9×10^{-7}	3.9×10^{-7}	1.8×10^{-7}
^{51}Cr	7.9×10^{-6}	3.5×10^{-6}	1.6×10^{-6}
^{65}Zn	2.4×10^{-5}	1.0×10^{-5}	4.9×10^{-6}
^{86}Rb	3.0×10^{-6}	1.3×10^{-6}	6.1×10^{-7}
$^{99}Mo(Tc)$	1.2×10^{-5}	5.2×10^{-6}	2.5×10^{-6}
^{103}Ru	5.8×10^{-6}	2.6×10^{-6}	1.2×10^{-6}
^{131}I	7.2×10^{-6}	3.2×10^{-6}	1.5×10^{-6}
^{134}Cs	4.1×10^{-6}	1.8×10^{-6}	8.4×10^{-7}
^{141}Ce	3.2×10^{-6}	1.4×10^{-6}	6.5×10^{-7}
^{152}Eu	1.7×10^{-6}	7.5×10^{-7}	3.5×10^{-7}
^{237}U	7.2×10^{-7}	3.2×10^{-7}	1.5×10^{-7}
^{239}Np	7.1×10^{-6}	3.1×10^{-6}	1.5×10^{-6}

[a]Composition defined in [McELROY] for 76-68 glass. The sample weight was 0.47 g, and the surface area (calculated) was 2.3 cm^2 (apparent geometric surface).

[b]These units of g/cm^2 day represent the gram equivalents that would have been leached had the entire matrix leached at the same rate as did the specific isotope studied.

Table 48. Leach Rates for PNL-Glass[a] in 25°C Stagnant Distilled Water for Three Sequential Tests

Isotope Analyzed	Leach Rate, g/cm^2d[b]		
	5.8 d[c,d]	21.0 d[d]	32.0 d[d]
^{51}Cr	1.9×10^{-6}	3.0×10^{-7}	4.2×10^{-7}
^{60}Co	4.8×10^{-6}	1.4×10^{-6}	1.2×10^{-6}
^{65}Zn	5.4×10^{-6}	8.7×10^{-7}	9.2×10^{-7}
^{95}Zr	4.5×10^{-7}	e	1.8×10^{-7}
^{134}Cs	7.8×10^{-7}	2.9×10^{-7}	9.8×10^{-7}
^{141}Ce	6.0×10^{-7}	7.1×10^{-8}	2.2×10^{-7}
^{152}Eu	5.1×10^{-7}	6.5×10^{-8}	1.7×10^{-7}
^{237}U	1.5×10^{-7}	f	f
^{239}Np	1.5×10^{-6}	f	f

[a]Composition defined in [McELROY] for 76-68 glass. The sample weight was 0.47 g and the surface area (calculated) was 2.3 cm^2 (apparent geometric surface).

[b]These units of grams per cm^2 day (g/cm^2d) represent the gram equivalents that would have been leached had the entire matrix leached at the same rate as the specific isotope studied.

[c]The values reported for 5.8 d are based on a data analysis separate from that in Table 47. Any differences between values in this table and Table 47 for the 5.8 d leach test are not regarded as significant.

[d]Length of time (in days) for each sequential leach test.

[e]Data not available because the gamma rays were not resolvable from the gamma spectrum.

[f]These isotopes have short half lives and had decayed away before the second leach measurements were made.

f. Comparison of Neutron Activation Technique with Soxhlet Leach Test Method

Experiments are in progress to compare the results of leach tests based on the nondestructive neutron activation technique [STEINDLER-1978A] and the more or less standard Soxhlet leach test method. Pyrex (borosilicate glass) beads and SWF granules were ground and sieved. The particle size distribution is shown in Fig. 75. Samples of these materials of SWF granules, and of Pyrex beads have been irradiated. The pulverized materials are being tested in a conventional Soxhlet apparatus and the results compared with those from simple stagnant leaching of unperturbed beads.

Surface areas have been measured for these samples, using the BET (krypton) method, and the apparent geometric surface has been calculated assuming the particles to be spheres with the particle size distribution shown

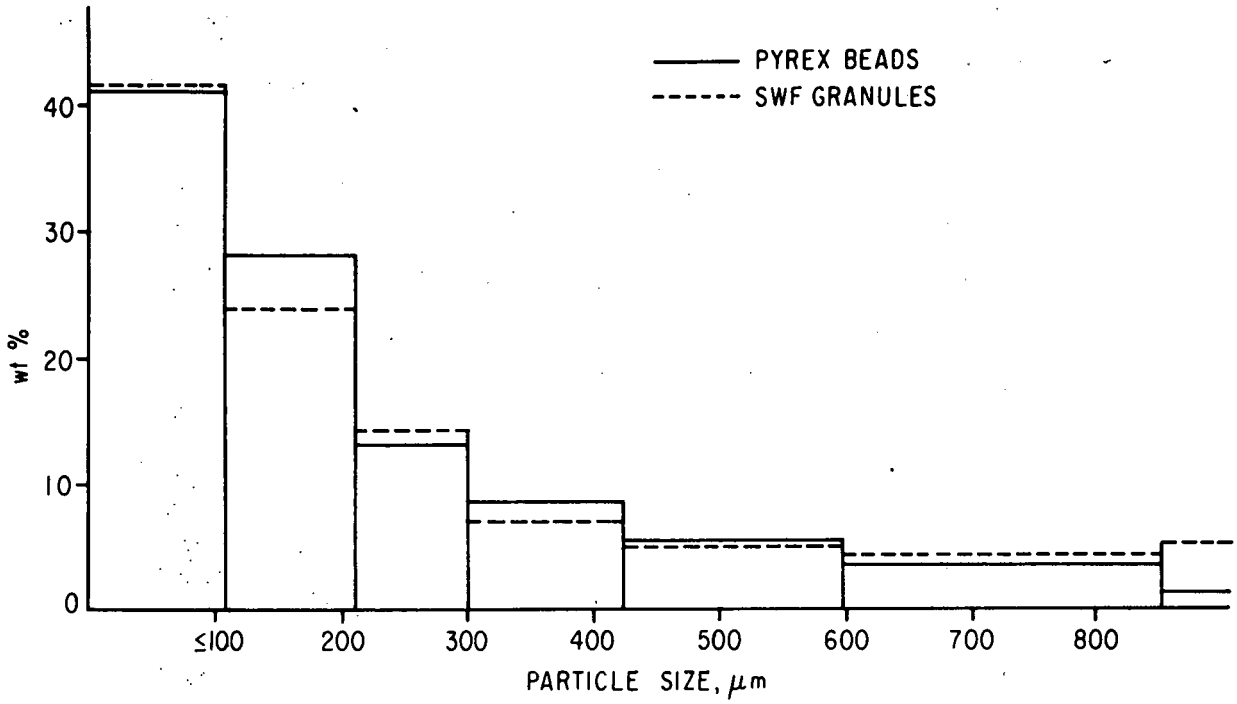

Fig. 75. Particle Size Distribution for Crushed and Ground Beads (Solid Lines, Pyrex Beads; Dashed Lines, SWF Granules). Based on a mechanical screening.

in Fig. 75. The surface area data are tabulated in Table 49. As has been reported previously [STEINDLER-1978C], the surface area available to the leaching medium is probably significantly greater than the surface area estimated from the apparent geometric shape but smaller than the surface area determined by BET gas adsorption techniques. Further work needs to be done

Table 49. Comparison of BET-Measured and Calculated Surface Areas

Sample	Surface Area, m^2/g	
	BET	Calculated[a]
Pyrex Beads	7×10^{-3}	3.9×10^{-4}
Ground Pyrex	0.11	0.01
SWF Granules	0.91	6.1×10^{-4}
Ground SWF Granules	2.0	0.015

[a] These surface areas were determined by assuming nonporous spherical shapes and calculating the geometric surface area. For the ground samples, the surface areas were calculated from particle sizes, using the weighted distribution given in Fig. 75.

in order to establish the actual surface areas of specimens exposed to leaching. In the meantime, the surface area based on the apparent geometric shape probably results in conservative estimates for the leach rates of the solids and is the value used in our studies.

g. Current and Planned Leach Tests

Leach tests currently in progress include the following:

Waste Form	Temperature, Leach Medium	pH
SWF granules in lead matrix	25°C, H_2O(distilled)	6.0
Pyrex beads in lead matrix	25°C, H_2O(distilled)	6.0
SWF powder - Soxhlet	100°C, H_2O(distilled)	7.3
Pyrex powder - Soxhlet	100°C, H_2O(distilled)	7.3
SWF granules	100°C, H_2O(distilled)	7.3
Pyrex beads	100°C, H_2O(distilled)	7.3
Pyrex beads	25°C, H_2O(distilled)	6.0
PNL glass (76-68)	25°C, H_2O(distilled)	6.0
PNL glass (76-68)	25°C, Brine	7.6
PNL glass (76-68)	110°C, Brine	7.6
PNL glass (76-68)	25°C, H_2O (tap)	9.7
PNL glass (76-68)	25°C, H_2O (CO_3^{2-})	3.9

Experiments have been planned to use an autoclave for study of the leach rates of various waste forms in various leaching media at elevated temperatures (up to 300°C) and pressures. The temperature range should be adequate to span the anticipated final storage conditions.

3. Conclusions

Experiments have shown that significant and meaningful leach rate data can be obtained with relatively simple laboratory-scale equipment coupled with neutron activation analysis techniques. More detailed information, or data for other radionuclides, can be procured by applying radiochemical separations and more sophisticated counting methods [STEINDLER-1978A, FLYNN].

The equipment and experimental techniques developed at ANL are capable of measuring the leach rates for all elements of interest, from any solid waste form, over a range of potential storage environments.

The results reported here support the following conclusions:

1. Compounds formed by interactions between solidified high-level stabilized calcined waste and molten lead (i.e., lead rare earth silicates) have sufficiently low leach rates that they are not likely to be detrimental to the overall leaching characteristics of metal-encapsulated waste forms.

2. Negligible fractions of the elements of concern for waste management may be leached into the lead matrix during the casting process.

3. Leach rates for Zircaloy and lead [STEINDLER-1978A] are sufficiently low that they are still considered suitable candidates for containing nuclear waste materials insofar as leaching is concerned.

4. Experiments to date with small laboratory-scale specimens indicate that the lead matrix provides little if any shielding effect from the leachant when relatively porous waste forms are used.

5. Leach rates consistently decrease with time; hence, estimates of leach rates for geologic storage based on initial measurements can be considered conservative estimates.

6. Leach rates of the various elements present in nuclear waste can vary widely; hence, the leach rate for each element of concern in each waste form considered must be measured.

7. A simulated high-level waste glass containing uranium has been prepared by PNL which has uniform leaching characteristics of many elements in 25°C distilled water.

8. Surface area estimates based on the apparent geometric shape of the waste form should give conservative upper limits of leach rates. Surface areas based on data obtained by BET gas adsorption techniques are probably greater than the surface areas actually exposed to the leaching medium. Hence, leach rates based on BET-measured surface areas are likely to be optimistic.

V. ESTABLISHMENT OF TENTATIVE CRITERIA FOR HULL TREATMENT
(L. E. Trevorrow and B. J. Kullen)

Criteria are being formulated for the safe management of waste hulls from the reprocessing of spent nuclear fuel. The expression of criteria for hulls handling in the form of a matrix of interactions between a set of safety policies and a set of factors that are basic to hulls operations (Table 39, ANL-78-68) has been found to be similar to a method used in the expression of criteria for engineering concepts in general. Thus, criteria are used to construct an index to be used in judging the effectiveness of an engineering concept. Such an idex has been given various names, e.g., criterion function, objective function, measure of effectiveness, or utility [WOODSON, MEREDITH].

Any concept for hulls management--in general a set of chemical and engineering operations that will convey hulls from the point of their generation to terminal storage--would be judged in the present concern primarily by its effectiveness in preserving the safety of both the general public and the persons directly involved in the operations. Criteria for hulls management can be developed around a format similar to that used in the expression of criterion functions. The main advantage in applying this format is that it analyzes the means of judging a concept in an orderly manner that explicitly displays the factors considered. Also, it was found to be similar to the analysis, already under way in this work, of the matrix of interactions of a set of safety policies and a set of general factors that are likely to be employed in hulls management operations.

For a given engineering concept (usually one of several alternatives) a criterion function is defined:

$$CF = a_1x_1 + a_2x_2 + a_3x_3,$$

where x_n are the criterion variables (i.e., criteria),

e.g., x_1 = durability

x_2 = simplicity

x_3 = cost,

and the a_n are assigned weight factors. The criterion variables, x_n, are in turn dependent on other (secondary) variables and also parameters, e.g., x_1 dependent on secondary variables such as bar strength and on parameters such as bar thickness and tensile strength of bar material. If it is possible to quantify all variables and parameters (which is not always the case), then the concept, among a set of alternatives, that yields a maximum or minimum criterion function, depending on the variables chosen, would be selected as optimum.

We believe that the appropriate objective of the present study is to formulate a set of criterion variables and to define the secondary variables and parameters that are considered to be of greatest importance; no attempt is made to calculate numerical values of criterion functions for alternative concepts of hulls management. The complete definition of weight factors, a_n, parameters, and secondary variables would be done by the organizations that would design and carry out the operations and by regulatory agencies. Commercial organizations would be especially interested in defining not only secondary variables and parameters, but also economic criteria. The criteria defined here are primarily safety criteria. Some of the parameters, e.g., permissible radiation levels, would be defined in Federal regulations to be promulgated by DOE, NRC, and EPA, or would be developed in licensing proceedings.

For the case of hulls management, let a criterion function be expressed by:

$$CF = a_1x_1 + a_2x_2 + a_3x_3 + \cdots + a_9x_9,$$

where x_n represents nine criteria:

x_1 = Ability to limit the release of radioactive particulate solids in normal operations,

x_2 = Ability to prevent accidents that would result in the release of radioactive particulate solids,

x_3 = Ability to minimize the consequences of accidents which result in the release of radioactive particulate solids,

x^4 = Ability to limit exposure to penetrating radiation in normal operations,

x_5 = Ability to prevent accidents that would result in exposure to penetrating radiation,

x_6 = Ability to minimize the consequences of accidents which would result in exposure to penetrating radiation,

x_7 = Ability to limit pyrophoric effects in normal operations,

x_8 = Ability to prevent accidents involving pyrophoricity,

x_9 = Ability to minimize the consequences of accidents involving pyrophoricity,

As in the general case described above, the criteria are functions of secondary variables and also of parameters. For this work, we propose that each criterion is a function of four variables and related parameters:

(1) Equipment variables and parameters

(2) Operations design variables and parameters

(3) Personnel factors and parameters

(4) Waste form variables and parameters

The criterion function for hulls management, i.e., $CF = a_1x_1 + a_2x_2 + a_3x_3 + \ldots + a_9x_9$, can be conceived to be a column vector that is related to a matrix of variables,

$a_1x_1 = f_1$ (equipment + operations + personnel factors + waste form)

$a_2x_2 = f_2$ (equipment + operations + personnel factors + waste form)

$a_3x_3 = f_3$ (equipment + operations + personnel factors + waste form)

and so on, up to

$a_9x_9 = f_9$ (equipment + operations + personnel factors + waste form)

It is convenient to use this matrix to label, arrange, and trace the relation of variables and parameters to the criteria. Current work involves the definition of the secondary variables and parameters that are considered important in complying with the nine criteria listed above.

This revision of format in expressing criteria will be incorporated into the document on criteria for hulls handling that is soon to be sent to reviewers in several organizations and agencies. Later, final hull treatment criteria that have been revised in response to opinions from the industry, technical and professional institutions, and government agencies will be issued.

VI. TRANSPORT PROPERTIES OF NUCLEAR WASTE IN GEOLOGIC MEDIA

(M. G. Seitz, P. Rickert,* S. Fried,* A. M. Friedman,* Jacqueline Williams,† and M. J. Steindler)

A. Introduction

The migration of trace elements that results from a solution flowing in a geologic medium depends on the extent of reaction of the trace elements with the solution and the medium and, hence, on the flow rate of the solution.

Different experimental approaches to studying nuclide migration have different advantages. Batch partitioning tests,‡ for example, can be performed quickly with any nuclide on any rock, independent of the porosity, brittleness, or other properties of the rock. Under specific conditions, the measured partitioning value may relate to the migration by fluid flow of the nuclide in the rock. Column-infiltration experiments have the advantage that nuclide migration by fluid flow in rocks is measured directly. The infiltration experiments have the disadvantage that they require porous or fractured rock of distinct geometry for fluid flow. By comparing results from different experimental techniques, we may determine under what conditions a simple experimental approach may be used in predicting migration without loss of understanding and accuracy.

This report describes column infiltration experiments** that used glauconite (a hydrous ferromagnesian silicate) in columns and in which strontium was eluted at different solution flow rates.

Also of concern to light water reactor waste disposal schemes is the isotope of tin, ^{126}Sn, a long-lived radioactive fission product of uranium. The behavior of tin in a glauconite column as observed in a column infiltration experiment is described in this report.

In this report, results are reported for the migration of strontium in oolitic limestone as determined by column infiltration experiments. These results are compared with migration characteristics predicted from batch partitioning data.

The chemical constituents of the solutions used in these experiments constitute one factor affecting the mobilities of trace elements in flowing aqueous solutions. The bicarbonate alkalinity and calcium content of solutions used in the experimental program have been determined by titration. Spectrochemical analyses for major cations were also made. These analyses are part of a continuing effort to characterize the chemical and physical state of rocks, trace elements, and solutions used in this program.

---

*Member of Chemistry Division.

†Member of Analytical Section, Chemical Engineering Division.

‡In a batch partitioning test, granulated rock and a solution in a test tube are agitated to establish partitioning of nuclides between solid and liquid phases.

**In a column infiltration experiment, liquid is pumped at high pressure through a column of mineral sand in a tube.

Also affecting the mobilities of trace elements are the oxidation potential (E_h) and the hydrogen ion concentration (expressed as pH) of flowing groundwater. For example, uranium in waters of high oxidation potential is mobilized as the hexavalent ion, while in waters of low oxidation potential it is immobilized as the quadrivalent ion (as insoluble silicates or oxides). Tin dissolves in high-pH solutions and precipitates as hydrolysis products in neutral solutions.

The migration of trace elements can be influenced by dissolved gases (notably carbon dioxide, oxygen, and hydrogen sulfide) in groundwater, which increase or decrease the E_h and pH of the water. In addition, carbonate ions may complex with trace elements, and oxygen in solution may oxidize multivalent trace elements. Described in this report are techniques and apparatus used to control the CO_2 and O_2 dissolved in solutions used in these experiments.

B. Analytical

Solutions used to elute strontium in glauconite and limestone columns were analyzed for their concentrations of common cations by spectrochemical means and for bicarbonate and calcium concentrations by titration. The solutions analyzed are (1) a "recipe" solution simulating the groundwater expected in limestone, (2) a REW solution made with oolitic limestone as described below (3) a 0.01M $CaSO_4$ solution, and (4) standard $NaHCO_3$ solutions.

The recipe solution was prepared according to the following Battelle Pacific Northwest Laboratory specifications for a controlled sample program. The ingredients of the recipe solution listed below were added to 1 L of distilled water:

Ingredient	mg
$Ca(OH)_2$	92.5
$MgSO_4$	18
NaCl	5.8
KCl	0.8

The mixture was sparged with CO_2 until all of the lime dissolved.

Our solution, after lime was dissolved, was at pH 6. Sparging with N_2 raised the pH to 8.5. (After the experiments, the pH decreased over a period of about 10 days to 8.0, and simultaneously a precipitate formed).

The REW solution was made by stirring 10 g of ground oolitic limestone in 1 L of distilled water for periods of 6 to 12 days and filtering the solution through 0.45-μm-pore-size Milipore filter. Strontium was added to the solution by adding and partially dissolving $SrCO_3$ (about 17 mg/L of solution) in the REW solution and refiltering the solution.

The bicarbonate alkalinity was measured by adding a known excess of standard NaOH to a solution to convert the HCO_3^- to CO_3^{2-} according to the reaction

$$Ca(HCO_3)_2 + 2NaOH \rightarrow CaCO_3 + Na_2CO_3 + 2H_2O$$

Barium chloride was added to precipitate carbonate from the solution. The excess sodium hydroxide was titrated with standard HCl to a phenolphtalein end point. The number of NaOH equivalents consumed before carbonate precipitation is equal to the number of HCO_3^- equivalents in the original solution. Reagent grade $NaHCO_3$ was used as a standard for the titration. Bicarbonate concentrations in the recipe solution, oolitic REW solution, and the standard solution are given in Table 50.

Table 50. Analyses of Solutions for Bicarbonate by Titration

Solution	Titration	HCO_3^-
Recipe Solution, Batch No. 1	1	124 mg/L
	2	121 mg/L
Recipe Solution, Batch No. 2	1	174 mg/L
	2	178 mg/L
Oolitic REW with $SrCO_3$	1	36 mg/L
	2	35 mg/L
0.1M $NaHCO_3$ Standard Solution	1	98.9% Recovery
	2	99.8% Recovery
	3	99.6% Recovery

Calcium in two solutions used in strontium-elution experiments was determined by direct pH 10 buffered titration, with the disodium salt of ethylenediaminetetracetic acid (2Na·EDTA) the titrant and Calmagite an indicator. The 2Na·EDTA was standardized with primary grade $CaCO_3$, which was converted to $CaCl_2$ (the 2Na·EDTA was determined to be 94.8% pure). No other primary grade calcium salt was readily available for use as a standard. The results for the two solutions analyzed are shown in Table 51.

Table 51. Calcium in Solution as Determined by 2Na·EDTA Titration

Solution	Titration	Calcium,[a] meq/mL (μg/mL)
0.01M $CaSO_4$ containing strontium	1	0.0102 (255)
	2	0.0102 (255)
Oolitic REW containing $SrCO_3$	1	3×10^{-4} (12)
	2	2×10^{-4} (8)

[a]The titration results are indicative of calcium, magnesium, strontium, and other titratable cations in solution. The concentration, in weight, was calculated considering that most of the titratable cations were calcium.

The 0.01M $CaSO_4$ solution containing 10^{-4}M strontium was determined by spectrochemical analyses to contain 18 μg/mL strontium, as well as measurable quantities of aluminum, iron, magnesium, and sodium (0.4, 0.005, 0.1, and 0.05 μg/mL, respectively) and calcium. The strontium concentration is twice that expected from the addition of $SrCO_3$ and suggests that strontium was present in the $CaSO_4$ used to prepare the solution.

The oolitic REW solution with added strontium was determined by spectrochemical analyses to contain calcium (10 μg/mL), strontium (1 μg/mL), magnesium (0.6 μg/mL), and sodium (0.6 μg/mL) as the major cations along with detectable quantities of aluminum, boron, chromium, praseodymium, lithium, and silicon (0.1, 0.4, 0.008, 0.15, 0.0008, and 2 μg/mL, respectively). Apparently, very little of the strontium, 8.8 μg/mL of which was added as $SrCO_3$, dissolved. The concentration of calcium is identical, within analytical error, to that determined by titration.

The nominal composition of the recipe solution in limestone is 50 μg/mL calcium, 3.6 μg/mL magnesium, 2.3 μg/mL sodium, 0.4 μg/mL potassium, and 153 μg/L bicarbonate, along with sulfate and chloride anions. Comparing the limestone REW with the recipe solution, we see that the limestone REW solution is more dilute (i.e., lower in major cations and bicarbonate) than is the recipe solution. The REW solution is more complex than is the recipe solution having present at detectable levels six elements that were not explicitly added to the recipe solution.

C. Strontium and Tin Migration in Glauconite

The apparatus used in the column infiltration experiments consists of a mineral column contained in a stainless steel tube and connected to a sample-injection valve and a solution-metering pump. Glauconite [a hydrous silicate, nominally $(K,Na)(Al,Fe^{3+},Fe^{2+},Mg)_2(Al,Si)_4O_{10}(OH)_2$] was used to prepare two mineral columns; glauconite sand was sifted to obtain a fraction having a uniform size (<40 and >70 mesh). The sand was washed repeatedly in distilled water to remove dust adhering to the particles and was packed in stainless steel tubing to form columns 15-cm long by 1.0-cm diameter and 53% porous.

We prepared one of the columns by eluting it with a solution of 0.01M $CaSO_4$ and 0.0001M $SrCO_3$. The solution was made with deaerated water and was kept under nitrogen atmosphere to maintain the low oxygen level.

Strontium-85 with $SrCl_2$ carrier was added to an aliquot of the calcium-strontium to form a radioactive solution containing about 1×10^{-6}M $SrCl_2$. To perform an experiment, we injected a small quantity (20 μL) of the radioactive solution into the solution stream above the glauconite column and eluted the radioactivity from the column. The eluate was collected in fractions, and each fraction was analyzed to determine the migration characteristics of the strontium in the column. Six infiltration experiments, each at a different flow rate, were performed in this manner.

The radioactive strontium in solution vs. the eluate fractions are plotted in Fig. 76. The shapes of the strontium peaks are dependent on the flow rate of the eluent. The sharpest peak is produced with the lowest flow rate; the widest peak is produced with the highest flow rate. The strontium peaks were delayed relative to the advancing water front (which would traverse the column in the first 6.5 mL of eluate). Moreover, each of the strontium peaks seen in Fig. 76, even the one produced at the lowest flow rate, is considerably wider than the 2-mL full width at half maximum seen for peaks of tritiated water eluted through the column [STEINDLER-1978C]. Therefore, the stronium interacted with the glauconite column. As indicated by the different peak shapes, it interacted differently at each flow rate. The flow rates given in Fig. 76 were measured by collecting eluate over specific periods of time. In each experiment, all of the radioactive strontium was eluted in the single peak seen in the figure.

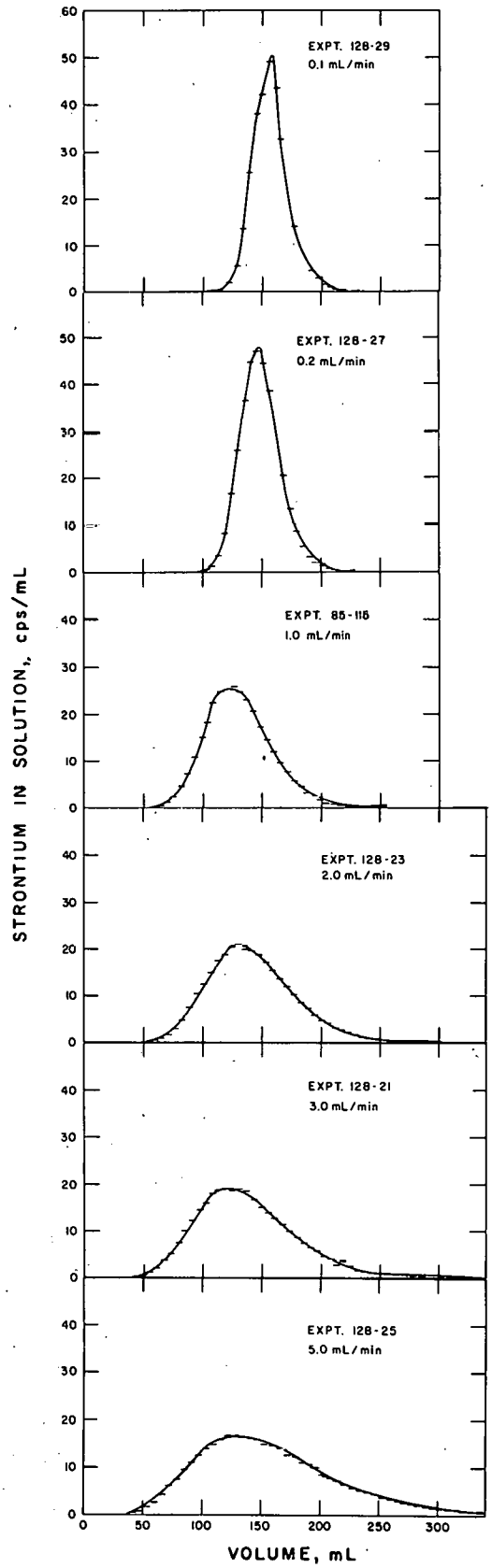

Fig. 76.

Elution of Strontium from a Column of Glauconite. Peak width increases with flow rate (top to bottom), indicating nonequilibrium behavior. Note that the scale for the eluate activity changes between the curves for 0.2 and 1 mL/min. ANL Neg. No. 122-78-837.

The results indicate that nonequilibrium effects dominate the shape of the migrating strontium peak at flow rates above 1.2 km/y in glauconite. In general, a trace element does not completely equilibrate between a solution and a rock because the equilibration usually involves liquid or solid diffusion at low temperatures over distances of 10 μm or more. In spite of this limitation, a criterion is suggested (below) from the experimental results to determine when "local equilibrium" may be used to model migration without loss of accuracy.

One glauconite column was prepared by eluting it with a 0.01M $CaSO_4$ solution which nominally contained 0.0001M $SnCl_2$. In the preparation of this solution, the stannous chloride dissolved, at first, in deoxygenated water used to make the solution, but the tin formed hydrolysis products (as identified by X-ray diffraction) that precipitated over a period of several days. The solution was filtered each day until it was stable and was kept under nitrogen gas that was low in oxygen ($\lesssim$2 ppm O_2) to prevent oxidation of the tin. The tin remaining in solution after precipitation ceased was found to be less than 1×10^{-7}M.

Tin-113, as stannous chloride, was added to an aliquot of the calcium sulfate solution to form the radioactive solution containing about 7×10^{-9}M ^{113}Sn. We injected 20 μL of the radioactive solution into the nonradioactive solution stream to introduce the radioactive tin to the glauconite column. Nonradioactive solution was pumped through the column at a rate of 0.2 mL/min for about 38 days but did not wash a detectable amount of tin out of the column. The location of the radioactive tin in the column, determined by disassembling and sampling the column, is plotted in Fig. 77. The tin was strongly retained on the glauconite; the peak activity was in the top sample of the glauconite. However, we detected radioactive tin in all samples of the glauconite, indicating that some of it migrated the length of the column. The migration of the very small amount of tin through the column may have been due to the movement of colloids of tin or of particles with adsorbed tin.

D. Strontium Migration in Oolitic Limestone

We prepared three columns of oolitic limestone by epoxy-mounting cores (approximately 5-cm long by 1-cm diameter) of limestone in stainless steel tubing. The ends of the limestone core and tubing were cut off to expose plane surfaces of limestone that were free of epoxy. The epoxy sealed the sides of the limestone column and prevented water from channeling between the column and tubing.

After running REW solution through the columns for several days, we eluted the columns with 20-μL quantities of tritiated water to determine the columns' flow characteristics. A tritium elution curve for column 1 is plotted in Fig. 78. Tritium moved through each column in a peak and was eluted in the first two milliliters. Porosities determined from the tritium peak elution volumes are given in Table 52.

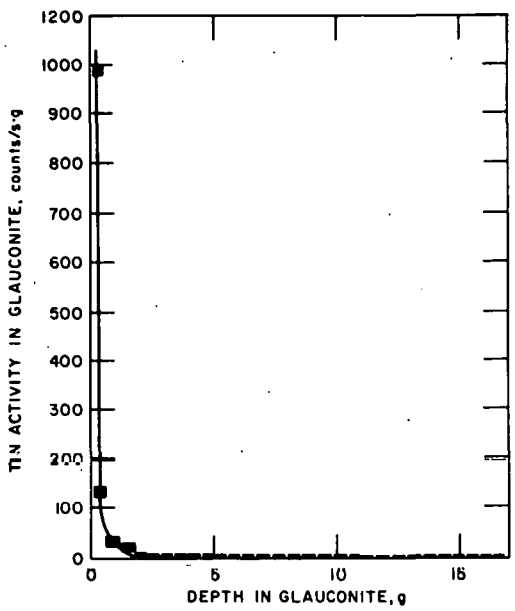

Fig. 77. Distribution of ^{113}Sn in a Glauconite Column after Elution with 5.5 L of 0.01M $CaSO_4$ Solution. Expt. 85-110.

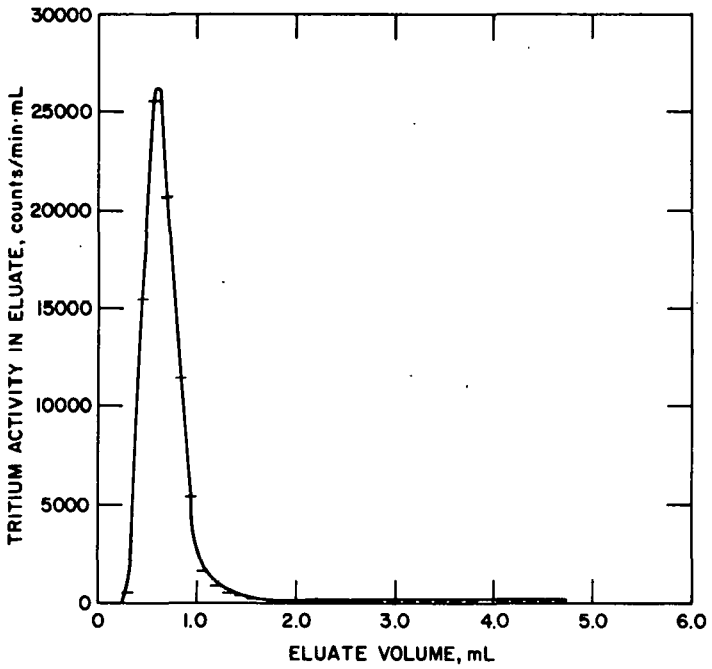

Fig. 78. Elution of Tritium through Column 1 of Oolitic Limestone. Flow rate, 0.1 mL/min. Expt. 85-123A.

Table 52. Porosities of Limestone Columns as Measured (1) by Weight Loss upon Drying a Water-Saturated Column and (2) by Tritiated-Water Elution.

		Porosity, %	
	Length	By Water Capacity	By Tritium Elution
Column 1	3.95	49	19
Column 2	3.56	—	19
Column 3	4.09	—	16

Limestone column 1 has a porosity subject to flow that is considerably less than its total porosity (as measured by weighing the column first dry and then saturated with water. This difference is probably due to dead-ended pores that do not link to form part of the water flow path. A low porosity of each column was measured with tritium, indicating that this difference is a common feature of the limestone.

Using a solution-metering pump, we prepared the columns by eluting them with a 0.1 mL/min flow of REW solution for 20 h before introducing radioactive strontium. An experiment was started by injecting into the solution upstream from the limestone column a 20-μL quantity of solution containing radioactive ^{85}Sr. The elution curve for each experiment was determined by measuring the strontium activity in the column eluate.

A ^{85}Sr elution experiment with the 0.01M $CaSO_4$ solution was run in column 1. Seven ^{85}Sr-elution experiments (three with oolitic REW, three with the recipe solution, and one with 0.1M $CaSO_4$ solution) were run in column 2. Column 3 was not used because of its low porosity (Table 52). Elution curves typical of those for the three different solutions are given in Figs. 79, 80, and 81.

With both the oolitic REW solution and the recipe solution, strontium is eluted in a peak and is retarded relative to the water front. The peak occurs at 6 to 9 mL for REW solution and at about 5 mL for the recipe solution, giving velocities of the strontium relative to the water front of 0.06 to 0.09 for REW water and of 0.11 for the recipe solution. The peaks are broad and skewed, indicating that the elution of strontium is complicated by kinetics, irreversibility, or other aspects of the strontium reaction with limestone.

As seen in Fig. 81, strontium is eluted immediately with the solution of 0.001M $CaSO_4$. Only that strontium activity in the skewed tail of the peak was slightly retarded in the limestone.

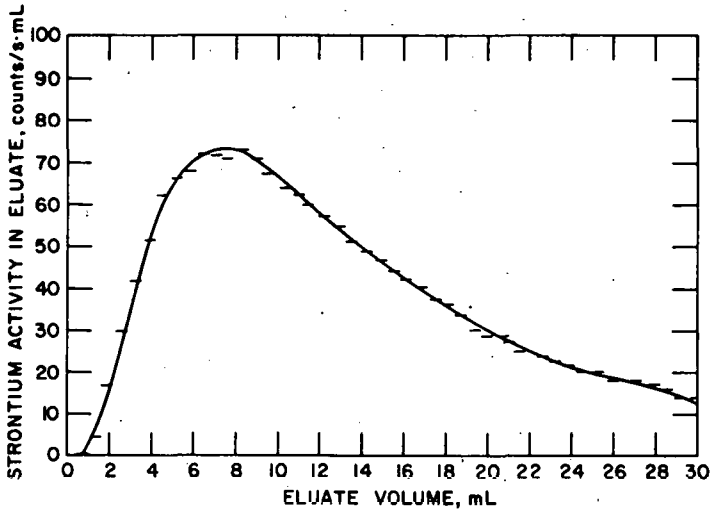

Fig. 79. Eluate Activity vs. Eluate Volume for ^{85}Sr Elution through Oolitic Limestone Column with Rock-Equilibrated-Water (REW) Solution. Expt. 128-33.

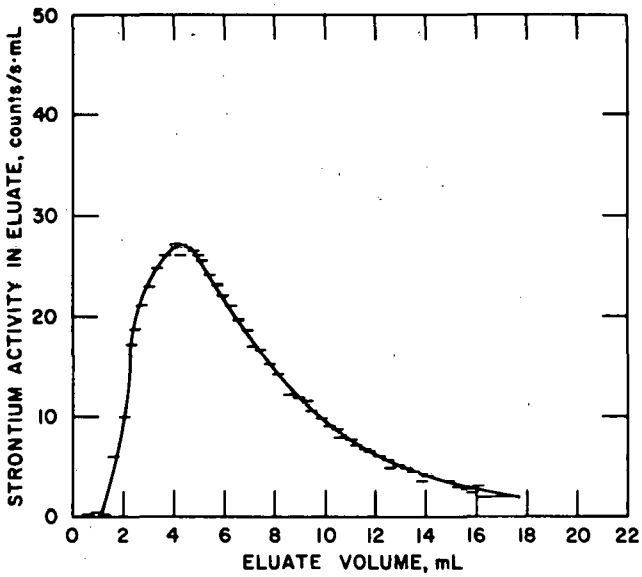

Fig. 80. Eluate Activity vs. Eluate Volume for ^{85}Sr Elution through Oolitic Limestone with Recipe Solution at 0.043 mL/min. Expt. 128-43.

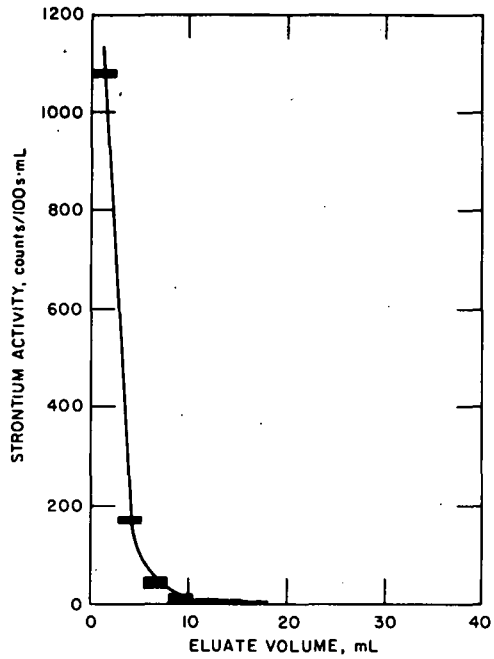

Fig. 81. Elution of Strontium-85 Through a Column of Oolitic Limestone in a 0.001M $CaSO_4$ Solution at 0.1 mL/min. Expt. 85-123B.

E. Dissolved-Gas Control

Gas-controlled glove boxes with transfer ports and gloved access (not described in this report) and in which CO_2 and O_2 concentrations are regulated are used in this program to contain "open air" experiments such as batch and static-absorption experiments. Apparatus used in "closed" experiments, such as in column infiltration experiments, is described. In column infiltration experiments, the solution is sealed from the atmosphere and is made to react with gases of known composition to dissolve CO_2 and O_2.

Solutions for column infiltration experiments were made by first deaerating distilled water by boiling. Then nitrogen gas purified as described below was bubbled through the water to obtain low concentrations of dissolved carbon dioxide and oxygen. One setup used to obtain nitrogen having the low CO_2 and O_2 levels desired experimentally is shown in Fig. 82. Solutions with low CO_2 and low O_2 levels produced by sparging with nitrogen purified in this apparatus can be mixed with solutions having high CO_2 or high O_2 levels (produced by reacting CO_2 gas, O_2 gas, or air with water) to produce solutions of intermediate CO_2 or O_2 levels.

In the apparatus diagrammed in Fig. 82, nitrogen gas derived from liquid nitrogen and containing about 2 ppm oxygen was dried and reacted with Ascarite to remove CO_2 ($f_{CO_2} = 10^{-17}$Pa). The nitrogen gas was then stripped of oxygen

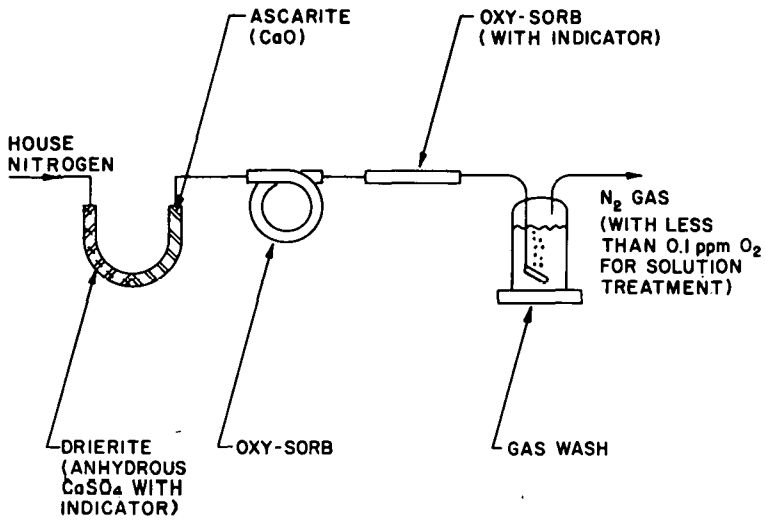

Fig. 82. Apparatus for Removing CO_2 and O_2 from Nitrogen Stream

by the chemical oxygen absorbents and passed through an oxygen-sorbent indicator that verifies an oxygen level in the gas below the detectable level. As an oxygen absorbent, we used dry flow-through traps (Oxy-sorb, supplied by Alltech Associates, Arlington Heights, Illinois) that do not require high temperatures to remove oxygen from the nitrogen gas. Alternatively, we used an oxygen-absorbing solution of chromous chloride (Oxsorbent, manufactured by Burrell Corporation, Pittsburgh, Pennsylvania), which is highly reactive with gaseous oxygen. After oxygen removal, the gas was washed in water to remove any entrained particulate or liquid and to restore water vapor to the gas.

The quantity of CO_2 in the solutions equilibrated with purified nitrogen is expected to be low. A solution in equilibrium with gas that has been reacted with CaO ($f_{CO_2} = 10^{-17}$ Pa) has a total-dissolved-carbonate content calculated to be $10^{-23.6}$M, which is significantly lower than the concentration of trace elements used in the experiments. With the dry flow-through oxygen traps used, the oxygen concentration in the nitrogen gas is indicated to be less than 0.1 ppm, and oxygen concentration in solutions can be reduced to less than 10^{-10}M. This is lower than the concentration of trace elements used in some of our experiments (about 10^{-4}M for strontium and tin in column infiltration experiments). By sparging the solution with nitrogen gas that has been reacted with chromous chloride, solutions are expected that have dissolved oxygen concentration* considerably below the concentration of the trace elements used in the experiments.

*Oxygen partial pressures of about 10^{-78} Pa, i.e., at the limit of stability of water, are calculated.

Solutions with low CO_2 and low O_2 levels produced in this apparatus can be mixed with solutions having high CO_2 or high O_2 levels (produced by reacting CO_2 gas, O_2 gas, or air with water) to produce solutions of intermediate CO_2 or O_2 levels.

The reduction of dissolved gas concentrations to levels expected in groundwaters permits experimentation which can reproduce migration characteristics of nuclides in natural geologic formations. However, the concentrations of dissolved gases in solutions do not, in themselves, control the E_h or pH of a solution reacted with a particular rock. These properties of the solution are determined rather by all of the constituents, including dissolved gases, in the solution-rock system.

A good method of controlling E_h and pH in solution is to reduce the concentrations of dissolved gases in the solution (as discussed) and then to allow the solution to react with the geologic material. In column infiltration experiments, the latter step has been performed in a column upstream from the sample-injection valve in the infiltration apparatus.

F. Discussion of Experimental Results

In experiments in which strontium was eluted through the glauconite column, the strontium peak moved through the column with a well-defined velocity equal to about 0.04 times the velocity of the water stream. This behavior for strontium arises, in all likelihood, from continuous and reversible partitioning of the strontium in liquid and solid phases. At the higher flow rates, there is a broadened curve shape and a slight increase in the velocity of the strontium as a result of less reaction of the liquid and solid. This effect, i.e., the effect that slow kinetics modify trace-element migration at flows of 0.1 mL/min or greater, is expected from the results of earlier static-absorption experiments [SEITZ].

Because no peak shape independent of flow was obtained in any experiment except, possibly, in the set of experiments at 0.1 mL/min, the condition of local equilibrium (in which solution and liquid can be considered to be locally equilibrated with respect to strontium) was not demonstrated for any experiment. This flow, for a column 1-cm in diameter and 53% porous, corresponds to a linear flow of 1.2 km/y and is comparable to the flow of water found in some geologic formations. The absence of a "local equilibrium" degrades the effectiveness of geologic media as a barrier to nuclide migration. Therefore, models of nuclide migration need to take into account reaction kinetics that cause increased dispersion (peak broadening) of a migrating species with increased flow rate, such as are seen in Fig. 76.

It is unlikely that the water flow can be made slow enough for "local equilibrium" to exist for strontium in glauconite. This is because although a fast reaction of strontium between the groundwater and a solid particle of glauconite occurs at the wetted surface adjacent to the fluid stream, continued but slower reaction of strontium with deeper layers of the glauconite (made accessible by capillaries, interlayer water, or crystalline defects) also proceeds.

Peak broadening may result not only from nonequilibration, but also from differences in stream paths within the column (hydrodynamic dispersion), from heterogeneous solid media within the column, and from the exchange process itself (finite size of a theoretical plate). At flow rates low enough that these effects dominate the width of the elution peak, the migrating nuclide may be considered to be in "local equilibrium" without loss of accuracy. Of course, the models, need to consider dispersive terms for hydrodynamic dispersion, etc., where these dominate the elution-curve shape. For strontium elution through the glauconite used in these experiments, "local equilibrium" occurs at flows of 0.1 mL/min (1.2 km/y) or lower.

This work with strontium in glauconite is an extension of work by Inoue and Kaufman [INOUE]. In that work, they modeled strontium migration in glauconite, assuming conditions of local equilibrium for flows up to 6.3 km/y. Although the model predicted the results of the experiments reasonably well, results for the model and the experiment differed, possibly due to the existence of nonequilibrium behavior (as seen in the results reported here).

In the experiments with oolitic limestone, radioactive strontium moved through the limestone as rapidly as did the fluid stream containing 0.01M calcium but moved through oolitic limestone with a peak velocity only 0.10 times the velocity of the REW solution stream and only 0.14 times the velocity of the recipe solution. The behavior for strontium in REW and in the recipe solution was nearly the same in spite of the great dissimilarities in the two solutions. The REW solution was more dilute than the recipe solution and more complex, containing six elements at detectable quantities not specifically added to the recipe solution. In addition, the REW solution presumably contained fine clay particles that were introduced by mixing the water with limestone and that were not filtered by the 0.45-μm-pore-size membrane filter. It is likely that the recipe solution also contains particulate matter introduced as insoluble contaminants from the chemicals. However, the characteristics and amounts of the particles in each solution must be fundamentally different. That there two solutions with gross differences produce similar migration behavior for strontium suggests that the differences are not important. However, migration behavior is clearly sensitive to solution composition as seen by the migration results using a solution with the elevated concentration of 0.01M $CaSO_4$. It may only be in dilute solutions that large variations in concentrations of major constituents do not affect migration behavior. Nevertheless, this behavior, if generally true, would considerably simplify predictions of nuclide migration.

The retardation of strontium on limestone columns with REW solution and recipe solution is a result of a significant fraction of the strontium in the column being bound by the limestone. The position of the elution peaks indicates an exchange capcity of 7×10^{-5} meq strontium per gram of limestone. Small exchange capacities such as this can retard the movement of trace elements in solution. Measurements of these small capacities are important in assessing geologic bodies as barriers to nuclide migration. Elution of rock with solutions containing trace quantities of the elements of interest is a good method of measuring that capacity.

Because strontium moves through oolitic limestone in a peak having a measurable velocity, we can compare the results of the column-infiltration experiments with the behavior predicted from earlier batch-absorption experiments. In batch tests (to be reported for the controlled-sample program of the Waste Isolation Safety Assessment Program), the measured coefficients, K_D, for strontium partitioning between the recipe solution and oolitic limestone were 5.09, 5.33, and 5.77. The coefficient, K_D, is related to the velocity of strontium relative to the velocity of water, v_{Sr}/v_w, by the equation

$$\frac{v_{Sr}}{v_w} = \frac{1}{1 + K_D \delta/\epsilon}$$

where δ, the density, is 2.35 g/cm^3 and ϵ, the porosity, is 0.19 for the limestone columns used in the experiments. In deriving this equation, we assumed that local equilibration and reversible reactions exist during nuclide transport.

Relative migration rates expected for the three measurements of K_D in the batch experiments are 0.016, 0.015, and 0.014, respectively. These predicted values are nearly one order of magnitude lower than the value, 0.14, measured in the elution experiment with the recipe solution. This difference suggests (1) that conditions in the experimental technique (the use of crushed limestone in batch tests versus the use of bulk limestone in infiltration experiments, for example) preclude comparison of results from the two experimental techniques or (2) that assumptions made to compare the results (equilibrium results in batch tests, local-equilibrium in infiltration experiments, etc) were not valid. We are examining transport models with saturation effects, irreversible reactions, and variable reaction kinetics that may help explain the discrepancy.

VII. TRACE-ELEMENT TRANSPORT IN LITHIC MATERIAL BY FLUID FLOW AT HIGH-TEMPERATURES

(M. G. Seitz and R. A. Couture)

A. Introduction

To study the expected migration of trace elements in natural geologic formations, we have assembled equipment for pumping solutions through packed mineral columns at elevated temperatures and at pressures high enough to prevent boiling. By using this approach, we have anticipated nonequilibrium phenomena which in the absence of direct experimental data are difficult to take into account in model calculations.

The two previous quarterly reports explore the geological relevance of this work and some of the capabilities of the technique [STEINDLER-1978B] and report on details of the experimental method and some preliminary experiments [STEINDLER-1978C]. In this report, experimental progress is summarized.

Work has focused on three areas: (1) design and perfection of equipment and techniques, (2) cesium-sodium ion exchange on kaolinite from room temperature to 225°C, and (3) sorption of iodine species by kaolinite at room temperature and 130°C. The last is particularly interesting because several chemical species of iodine are simultaneously present which migrate at different rates through the columns. Column absorption experiments were done rather than static absorption experiments; the latter are generally not suitable for study of a system of this complexity because the experiments do not distinguish between species. The Cs^+–Na^+ exchange reaction on kaolinite is being studied to determine the enthalpy of reaction at different temperatures. Few studies have been made of ion exchange on minerals above 100°C.

In these column infiltration experiments, we inject radioactive solutions in trace quantities onto a mineral column, elute the column with an aqueous solution, and analyze the effluent to determine the migration velocity of the radioactive material. Temperature, pressure, and flow rate are controlled; the pressures are high enough to prevent boiling of the aqueous solutions.

The mineral kaolinite [$Al_2Si_2O_5(OH)_4$] has been used in all of the experiments. This mineral was selected for the initial parts of the work because it does not swell and is stable at high temperatures, it is mineralogically simple, it is common, and few data on ion exchange with kaolinite have been obtained. Furthermore, fewer ion exchange mechanisms operate on kaolinite than on swelling clays since no interlayer exchange sites (sites located between the oxygen sheets) are involved.

B. Preparation of the Mineral Columns

Design of the columns is still evolving. Commercial chromatographic fittings work well at temperatures at least up to 130°C. We have used such fittings for a few hours up to 225°C, but the plastic (Kel-F) seals on the frits flow, causing the columns to plug up. For high-temperature use we have obtained soft nickel seals for the frits. With commercial fittings, where

the main seals are made with swaged ferrules, a 1-cm-diameter column cannot be made shorter than about 6 cm. To make short columns which are usable at moderate temperatures, these seals can be omitted; instead, the column end fittings with Kel-F seals can be made leak-tight by an exterior clamp.

The columns were prepared by pumping a slurry into an empty tube having a frit on the bottom. Initial porosity was generally about 40-50%, and compaction after preparation was minimal.

Two types of kaolinite were used for the experiments. Hydrite R is a commercially prepared kaolinite which has a mean equivalent spherical particle diameter of 0.8 μm. The clay has been treated to remove manganese and iron oxides and is pure white. X-ray diffraction analysis shows that the clay is very well crystallized, with no impurities detectable. American Petroleum Institute standard kaolinite 9 was also used. The clay occurs in massive white blocks. Hand-picked specimens were ground in acetone and sieved to <125-μm diameter. The ground particles presumably consist of cemented aggregates of much finer grains. X-ray diffraction analysis shows only kaolinite and quartz; the kaolinite is not as well crystallized as the Hydrite R.

C. Transport of Tritium

Tritiated water was used to monitor column performance. Tritium follows the flow of water through the column with a minimum of interaction with the mineral and is a good indicator of experimental problems such as channeling and the presence of voids in the column. At room temperature, the tritium peak velocity was found to agree with the value calculated from the free column volume, verifying proper performance of the columns. Tritium-elution experiments of the type described in [STEINDLER-1978C] are now used routinely for column diagnostics.

D. Behavior of Cesium

We have used cesium to develop the high-temperature infiltration technique because cesium is convenient, being univalent, forming stable solutions and having a moderate-life (about 2.1 y) isotope that decays with an energetic gamma. Furthermore, kaolinite has a stronger affinity for Cs^+, which is weakly hydrated, than for Na^+, which is more strongly hydrated. It was interesting to determine to what extent kaolinite loses its preference for Cs^+ at elevated temperatures, especially above 100°C where few measurements have been made. To do this, we injected cesium chloride dissolved in $NaHCO_3$ solution onto kaolinite columns at several different temperatures. The measurements made in these experiments may be the only ones existing for Cs^+-Na^+ exchange on clay minerals above 100°C. We plan to derive the change in free energy and enthalpy above 100°C for this ion exchange and ion exchanges of other elements and minerals.

Spikes of dissolved cesium-134 in trace quantities were injected onto kaolinite columns, and $NaHCO_3$ solutions in various concentrations were pumped through the columns at constant rates. The effluent solutions were analyzed continuously for activity; in two cases, the columns were opened

at the end of an experiment and the clay was analyzed for activity. The results are summarized in Table 53, and three of the activity profiles are shown in Figs. 83-85. In the first three experiments listed (columns 1-3), the effective free column volume was determined by pumping tritiated water through the columns. In the first two experiments, the free column was also measured gravimetrically (porosity times volume) and was found to be equal to that measured with tritium. The fraction of cesium in solution was assumed to be the peak velocity of cesium divided by the velocity of the solvent.

The effects of temperature and solution concentration are shown clearly. An increase in competing ion concentration (Na^+) increases the relative velocity of Cs^+. It also appears that increasing the temperature decreases the affinity of kaolinite for Cs^+ in comparison to its affinity for Na^+.

Table 53. Results of Cesium Experiments with Kaolinite

Column	Clay	Temperature, °C	[$NaHCO_3$], M	Percent of Co in Solution in the Column
1	Hydrite R	∿25	0.001	≤0.028
2	Hydrite R	∿25	0.5	0.23
4	Kaolinite 9	118	0.10	3.4
3	Kaolinite 9	224	0.10	∿25-50

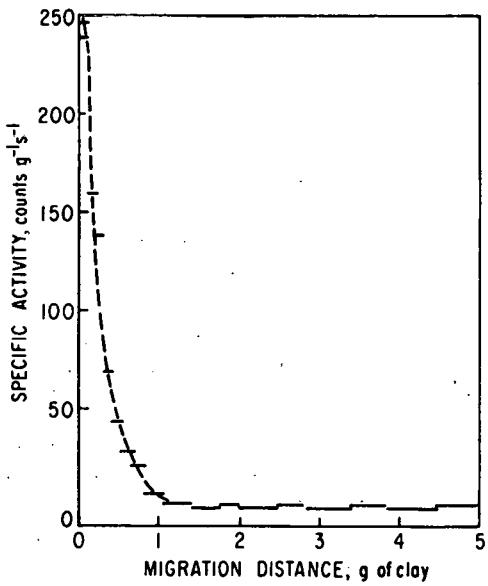

Fig. 83.

Migration of Cesium-134 in a Column of Kaolinite at Room Temperature in 0.001M $NaHCO_3$. Total solution pumped through the column corresponded to eighty-nine free column volumes.

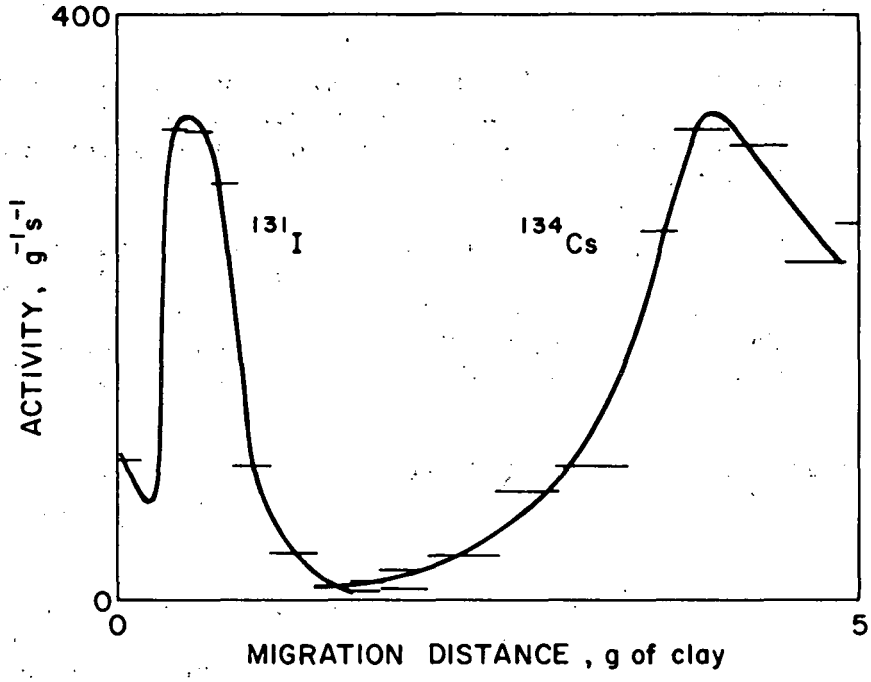

Fig. 84. Activity of Iodine-131 and Cesium-134 on Kaolinite Column 2 at Room Temperature

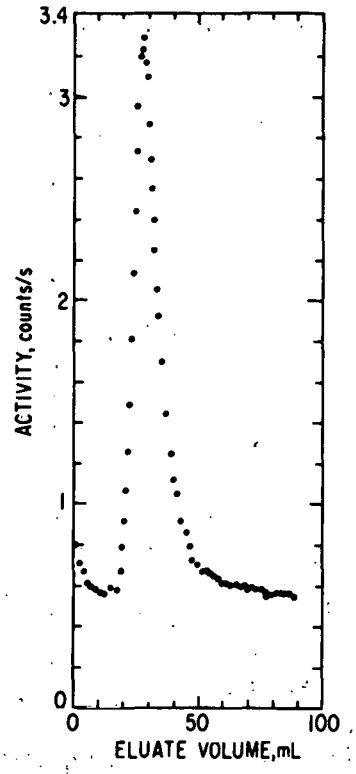

Fig. 85.

Elution of Cesium-134 from Kaolinite Column 4 by 0.10M $NaHCO_3$ at 118°C

E. Behavior of Iodine

Iodine absorption on kaolinite is complicated by the existence of several oxidation states of iodine which behave differently in kaolinite. Different species of iodine in a single sample are capable of moving through kaolinite columns at several distinct rates.

The experiments were performed as follows: Two samples of ^{131}I (reportedly present as I^- in 0.1M NaOH) were obtained from New England Nuclear Company. In the column experiments, diluted spikes were injected into streams of $NaHCO_3$ solutions and were pumped through kaolinite columns. Some of these experiments were described in [STEINDLER-1978C] and are summarized here.

In experiments at 130°C reported previously, all of the iodine moved through columns of kaolinite at the same rate as the aqueous solution of 0.001M $NaHCO_3$.

At room temperature, the iodine moved through columns of kaolinite in as many as three peaks representing three different velocities. Results of one experiment are shown in Fig. 86. In various experiments, from about 5 to 20% of the iodine moved at the same rate as the solvent, while movement of the remainder of the iodine was greatly retarded. The results were time-dependent: one peak was prominent in one experiment but entirely absent in the next experiment.

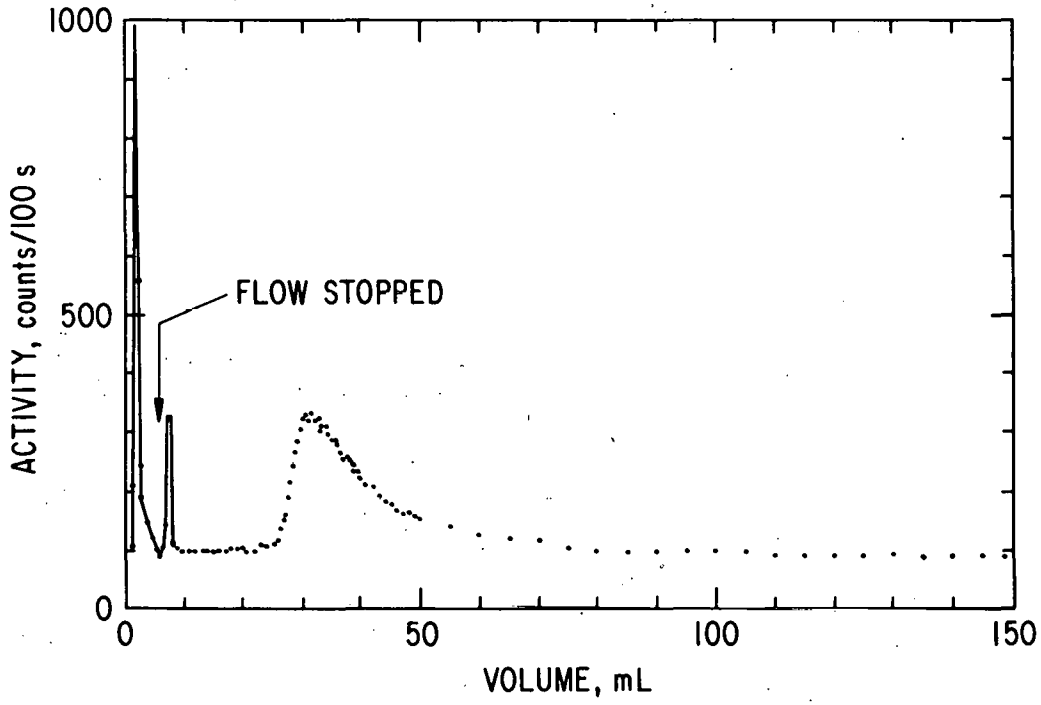

Fig. 86. Elution of Iodine-131 from Kaolinite in Column 2 at Room Temperature. 0.025 mL/min. 0.001M $NaHCO_3$

Finally, in one experiment, about 5% of the iodine was eluted with the solvent front, while the remainder of the iodine was firmly bound. The ^{131}I samples used were supplied as I^-, but the results strongly suggested that as many as three or possibly more iodine species were present.

More recently, an infiltration experiment was performed after which the column was dissected to determine whether the firmly bound iodine was actually bound to the clay; solvent extraction and paper chromatography were used in an attempt to identify iodine species.

In the infiltration experiment, a spike of ^{131}I was injected onto a packed column of kaolinite and was infiltrated with more than 43 mL of 0.001M $NaHCO_3$ solution. Another spike of the same size was injected, followed by 147.2 mL of 0.001M $NaHCO_3$. A spike of $^{134}CsCl$ in 0.5M $NaHCO_3$ was then injected, and 663 mL of 0.5M $NaHCO_3$ was pumped through the column. The clay was then removed from the column and segments were analyzed radiometrically for ^{131}I and ^{134}Cs with a NaI gamma detector. The results are shown in Fig. 84. Only 4.7% of the iodine was eluted from the column; most or all of the remainder was bound to the clay. (Roughly 82% of the iodine is accounted for by a semiquantitative analysis of the amount bound, but the uncertainty is large and unknown because of absorption effects and other uncertainties.) Most of the iodine migrated through less than one-fifth of the clay.

We can estimate roughly how strongly the iodine in the second peak was bound if we consider the experiments in 0.5M $NaHCO_3$ and 0.001M $NaHCO_3$ together. Total fluid flow was 853 mL, or 446 free-column volumes. The peak moved through 10% of the column. Only about 0.1/446 = 0.022% of the iodine was in solution, on the average.

Investigation by paper chromatography confirms that two or more species were present in samples from various experiments at various times. Figure 87 shows paper chromatograms of three iodine-containing solutions developed in 1:1:10 H_2O:n-butanol:acetone. Two or three peaks appear in each chromatogram. In order to prove that the two peaks at R_F = 0 and 0.87 are due to different species, a two-dimensional chromatogram was developed, using two solvents: first, 1:1:10 H_2O:n-butanol:acetone; and second, 3:2 i-propanol: 1.5M NH_3. The results, shown in Fig. 88, clearly indicate different behavior for the two peaks in the second solvent; the smaller one shows a prominent "tail." Therefore, there are at least two species on the paper.

An attempt was made to identify the species by chromatography of microamounts of iodine-containing salts. The iodine was detected by dusting the paper with soluble starch and (1) oxidation or (2) reduction to I_2. The R_F values for various iodine species are

NaI	broad band about	0.2-0.55
KIO_3		0
KIO_4		0

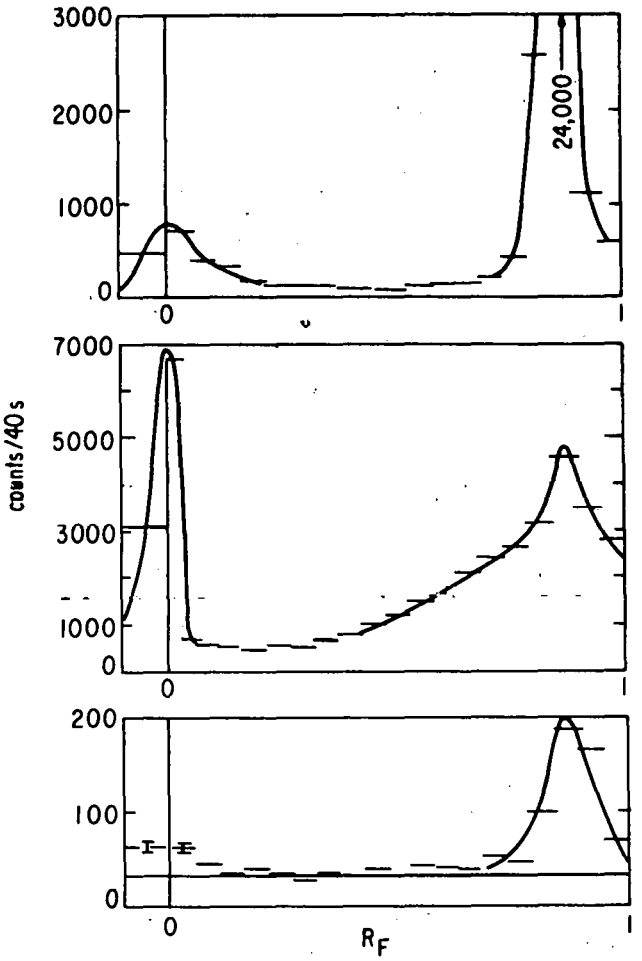

Fig. 87. Paper Chromatography Results of Iodine Samples.
Top: Sample diluted with 0.001M $NaHCO_3$, dried with air, then redissolved in water.
Center: The same sample dried in air, then dissolved in water.
Bottom: A different sample, diluted with water.

An attempt to detect HOI produced by the reaction

$$2I_2 + 2H_gO + H_2O \rightarrow HgO \cdot HgI_2 + 2HOI$$

[COTTON] was not successful, since HOI is rather unstable. That HOI exists in the radioactive samples seems unlikely.

Several experiments with the addition of acids and bases (0.01M H_2SO_4, 0.01M NaOH, 0.25M NaOH) to the iodine spot on the paper demonstrate that the R_F values are not very dependent on the composition of iodine-containing solution. However, if two or more oxidation states are present on the paper,

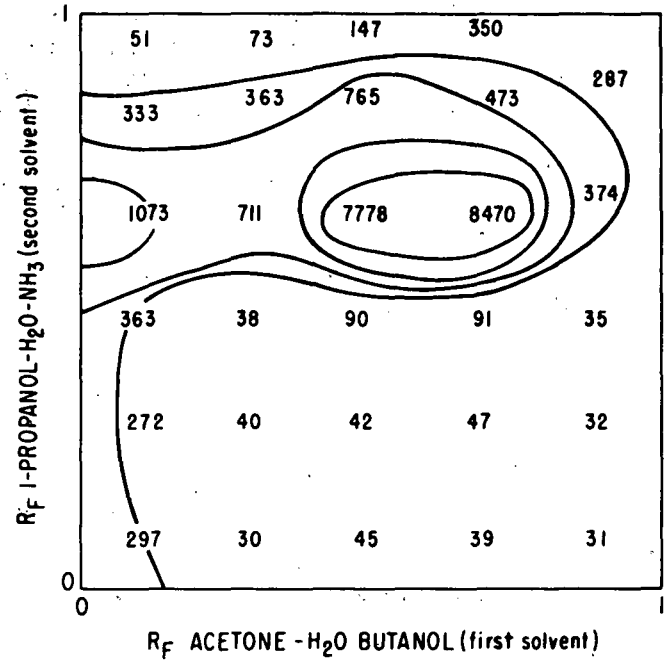

Fig. 88. Paper Chromatogram of an Iodine-131 Solution in Two Solvents

exchange during development is possible. To demonstrate exchange, I_2 was reacted with 1.5M NH_4OH to give I^- and IO_3^-, according to the reaction

$$3I_2 + 6OH^- \rightarrow 5I^- + IO_3^- + 3H_2O \qquad (1)$$

The excess NH_3 evaporated, and the result was a very long band visible from R_F = 0.05 to 0.65 and indicating exchange among I_2, I^-, and IO_3^-. Likewise, I_2 plus dilute HNO_3 gave R_F = 0.70 to 0.92, evidently due to $I^- + I_2 + I_3^-$. The radioactive samples (Fig. 87) showed similar behavior. The position of the peak shown at R_F = 0.87 in Fig. 87 and the relative heights of the peaks at R_F = 0 were found to depend on such factors as the presence of NH_3 and whether the spot dried completely before development. The results are consistent with the reaction of I^- and IO_3^- with I_2 on the paper.

Presumably, such reactions will not occur if only one species is present in the solution. Thus, paper chromatography might be useful for characterizing solutions which have emerged from the mineral columns. It should also be possible to ensure that only one oxidation state is present by adding a carrier or an oxidizing or reducing agent as a preservative. We have now begun investigations using these techniques.

Although I_2 is apparently present on the paper, little I_2 is present in the radioactive solutions. Aliquots of the solutions were extracted with CCl_4. From top to bottom in Fig. 87, the amounts of extractable iodine are

0.62, 1.8, and about 0%, respectively. Thus, most of the I_2 present on the paper is apparently due to reaction between I^- and oxidized species, most probably IO_3^-. One may well ask whether it is possible to have I^- and IO_3^- coexisting in solution without I_2. For reaction 1, log K is 37. If a reasonable pH (e.g., 6) and reasonable upper limits for the concentrations [$(I^-) = (IO_3^-) = \overline{10^{-7}}$] are assumed, (I_2) is calculated to be only $10^{-10.3}$. Thus the presence of very little I_2 does seem reasonable.

The results obtained during this report period show that we now have the tools for a straightforward investigation of sorption of iodine species by kaolinite.

F. Discussion

Despite its small ion exchange capacity in comparison with expanding clay minerals, kaolinite may have significance in the disposal of radioactive waste. Because of its large surface area, it has a higher exchange capacity than most of the minerals in igneous rocks. Kaolinite is stable in warm, humid environments where montmorillonite does not form or is rapidly weathered. It is highly abundant in some locations; in others, it is the only clay mineral present. Therefore, its characteristics may determine the migration of radioactive isotopes in some soils, particularly in the southeastern United States. It is also cheap and could be used in engineered disposal sites. Thus, it is interesting to note that kaolinite is capable of strongly binding cesium and iodine in solutions having ionic strengths comparable to or higher than those in groundwater.

The temperature dependence of absorption of both cesium and iodine may be of considerable practical interest. The use of clay in high-level radioactive waste disposal sites has been proposed. Our results suggest that such a procedure might be ineffective for some elements because of accelerated migration at high temperatures.

Kaolinite may also have relevance to many other rock-forming silicates. The sites of ion exchange are at the surfaces of kaolinite particles, and the cation exchange capacity is proportional to the surface area [CARROLL] but does not depend on the composition of the clay. Since kaolinite is a layer-lattice silicate whose surface probably consists of an oxide layer, its exchange properties may be similar to those of many other rock-forming silicates which exchange ions mainly at the surface.

In order to obtain meaningful results, it is essential to determine which species were retained by the clay and why. Two factors may be relevant: the oxidation state and the history of the clay. Possibly, a change in the oxidation state with time accounts for the sudden strong binding of 95% of the iodine to the clay. (In previous experiments, the iodine was less strongly bound.) It is also possible that prolonged washing with 0.001M $NaHCO_3$

accounts for the behavior. This solution is slightly alkaline, while the clay (Hydrite R) was treated by the supplier with slightly acidic solutions to remove iron and manganese oxides. The residual acid may not have been completely washed out. The temperature history of the clay can be ruled out as an important factor. The clay was heated to 132°C in some experiments, but the heating did not permanently affect its migration properties.

It is important to realize that for a clay-water system, the distribution coefficient, K_d, for any exchangeable ion is proportional to the ion exchange capacity and also depends on porosity. For a substance such as kaolinite which exchanges mostly at the crystal surface, K_d should be nearly proportional to specific surface area. Migration velocity is an inverse function of K_d and therefore depends on surface area and porosity. In order to compare the results obtained with different mineral samples, it is desirable to determine the exchange reaction constant, which is a more fundamental property of the substances than is K_d. We are now measuring exchange constants at elevated temperatures.

THIS PAGE

WAS INTENTIONALLY

LEFT BLANK

APPENDIX A

THE VAPOR PRESSURES OF THE ELEMENTS

Presented below is a table (Table A-1) of vapor pressures for the elements at specific temperatures (from 800 K to 1400 K in steps of 200 K). The table is a compilation from several sources, the major one being [HULTGREN]. The latter publication evaluates and re-evaluates thermodynamic data as it becomes available.

Vapor pressures not available in the aforementioned article were obtained from numerous publications. The use of estimates and interpolations in this table is indicated by parentheses. The vapor pressures presented in this table are reported in millimeters of mercury (mm Hg). One millimeter of mercury is equivalent to 133 pascals.

Table A-1. Vapor Pressure mm of Hg

	800 K	1000 K	1200 K	1400 K	Reference
Ac	-	(1×10^{-8})	(3.7×10^{-6})	(2.7×10^{-4})	[MARGRAVE]
Ag	1.06×10^{-9}	4.96×10^{-6}	1.32×10^{-3}	6.06×10^{-2}	[HULTGREN]
Al	-	4.03×10^{-8}	2.09×10^{-5}	1.76×10^{-3}	[HULTGREN]
Am	-	2.05×10^{-6}	3.65×10^{-4}	1.29×10^{-2}	[HULTGREN]
As	2.05×10^{-10}	1.63×10^{-6}	6.26×10^{-4}	-	[HULTGREN]
As_2	1.03×10^{-3}	0.590	37.5	-	[HULTGREN]
As_3	1.28×10^{-4}	0.241	33.1	-	[HULTGREN]
As_4	1.21×10^{2}	7.75×10^{3}	1.10×10^{5}	-	[HULTGREN]
Au	4.86×10^{-15}	2.81×10^{-10}	4.10×10^{-7}	6.82×10^{-5}	[HULTGREN]
B	-	6.99×10^{-10}	7.66×10^{-15}	2.38×10^{-11}	[HULTGREN], [SMITHELLS]
Ba	4.65×10^{-5}	3.93×10^{-20} @ 1002 K	0.920	8.44	[SMITHELLS], [HULTGREN]
Be	2.17×10^{-12}	3.59×10^{-8}	2.28×10^{-5}	2.23×10^{-3}	[HULTGREN]
Bi	3.37×10^{-5}	1.14×10^{-2}	0.545	8.44	[HULTGREN]
Bi_2	7.29×10^{-5}	1.95×10^{-2}	0.768	9.96	[HULTGREN]
$Bi(P_{total})$	1.06×10^{-4}	3.09×10^{-2}	1.31	18.4	[HULTGREN]
C	1.52×10^{-36}	3.88×10^{-27}	7.07×10^{-21}	2.13×10^{-16}	[HULTGREN]
C_2	1.36×10^{-41}	8.36×10^{-31}	1.29×10^{-23}	1.75×10^{-18}	[HULTGREN]
C_3	2.28×10^{-39}	5.17×10^{-29}	4.03×10^{-22}	3.27×10^{-17}	[HULTGREN]
$C(P_{total})$	1.52×10^{-36}	3.95×10^{-27}	7.45×10^{-21}	2.51×10^{-16}	[HULTGREN]
Ca	1.19×10^{-3}	0.194	5.30	50.6	[HULTGREN]
Cd	23.2	4.81×10^{2}	-	-	[HULTGREN]
Ce	-	1.29×10^{-13}	5.32×10^{-10}	1.98×10^{-7}	[HULTGREN]
Co	-	1.67×10^{-12}	8.36×10^{-9}	3.28×10^{-6}	[HULTGREN]
Cr	8.07×10^{-16}	6.84×10^{-11}	1.75×10^{-7}	4.51×10^{-5}	[SMITHELLS], [HULTGREN]
Cs	1.50×10^{2}	1.27×10^{3}	5.13×10^{4}	1.22×10^{4}	[HULTGREN]
Cu	5.7×10^{-13}	1.29×10^{-8}	9.96×10^{-6}	1.09×10^{-3}	[HULTGREN]
Dy	1.22×10^{-10}	6.74×10^{-7}	1.98×10^{-4}	1.11×10^{-2}	[HULTGREN]
Er	-	2.58×10^{-8}	1.28×10^{-5}	1.04×10^{-3}	[HULTGREN]
Eu	8.36×10^{-4}	0.138	3.46	31.2	[HULTGREN]
Fe	4.94×10^{-17}	1.14×10^{-11}	3.8×10^{-8}	1.18×10^{-5}	[HULTGREN]
Ga	1.60×10^{-9}	4.73×10^{-6}	9.65×10^{-4}	4.25×10^{-2}	[HULTGREN]
Gd	-	4.33×10^{-12}	1.14×10^{-8}	3.15×10^{-6}	[HULTGREN]
Ge	4.86×10^{-15}	4.03×10^{-10}	7.68×10^{-7}	1.0×10^{-4}	[HULTGREN]

(contd)

Table A-1. (Contd)

	800 K	1000 K	1200 K	1400 K	Reference
Hf	2.28×10^{-30}	7.37×10^{-23}	4.02×10^{-17}	2.4×10^{-13}	[SMITHELLS], [HULTGREN]
Hg	8.41×10^{3}	-	-	-	[HULTGREN]
Ho	-	1.82×10^{-7}	6.71×10^{-5}	4.34×10^{-3}	[HULTGREN]
In	5.93×10^{-8}	7.14×10^{-5}	7.98×10^{-3}	0.232	[HULTGREN]
Ir	2.04×10^{-33}	1.06×10^{-24}	6.3×10^{-19}	8.47×10^{-15}	[SMITHELLS], [HULTGREN]
K	45.1	5.56×10^{2}	2.94×10^{3}	9.27×10^{3}	[HULTGREN]
La	6.05×10^{-19}	6.99×10^{-14}	8.55×10^{-10}	1.44×10^{-7}	[SMITHELLS], [HULTGREN]
Li	8.13×10^{-3}	0.775	15.8	1.36×10^{-2}	[HULTGREN]
Lu	-	2.51×10^{-13}	1.22×10^{-9}	5.24×10^{-7}	[HULTGREN]
Mg	0.183	11.9	1.63×10^{2}	1.03×10^{3}	[HULTGREN]
Mn	4.26×10^{-9}	1.75×10^{-5}	4.04×10^{-3}	0.185	[HULTGREN]
Mo	3.05×10^{-33}	2.43×10^{-24}	6.96×10^{-19}	8.48×10^{-15}	[SMITHELLS], [HULTGREN]
Na	7.35	1.5×10^{2}	1.12×10^{3}	4.7×10^{3}	[HULTGREN]
Nb	6.61×10^{-37}	1.29×10^{-27}	3.69×10^{-21}	1.16×10^{-16}	[SMITHELLS], [HULTGREN]
Nd	-	6.2×10^{-9}	3.8×10^{-6}	3.29×10^{-4}	[HULTGREN]
Ni	4.88×10^{-18}	1.6×10^{-12}	8.36×10^{-9}	3.77×10^{-6}	[SMITHELLS], [HULTGREN]
Os	-	8.36×10^{-31}	-	-	[HULTGREN]
Pa	-	-	-	(1.68×10^{-8})	[MARGRAVE]
Pb	4.62×10^{-5}	1.22×10^{-2}	0.483	6.59	[HULTGREN]
Pd	7.55×10^{-16}	6.16×10^{-11}	1.06×10^{-7}	2.04×10^{-5}	[SMITHELLS], [HULTGREN]
Po	(3.16)	(73.6)	(5.69×10^{2})	-	[MARGRAVE]
Pr	3.95×10^{-15}	1.52×10^{-10}	1.6×10^{-7}	1.98×10^{-5}	[HULTGREN]
Pt	1.81×10^{-26}	2.99×10^{-19}	1.88×10^{-14}	4.18×10^{-11}	[SMITHELLS], [HULTGREN]
Pu	9.12×10^{-15}	2.36×10^{-10}	1.9×10^{-7}	2.24×10^{-5}	[HULTGREN]
Rb	1.16×10^{2}	1.1×10^{3}	4.72×10^{3}	-	[HULTGREN]
Re	6.8×10^{-44}	1.67×10^{-30}	4.25×10^{-24}	2.56×10^{-19}	[SMITHELLS], [HULTGREN]
Rh	1.76×10^{-26}	8.36×10^{-19}	2.11×10^{-14}	5.75×10^{-11}	[SMITHELLS], [HULTGREN]
Ru	-	1.14×10^{-23}	-	-	[HULTGREN]
S	2.24×10^{3}	-	-	-	[HULTGREN]
Sb	3.42×10^{-8}	6.78×10^{-5}	8.06×10^{-3}	0.239	[HULTGREN]

(contd)

Table A-1. (Contd)

	800 K	1000 K	1200 K	1400 K	Reference
Sb_2	1.12×10^{-4}	5.09×10^{-2}	1.73	19.8	[HULTGREN]
Sb_4	5.46×10^{-3}	0.599	4.65	17.7	[HULTGREN]
$Sb(P_{total})$	5.57×10^{-3}	0.651	6.38	37.8	[HULTGREN]
Sc	2.66×10^{-15}	2.05×10^{-10}	3.53×10^{-7}	7.07×10^{-5}	[HULTGREN]
Se	4.79×10^{-5}	3.5×10^{-2}	-	-	[HULTGREN]
Se_2	15.2	4.4×10^{2}	-	-	[HULTGREN]
Se_3	45.6	7.6×10^{2}	-	-	[HULTGREN]
$Se(P_{total})$	63.8	1.29×10^{3}	-	-	[HULTGREN]
Si	8.36×10^{-20}	6.76×10^{-14}	5.93×10^{-10}	3.8×10^{-7}	[HULTGREN]
Si_2	9.12×10^{-27}	4.18×10^{-19}	5.02×10^{-14}	2.05×10^{-10}	[HULTGREN]
Si_3	6.99×10^{-28}	5.93×10^{-20}	1.06×10^{-14}	5.78×10^{-11}	[HULTGREN]
$Si(P_{total})$	8.36×10^{-20}	6.76×10^{-14}	5.93×10^{-10}	3.8×10^{-7}	[HULTGREN]
Sm	1.71×10^{-12}	7.36×10^{-3}	0.396	6.01	[HULTGREN]
Sn	7.16×10^{-12}	6.46×10^{-8}	2.35×10^{-5}	1.61×10^{-3}	[SMITHELLS], [HULTGREN]
Sr	2.91×10^{-3}	0.783	14.7	1.16×10^{2}	[SMITHELLS], [HULTGREN]
Ta	1.95×10^{-41}	2.81×10^{-31}	1.95×10^{-24}	1.4×10^{-19}	[SMITHELLS], [HULTGREN]
Tb	-	1.67×10^{-11}	3.65×10^{-8}	8.51×10^{-6}	[HULTGREN]
Tc	-	(1.22×10^{-25})	-	-	[HULTGREN]
Te	5.54×10^{-4}	9.88×10^{-2}	3.06	-	[HULTGREN]
Te_2	1.25	43.3	4.2×10^{2}	1.83×10^{3}	[HULTGREN], [SMITHELLS]
Th	1.98×10^{-28}	5.62×10^{-21}	5.06×10^{-16}	1.71×10^{-12}	[SMITHELLS] [HULTGREN]
Ti	9.12×10^{-21}	1.06×10^{-14}	1.14×10^{-10}	8.36×10^{-8}	[HULTGREN]
Tl	7.98×10^{-4}	0.137	4.13	45.5	[HULTGREN]
Tm	4.56×10^{-7}	4.29×10^{-14}	3.96×10^{-2}	0.973	[HULTGREN]
U	-	1.37×10^{-17}	-	5.4×10^{-10} @ 1405 K	[HULTGREN]
V	1.74×10^{-23}	9.12×10^{-17}	2.66×10^{-12}	4.03×10^{-9}	[HULTGREN], [SMITHELLS]
W	1.63×10^{-45}	8.36×10^{-35}	4.29×10^{-27}	8.03×10^{-22}	[SMITHELLS], [HULTGREN]
Y	1.44×10^{-18}	4.56×10^{-13}	2.05×10^{-9}	8.21×10^{-7}	[HULTGREN]
Yb	5.2×10^{-2}	4.29	69.9	4.58×10^{2}	[HULTGREN]
Zn	2.56	89.7	9.27×10^{2}	4.73×10^{3}	[HULTGREN]
Zr	-	3.04×10^{-22}	5.29×10^{-17}	3.01×10^{-13}	[HULTGREN] [SMITHELLS]

APPENDIX B.

FISSION YIELDS FROM ^{235}U FISSION*

Atomic No.	Element Symbol	Mass No.	T 1/2	Independent Fission Yield[a]	Cumulative Fission Yield[b]	Est. wt % of Total Non-Volatile Fission Products[c]
30	Zn	72	46. h	1.6×10^{-5}	2.37×10^{-5}	ΣZn = <0.0001
31	Ga	72	14. h			
		73	5.0 h	2×10^{-6}		ΣGa = <0.001
32	Ge	72	S[d]		2.7×10^{-5}	
		73	S		1.1×10^{-4}	
		74	S	3×10^{-4}	3.6×10^{-4}	
		75m	49 s			
		75	82 m	8×10^{-4}		
		76	S	2×10^{-3}	3.8×10^{-3}	
		77m	54 s			
		77	11 h	3.1×10^{-3}		
		78	1.5 h			ΣGe = <0.01
33	As	75	S		1.2×10^{-3}	
		76	26 h	0		
		77	39 h			
		78	1.5 h	2×10^{-3}		
		79	9.0 m	5.6×10^{-2}		
		80	16 s			
		81	32 s			ΣAs = <0.001
34	Se	76	S		0	
		77m	17 s	2×10^{-4}		
		77	S		8.5×10^{-3}	
		78	S		1.9×10^{-2}	
		79m	3.9 m			
		79	7×10^{4} y			
		80	S	8×10^{-2}	0.13	
		81m	57 m	8.4×10^{-3}		

(contd)

*To convert megawatt days per metric ton of uranium fuel (about 3.3% ^{235}U) to the percent of uranium atoms fissioned, multiply by 1.74×10^{-4}.

Appendix B. (contd)

Atomic No.	Element Symbol	Mass No.	T 1/2	Independent Fission Yield[a]	Cumulative Fission Yield[b]	Est. wt % of Total Non-Volatile Fission Products[c]
		81	18 m	1.4×10^{-1}		
		82	S	0.25	0.35	
		83m	70 s			
		83	23 s			
		84	3.3 m			ΣSe = <0.2%
35	Br	79	S		5.3×10^{-2}	
		80m	4.4 h			
		80	17 m			
		81	S		0.22	
		82	35 h	3.8×10^{-5}	3.8×10^{-5}	
		83	2.4 h			
		84m	6 m	1.9×10^{-2}		
		84	32 m			
		85	2.9 m		1.33	
		86	55 s			
		87	56 s			
		88	16 s			
		89	4.5 s			(ΣBr = <0.15%)
36	Kr	82	S		0	
		83m	1.8 h			
		83	S		0.53	
		84	S		0.99	
		85m	4.5 h		1.33	
		85	11 y		0.27	
		86	S		1.95	
		87	76 m		2.55	
		88	2.8 h	0.8	3.61	(ΣKr = <2.0%)
37	Rb	85	S		1.31	
		86	19 d	2.8×10^{-5}		
		87	S(4.7×10^{10} y)		2.55	
		88	18 m			
		89	15 m	0.2	4.71	
		90	3 m	0.7	4.63	ΣRb = 1.2%

(contd)

Appendix B. (contd)

Atomic No.	Element Symbol	Mass No.	T 1/2	Independent Fission Yield[a]	Cumulative Fission Yield[b]	Est. wt % of Total Non-Volatile Fission Products[c]
38	Sr	86	S		0	
		87	S		0	
		88	S		3.62	
		89	50 d		4.71	
		90	28 y		5.86	
		91	9.5 h	0.07	5.90	
		92	2.7 h		5.98	ΣSr = 3.02%
39	Y	89	S		4.85	
		90	64 h		(see ^{90}Sr)	
		91m	50 m			
		91	59 d		5.90	
		92	3.5 h			
		93	10 h	0.1	6.41	ΣY = 1.63%
40	Zr	90	S		(see ^{90}Sr)	
		91	S		5.92	
		92	S		5.96	
		93	9.5 x 10^5y		6.37 (at 1-y decay)	
		94	S		6.41	
		95	65 d		6.50	
		96	S		6.25	
		97	17 h		5.86	ΣZr = 12.8%
41	Nb	93m	3.7 y		6.37 (see ^{93}Zr)	essentially 0
		93	S		6.37 (see ^{93}Zr)	essentially 0
		94	2 x 10^4y		0	
		95m	3.6 d			
		95	35 d	<4 x 10^{-5}	<4 x 10^{-5} (see ^{95}Mo)	
		96	23 h	6.36 x 10^{-4}	∿6.36 x 10^{-4} (see ^{96}Mo)	
		97m	54 s			
		97	74 m			ΣNb = <0.1% at 1 y decay

(contd)

Appendix B. (contd)

Atomic No.	Element Symbol	Mass No.	T 1/2	Independent Fission Yield[a]	Cumulative Fission Yield[b]	Est. wt % of Total Non-Volatile Fission Products[c]
42	Mo	95	S		6.46	
		96	S		$\sim 6 \times 10^{-4}$	
		97	S		5.96	
		98	S		5.78	
		99	66 h		~6.25	
		100	S		6.33	
		101	15 m		5.10	ΣMo = 12.1%
43	Te	99m	6.0 h			
		99	2.1×10^5 y		6.13	
		100	16 x	~0		
		101	14 m			ΣTc ≅ 2.9% at 1 y decay
44	Ru	99	S		~0 (see ^{99}Tc)	
		100	S		~0	
		101	S		5.04	
		102	S		4.20	
		103	40 d		3.00	
		104	S		1.82	
		105	4.4 h			
		106	1 y		0.39	
		107	4 m	0.04		ΣRu ≅ 7.54%
45	Rh	103m	56m			
		103	S		3.14	
		104m	4.4m	0		
		104	42 s	0		
		105m	38 s			
		105	36 h		0.95	
		106	30 s			ΣRh ≅ 1.28%
46	Pd	104	S	~0	0	
		105	S		0.99	
		106	S		0.392 (see ^{106}Pu)	

(contd)

Appendix B. (contd)

Atomic No.	Element Symbol	Mass No.	T 1/2	Independent Fission Yield[a]	Cumulative Fission Yield[b]	Est. wt % of Total Non-Volatile Fission Products[c]
46	Pd	107	7×10^6 y		0.173	
		108	S	~0.08	7.4×10^{-2}	
		109	13 h		2.4×10^{-2}	
		110	S	~0.02	2.33×10^{-2}	
		111m	5.5 h			
		111	22 m			ΣPd = 4.67%
47	Ag	107m	44 s			
		107	S		<<0.173 (see ^{107}Pd)	
		108m	130 yr	~0	~0	
		108	2.4 m	~0	~0	
		109m	40 s			
		109	S		3.08×10^{-2}	
		110m	250 d	~0	very small (capture from ^{109}Ag)	
		110	24 s			
		111m	74 s			
		111	7.5 d		1.83×10^{-2} (see ^{113}In)	ΣAg = 0.2%
48	Cd	110	S		~0	
		111	S		1.87×10^{-2}	
		112	S		1.29×10^{-2}	
		113m	14.6 y			
		113	S		1.25×10^{-2}	
		114	S		1.16×10^{-2}	
		115m	45 d		7.89×10^{-2}	
		115	54 h		1.16×10^{-2}	
		116	S	~0.01	1.10×10^{-2}	
		117m	3.4 h			
		117	2.6 h			
		118	50 m	~0.01	1.48×10^{-2}	ΣCd = 0.29%
49	In	113	S		~0	
		114m	49.5 d			
		114	72 s			

(contd)

Appendix B. (contd)

Atomic No.	Element Symbol	Mass No.	T 1/2	Independent Fission Yield[a]	Cumulative Fission Yield[b]	Est. wt % of Total Non-Volatile Fission Products[c]
49	In	115m	4.5 h			
		115	S(5×10^{14}y)		1.06×10^{-2}	ΣIn $\leq$ 0.1%
50	Sn	115	S		$\sim$0	
		116	S		$\sim$0	
		117m	14 d			
		117	S		1.08×10^{-2}	
		118	S		1.18×10^{-2}	
		119m	245 d			
		119	S		1.17×10^{-2}	
		120	S	$\sim$0.01	1.23×10^{-2}	
		121m	50 y			
		121	27 h	$\sim$0.015	1.78×10^{-2}	
		122	S	$\sim$0.013	1.39×10^{-2}	
		123	40 m			
		123	129 d		$\sim 1.6 \times 10^{-2}$	
		124	S	$\sim$0.02	2.29×10^{-2}	
		125m	9 m			
		125	9.7 d			
		126	10^5y		5.90×10^{-2}	ΣSn = 1.7%
51	Sb	121	S		1.30×10^{-2}	
		122m	4.2 m			
		122	2.7 d	$\sim$0	$\sim$0	
		123	S		1.69×10^{-2} (see ^{123}Sn)	
		124		$\sim$0	$\sim$0	
		125	2.7 y		2.53×10^{-2}	
		126m	19 m			
		126	12 d		1.7×10^{-4} (see ^{126}Sn)	
		127	93 h		0.104	
		128m	10 m			
		128	9.0 h			ΣSb $\simeq$ 0.05%

(contd)

Appendix B. (contd)

Atomic No.	Element Symbol	Mass No.	T 1/2	Independent Fission Yield[a]	Cumulative Fission Yield[b]	Est. wt % of Total Non-Volatile Fission Products[c]
52	Te	122	S		0	
		123	S		0	
		124	S	∿0	0	
		125m	58 d		$<3 \times 10^{-2}$	
		125	S		3.00×10^{-2}	
		126	S		$<5.90 \times 10^{-2}$	
		127m	109 d		5.6×10^{-2}	
		127	9.4 h			
		128	S		0.351	
		129m	33 d		0.337	
		129	70 m			
		130	S		1.46	
		131m	30 h		2.50	
		131	25 m	0.2		
		132	78 h	1.0	4.29	ΣTe = 1.95%
53	I	127	S		1.29	
		128	25 m			
		129	1.6×10^7 y		0.665	
		130	12 h			
		131	8.0 d		2.87	
		132	2.3 h			
		133	21 h	0.5	6.76	(ΣI = 0.4%)
54	Xe	128	S	0	0	
		129	S	4×10^{-4}	0.665	
		130	S	0	0	
		131m	12 d	3.12×10^{-2}		
		131	S		2.84	
		132	S		4.22	
		133m	2.2 d	0.200		
		133	5.3 d		6.77	
		134	S		7.68	
		135m	15 m	1.17		
		135	9.2 h	0.3	6.73	(ΣXe ≳ 15%)

(contd)

Appendix B. (contd)

Atomic No.	Element Symbol	Mass No.	T 1/2	Independent Fission Yield[a]	Cumulative Fission Yield[b]	Est. wt % of Total Non-Volatile Fission Products[c]
55	Cs	133	S		6.77	
		134m	2.9 h	∿0		
		134	2.1 y	5.7×10^{-5}		
		135	2×10^{6} y		6.64	
		136	13 d	5.9×10^{-3}		
		137	30 y		6.28	
		138	32 m	0.04	6.74	ΣCs = 9.00%
56	Ba	134	S		0	(see ^{134}Xe, ^{134}Cs)
		135m	29 h			
		135	S		6.63	
		136	S		∿5.9×10^{-3} (see ^{136}Xe, ^{136}Cs)	
		137m	2.6 m			
		137	S		<6.26 (see ^{137}Cs)	
		138	S		6.85	
		139	83 m	0.012	6.59	
		140	13 d	0.066	6.31	ΣBa = 5.20%
57	La	139	S		6.59	
		140	40 h		∿6.31	
		141	3.9 h	0.004	5.70	
		142	93 m	0.019	5.96	ΣCa = 4.39%
58	Ce	140	S		6.32	
		141	33 d		5.70	
		142	S		5.93	
		143	33 h	4.4×10^{-3}	5.85	
		144	285 d	0.3	5.42	ΣCe = 8.79%
59	Pr	141	S		6.32	
		142	19 h		∿0	
		143	14 d		>5.85	
		144	17 m			
		145	6.0 h		3.95	ΣPr = 4.16%

(contd)

Appendix B. (contd)

Atomic No.	Element Symbol	Mass No.	T 1/2	Independent Fission Yield[a]	Cumulative Fission Yield[b]	Est. wt % of Total Non-Volatile Fission Products[c]
60	Nd	142	S		0	
		143	S		5.97	
		144	S (2×10^5y)		<5.46	
		145	S		3.94	
		146	S		3.00	
		147	11 d		2.23	
		148	S		1.69	
		149	1.7 h			
		150	S		0.649	ΣNd = 14.0%
61	Pm	147	2.6 y		<2.28	(see ^{147}Sm, ^{147}Nd)
		148m	41 d	∿0	<0.01	
		148	5.4 d	∿0	<0.01	
		149	53 h		1.07	
		150	2.7 h			
		151	28 h	0.02	<0.44	ΣPm = 0.23%
62	Sm	147	S (1×10^{11}y)		2.28	
		148	S (8×10^{15}y)	∿0	∿0.01	
		149	S		1.09	
		150	S	∿0	<0.01	
		151	93 y		0.422	(see ^{151}Eu)
		152	S		0.272	
		153	47 h		0.15	
		154	S		7.5×10^{-2}	
		155	22 m			ΣSm = 2.90%
63	Eu	151	S		<<0.422	
		152m	96 m	∿0	0	
		152	13 y	∿0	0	
		153	S		0.163	
		154	S		7.5×10^2	

(contd)

Appendix B. (contd)

Atomic No.	Element Symbol	Mass No.	T 1/2	Independent Fission Yield[a]	Cumulative Fission Yield[b]	Est. wt % of Total Non-Volatile Fission Products[c]
63	Eu	155	22 m		3.33×10^{-2}	
		156	9.4 h		1.33×10^{-2}	
		157	15 h		6.4×10^{-3}	ΣEu = 0.62%
64	Gd	152	S (1×10^{14}y)		0	
		153	241 d (EC)	0	0	
		154	S		0	
		155	S		<0.033	
		156	S		1.4×10^{-2}	
		157	S		6.6×10^{-3}	
		158	S		3.3×10^{-3}	
		159	19 h		1.09×10^{-3}	
		160	S		4.0×10^{-4}	
		161	3.7 m		$<8.4 \times 10^{-5}$	ΣGd = 0.42
65	Tb	159	S		1.05×10^{-3}	
		160	72 d		3.7×10^{-8}	
		161	7 d		8.4×10^{-5}	
		162	7.5 m			ΣTb = <0.01
66	Dy	160	S		0	
		161	S		$<8.8 \times 10^{-5}$	ΣDy = <0.0001

[a] Independent fission yield for the isotope listed is atoms per 100 ^{235}U fissions for the isotopes listed.

[b] Cumulative fission yield is a summation of the independent fission yields plus the total isobaric chain yield for the isotopes of lower Z, expressed in atoms per 100 ^{235}U fission events [NETHAWAY]. Cumulative fission yields for all stable isotopes will sum to 200% (two fragments per fission event). Cumulative fission yields for the stable isotopes is the isobaric chain yield. Data taken from [MEEK].

[c] Estimated weight percent of total nonvolatile fission products, taken from [SCHINDLER]. Note this is in mass % not atom %.

[d] S--stable isotope.

APPENDIX C

PRELIMINARY FLOWSHEET FOR REPROCESSING FUEL IN LIQUID TIN

The accompanying flowsheet (Fig. C-1) represents a concept for a pyrochemical reprocesssing scheme based on selective nitriding of uranium in tin solvent. All numbers on the flowsheet are kilograms of material, based on 1 metric ton of UO_2 fuel at 3.5% burnup, plus an appropriate amount of cladding.

The assumptions made are explained as follows.

1. Declad Step

The tin used for dissolving the cladding is cooled at the end of the decladding step to precipitate the contaminants at about 240°C, and the recycle from the first stage of tin recovery is shown as saturated with cladding components, so that essentially all of the cladding appears in the material sent for tin reclamation (reclamation method not yet clearly defined).

Only 80% of the volatile fission products are shown leaving in the vapor phase from decladding. This is an estimate, and it will vary, depending on the degree to which the UO_2 is disturbed.

Tin is not anticipated in the overhead product.

2. Reduction

The reduction of UO_2 with carbon is shown here as a separate step to illustrate that not all fission products have appreciable solubility in tin, even at elevated temperature. A solid molybdenum phase, which might also contain Nb, Tc, or Ru, will probably be formed.

Nickel is added (possibly) to enhance carbon solubility and hasten the reduction process.

3. Nitriding

Not shown is a sink-float or similar separation of rare earth nitrides, along with ZrN and YN, pending laboratory demonstration at near operating conditions.

The tin remaining with the nitrides at the end of this step is an estimate based on wetting of the nitrides by tin.

The uranium content of the liquid phase is based on the assumption of 97% conversion to UN at 1.013×10^5 pascals (1 atm) N_2 pressure.

4. Oxidation

The tin should be vaporized overhead as SnO_2, leaving the refractory oxides for refabrication.

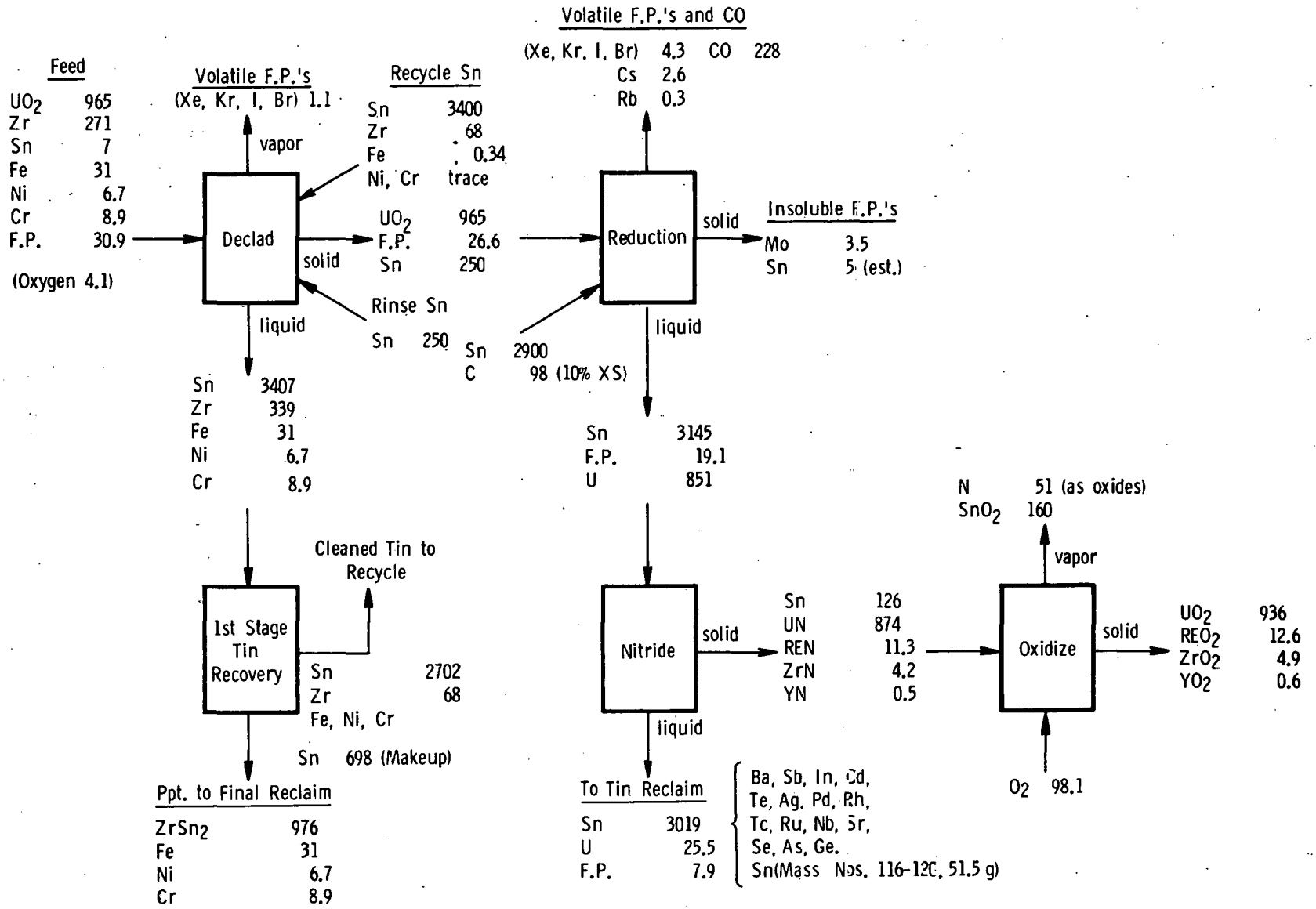

Fig. C-1. Fuel Reprocessing in Liquid Tin - Flowsheet (Revision 1). All numbers are kilograms of material, based on 1 metric ton of UO_2 fuel at 3.5% burnup, plus an appropriate quantity of cladding.

Tin reclamation remains an undefined area, and only the feedstocks are shown. Tin from the nitriding step can probably be cooled to 240°C to precipitate the balance of dissolved species (as was done in the decladding step). A solid material would thereby be produced which is an alphabet soup of intermetallic compounds, uncombined metals, and entrained tin.

Since tin is quoted at $5.95/lb, recovery of the tin from waste products is critical. Fuming, liquid metal leaching, and other techniques are under consideration for tin recovery.

REFERENCES

AI

1000 MW(e) Liquid Metal Fast Breeder Reactor Follow-On Study Conceptual Design Report, AI-AEC-12792, p. 97 (1969).

Amecke

B. Amecke, Bertraege zur Wiederaufbereitung von Thorium-Uranern Brennstoffen mit Salztransportverfahren, Dissertation Technische Universitaet Carolo-Wilhelmina zu Braunschweig (1971).

ANL-1965

R. C. Vogel et al., Chemical Engineering Division Semiannual Report, January-June 1965, Argonne National Laboratory Report ANL-7055, p. 42 (October 1965).

ANL-1966

L. E. Link et al., 1000-MW(e) Metal Fueled Fast Breeder Reactor, Argonne National Laboratory Report ANL-7001 (June 1966).

ANL-1970

R. C. Vogel et al., Chemical Engineering Division Annual Report-1970, Argonne National Laboratory Report ANL-7775 (April 1971).

Anselin

F. Anselin, Preparation of Metallic Plutonium, Extractive and Physical Metallurgy of Plutonium and Its Alloys XX, D. Wilkinson, Ed., Interscience Publishers, New York, pp. 61-74 (1960).

Archer

R. S. Archer, Molybdenum, Rare Metals Handbook, Reinhold Publishing Corporation (1961).

Arsene

A. Arsene and M. Germain, Etude du Partage de L'acide Formique, de L'uranium(VI) et du Plutonium(IV) dans le Systeme Tributylphosphate-dodecane-Acide Nitrique - Acide Formique - Eau, Revue Roum. Chim. 20, 251 (1975).

ASTM

Spec for Nuclear Grade Sinterable Uranium Dioxide Powder, ASTM-C-753-73, American Society for Testing Materials, Philadelphia (1973).

Avogadro-1971

A. Avogadro and J. Wurm, A Method of Processing Nuclear Fuels, British Patent Specification 1,221,604 (1971).

Avogadro-1972

A. Avogadro and A. DePlano, Pyrochemical Pretreatment of Fuels Derived from Fast Power Reactors: Oxidation with Fused Alkaline Nitrates, European Atomic Energy Community Report EUR-47841 (1972).

Bagnal
K. W. Bagnal, D. Brown, and J. G. H. duPreeze, J. Chem. Soc. 1964, 2603.

Baker
R. D. Baker and W. J. Maraman, Calcium Reduction of Plutonium Halides to Metal, Extractive and Physical Metallurgy of Plutonium and Its Alloys, W. D. Wilkinson, Ed., Interscience Publishers, New York, pp. 43-59 (1960).

Baldwin
C. E. Baldwin et al., Rocky Flats, private communication (March 1978).

Barr
M. J. Barr et al., Characterization of Some UO_2 and PuO_2 Powders Battelle Northwest Laboratory Report BNWL-1441 (July 1970).

Barton
C. J. Barton et al., Phase Diagrams of Nuclear Reactor Materials, Oak Ridge National Laboratory Report ORNL-2548 (1959).

Bayanov
A. P. Bayanov, Russ. Chem. Rev. 44(2), 122 (1975).

Benz
R. Benz, J. Inorg. Nucl. Chem. 24, 1191 (1962).

Bernstein
G. J. Bernstein, D. E. Grosvenor, J. F. Lenc, W. E. Miller, I. O. Winsch, J. Wolkoff and R. C. Paul, The EBR-II Skull Reclamation Process, Part V Design and Development of Plant Scale Equipment, Argonne National Laboratory Report ANL-7772 (January 1971).

Blocher
J. M. Blocher, Jr., Structure/Property/Process Relationships in Deposition, CVD, J. Vac. Sci. Technol., 680-686 (July-August 1974).

Bodine-1964
J. E. Bodine, I. J. Grace, J. Guon, and L. A. Hanson, Oxidative Decladding of Uranium Dioxide Fuels, Nucl. Sci. Eng. 19, 1 (1964).

Bodine-1965
J. E. Bodine, J. Guon, and R. J. Sullivan, Second-Cycle AIROX Reprocessing and Pellet Refabrication of Highly Irradiated Uranium Dioxide, North American Aviation Report NAA-SR-11375 (1965).

Bohnenstingl
J. Bohnenstingl, E. Fischer, M. Laser, and H. Gabbard, Reprocessing of Thorium-Containing Nuclear Fuels: Activity Report for Second Half Year 1970, United States-German High Temperature Reactor Research Exchange Program Report GERHTR-43 (February 1971).

Bonner

W. F. Bonner, H. T. Blair, and L. S. Romero, Spray Solidification of Nuclear Waste, Battelle Pacific Northwest Laboratories Report, BNWL-2059 (August 1976).

Booman

G. L. Booman, M. C. Elliot, R. B. Kimball, F. O. Cartan, and J. E. Rein, Determination of Free Acid in the Presence of Hydrolysable Ions, Anal. Chem. 30, 284 (1958).

Borzone

G. Borzone, A. Borese, A. Calabretta, and R. Ferro, J. Less-Common Metals 58, 31 (1978).

Bourgeois

M. Bourgeois and P. Nollet, Study of the Chemical Treatment of Uranium-Zirconium Fuel by Dry Methods, Energ. Nucl. 8 3, 165-174 (May 1966).

Bowersox

D. F. Bowersox, A Pyrochemical Head-End Treatment for Spent Nuclear Fuels, Los Alamos Scientific Laboratory Report LA-6596-MS (January 1977).

Bradbury

B. T. Bradbury, J. T. Dement, and P. M. Martin, Solid Fission Products in Irradiated Uranium Dioxide, Atomic Energy Research Establishment Report AERE-R-5149 (1966).

Brambilla-1973

G. Brambilla, G. Caporali, and M. Zambianchi, Process for the Dissolution of Ceramic Nuclear Fuels, Ger. Offen. 2,319,717 (1973).

Brambilla-1976

G. Brambilla and G. Caporali, Process for the Pyrochemical Separation of Plutonium from Irradiated Nuclear Fuels, Ger. Offen. 2,611,333 (1976).

Bramman

J. I. Bramman, R. M. Sharpe, D. Thom, and G. Yates, Metallic Fission-Product Inclusions in Irradiated Oxide Fuels, J. Nucl. Mat. 25, 201 (1968).

Brand

G. E. Brand and E. W. Murbach, Pyrochemical Reprocessing of UO_2 by AIROX: Summary Report, NAA-SR-11389 (1965).

British Patent

Brazing Alloys for Tungsten, Molybdenum and Alloys Thereof, British Patent 1,063,274 (June 14, 1965).

Brown

F. Brown et al., The Preparation of Mixed U-Pu Carbides by the Metal-Hydrocarbons Gas Reactivity, Compounds of Interest in Nuclear Reactor Technology. Nuclear Metallurgy Symposium, Boulder, Colorado, August 1964 IMD Special Report 13, The Metallurgical Soc. of AIME.

Burman

R. W. Burman, R. W. Gilbert, Jr., and R. Q. Barr, Molybdenum - 30% Tungsten Alloy Handles Liquid Zinc, Molybdenum Metal, Climax Molybdenum Company of Michigan (Inc.) (June 1970).

Cafasso

F. A. Cafasso, H. M. Feder, and I. Johnson, Partition of Solutes Between Liquid Metals, I. The Aluminum-Cadmium System, J. Phys. Chem. 66, 1028-1030 (1962).

Carroll

D. Carroll, Ion Exchange in Clays and Other Minerals, Geol. Soc. Am. Bull. 70, 749-780 (1959).

CEN

Centre d'Etude de l'Energie Nucleaire 'C.E.N.' at Brussels, Process for the Conditioning of Irradiated Nuclear Fuel, Netherlands Patent 7,500,663 (1975). Available also as BNWL-TR-319 (1978).

Chilton

J. D. Chilton, L. A. Hanson, E. W. Murbach, and F. W. Dodge, Separation of Uranium from Thorium by Liquid Metal Extraction, Thorium Recovery, and Fission Product Distribution, North American Aviation Report NAA-SR-6666 (1962).

Chiotti-1961

P. Chiotti and K. J. Gill, Phase Diagram and Thermodynamic Properties of the Thorium-Zinc System, Trans. Metall. Soc. AIME, 221, 573-579 (June 1961).

Chiotti-1964

P. Chiotti and P. F. Woerner, J. Less-Common Metals 1, 111 (1964).

Christensen-1969

J. A. Christensen, Research at Battelle - Northwest on Transport Processses in Oxide Nuclear Fuel, BNWL-1202 (1969).

Christensen-1970

J. A. Christensen, Structure Evolution in an Oxide Fuel Pin, WHAN-SA-79 (1970).

Cleveland

J. M. Cleveland, The Chemistry of Plutonium, Gordon and Breach: Science Publishers, New York (1970).

Cole

N. C. Cole, R. G. Gilliland, and G. M. Slaughter, Weldability of Tungsten and Its Alloy, Welding Research Supplement, 4195-4265 (September 1971).

Corn

M. Corn, Adhesion of Particles, Aerosol Science, C. N. Davies, Ed., Academic Press, New York, Chapter XI (1960).

Cotton
F. A. Cotton and G. Wilkinson, Advanced Inorganic Chemistry, 2nd Ed., Interscience Publishers, New York (1966).

Davies
J. H. Davies and F. T. Ewart, The Chemical Effects of Composition Changes in Irradiated Oxide Fuel Materials, J. Nucl. Mat. 41, 143 (1971).

DeGrazio
R. P. DeGrazio, A Prototype Hydriding Apparatus (Application for Plutonium Recovery, RFP-2340 (1975).

DeHalas
D. R. DeHalas and G. R. Horn, Evolution of Uranium Dioxide Structure During Irradiation of Fuel Rods, J. Nucl. Mat. 8(2), 207 (1963).

De Kany
J. P. De Kany, H. W. Lavendel, and L. Burris, Jr., Studies of Corrosion by Molten Zinc and Cadmium Systems, Argonne National Laboratory Report ANL-6243 (October 1960).

Dimmick
R. L. Dimmick, M. T. Hatch, and J. Ng, A Particle-Sizing Method for Aerosols and Fine Powders, AMA Arch. Public Health 18, 23 (1958).

DMIC Review
DMIC Review of Metal Joining, Battelle Memorial Institute (Dec. 10, 1965).

Dwyer
O. E. Dwyer, H. E. Howe, and E. R. Avrutic, Nucl. Sci. Eng. 12, 15 (1962).

Elliott
R. P. Elliott, Constitution of Binary Alloys-First Supplement, McGraw-Hill Book Co. (1965).

Ewart
F. T. Ewart and R. G. Taylor, The Chemical Effects of Composition Changes in Irradiated Oxide Fuel Materials II - Fission Product Segregation and Chemical Equilibria, J. Nucl. Mater. 61, 254 (1976).

Feder-1958
H. M. Feder and R. J. Teitel, Purification of Reactor Fuels and Blankets by Crystallization from Liquid Metal Solvents, Second International Conference on the Peaceful Uses of Atomic Energy, Vol. 17 (1958).

Feder-1961
H. M. Feder and R. J. Teitel, Purification of Reactor Fuels and Blankets by Crystallization from Liquid Metal Solvents, Progr. Nucl. Energy. Ser., 3, Process Chemistry, Pergamon Press Ltd., 365 (1961).

Fee

D. C. Fee and C. E. Johnson, Phase Equilibria and Melting Point Data for Advanced Fuel Systems, Argonne National Laboratory Report ANL-AFP-10 (June 1975).

Ferris-1971

L. M. Ferris et al., J. Less-Common Metals 25, 83 (1971).

Ferris-1972

L. M. Ferris et al., J. Inorg. Nucl. Chem. 34, 313, 2921 (1972).

Findlay

J. R. Findlay, The Migration of Fission Products Through Reactor Fuel Materials, Proceedings of a Panel on Behavior and Chemical State of Irradiated Ceramic Fuels, Vienna, International Atomic Energy Agency Report IAEA-PL-463/10, p. 211 (1972).

Flynn

K. F. Flynn, L. J. Jardine, and M. J. Steindler, Method for Determining Leach Rates of Simulated Radioactive Waste Forms, American Chemical Society Symposium on Radioactive Waste in Geologic Storage, ACS Symp. Ser. 100, p. 115 (1979).

Frost

B. R. T. Frost, Studies of Irradiation Effects in Ceramic Fuels at Harwell, Ceramic Nuclear Fuels, O. L. Kruger, Ed., American Ceramic Society, Inc., Columbus, Ohio, pp. 225-243 (1969).

Ger Offen

Ger. Offen. 1,197,630 (1975).

Gittus

J. H. Gittus, Uranium, Butterworths, Washington, pp. 124-126 (1963).

Glassner

A. Glassner, The Thermochemical Properties of the Oxides, Fluorides, and Chlorides to 2500 K, Argonne National Laboratory Report ANL-5750 (1957).

Goode-1970A

J. H. Goode and O. L. Kirkland, Effect of Voloxidation Time, Temperature, and Fuel Particle Size on the Release of ^{85}Kr, LMFBR Fuel Cycle Studies Progress Report for September 1970, No. 19, Oak Ridge National Laboratory Report ORNL-TM-3180 (1970).

Goode-1970B

J. H. Goode and O. L. Kirkland, Voloxidation from Oxide Fuels, LMFBR Fuel Cycle Studies Progress Report for August 1970, No. 18, Oak Ridge National Laboratory Report ORNL-TM-3127 (1970).

Gorbunov

V. F. Gorbunov et al., Sov. Radiochem. 18(1), 101-105 (1975).

Grimes
W. R. Grimes, J. H. Shaffer and F. A. Doss, U.S. Patent 3,806,581 (April 1974).

GTE Sylvania
Custom Fabricated Parts of Tungsten, Molybdenum, and Their Alloys, GTE Sylvania.

Guertler
W. Guertler, A Compendium of Constitutional Ternary Diagrams of Metallic Systems, Wright Air Development Center, WADC Tech. Report 58-615, part 1 (March 1959).

Guon-1962
J. Guon, J. E. Bodine, R. J. Sullivan, and F. W. Gandolfo, Low Decontamination Reprocessing Studies on Irradiated Uranium Dioxide Reactor Fuel, North American Aviation Report NAA-SR-7136 (1962).

Guon-1964
J. Guon, J. E. Bodine, and R. J. Sullivan, Refabrication and Encapsulation of Highly Irradiated Uranium Dioxide, North American Aviation Report NAA-SR-8213 (1964).

Haire
R. G. Haire, R. D. Baybarz, and L. G. Farrar, A Study on the Oxidation Behavior of (U, Pu)O_2 Fuels which Relates to the Voloxidation Process, Oak Ridge National Laboratory Report ORNL-TM-3724, 9 (1972).

Hampel
C. A. Hampel, Tantalum, Rare Metals Handbook, Reinhold Publishing Corporation, pp. 469-518 (1961).

Hansen
M. Hansen and K. Anderko, Constitution of Binary Alloys, 2nd Ed., McGraw-Hill Book Co., (1958).

Hanson
L. A. Hanson, Removal of Irradiated UO_2 Fuel from the Cladding by Controlled Oxidation, North American Aviation Report NAA-SR-3591 (1959).

Hariharan
A. V. Hariharan et al., in Symposium on Reprocessing of Nuclear Fuels, Vol. 15, p. 261, Report CONF-690801 (1969).

Henrion
P. N. J. Henrion, W. F. Johannes, and L. Claes, Belgian Patent 815,189.

Heylen
P. R. Heylen, et al., Nuclear Energy Maturity, Proceedings of the European Nuclear Conference, Paris, Vol. 8, Reprocessing, Transport, and Waste Disposal, Pergamon Press, Oxford, p. 68 (1975).

Hidy

G. M. Hidy and J. R. Brock, The Dynamics of Aerocolloidal Systems, Vol. 1, Pergammon Press, New York (1970).

Hildebrand

J. H. Hildebrand and R. L. Scott, The Solubility of Nonelectrolytes, Reinhold Publishing Corp., New York (1950).

Hodge

W. Hodge, R. M. Evans, and A. F. Haskins, Metallic Materials Resistant to Molten Zinc, J. Met., 824-832 (July 1955).

Hofmann

P. Hofmann, United States - Euratom Fast Reactor Exchange Program Report EURFNR-1177 (1974).

Hultgren

R. Hultgren, R. L. Orr, and K. K. Kelley, Supplement To Selected Values of Thermodynamic Properties of Metals and Alloys, Department of Mineral Technology, College of Engineering and Inorganic Materials Research Division, Lawrence Radiation Laboratory, University of California, Berkeley, California, Rev. 1970.

Inoue

Y. Inoue and W. Kaufman, Prediction of Movement of Radionuclides in Solution Through Porous Media, Health Phys. 9, 705-715 (1963).

Ishihara

T. Ishihara, K. Hirano, and T. Honda, Processing of Uranium Dioxide Fuel by Chloride Fractional Distillation, Nippon Genshiryoku Gakkaishi 4, 231-239 (April 1962).

Iverson

P. M. Iverson, Reactions of Thorium Carbide in a Fused Salt-Liquid Metal System, Unpublished M.S. Thesis, Library, Iowa State University, Ames, Iowa (1969).

Jardine

L. J. Jardine and M. J. Steindler, A Review of Metal-Matrix Encapsulation of Solidified Radioactive High-Level Waste, Argonne National Laboratory Report ANL-78-19 (1978).

Jeffery

B. M. Jeffery, Microanalysis of Inclusions in Irradiated UO_2, J. Nucl. Mater. 22, 33 (1967).

Jenkins

I. L. Jenkins, N. J. Keen, and A. G. Wain, Alternative Routes for the Conversion of Plutonium Salts to Metal and Their Recovery Problems Extractive and Physical Metallurgy of Plutonium and Its Alloys, W. D. Wilkinson, Ed., Interscience Publishers, Inc., New York, pp. 25-42 (1960).

Johnson
T. R. Johnson et al., The EBR-II Skull Reclamation Process, Part II, Argonne National Laboratory Report ANL-6874 (April 1964).

Kanellakopulos
B. Kanellakopulos and H. Parthey, The Oxidation of Uranium Tetrachloride, J. Inorg. Nucl. Chem. 28, 2541-2549 (1966).

Kendall
J. Kendall, E. D. Crittendan, and H. K. Miller, J. Am. Chem. Soc. 45, 977 (1923).

Kleykamp
H. Kleykamp, Formation of Phases and Distribution of Fission Products in an Oxide Fuel, Proceedings of a Panel on the Behavior and Chemical State of Irradiated Ceramic Fuel, International Atomic Energy Agency Report IAEA-PL-463/8 (1972).

Klima
J. Klima, M. Prodest, and V. Vins, Contribution to the Studies of the Fission Gases Released from Irradiated Uranium Dioxide, Proceedings of a Panel on Behavior and Chemical State of Irradiated Ceramic Fuels, Vienna, International Atomic Energy Report IAEA-PL-463/11, p. 211 (1972).

Knighton-1957
J. B. Knighton, H. M. Feder, L. Burris, Jr., and A. A. Chilenskas, Use of Zinc in Pyrometallurgical Processing of Reactor Fuels, presented at A.N.S. meeting, June 1957.

Knighton-1961
J. B. Knighton and R. K. Steunenberg, Effect of Flux Composition on the Reduction of Uranium, Thorium and Plutonium Oxides by Zinc-Magnesium Alloy, Trans. Am. Nucl. Soc. 4(2), 352-3 (1961).

Knighton-1963
J. B. Knighton and R. K. Steunenberg, Reduction of Plutonium Dioxide by Zinc-Magnesium Alloys and Molten Halide Salt Systems, Trans. Am. Nucl. Soc. 6(1), 166 (1963).

Knighton-1965A
J. B. Knighton and R. K. Steunenberg, Preparation of Metals by Magnesium-Zinc Reduction. Part I. Reduction of Uranium Oxides, Argonne National Laboratory Report ANL-7057 (June 1965).

Knighton-1965B
J. B. Knighton and R. K. Steunenberg, Preparation of Metals by Magnesium-Zinc Reduction. Part III. Reduction of Plutonium Dioxide, Argonne National Laboratory Report ANL-7059 (June 1965).

Knighton-1965C
J. B. Knighton, R. A. Mancini, and R. K. Steuenberg, Consolidation of Lanthanon Fission Products in Alloys, Argonne National Laboratory Report ANL-7064 (August 1965).

Knighton-1966
J. B. Knighton, R. Tiffany, and K. Tobias, Solubility of Uranium in Zinc-Magnesium, Chemical Engineering Division Semiannual Report, July-December 1966, Argonne National Laboratory Report ANL-7325.

Knighton-1969A
J. B. Knighton, I. Johnson, and K. K. Steunenberg, Uranium Purification by the Process of Salt Transport, Argonne National Laboratory Report ANL-7524 (March 1969).

Knighton-1969B
J. B. Knighton, I. Johnson, and R. K. Steunenberg, Uranium and Plutonium Purification by the Salt Transport Method, Symposium on the Reprocessing of Nuclear Fuels, Atomic Energy Commission Report (AEC Conf. 690801, August 25-27, pp. 337-361 (1969).

Knoch
W. Knoch, Solubility of Plutonium in Liquid Cu-Mg Alloys, Chemical Engineering Division Semiannual Report, January-June 1966, Argonne National Laboratory Report ANL-7225.

Koch-1965A
V. G. Koch, Extraction von Uran VI durch Tricaprylmethylammiumnitrat, Radiochim. Acta 4, 128 (1965).

Koch-1965B
V. G. Koch, Zur Wiederaufarbeitung von Kernbrennstoffen durch Flussig-Flussig-Extraction mit quartares Ammoniumitraten. On the Reprocessing of Nuclear Fuels by Liquid-Liquid Extraction with Quaternary Ammonium Nitrates, Kerntechnik 7, 394 (1965).

Kyle-1965
M. L. Kyle, P. A. Nelson, and L. Burris, Jr., Corrosion of Steels and Tantalum by Molten Cadmium-Magnesium-Zinc Systems, Electrochem. Technol., 258-262 (September-October 1965).

Kyle-1969
M. L. Kyle, R. D. Pierce, and V. M. Kolba, Containment Materials for Pyrochemical Processes, in Reprocessing of Nuclear Fuels, CONF-690801, Ames, Iowa (1969).

Laughlin
W. C. Laughlin and N. W. Gregory, Inorg. Chem. 14, 1263 (1975).

Lawroski-1962
S. Lawroski, R. C. Vogel, and V. H. Munnecki, Chemical Engineering Division Summary Report, October, November, December, 1961, Argonne National Laboratory Report ANL-6477 (March 1962).

Lawroski-1964
S. Lawroski and L. Burris, Jr., Processing of Reactor Fuel Materials by Pyrometallurgical Methods, At. Energy Rev. 2(3), 3-69 (1964).

Layne-1963
G. S. Layne and R. J. Teitel, Uranium-Molybdenum-Aluminum Ternary Alloy, U.S. Patent 3,098,742 (July 23, 1963).

Layne-1965
G. S. Layne and J. O. Huml, Uranium-Niobium-Aluminum Ternary Alloy, U.S. Patent 3,183,079 (May 11, 1965).

Leitnaker
J. M. Leitnaker, Applications of Thermodynamics for Predicting and Understanding the Performance of Fast Breeder Reactor Oxide Fuels, J. Nucl. Mater. 51, 95 (1974).

Li
K. C. Li, Tungsten, Rare Metals Handbook, Reinhold Publishing Corporation (1961).

Lukens
H. R. Lukens, C. A. Preskett, and R. J. Teitel, Aluminum Alloy Processing of Th- and U-Based Fuels, private communication (May 16, 1978).

McDuffie
H. M. McDuffie, D. H. Smith, and P. T. Owen, Oak Ridge National Laboratory, private communication (May 1978).

McElroy
J. L. McElroy, Quarterly Progress Report Research and Development Activities, Waste Fixation Program, Oct-Dec 1976, Battelle Pacific Northwest Laboratories Report PNL-2264 (November 1977).

McKay
H. A. C. McKay, J. H. Miles, and H. S. Park, Possible Uses of Carboxylic Acids for U/Pu Separation in Nuclear Fuel Reprocessing, AERE-8509 (1976).

Mailen
J. C. Mailen and L. M. Ferris, Inorg. Nucl. Chem. Lett. 7, 431 (1971).

Margrave
J. L. Margrave, Appendix VI. Melting Points and Vapour Pressures of the Elements, Physicochemical Measurements at High Temperatures, J.O.M. Bockris, Ed., 1959, pp. 369-371, Butterworths, London, England.

Marshall
W. R. Marshall, Jr., Atomization and Spray Drying, Chem. Eng. Prog. Monogr. Ser. 50, 2 (1954).

Meek
M. E. Meek and B. F. Rider, Compilation of Fission Product Yields, Vallecitos Nuclear Center Report NEDO 12154-1 (1974).

Megerth

F. H. Megerth, Zircaloy-Clad UO_2 Fuel Rod Evaluation Program, General Electric Co. Report GEAP-5746 (1969).

Meredith

D. D. Meredith, K. W. Wong, R. W. Woodhead, R. H. Wortman, Design and Planning of Engineering Systems, Prentice-Hall, Inc., Englewood Cliffs, New Jersey, Ch. 4,5 (1973).

Metcalfe

A. G. Metcalfe, Reactive Brazing, A New Joining Method, Met. Prog., 88-86 (May 1963).

Mishima-1968A

J. Mishima et al., Plutonium Release Studies: III. Release from Heated Plutonium-Bearing Powders, Battelle-Northwest Report BNWL-786 (July 1968).

Mishima-1968B

J. Mishima et al., Plutonium Release Studies: IV. Fractional Release from Heating Plutonium Nitrate Solutions in a Flowing Air Stream, Battelle-Northwest Report BNWL-931 (November 1968).

Mishima-1973A

J. Mishima and L. S. Schwendiman, Fractional Airborne Release of Uranium (Representing Plutonium) During the Burning of Contaminated Wastes, Battelle-Northwest Report BNWL-1730 (April 1973).

Mishima-1973B

J. Mishima and L. S. Schwendiman, Some Experimental Measurements of Airborn Uranium (Representing Plutonium) in Transportation Accidents, Battelle-Northwest Report BNWL-1732 (August 1973).

Monk

G. W. Monk, Viscous Energy Dissipated During Atomization of a Liquid, J. Appl. Phys. 23, 288 (January-December 1952).

Moore

R. H. Moore, J. R. Morrey, and E. E. Voiland, The Equilibrium Controlled Reduction of Uranium Chloride by Molten Aluminum in a Fused Salt Solvent, J. Phys. Chem. 67, 744-747 (1963).

Moulton-1970A

D. M. Moulton and J. H. Shaffer, Oak Ridge National Laboratory Report, ORNL-4548, p. 171 (February 1970).

Moulton-1970B

D. M. Moulton, Oak Ridge Naional Laboratory Report, ORNL-4548, p. 174 (February 1970).

Nelson

P. A. Nelson, M. L. Kyle, G. A. Bennett, and L. Burris, Jr., Corrosion of Refractory Metals by Zinc-Magnesium-Uranium and Halide Salt Systems, Electrochem. Technol. 3(9-10), 263-269 (September-October 1965).

Nethaway
P. R. Nethaway and G. W. Barton, A Compilation of Fission Product Yields in Use at Lawrence Livermore Laboratory, Report UCRL-51428 (October 3, 1973).

Newkirk
H. W. Newkirk, Jr., J. L. Daniel, and B. Mastel, Electron Microscope Studies of Damage in Irradiated Uranium Dioxide, J. Nucl. Mater. 2(3), 269 (1960).

O'Boyle-1969
D. R. O'Boyle, F. L. Brown, and J. E. Sanecke, Solid Fission Product Behavior in Uranium-Plutonium Oxide Fuel Irradiated in a Fast Neutron Flux, J. Nucl. Mater. 29, 27 (1969).

O'Boyle-1970
D. R. O'Boyle, F. L. Brown, and A. E. Dwight, Analysis of Fission Product Ingots Formed in Uranium-Plutonium Oxide Irradiated in FBR-II, J. Nucl. Mater. 35, 257 (1970).

Oi-1964
Noboru Oi and Keiji Naito, Relocation of Fission Products and Pu in Irradiated UO_2 Pellets, Nucl. Sci. Technol. 2(8), 284 (1964).

Oi-1965
Noboru Oi and Jizaburo Takagi, Distribution of Fission Products in Irradiated UO_2, Nucl. Sci. Technol. 2, 127 (1965).

ORNL-1957
Reactor Chem. Div. Semi-Annual Report January-June 1957, Oak Ridge National Laboratory Report ORNL-2392, p. 29 (August 1957).

ORNL-1970
Oak Ridge National Laboratory Report ORNL-4436, Sect. 4.3.1 (1970).

ORNL-1973
Voloxidation - Removal of Volatile Fission Products from Spent LMFBR Fuels, J. H. Goode, Ed., Oak Ridge National Laboratory Report ORNL-TM-3723 (1973).

Patterson
F. H. Patterson, W. C. Robinson, Jr., and C. F. Leitten, Jr., Conversion, of Uranium Chlorides to Urania by Gas-Phase Reduction Hydrolysis, Oak Ridge National Laboratory Report ORNL/TM-1701 (April 1967).

Petkus
E. J. Petkus, et al., Fluidized Bed Technique for Preparation of Uranium-Plutonium Monocarbide, Chem. Eng. Progr. Symp., Ser 80, 63, 111-120 (1967).

Powell
H. J. Powell, Fission Product Distribution in Fast Reactor Oxide Fuels, Proceedings of a Panel on Behavior and Chemical State of Irradiated Ceramic Fuels, Vienna, International Atomic Energy Agency Report IAEA-PL-463/10, 211 (1972).

Prasad
R. Prasad, K. Rengan, and A. V. Hariharan, Laboratory Investigations on Direct Chlorination Volatility Reprocessing of Nuclear Fuels, Part IV, BARC-406 (1969).

Qureshi
M. Qureshi, H. S. Rathore, and R. C. Kaushik, Cation and Anion Exchange Studies of Twenty Cations in Aqueous Solutions of Formic, Oxalic, Tartaric and Citric Acids and Their Alkali Metal Salts, Anal. Chem. 47, 1710 (1975).

Rand
M. H. Rand and L. E. J. Roberts, Thermochemistry and Nuclear Engineering, Proceedings of the Symposium on Thermodynamics, Vienna, July 22-27, 1965 (1966).

Reilly
J. J. Reilly, W. H. Regan, E. Wirsing, and L. P. Hatch, Uranium Recovery from Unirradiated Reactor Fuel Elements, Ind. Eng. Chem. Process Des. Dev. 2(2), 127-133 (April 1963).

RESAR-3
Reference Safety Analysis Report (RESAR-3), Consolidated Version, Westinghouse Nuclear Energy Systems, Docket-RESAR-23 (November 1973).

Richardson-1970
D. M. Richardson and J. H. Shaffer, Oak Ridge National Laboratory Report ORNL-4548, p. 172 (February 1970).

Richardson-1972
D. M. Richardson, Oak Ridge National Laboratory Report ORNL-4622, p. 107 (August 1972).

RI-AI
Rockwell International-Atomics International, Test Plan to Demonstrate the AIROX Process with Spent Fuel, private communication.

Schindler
R. E. Schindler, J. K. Berreth, G. G. Simpson, J. H. Valentine, and M. S. Walker, Development of a Fluidized Bed Calciner and Post Treatment Processes for Solidification of Commercial Fuel Reprocessing Liquid Wastes, Report ICP-1136 (December 1977).

Schraidt
J. H. Schraidt and M. Levenson, Development in Pyrometallurgical Processing Second Conference on Peaceful Uses of Nuclear Energy, Vol. 17 (September 1958).

Seitz

M. G. Seitz, P. G. Rickert, S. M. Fried, A. M. Friedman, and M. J. Steindler, Studies of Nuclear-Waste Migration in Geologic Media, Annual Report November 1976-October 1977, Argonne National Laboratory Report ANL-78-8 (1978).

Selby

J. M. Selby et al., Considerations in the Assessment of the Consequences of Effluents from Mixed Oxide Fuel Fabrication Plants, Battelle-Northwest Report BNWL-1697, Rev. 1 (June 1975).

Selvaduray

G. S. Selvaduray, M. K. Goldstein, and R. N. Anderson, A Methodology for Evaluation of Alternative Technologies Applied to Nuclear Fuel Reprocessing, Brookhaven National Laboratory Report BNL-50700 (July 1977).

Semenenko

K. N. Semenenko, V. N. Sulov, and N. S. Kedrova, Russ J. Inorg. Chem. 14, 481 (1969).

Sharma

R. A. Sharma and I. Johnson, Study of the Reduction of UO_2 by Magnesium or Calcium Dissolved in Molten Chloride, Metall. Trans. 1, 291-7 (1970).

Shunk

F. A. Shunk, Constitution of Binary Alloys-Second Supplement, McGraw-Hill Book Co. (1969).

Siddall-1959A

T. D. Siddall, III, Trialkyl Phosphates and Dialkyl Alkylphosphonates in Uranium and Thorium Extraction, Ind. Eng. Chem. 51, 41 (1959).

Siddall-1959B

T. H. Siddall, III, Thermodynamics for the Extraction of Uranyl Nitrate and Nitric Acid by Esters of the Type (RO), P = D and $(RO)_2RP = O$, J. Am. Chem. Soc. 81, 4176 (1959).

Slinn

W. G. N. Slinn, Parametrizations for Resuspension and for Wet and Dry Deposition of Particles and Gases for Use in Radiation Dose Calculations, Nucl. Saf. 19(2), 205-238 (March-April 1978).

Smith-1970

F. J. Smith et al., Oak Ridge National Laboratory Report ORNL-4548, p. 289 (February 1970).

Smith-1971

F. J. Smith et al., Oak Ridge National Laboratory Report ORNL-4676, p. 242 (February 1971).

Smith-1972
F. J. Smith, J. Less-Common Metals 29, 73 (1972).

Smithells
C. J. Smithells, Ed., Metals Reference Book, 5th Ed., Butterworths, London and Boston, pp. 231-233 (1976).

Sood-1967
S. P. Sood and A. V. Hariharan, Chlorination Volatility Separation of Th and U, Proceedings of the Nuclear and Radiation Chemistry Symposium, Poona, India, March 6-9, 1967, CONF-670335.

Sood-1969
S. P. Sood et al., Laboratory Investigation on Direct Chlorination Volatility Processing of Nuclear Fuels. Part II. Chlorination of Uranium Oxides, Bhabha Atomic Research Centre Report BARC-404 (1969).

Stehle
H. Stehle, H. Assmann, and F. Wunderlick, Uranium Dioxide Properties for LWR Fuel Rods, Nucl. Eng. Des. 33, 230 (1975).

Steindler-1977
M. J. Steindler et al., Chemical Engineering Division Fuel Cycle Programs Quarterly Progress Report, October-December 1976, Argonne National Laboratory Report ANL-77-36.

Steindler-1978A
M. J. Steindler et al., Chemical Engineering Division Fuel Cycle Programs Quarterly Progress Report, January-September 1977, Argonne National Laboratory Report ANL-78-11.

Steindler-1978B
M. J. Steindler et al., Chemical Engineering Division Fuel Cycle Programs Quarterly Progress Report, October-December 1977, Argonne National Laboratory Report ANL-78-37.

Steindler-1978C
M. J. Steindler et al., Chemical Engineering Division Fuel Cycle Programs Quarterly Progress Report, January-March 1978, Argonne National Laboratory Report ANL-78-68.

Steunenberg-1967A
R. K. Steunenberg, Salt Transport Processes for Ceramic Fast Breeder Fuels, Advanced Course in Fuel Reprocessing, pp. 476-493, KR-126, Institutt for Atomenergi, Kjeller, Norway (1967).

Steunenberg-1967B
R. K. Steunenberg, Pyrometallurgical Processing of Fast Breeder Fuel, Reprocessing of Fuel from Present and Future Power Reactors, Institute for Atomenergi, Kjeller Research Establishment, pp. 452-493 (1967).

Steunenberg-1968A
R. K. Steunenberg and J. D. Arntzen, Compact Pyrochemical Processes, Chemical Engineering Division Semiannual Report, July-December 1967, Argonne National Laboratory Report ANL-7425 (May 1968).

Steunenberg-1968B
R. K. Steunenberg and J. D. Arntzen, Compact Pyrochemical Processes, Chemical Engineering Division Annual Report-1968, Argonne National Laboratory Report ANL-7575 (April 1969).

Steunenberg-1969A
R. K. Steunenberg, R. D. Pierce, and L. Burris, Pyrometallurgical and Pyrochemical Fuel Processing Method, Prog. Nucl. Energy., Ser. 3, Process Chemistry, Vol. 4, 461-503 (1969).

Steunenberg-1969B
R. K. Steunenberg, R. D. Pierce, and A. Johnson, Status of the Salt Transport Process for Fast Breeder Reactor Fuels in Reprocessing of Nuclear Fuels, CONF-690801 (August 1969).

Strausberg-1959
S. Strausberg and T. E. Luebben, Chemical Pulverization of Sintered Uranium Dioxide Bodies, Part I, North American Aviation Report NAA-SR-3910 (1959).

Strausberg-1960
S. Strausberg, Chemical Pulverization of Sintered Uranium Dioxide Bodies, Part II, North American Aviation Report NAA-SR-3911 (1960).

Strausberg-1962
S. Strausberg, Multicycle Reprocessing and Refabrication Experiments on Simulated UO_2 - Fissia Pellets, North American Aviation Report NAA-SR-7138 (1962).

Teitel-1958
R. J. Teitel, The Aluminum-Magnesium Pyrometallurgical Process, The Dow Chemical Company Status Report (August 12, 1958).

Teitel-1959
R. J. Teitel, Separation of Uranium from Zirconium-Uranium Alloy, U.S. Patent 2,974,942 (filed August 7, 1959).

Teitel-1960A
R. J. Teitel and G. S. Layne, The Dow Aluminum Pyrometallurgical Process, USAEC Report TID-11692 (August 1960).

Teitel-1960B
R. J. Teitel, Separation of Uranium from Zirconium-Uranium Alloy, U.S. Patent 2,963,461 (December 6, 1960).

Teitel-1962
R. J. Teitel, Process for Recovering Uranium Values, U.S. Patent 3,053,650 (September 11, 1962) and Canadian Patent 629,781.

Teitel-1963
R. J. Teitel, Reduction of Uranium Oxide, U.S. Patent 3,099,555 (July 30, 1963).

Teitel-1964A
R. J. Teitel, Recovery of Uranium (Cu-Al Process), U.S. Patent 3,148,976 (September 15, 1964).

Teitel-1964B
R. J. Teitel, Processing Impure Uranium, U.S. Patent 3,148,976 (September 15, 1964).

Teitel-1964C
R. J. Teitel and G. S. Layne, Processing Impure Uranium, U.S. Patent 3,148,975 (September 15, 1964).

Teitel-1964D
R. J. Teitel and G. S. Layne, Methods of Purifying Uranium Metal, U.S. Patent 3,148,977 (September 15, 1964).

Teitel-1964E
R. J. Teitel, Reduction of Uranium Oxide, U.S. Patent 3,119,686 (January 28, 1964).

Threadgill
W. D. Threadgill, Preparation of Metallic Calcium by Electrolysis of Calcium Oxide Dissolved in Molten Calcium Chloride, J. Electrochem. Soc. III, 1408 (1964).

Turnbull
J. A. Turnbull and R. M. Cornell, The Re-solution of Gas Atoms from Bubbles During the Irradiation of UO_2, J. Nucl. Mater. 36, 161 (1970).

Van Vucht
J. H. N. Van Vucht, Ternary System Th-Ce-Al, Philips Res. Rep. 16(1), 1-40 (1961).

Vogel-1964A
R. C. Vogel, M. Levenson, and V. H. Munnecke, Chemical Engineering Division Semiannual Report, July-December 1963, Argonne National Laboratory Report ANL-6800 (May 1964).

Vogel-1964B
R. C. Vogel, M. Levenson, and V. H. Munnecke, Chemical Engineering Research Highlights, May 1963-April 1964, Argonne National Laboratory Report, ANL-6875 (1964).

Vogel-1968A
R. C. Vogel, E. R. Proud, and J. Royal, Chemical Engineering Division Research Highlights, May 1967-April 1968, Argonne National Laboratory Report ANL-7450 (1968).

Vogel-1968B
R. C. Vogel, M. Levenson, E. R. Proud, and J. Royal, Chemical Engineering Division Research Highlights, May-December 1968, Argonne National Laboratory Report ANL-7550.

Wenz-1966
D. A. Wenz and R. D. Wolson, Chemical Interactions of Uranium Oxides in Molten Salts, Chemical Engineering Division Semiannual Report, July-December 1966, Argonne National Laboratory Report ANL-7325 (April 1967).

Wenz-1968
D. A. Wenz, R. D. Wolson, and I. Johnson, Reduction of Uranium Dioxide in Molten Salt-Metal Systems, Argonne National Laboratory Report ANL-7463 (November 1968).

Wenz-1969
D. A. Wenz and R. D. Wolson, The $CaCl_2$-Rich Region of $CaCl_2$-CaF_2-CaO System, Chemical Engineering Division Annual Report-1968, Argonne National Laboratory Report ANL-7575 (April 1969); J. Chem. Eng. Data 14, 250 (1969).

Winsch-1967
I. O. Winsch, M. L. Kyle, R. D. Pierce, and L. Burris, Tungsten Crucibles in Pyrochemical Processing of Nuclear Fuels, Nucl. Appl. 3, 245-251 (April 1967).

Winsch-1969
I. O. Winsch, R. D. Pierce, G. J. Bernstein, W. E. Miller, and L. Burris, EBR-II Skull Reclamation Process, Symposium on Reprocessing of Nuclear Fuels at Ames Iowa, August 1969, CONF 690801.

Woodson
T. T. Woodson, Introduction to Engineering Design, McGraw-Hill Book Co., New York, Ch. 12, 13, 15 (1966).

Wurm-1968
J. G. Wurm and A. Avogadro, Process for Reprocessing Nuclear Fuels, British Patent Specification 1,108,042 (1968).

Wurm-1970
J. G. Wurm, P. R. Heylen, R. C. Debeukelaer, and A. DeConinck, Pyrochemical Head-End Conception for Fast Breeder Fuel Processing, European Atomic Energy Community Report EUR-4614e (1970).

Yamagishi

S. Yamagishi and Y. Kamemoto, Separation of Fission Products from Irradiated Uranium Dioxide in Fused Nitrate Systems, J. Nucl. Sci. Technol. 2(11), 457-462 (November 1965).

Zebel

G. Zebel, Coagulation of Aerosols, Aerosol Science, C. N. Davies, Ed., Academic Press, New York, Chapter II. (1966).

Distribution for ANL-78-76

Internal:

W. E. Massey
M. Ader
R. E. Barletta
J. K. Bates
C. H. Bean
G. J. Bernstein
L. Burris
F. A. Cafasso
T. F. Cannon
R. A. Couture
E. J. Croke
L. Cuba
P. R. Fields
K. F. Flynn
S. Fried
A. M. Friedman
B. R. T. Frost
T. J. Gerding
L. J. Jardine
G. Kesser
M. Krumpelt
B. J. Kullen
S. Lawroski
R. A. Leonard
W. J. Mecham
J. H. Meisenhelder
A. Melton
K. M. Myles
M. V. Nevitt
R. H. Pelto
W. B. Seefeldt
M. G. Seitz
A. A. Siczek
J. Simmons
M. J. Steindler (15)
L. E. Trevorrow
S. Vogler
D. S. Webster
A. A. Ziegler
A. B. Krisciunas
ANL Contract File
ANL Libraries (5)
TIS Files (6)

External:

DOE-TIC, for distribution per UC-10 and UC-70 (330)
Manager, Chicago Operations and Regional Office, DOE
Chief, Office of Patent Counsel, DOE-CORO
President, Argonne Universities Association
Chemical Engineering Division Review Committee:
  C. B. Alcock, U. Toronto
  R. C. Axtmann, Princeton U.
  R. E. Balzhiser, Electric Power Research Inst.
  J. T. Banchero, U. Notre Dame
  T. Cole, Ford Motor Co.
  P. W. Gilles, U. Kansas
  R. I. Newman, Allied Chemical Corp.
  G. M. Rosenblatt, Pennsylvania State U.
T. W. Ambrose, Battelle Pacific Northwest Lab.
C. K. Anderson, Combustion Engineering
F. H. Anderson, Allied Chemical Corp., Idaho Falls
J. F. Bader, Westinghouse Electric Corp., Pittsburgh
Battelle-Columbus Labs.
R. C. Baxter, Allied-General Nuclear Services
J. E. Bennett, Clemson U.
M. Binstock, Kerr-McGee Nuclear Corp.
B. C. Blanke, USDOE-DA, Miamisburg, O.
D. Bowersox, Los Alamos Scientific Lab.
K. Bowlman, General Electric Co., San Jose
M. G. Britton, Corning Glass Works
C. L. Brown, Battelle Pacific Northwest Lab.
R. Brown, Allied Chemical Corp., Idaho Falls
H. L. Browne, Bechtel, Inc.
J. K. Bryan, Clemson U.
L. L. Burger, Battelle Pacific Northwest Lab.
D. Camp, Lawrence Livermore Lab.
D. O. Campbell, Oak Ridge National Lab.

D. Camp, Lawrence Livermore Lab.
D. O. Campbell, Oak Ridge National Lab.
J. Carp, Edison Electric, New York City
W. T. Cave, Mound Lab.
B. H. Cherry, GPU Services Corp.
E. D. Clayton, Battelle Pacific Northwest Lab.
F. E. Coffman, USDOE-MFE
J. J. Cohen, Lawrence Livermore Lab.
W. J. Coleman, Battelle Pacific Northwest Lab.
C. R. Cooley, Office of Nuclear Waste Management, USDOE
G. R. Corey, Commonwealth Edison, Chicago
R. Cunningham, USNRC, Nuclear Materials Safety & Safeguards
R. E. Dahl, Hanford Engineering Development Lab.
J. C. Dempsey, Office of Nuclear Waste Management, USDOE
R. L. Dickeman, Exxon Nuclear Co., Inc., Bellevue
M. Dickerson, Lawrence Livermore Lab.
B. R. Dickey, Allied Chemical Corp., Idaho Falls
J. Dietz, Los Alamos Scientific Lab.
R. L. Dillon, Battelle Pacific Northwest Lab.
R. F. Duda, Westinghouse Electric Corp., Pittsburgh
G. H. Dyer, Bechtel Corp.
Eastern Environmental Radiation Lab., HEW
D. Eldred, General Electric Co., Sunnyvale
E. D. Erickson, Rocky Flats Plant
D. Ferguson, Oak Ridge National Lab.
R. L. Ferguson, USDOE-ANE
J. L. Fletcher, Hanford Engineering Development Lab.
Foster Wheeler Corporation, Library (HQAP)
R. G. Geier, Rockwell Hanford Operations, Richland
General Electric Co., San Jose (DOE)
A. Giambusso, USDOE-AIA
R. W. Gilchrist, Clemson U.
S. Goldsmith, Battelle Pacific Northwest Lab.
R. L. Grant, Boeing Engineering and Construction Div., Seattle
J. L. Heffter, NOAA, Silver Spring
R. S. Hemper, Battelle Pacific Northwest Lab.
T. B. Hindman, Jr., USDOE-SR
A. H. Hines, Jr., Florida Power Corp.
C. A. Hirenda, Proposal Management, Inc., Philadelphia
R. Hoskins, Tennessee Valley Authority
H. A. Hurstadt, Virginia Polytechnic Inst.
R. H. Ihde, Babcock & Wilcox Co., Lynchburg
W. Johnson, Yankee Atomic Electric Co.
B. F. Judson, General Electric Co., San Jose
W. A. Kalk, Holmes & Narver, Inc., Anaheim
S. V. Kaye, Oak Ridge National Lab.
G. R. Keepin, Los Alamos Scientific Lab.
C. J. Kershner, Mound Lab.
F. J. Kiernan, Aerojet Energy Conversion Co., Washington
K. Killingstad, Battelle-Human Affairs Research Centers, Seattle
H. J. C. Kouts, USNRC
G. Lehmkul, Rocky Flats Plant
D. Lester, Battelle Pacific Northwest Lab.
S. Levine, USNRC, Div. of Reactor Safety Reasearch
F. W. Lewis, Middle South Utilities, Inc., New Orleans
W. H. Lewis, Nuclear Fuel Services, Rockville

R. C. Liikala, Battelle Pacific Northwest Lab.
J. L. Liverman, Deputy Asst. Secy. for Environment, USDOE
Los Alamos Scientific Lab., Director
L. Machta, NOAA, Silver Spring
J. C. Mailen, Oak Ridge National Lab.
W. J. Maraman, Los Alamos Scientific Lab.
M. L. Matthews, Nuclear Power Development, USDOE
W. H. McVey, USDOE-NPD
R. B. Minogue, USNRC, Office of Standards Development
E. Morgan, Babcock & Wilcox Co., Lynchburg
B. C. Musgrave, Allied Chemical Corp., Idaho Falls
M. I. Naparstek, Burns & Roe, Inc., Paramus, NJ
NASA, John F. Kennedy Space Center
L. W. Nelms, Todd Company, Galveston
Y. Ng, Lawrence Livermore Lab.
R. D. Oldenkamp, Atomics International
D. Orloff, U. South Carolina
R. C. Orphan, Lawrence Livermore Lab.
D. A. Orth, Savannah River Plant
B. Paige, Allicd Chemical Corp., Idaho Falls
J. H. Pashley, Oak Ridge Gaseous Diffusion Plant
H. Postma, Oak Ridge National Lab.
C. A. Preskitt, IRT Corp., San Diego
J. J. Reilly, Brookhaven National Lab.
C. Rhoades, U. South Carolina
G. K. Rhode, Niagara Mohawk Power Corp., Syracuse
L. M. Richards, Atlantic Richfield Co., Los Angeles
G. L. Ritter, Exxon Nuclear Corp., Richland
D. M. Rohrer, Los Alamos Scientific Lab.
H. E. Roser, USDOE, Albuquerque Operations Office
K. J. Schneider, Battelle Pacific Northwest Lab.
R. L. Scalc, U Arizona
T. A. Sellers, Sandia Labs.
J. Shefcik, General Atomic Co.
W. G. N. Slinn, Oregon State U.
B. Smenoff, Hudson Inst. Croton, NY
L. E. Smith, Carolina Power & Light Co., Raleigh
A. Squire, Hanford Engineering Development Lab.
T. Stanford, U. South Carolina
C. Stephens, Virginia Electric Power Co., Richmond
J. A. Stiegler, Sandia Labs.
S. Stoller, The S. M. Stoller Corp.
E. Straker, Science Applications, Inc., La Jolla
K. Street, Lawrence Livermore Lab.
G. Stukenbroeker, NL Industries, Wilmington, Del.
J. L. Swanson, Battelle Pacific Northwest Lab.
R. Uhrig, Florida Power & Light Co., Miami
USDOE Div. of Nuclear Power Development, Nuclear Fuel Cycle Programs Br.
USDOE Office of Basic Energy Sciences
USDOE Div. of RRT, Engineering
USDOE Div. of RRT, Technology
USDOE Idaho Operations Office
USDOE New Brunswick Laboratory
USDOE San Francisco Operations Office

USDOE Southern California Energy Office
V. Van Brunt, U. South Carolina
H. H. Van Tuyl, Battelle Pacific Northwest Lab.
V. C. A. Vaughn, Oak Ridge National Lab.
E. E. Voiland, General Electric Co., Morris, IL
B. L. Vondra, Oak Ridge National Lab.
R. D. Walton, Jr., Office of Nuclear Waste Management, USDOE
C. D. Watson, Oak Ridge National Lab.
L. L. Wendell, Battelle Pacific Northwest Lab.
W. J. Wilcox, Oak Ridge Gaseous Diffusion Plant
A. K. Williams, Allied-General Nuclear Services, Barnwell
R. O. Williams, Rocky Flats Plant
D. D. Wodrich, Atlantic Richfield Hanford Co.
J. E. Yanoski, Office of Nuclear Energy Programs, USDOE
D. Zeigler, Rocky Flats Plant
Arizona, U. of, Dept. of Nucl. Engineering
C. F. Bonilla, Columbia U.
W. Brandt, U. of Wisconsin-Milwaukee
R. G. Cochran, Texas A&M U.
D. A. Daavettila, Michigan Technological U.
A. H. Emmons, U. Missouri
E. R. Epperson, Michigan Technological U.
Fermi National Accelerator Lab., Library
P. J. Fulford, Purdue U.
H. E. Hungerford, Purdue U.
H. S. Isbin, U. Minnesota
Y. W. Kang, National Accelerator Lab.
W. R. Kimel, U. Missouri
Maine Univ., Prof. in charge of Chem. Engr. Lib.
Marquette U., Dept. of Chemistry
Michigan Technological U., Library
D. W. Moeller, Kresge Ctr. for Environmental Health, Boston
G. Murphy, Iowa State U.
H. Rosson, U. Kansas
L. Schwendiman, Pacific Northwest Lab.
E. R. Stansberry, Purdue U.
B. S. Swanson, Illinois Inst. of Technology
H. G. Swope, Madison, Wis.
B. W. Wilkinson, Michigan State U.
W. E. Wilson, Washington State U.
W. F. Witzig, Pennsylvania State U.